Development and Deployment of an Autonomous Micro-Drilling System for Cochleostomy

Robin Peter Taylor

Doctor of Philosophy

Aston University

May 2008

Aston University

Development and Deployment of an Autonomous Micro-Drilling System for Cochleostomy

Robin Peter Taylor

Doctor of Philosophy
May 2008

This thesis describes the design and development of an autonomous micro-drilling system capable of accurately controlling the penetration of compliant tissues and its application to the drilling of the cochleostomy; a key stage in the cochlea implant procedure.

There are many surgical procedures where the penetration of soft or compliantly mounted tissues is required to a high degree of accuracy, without excessive protrusion of the tool. Under these circumstances, deflection of the tissue under the tool action or as a result of movement of the target makes this task difficult to achieve using conventional surgical robotic systems.

The drilling of the cochleostomy is a precision micro-surgical task in which the control of the burr penetration through the outer bone tissue of the cochlea is vital to prevent damage to the structures within and requires a high degree of skill to perform successfully. The micro-drilling system demonstrates that the penetration of the cochlea can be achieved consistently and accurately. Breakthrough can be detected and controlled to within 20 μm of the distal surface and the hole completed without perforation of the underlying endosteal membrane, leaving the membranous cochlea intact.

This device is the first autonomous surgical tool successfully deployed in the operating theatre. The system is unique due to the way in which it uses real-time data from the cutting tool to derive the state of the tool-tissue interaction. Being a smart tool it uses this state information to actively control the way in which the drilling process progresses. This sensor guided strategy enables the tool to self-reference to the deforming tissue and navigate without the need for pre-operative scan data. It is this capability that enables the system to operate in circumstances where the tissue properties and boundary conditions are unknown, without the need to restrain the patient.

Keywords: robotic surgery, sensor guided, smart tool

Dedicated to Natalie and my family

Acknowledgments

This research, whilst it was a fascinating insight into surgical robotics, was a very challenging and intense project encompassing skills across many fields and I would like to thank all those that helped me along the way.

I would like to thank my supervisor Peter Brett for guiding and supporting me for the duration of my research, for trusting in my abilities and allowing me the scope to develop the research as I saw fit.

I would like to thank Lionel Reyes and Geoff Shand for their role in the design and development of the hardware; without their continued support much of this project would not have been possible.

Thanks are due to all the staff in the ENT Department at the Queen Elizabeth Hospital for their enthusiasm regarding the project and their expertise and professionalism. Special thanks go to Mansel Griffiths, David Proops and Chris Coulson for giving up their own time to make this project the success it was. Special thanks to David, whose enthusiasm and unwavering support got us into the operating theatre and to Chris, who has kept the project going when my time at Aston had run out and for his faith in my abilities which gave me the confidence to see the clinical trials through.

I would also like to thank all those in the Biomedical Engineering Research Group, particularly Mark Prince, Paul Slack, Mark Elliot and Dheeraj Bansal. They made the research group a fantastic place to work and helped form a strong research team who not only helped and supported one-another but are also great friends.

Lastly I would like to thank my family for their love and support, particularly my girlfriend Natalie who kept me sane through the hard times and drove me mad through the rest.

Contents

List of Tables

List of Figures

Nomenclature

$\bar{F}$	Filtered force signal
$\bar{T}$	Filtered torque signal
β	Friction Coefficient
ΔF	Force Difference
ΔT	Torque Difference
δY	Deflection in the Y direction
$\dot{x}$	Feed rate
$\frac{dF}{dx}$	Force Gradient
$\frac{dT}{dx}$	Torque Gradient
γ	Cutting Rate
ω	Rotational Velocity
$\overline{V}$	Mean Velocity
σ	Standard Deviation
θ_1	Angular dimension: Location of near tissue interface.
θ_2	Angular dimension: Location of far tissue interface.
ay	Force gradient intersect with y axis

$ayLB$	Bound of ay
az	Torque gradient intersect with y axis
$azLB$	Bound of az
b	Breadth
c	Chord length
c	Damper Constant
d	Depth
dt	Time Interval
E	Yung's Modulus
F''	Force deviation rate
F'	Force deviation magnitude
F_x	Feed force
F_{lim}	Force threshold
g	Gravitational constant
h_{dp}	Drill penetration
I	Second Moment of Area
i	i^{th} sample
J	Total Inertia
j	Mean window width
J_L	Load Inertia
J_M	Motor Inertia
k	Filter window width

k	Stiffness
K_d	Derivative Gain
K_i	Integral Gain
K_p	Proportional Gain
K_v	Motor voltage constant
K_{ffa}	Acceleration Feed-forward Gain
K_{pc}	Current Loop Gain
l	Length
m_2	Mass of constant force load
n	Current sample
R	Resistance of the stator windings
r	Burr radius
S	Motor Rotational Direction
t	Time
T''	Torque deviation rate
T'	Torque deviation magnitude
T_A	Acceleration Torque
T_F	Friction Torque
T_G	Gravitational Torque
T_x	Torque
T_{Fm}	Motor friction Torque
T_{lim}	Torque threshold

T_L	Load Torque
V	Voltage
V_A^t	Actual Motor Velocity
V_A^t	Time Interval
$V_{errdiff}^t$	Differential Velocity Error
V_{err}	Velocity Error
V_{err}^t	Integral Velocity Error
W	Load
X	Horizontal distance from the pivot
x	Displacement
x_0	Start Position
x_2	Horizontal distance from the drill tip to the load m_2
x_d	Deflection
x_h	Hole Depth
x_t	Material Thickness

Chapter 1

Introduction

1.1 Compliant Tissue

The human body is a highly complex organic system consisting of many tissue types with varying mechanical properties. These flexible tissues are both mobile, fragile and are often easily damaged. That is to say that they are free to move whether it be through, change in orientation, movement of the patient or as a result of deformation caused by the action of a tool itself.

Human strengths lie in a sophisticated tactile and visual feedback system that combines high levels of spatial awareness and co-ordination with dexterity and the ability to make use of all the available information to control the task at hand (27). As such, when operating on a macro scale in conventional surgical procedures, tissue movenet or deformation is generally not an issue as the surgeon can sense the displacement and take the appropriate corrective action.

When operating at the opposite end of the scale, at the micro level when perception and dexterity are greatly reduced, the challenges are significantly greater. This particularly relevant with the use of Minimally Invasive Surgical (MIS) procedures and minimal Access Surgery (MAS) increasing, more and more techniques are being developed to replace conventional procedures.

These techniques present many potential benefits over conventional 'open' surgeries including:

1. smaller access,
2. reduced bleeding and trauma,
3. reduced scarring,
4. faster recovery times,
5. shorter hospital stays (59).

Whilst there are many potential benefits there are also significant challenges to be overcome to fully realise this potential, particularly as procedures are both reducing in scale and becoming increasingly complex, requiring a greater level of skill and training.

1.2 Compliant Tissue Challenges

Due to the limited access and confined working volume the visual field is severely limited as is the range of motion that can be achieved with the surgical instruments. Perhaps the biggest concern is the lack of tactile feedback to the clinician, this can result in extensive accidental soft tissue damage.

Given the stiffness of the tissues and the scale of the motion, the demands on the clinician are high. The manipulation of these tissues requires the clinician to work at the limit of human perception and dexterity. Under these circumstances and in micro-surgical procedures in general, human limitations become a factor in the successful outcome of surgical procedures. These limitations include:

- manipulative precision and dexterity are decreased as a result of narrow access;
- sensory perception is negligible and qualitative, often relying on poor visual feedback;

- responsivity is reduced due to delayed perception of forces at the tool tip;
- tool position and stability can be affected by tremor due to fatigue, particularly during lengthy procedures (87);
- disorientation in the enclosed environment.

While more training can reduce any skill deficit and aid in the more complex tasks, it can do little to increase the clinicians dexterity and the perception of forces at the tool tip. As such there is scope to build on the clinicians skills to improve the outcome of procedures so that it is not only more efficient, but less traumatic and more repeatable. It is here that surgical mechatronic and robotic systems can offer significant benefits over conventional techniques:

- precise and repeatable tool positioning;
- high degree of tool stability;
- precise and repeatable tool motion;
- accurate and quantitive sensory feedback from the tool point;
- highly responsive;
- unaffected by long or repetitive tasks;
- can maintain tool position for long periods.

Soft and compliant tissues present a significant challenge for robotic systems in surgery. As most conventional robotic systems rely on pre-operative scan data to calculate the tool path, tissue movement often results in the loss of the target. In order to achieve the benefits described above, a means of registering the tool to the deforming tissue is required so that the motion can be compensated.

1.3 Smart Surgical Tools

Given the human limitations and those of conventional robotic systems this research aims to explore the new concept of smart surgical tools.

A new approach to surgical robotics is proposed that uses simple, custom designed mechatronic devices coupled with modern sensing technologies to create a new generation of smart surgical tools.

Smart tools employ a multi-element sensing strategy to derive state information directly from the tool tip. This strategy uses more than just absolute measurements from individual sensors; data from sensing elements coupled directly, or indirectly to the tool combined with additional information available to the device is acquired and processed in real-time. Employing advanced multivariate algorithms and the relationships between the sensor transients for the analysis significantly increases the amount of information available. It is therefore possible to differentiate between different states that may occur at the tool tip through a process of discrimination. Through further characterisation, this information can be used to accurately describe the tool-tissue interaction, this is particularly important in biological systems where conditions are often neither absolute or repeatable.

Using this information as feedback to close the control loop enables a device to control a process or navigate without the need for external tracking or pre-operative planning. More-over, by looking at this information in real-time, indications of impending events can be detected and steps can be taken to control the process, even when the mechanical tissue properties and boundary conditions are unknown.

1.4 Aims and Objectives

The principal aims of this research are to design and build a surgical robotic system suitable for clinical deployment, capable of accurately controlling the penetration of a cutting burr through compliant tissues of unknown mechanical properties and boundary conditions at the medial surface.

The development of this device will explore the concept of a smart tool points; bringing together multi-modal sensing strategies and advanced control algorithms to implement the controlled compliant drilling technique (42).

This research will culminate in a series of research clinical trials in which the

system will be deployed in the operating theatre and used in general surgery. The ultimate aim of this is to demonstrate that smart tools can improve clinical results by building on a clinician's skills, enhancing sensing and control capabilities and therefore have a future in general surgical practice.

To achieve this the objectives of this work are as follows:

1. explore the drilling characteristics and devise a technique for the control of penetration through compliant tissues;
2. identify key requirements of a suitable clinical application;
3. identify general surgical requirements necessary to deploy a new device in the operating theatre;
4. design and build a complete surgical robotic system.
5. implement the compliant drilling technique;
6. verify and validate the system performance;
7. conduct a series of clinical trials.

1.5 Thesis Outline

This thesis is presented in nine chapters.

Chapter 2 describes the basis of the compliant drilling technique and a model of the compliant drilling characteristics is presented and evaluated. Using this model a technique is derived for the control of burr penetration through compliant tissues. The technique is broken down into a number of phases and different strategies are explored to control each phase. A technical specification is derived.

Chapter 3 presents the challenges involved in working with compliant tissues and the limitations of manual surgical techniques in contrast to the benefits that arise from the use of robotic systems. A review of past and present robotic surgical devices and their limitations are discussed.

Chapter 4 reviews earlier work on previous micro-drilling systems leading to a series of feasibility studies to evaluate different technological approaches to some of the challenges presented and forms the basis for a technical specification of the new device.

Chapter 5 begins by discussing deafness and some of the possible causes. Current surgical techniques in the field that may benefit from use of robotic systems are reviewed. The challenges, possible complications and approach to each procedure is discussed, as well as the general surgical requirements of such a system and a clinical and environmental specification for the device is derived.

Chapter 6 details the specification of the complete system and explores the philosophy behind the design of the surgical micro-drilling system in its entirety including the mechanical, electronic, firmware and software architectures of the device. The chapter concludes with a system wide summary of the device and additional design considerations.

Chapter 7 describes the verification and validation process, from initial laboratory trials up to a full cadaver trial of the device.

Chapter 8 builds on the learning from the trials in the previous chapter and defines the operating and surgical protocols for the use of the system in the operating theatre. The results of the clinical trials are presented and discussed.

Chapter 9 concludes the thesis by reviewing the work carried out and what has been achieved, exploring possible avenues for further work and the future of smart tool in the operating theatre.

Chapter 2

Controlled Compliant Drilling

2.1 Compliant Drilling

The compliant drilling technique was first conceived by Brett *et al* (37, 42) in 1993 in anticipation of the growing trends in clinical practice moving toward the use of minimally invasive and micro-surgical techniques, the expectation being that surgeons will be working on such a scale that perception of the tool forces involved would be almost impossible, greatly increasing the skill requirement for performing such tasks successfully. Automatic tools were being investigated as a potential solution, lowering skill requirements while still achieving high-quality results ultimately leading to advanced treatments becoming more widely available. The compliant drilling technique was designed to take the accuracy and precision achievable when drilling rigid materials and apply it to compliant materials such as soft tissues in the body.

The drilling of a compliant material is a particularly challenging task when any degree of precision is required. By its very nature drilling is a mechanical process that requires the application of force to remove the material ahead of the tool tip. When drilling a rigid material this is not a problem assuming the material is securely held in position. Precision can be maintained by referencing

the tool to the face of the material and then simply controlling the linear feed of the drill itself. In the case of drilling a compliant material, the application of force via the tool point deforms the target material and as such any reference to a fixed datum is lost. There are only two or three points (depending on the material thickness) during the compliant drilling process at which the precise position of the tool tip relative to the deformed material is known. What is required is a technique that is capable of self referencing to the deforming material, and allows the monitoring and control of the drilling process.

2.2 Compliant Drilling Model

The mathematical model described in this chapter was presented by Baker (27) in which various cutting burr geometries were modeled and their drilling characteristics explored. It was found that cutting burrs with spherical geometry generate the optimum drilling characteristics for detecting and controlling burr penetration. As such, only the use of this geometry will be considered in this work.

The model derived operates under the following basic assumptions:

1. the target tissue is compliant or compliantly mounted;
2. the tissue stiffness is sufficient to achieve the minimum force required to cut, without excessive deformation;
3. the target is only compliant along the drilling axis, orthogonal to the target tissue;
4. and the tissue is of uniform density and hardness.

While all efforts will be taken to provide these conditions during the actual drilling process, it is unlikely that these assumptions will remain true. Despite this, the model provides valuable insight into how breakthrough can be predicted and controlled. In order to achieve this, it is necessary to understand the key stages of the drilling process and the resulting characteristics that occur in the drilling transients.

2.2.1 Compliant Drilling Stages

Although drilling force and torque transients may vary depending on the control strategy, the key stages are specific to the drilling process and will occur regardless. These key stages are listed below:

1. the start of drilling;
2. when hole depth is equal to the radius of the burr;
3. the start of equilibrium drilling;
4. the start of breakthrough;
5. the completion of the hole.

It is possible to model the force and torque characteristics by considering the tool-tissue interaction at each of these stages based on the geometric progression of the burr.

The geometric relationships between the cutting burr and the tissue during the drilling process are depicted in figure 2.1 and the corresponding transients for constant feed rate drilling are shown in figure 2.2. Figure 2.2 shows a typical set and drilling transients obtained using the re-assembled clinical demonstrator described in section 4.1. The target material was compliantly mounted egg shell with a mounting stiffness of between 1.5 N/mm and 3.0 N/mm. The drill rotational velocity was 2 Hz and constant feed rate control strategy was used *(feed control strategies are discussed in section 2.3.2)*.

The start of drilling *(Stage 1 in figures 2.1 and 2.2)* is the point at which the burr is sat on the surface of the material, but is not yet exerting any force. The drill feed and rotation is then commenced and the process continues to the next stage. When drilling is initiated the burr does not begin to cut immediately, Baker (27) discovered that there is a minimum force required to begin cutting that is dependent on the type of burr and the properties of the target tissue. This can be observed at the beginning of the force transient in figure 2.2. As drilling is initiated the linear feed advances and the force increases. When only considering deflection along the drilling axis, orthogonal to the target, the force increase is

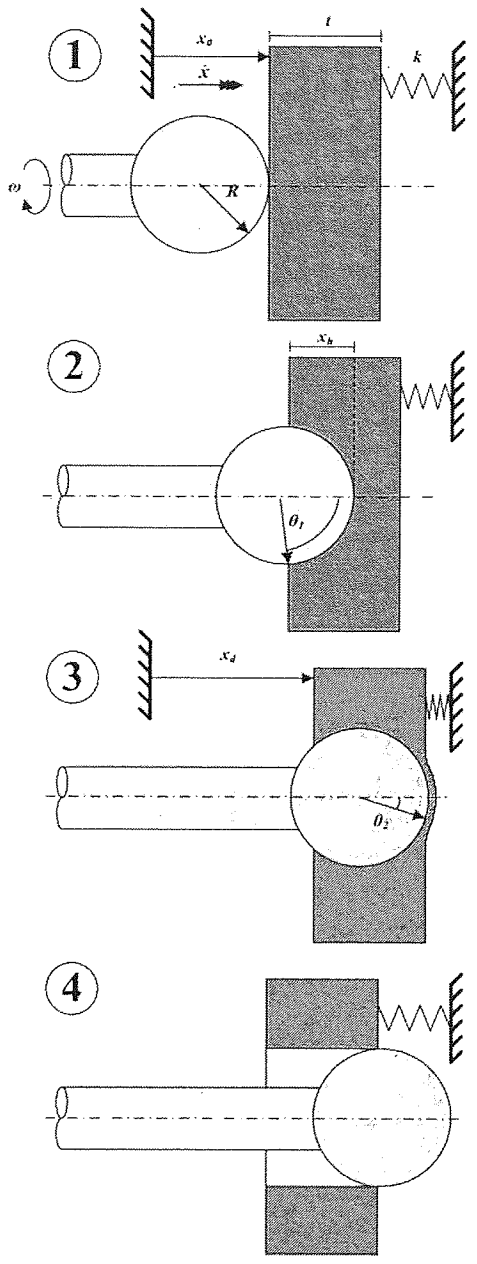

Figure 2.1: *Key stages in the drilling process.*

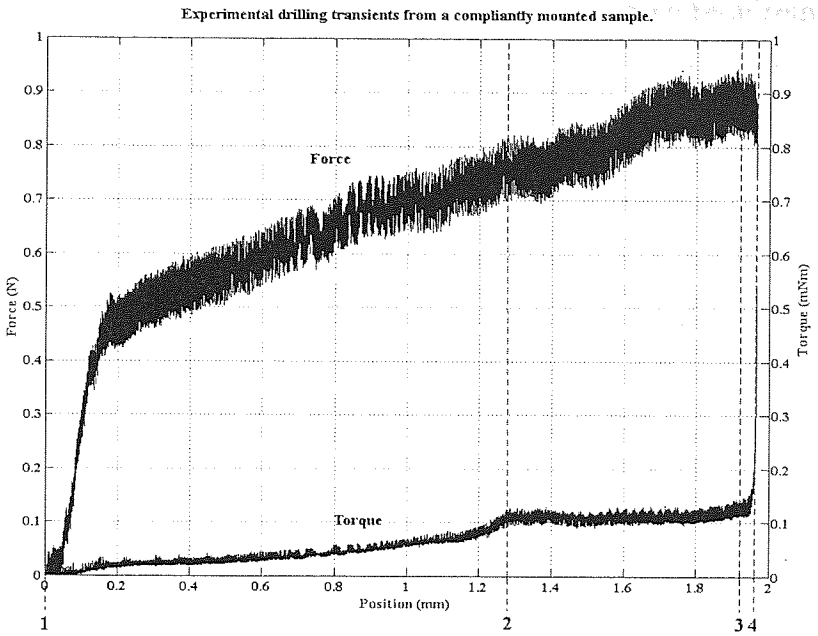

Figure 2.2: *Experimental force and torque transients.*

directly proportional to the displacement and thus obeys Hookes Law 2.1 (36) until the cutting threshold is reached.

$$F_x = kx \tag{2.1}$$

Where k is the tissue stiffness and x is the feed displacement.
The torque is proportional to the feed force and the surface area of the burr in contact with the material. As such the torque begins to rise steadily once cutting has begun and the feed force obeys equation 2.2.

$$F_x = k(x - x_h) \tag{2.2}$$

Where F_x is the linear force, k is an approximation of the bone stiffness, x is the linear displacement and x_d the hole depth.
In this configuration, it can be seen the force required to begin cutting is approximately 0.4 N. Thus, when drilling compliant tissue it is necessary that the

stiffness of the tissue is sufficient to meet the minimum force requirements without excessive deflection or deformation of the tissue. It should be noted that this is application dependent.

The next stage *(Stage 2 in figures 2.1 and 2.2)* occurs when the burr has drilled a hole to a depth equal to the radius of the burr. At this point the surface area of the cutting face has reached a maximum and the torque levels out and the cutting rate becomes directly proportional to the feed force. If the feed rate equals the cutting rate, this is termed as 'Equilibrium Drilling' and the force and torque remain constant until the onset of breakthrough.

This is unlikely to occur when using a constant feed rate control strategy *(feed strategies are discussed in section 2.3.2)* as the cutting rate is directly proportional to the feed force, thus the force required to reach equilibrium would exceed acceptable limits for use in any surgical application. For example, in the stapedotomy procedure described in section 5.3.2, the maximum feed force should not exceed 0.7 N as this would cause excessive deflection of target tissue increasing the risk of further damage.

For this reason equilibrium drilling is not shown in figure 2.1 and it does not occur in 2.2, hence there are only four stages depicted. In most cases the cutting rate is lower than the feed rate and as the force increases, so does the cutting rate resulting in a reduction in both the force and torque gradients. However this is not the case with constant feed force drilling, in actual fact the process of constant feed force drilling can be said to be entirely 'Equilibrium Drilling'.

Stage 4 *(Stage 3 in figures 2.1 and 2.2)* indicates the onset of breakthrough. As the burr approaches the medial surface the thinning of the material ahead of the burr causes local deformation resulting in a force drop and corresponding increase in the torque. The torque responds to an increase in the cutting rate as the surface area of the burr in contact with tissue begins to reduce. Due to the high force level and the reducing area over which the force is acting the cutting rate increases rapidly causing a further increase in the torque and a corresponding drop in force.

This is clearly shown between stages 3 and 4 in figure 2.2, stage 4 being when the hole is complete.

It is worth noting that these stages may not occur in this order, if at all, depending on the conditions at the tool tip. For example, if the tissue thickness is less than the radius of the burr then it will not be possible to reach stage 2.

2.2.2 Mathematical Model

In order to analyse and interpret the drilling transients in order to anticipate events during the drilling process it is necessary to understand the relationship between the force, torque and other associated drilling parameters such as the linear and rotational velocities.

Having identified the key stages of the drilling process a model can be used to further characterise the drilling transients to better understand their relationship to one another. A model can also provide a basis to which real-time data can be compared such that the current state of the drilling process can be deduced and the subsequent stages predicted.

The rate at which a drill bit progresses through the bone tissue is dependent upon factors such as the drill rotational velocity ω, cutting efficiency represented by the cutting coefficient γ, a coulomb friction coefficient β, and the feed force F_x. A model combining these factors was demonstrated by Brett *et al* (38) to provide an accurate representation of the drilling characteristics in compliant tissue when using a constant feed rate $\dot{x}$, and low shaft speeds in the order of 2 Hz. The relationships are given by equations 2.3 and 2.5.

$$\frac{\delta F_x}{\delta t} = \left(1 - \frac{2F_x\omega\gamma}{\pi R\dot{x}}\right) \frac{1}{(\sin 2\theta_2 - \sin 2\theta_1) + 2(\theta_2 - \theta_1)} \tag{2.3}$$

$$F_x = \left(\frac{\pi R\dot{x}_h}{2\omega\gamma}\right) [2(\theta_2 - \theta_1) + \sin 2\theta_2 - \sin 2\theta_1] \tag{2.4}$$

$$T_x = \beta R F_x \frac{[\cos 2\theta_1 - \cos \theta_1]}{[2(\theta_2 - \theta_1) + \sin 2\theta_2 - \sin 2\theta_1]} \tag{2.5}$$

It should be noted that the displacement x_h is the current hole depth, x is the drill displacement relative to the start position x_0 and x_d is the deflection of the surface. x_h is related to the feed force and the feed rate by equation 2.6, where k is an approximation of the material stiffness. θ_1 and θ_2 give the angles subtended from the axial centre of the burr along the drill axis to the intersection of the orthogonal plane of the tissue interfaces each side of the material being drilled as shown in figure 2.1.

$$\frac{dx_h}{dt} = \frac{dx}{dt} - \frac{d}{dt}\left(\frac{F_x}{k}\right) \tag{2.6}$$

The model so far is based on constant feed rate drilling, an equivalent model for constant feed force rather than constant feed rate is given by equation 2.7. The relationships between the force and torque as shown in equation 2.5 and the force and hole depth given by equation 2.6 remains the same. Although the relationship between force and torque is unchanged, the torque-displacement transients will differ due to the different force-displacement characteristic.

$$\frac{\delta x_h}{\delta t} = F_x \left(\frac{2\omega\gamma}{\pi R}\right) \frac{1}{(\sin 2\theta_2 - sin2\theta_1) + 2(\theta_2 - \theta_1)} \tag{2.7}$$

The model demonstrates that the the torque is directly proportional to the feed force, assuming the drilling axis is orthogonal to the target tissue, and that it is a function of the surface area of the burr in contact with the tissue and the rotational velocity of the burr. To validate the model it can be numerically evaluated and compared against real data.

Table 2.1: *Drilling model parameters.*

Parameter	Value	Units
ω	25	Hz
R	0.6	mm
$\dot{x}$	0.01	mm/s
γ	$0.1\text{x}10^{-9}$	m^2N
β	0.60	rad
x_t	1.0	mm
k	2000	Nm

2.2.3 Evaluating the Model

In order to evaluate the model it is necessary to determine values for parameters such as ω, γ, β and k. The material stiffness k can be easily calculated using Hookes law (36) by deflecting the target tissue a known distance and measuring the resulting force. The stiffness can then be calculated using equation 2.1. Although this model was originally developed for low shaft speeds it can be equally applied for higher velocities, in this instance 25 Hz was used.

Due to the unpredictable nature of human bone structure it is not possible to measure values for γ and β, as such γ, β were empirically determined using the drilling characteristics of compliantly mounted porcine cochlear. The parameters used for the evaluation of the model are shown in table 2.1.

The values of θ_1, θ_2 and F_x are numerically determined inside the model as a function of the burr displacement.

2.2.4 Simulation Results

Figure 2.3 shows the drill bit feed force and torque plotted as a function of displacement when drilling with constant feed rate. These results are derived by numerically integrating equation 2.3 and evaluating equation 2.5.

The force and torque transients clearly show the key stages in the drilling process discussed in section 2.2.1, demonstrating that the model incorporates the principle mechanics taking place. The point at which the hole depth is equal to the burr radius can be seen at position 1 at approximately 1.05 mm and is

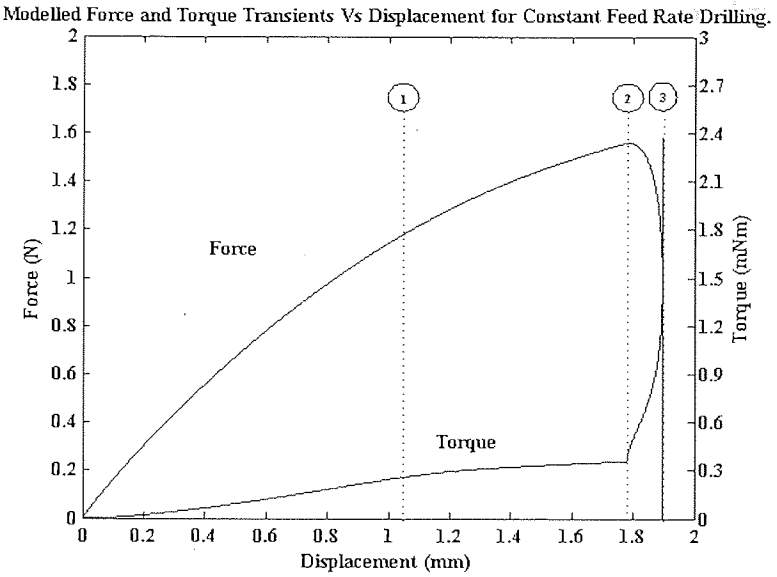

Figure 2.3: *Simulated drilling transients using a constant feed rate.*

indicated by an observable change in gradient of the torque transient. The onset of breakthrough occurs at position 2 at approximately 1.78 *mm* resulting in the sharp increase and subsequent roll off of the force signal. The hole was completed at position 3 at approximately 1.90 *mm*, shown by the force and torque dropping to zero. If drilling is stopped instantly as the force and torque reach zero *(position 3)*, the tip of the drill bit would have penetrated approximately 0.92 *mm* further beyond the far surface than is necessary to complete the hole due to the material returning to its neutral position.

It can be observed that the compliance of the material manifests itself in two ways:

- equilibrium drilling conditions are never reached even though the drill bit radius is less than the material thickness.
- due to the deflection of the material the drill displacement exceeds the thickness of the material and the burr radius combined.

In light of this, a technique to control penetration through the tissue will be required to compensate for this displacement by referencing to the deforming

tissue rather than to the absolute value of the drill position in order to maintain accuracy and precision.

2.3 Controlled Compliant Drilling Technique

Having identified the key stages in the drilling process and characterised the drilling transients using the mathematical model it is possible to develop a technique for controlling the drill penetration through compliant tissue. There are three phases to which a specific control strategy has to be applied:

- start of drilling to the onset of breakthrough;
- breakthrough detection and control;
- and hole completion.

Before drilling can commence the burr must be registered to the target by finding the surface and positiong the drill a known distance from it. As soon as drilling commences this reference is lost due to tissue deflection, but once the drill is re-referenced later in the drilling process this is an important datum.

The first phase begins when drilling is initiated and is termed Investigative drilling. This phase employs the drill feed control strategy that governs the way in which the drill advances forward. This can be done in one of two ways, firstly constant feed rate in which the actuator advances at a fixed velocity for the duration of the drilling process. The second is constant feed force, this is where the displacement of the actuator is governed by the force at the drill tip. The system aims to maintain the force at a predefined level by advancing the drill forward proportionally. The drill proceeds, interrogating the drilling transients looking for signs of the onset of breakthrough.

The aim of the breakthrough detection is to identify the initial stages of breakthrough by identifying characteristics in the drilling transients; this can be done by looking at one or both of the sensor signals.

The second phase is initiated when the first signs of breakthrough are detected. The breakthrough process has to be controlled and be prevented from progressing in order to reach the final phase.

The final phase is the hole completion. At the beginning of this phase the burr is positioned on the medial surface of the tissue. The control strategy for this stage aims to complete the hole to the full radius of the burr while achieving the minimum protrusion possible, in the case of a spherical cutting burr this is equal to the burr radius.

2.3.1 Target Registration

Initial registration can be a relatively simple process as long as the assumptions described in section 2.2 are met. With drill rotation disabled, the drill unit can be advanced slowly until contact with the surface is detected by looking at the force magnitude and gradient. Once detected the drill can be retracted until the force is zero, at which point the burr can be considered to be positioned on the surface of the material.

This process can be taken a step further by using the force level achieved through contact and the displacement to return the force to zero combined with equation 2.1 to calculate the stiffness of the target material.

To ensure effective registration the drilling axis must be orthogonal to the target tissue or within an acceptable tolerance. Using the drilling example shown in figure 2.2, the minimum force to begin cutting is approximately 0.4 N. If a maximum drilling angle of 20° is permitted and the nominal feed force is 1.5 N, the axial force component, F_x, equates to 1.4 N and the lateral force component, F_y, equates to 0.4 N. While this itself may result in a small degree of lateral deformation of the tissue, it is at the threshold for cutting and thus will result in minimal deviation of the burr from the desired trajectory. As such, the registration method and the predictive model remain effective if the drilling axis is within 20° of the axis orthogonal to the target tissue.

2.3.1.1 Stiffness Estimation

When considered a static system, a compliantly mounted sample can be approximated by Hooke's Law. However, when under dynamic conditions the material's behavior can be approximated to a mass-spring-damper system. For this reason measuring the stiffness by advancing until contact is achieved and then measuring the force may provide an inaccurate measurement of the material stiffness.

The force exerted against a mass-spring-damper system is given by equation 2.8.

$$F_x = kx + c\dot{x} \tag{2.8}$$

Where F_x is the axial force, k the stiffness, x is the feed displacement, c is the damping constant and $\dot{x}$ is the feed rate.

To measure the true static stiffness the drill feed must be stationary long enough for the force to settle to a steady state or the velocity has to be sufficiently low to minimize the $c\dot{x}$ term.

As such, a typical strategy for registering the device to the target and measuring the system stiffness is described in figure 2.4.

2.3.2 Feed Control Strategies

The feed control strategies dictate the way in which the linear movement of the drilling system is controlled. The implications of the drill feed control strategies that need to be considered include:

- the effects on the drilling data and therefore the ability to determine the state of the drilling process and detect breakthrough;
- the effects on the ability to control breakthrough;
- the implications for tool safety.

To demonstrate the difference between the control strategies of feed force and feed rate control, equations 2.3 - 2.7 have been plotted in figures 2.5 - 2.13.

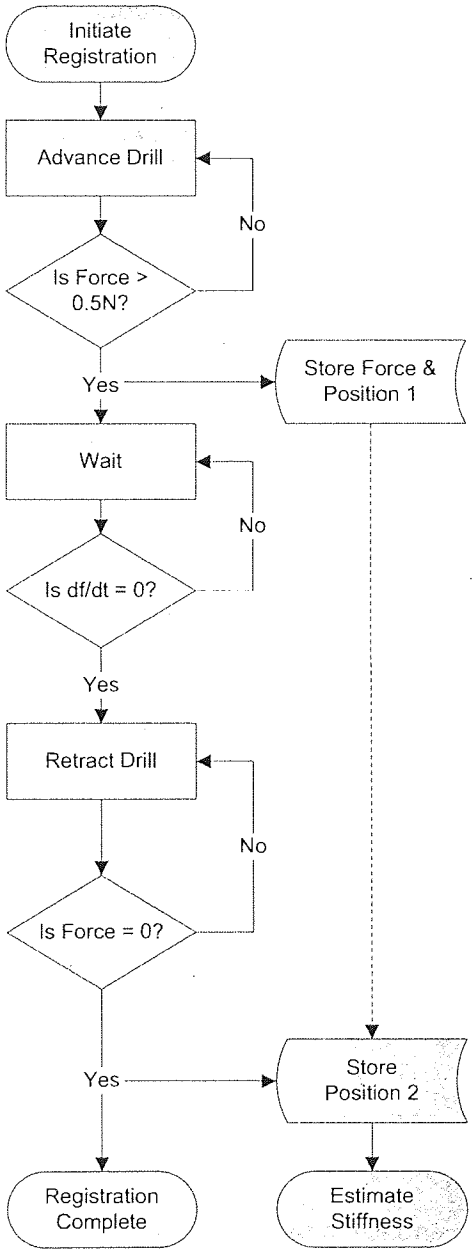

Figure 2.4: *Contact Strategy for device registration.*

2.3.2.1 Constant Feed Rate

Figure 2.5 shows the drilling transients when using a constant feed rate control strategy; figures 2.6 and 2.7 show the hole depth versus time and feed/cutting rate versus time respectively.

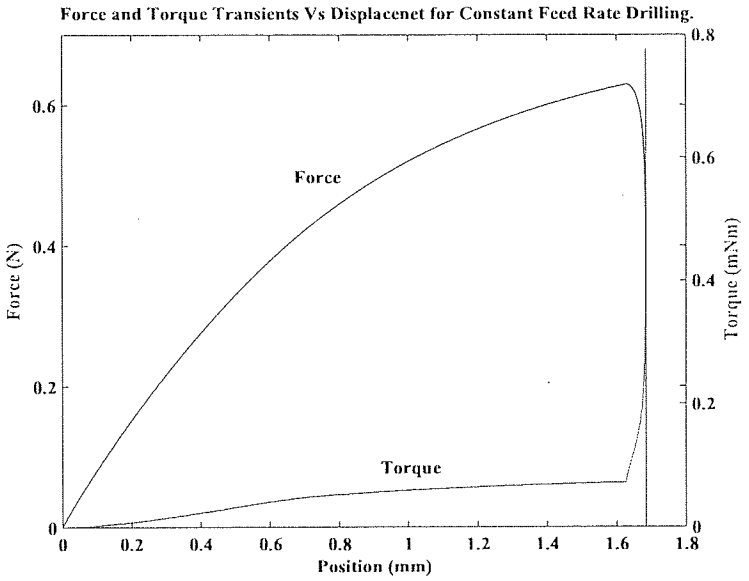

Figure 2.5: *Simulated drilling transients using a constant feed rate.*

To this point all the discussion around the drilling characteristics has described the use of the constant feed rate control strategy thus the characteristics will not be explained again, rather they will be used as a model against which alternative strategies can be compared.

2.3.2.2 Constant Feed Force

The constant feed force control strategy will not be considered for implementation in the clinical device due to the safety implications that may arise as a result of sudden changes in feed acceleration that may occur in the event of a drop in the feed force. The strategy is discussed in this section primarily to highlight some of the benefits such a strategy could provide over that of a constant feed rate strategy.

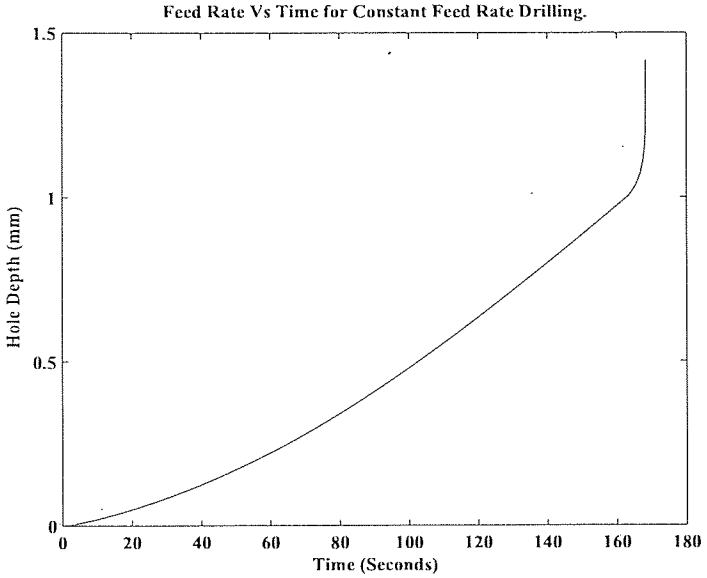

Figure 2.6: *Simulated hole depth using a constant feed rate.*

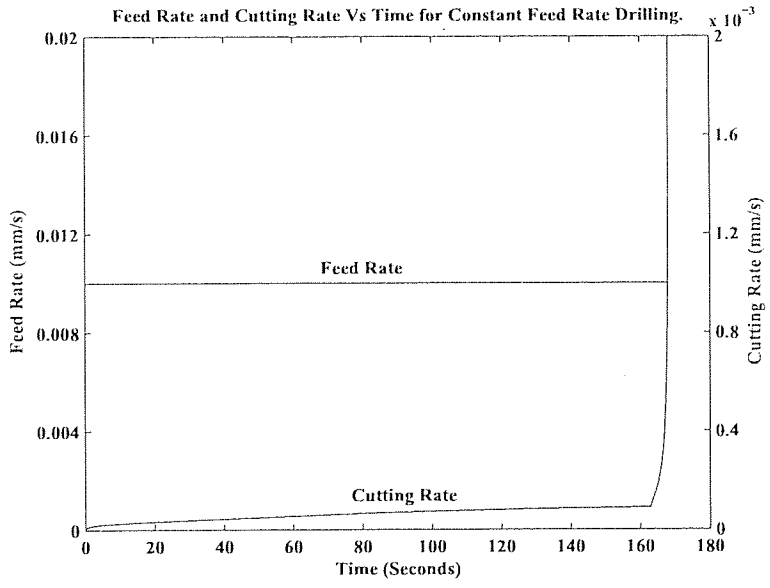

Figure 2.7: *Simulated feed and cutting rate using a constant feed rate.*

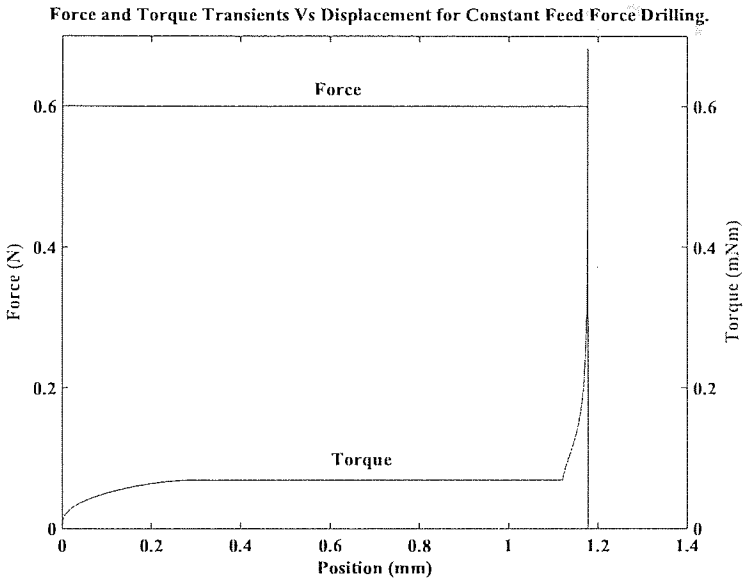

Figure 2.8: *Simulated drilling transients using a constant feed force control strategy.*

Figure 2.8 shows that when using a constant feed force control strategy there are similar variations in torque to the of constant feed rate. However, the gradient up to the point when the hole depth is equal to the burr radius (the equilibrium drilling point) falls to zero and then remains zero until the onset of breakthrough occurs. The feed rate has to remain equal to the cutting rate in order to keep the force constant for the duration of the drilling process. This is not the case when using a constant feed rate strategy as the continual advancement of the drill increases the force and thus the torque. The force transients of figures 2.5 and 2.8 are noticeably different in that the force profile for a constant feed force is simply a reference signal and conveys no information about the state of drilling process. Instead, the rate of feed displacement plotted as a function of time can be used to convey information on the progress of drilling as shown in 2.9.

The rising feed rate after a period of falling or steady feed rate indicates breakthrough. The feed rate profile for constant feed force drilling is similar to an inverted version of the constant feed rate force profile shown in figure 2.5 and therefore conveys similar information.

In terms of automatically characterising the drilling process from sensory data,

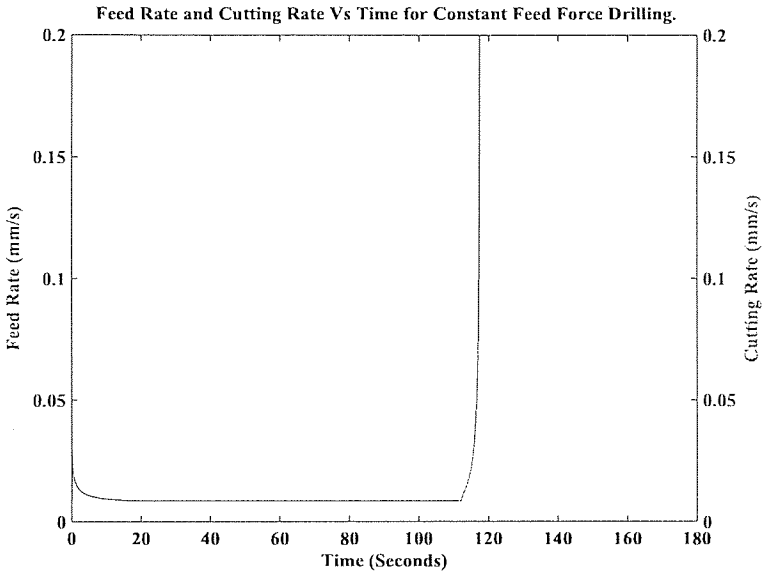

Figure 2.9: *Simulated feed rate and cutting rate using a constant feed force.*

the same information can be extracted from both feed strategies. In the drilling process, such information can be used to change the control strategy to maximise either performance or safety. With regard to these aspects one is led to investigate the rate of progress during drilling. Figures 2.6 and 2.10 show the transients of drilled-hole depth for constant feed rate and feed force control strategies respectively.

In both examples, the results show that hole depth increases rapidly on the approach to drill bit breakthrough. The shorter drilling time under the constant feed force strategy provides obvious advantages by achieving the drilling process more quickly and limiting the force exerted on the target. Set against this is the sharp feed acceleration as breakthrough starts as this reduces the time available for detecting the onset of breakthrough and raises the question of safety of a force control strategy (50) in this application. At the same time when drilling tissue of unknown stiffness using a constant feed rate strategy it is possible to apply excessive force due to insufficient compliance in the material. Given the advantages and disadvantages of the two control strategies what is clearly the most desirable solution is a hybrid strategy that combines the advantages of both

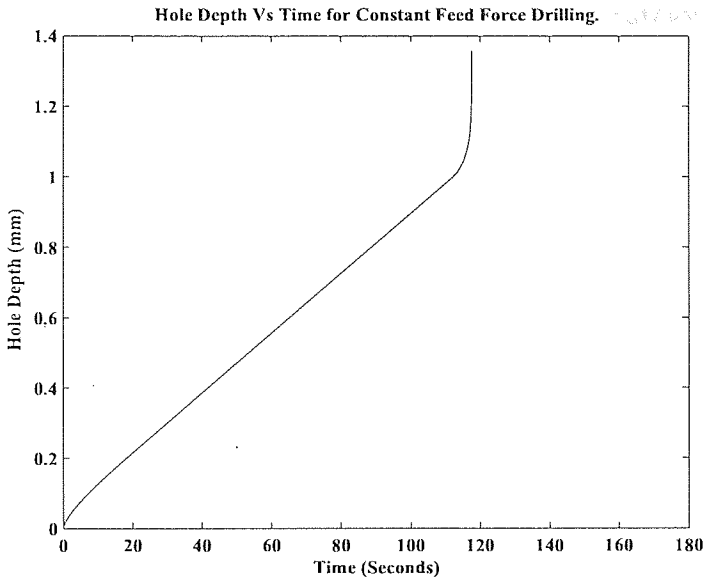

Figure 2.10: *Simulated hole depth using a constant feed force.*

and reduces the risk. This can be achieved by implementing a hybrid control strategy.

2.3.2.3 Force Limited Feed Rate

This strategy begins as a constant feed rate strategy with a maximum force setting. If this threshold is never reached the control strategy will remain that of the constant feed rate, however if the force limit is exceeded the constant feed force strategy is initiated with a fixed rather than proportional feed acceleration in the direction patient. This removes the risk of sharp feed acceleration should the feed force drop or breakthrough occur. The force limitation allows the use of higher feed rates without the risk of exerting too greater force and significantly reduces the drilling time.

Figures 2.11, 2.12 and 2.13 show simulated results using a hybrid control strategy. Comparing figures 2.11, 2.8 and 2.5 is can be seen that figure 2.11 shares the desirable features of both control strategies. The drill time is considerably shorter that of the constant feed rate control, yet the force is limited to a max-

imum of $0.7N$ as it would be in a constant feed force strategy. The combined strategies also reduce the rate at which breakthrough progresses retaining the sharp roll-off you would expect in the constant feed rate force transient, as do the other transients (See figures 2.12 and 2.13). This increases the amount of data available to accurately detect breakthrough.

As a further implication, figures 2.6 and 2.10 illustrate a significant problem when drilling manually in critical or delicate situations. As the target surface is reached and breakthrough starts to occur, breakthrough advances rapidly. The fast and accurate response required to avoid excessive penetration of the tool point is typically beyond that achievable by human response to tactile stimulus (40). Therefore an automated tool action is most appropriate for controlling breakthrough in these applications.

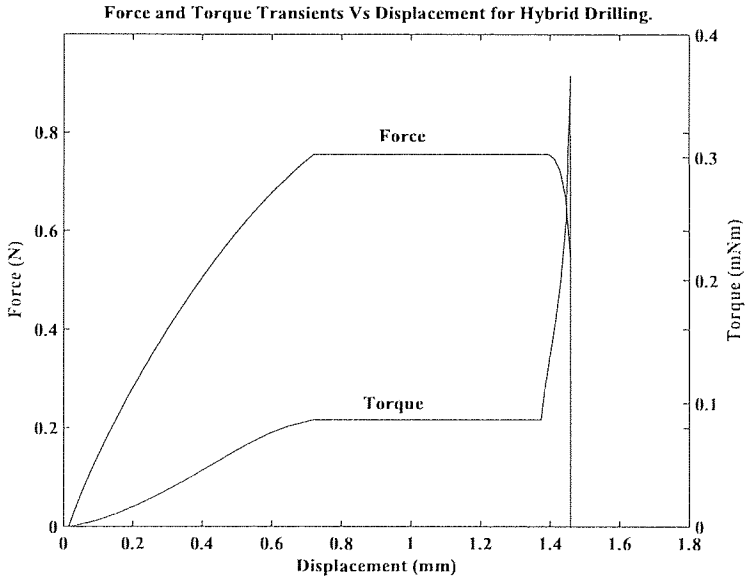

Figure 2.11: *Simulated drilling transients using a hybrid control strategy.*

2.3.3 Breakthrough Detection

The start of breakthrough and its identification are key to controlling the drilling process. The local deformation of the thinning tissue ahead of the cutting burr

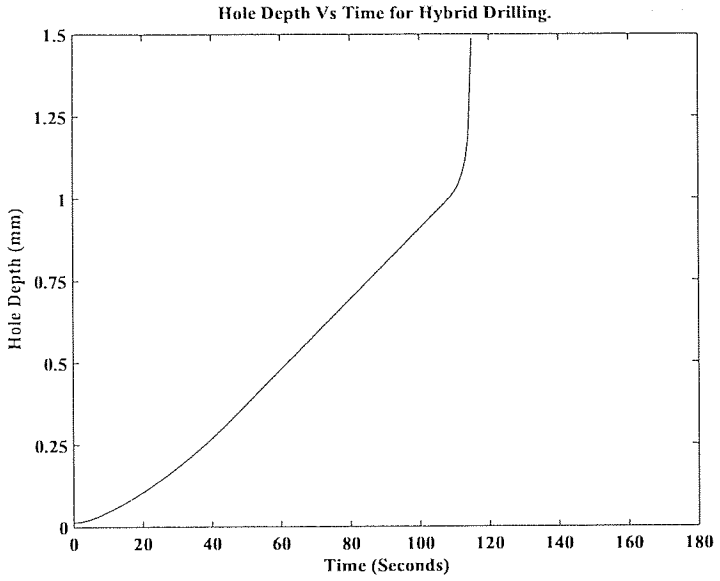

Figure 2.12: *Simulated hole depth using a hybrid control strategy.*

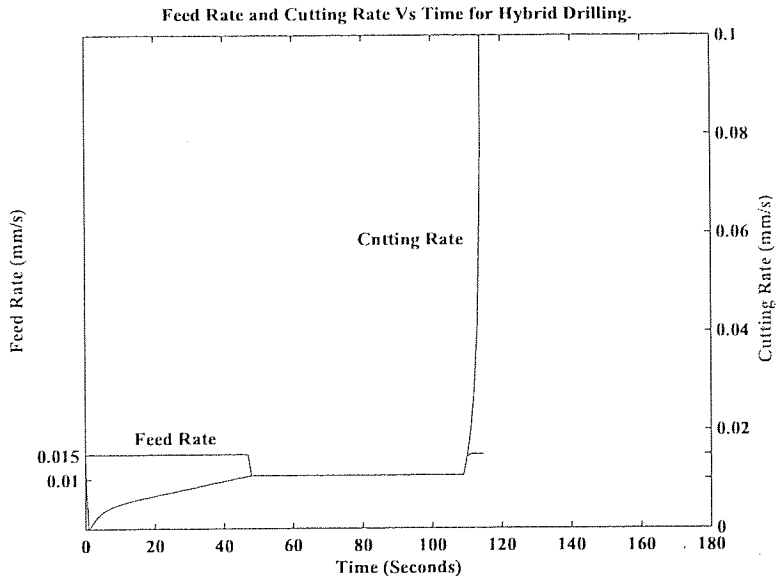

Figure 2.13: *Simulated feed rate and cutting rate using a hybrid control strategy.*

results in a drop in the axial force. The reducing contact area causes an increase in torque and accelerating cutting rate. It is these events that generate the characteristic breakthrough transients. The start of breakthrough determines the location of the far surface of the drilled material and thus, the amount the material has deflected and its thickness. This is an important reference point as the drill is advancing into the unknown region where sensitive structure may lie. Furthermore it is breakthrough that presents the challenge in terms of controlling the drill bit penetration. The presence of compliance results in the deflection of the drilled material under the action of the tool as such at the point of breakthrough the material starts to return to its neutral position. If the completion of breakthrough occurs and the material is allowed to return to its neutral position uncontrolled, the protrusion of the burr will be significantly higher than necessary to complete the hole. This can be complicated further if too high a force is exerted, breakthrough can be drastically accelerated, potentially leaving the drill bit protruding dangerously beyond the far surface.

The system employs dynamic breakthrough control by analysing the drilling transients in real-time looking for indications of breakthrough. Having explored the characteristic transients of compliant drilling, neglecting noise, it is true to say that the only circumstances under which the gradients of the force and torque undergo significant change is when the onset of breakthrough occurs as shown in figure 2.14.

The simplest method of breakthrough detection is to simply apply a threshold to the force and torque magnitude. In theory this is sufficient to differentiate between normal drilling and the breakthrough condition, however, this is not the case in practice for several reasons:

- as the force drops as breakthrough occurs it will already be below the threshold, making the detection essentially based on a single variable; Torque.
- Each drilling profile is unique, requiring different thresholds.
- When drilling in a noisy environment, rapid fluctuations cause false positive results;
- tissue inconsistencies result in addition noise that may be misinterpreted.

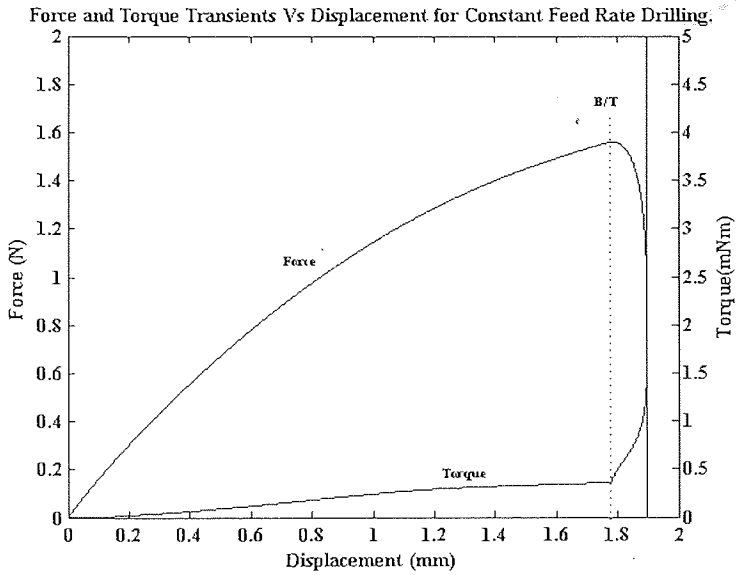

Figure 2.14: *Simulated drilling transients.*

What is required is a method independent of the force and torque magnitude to make it universally applicable. The method must also be able to discriminate between breakthrough and environmental noise such as electro-magnetic interference, target movement and target displacement.

The next logical step would be to incorporate the rates of change of the drilling transients and apply thresholds to the magnitude of gradient.

2.3.3.1 Gradient Method

The gradient method, again is a simple method of breakthrough detection. The gradients of the drilling transients shown in figure 2.14 are shown in figure 2.15.

The point at which breakthrough begins is denoted as B/T. By inspection it can be seen that the gradients change rapidly, in opposing directions. For constant feed rate drilling the force gradient should not be less than zero until the onset of breakthrough occurs. If thresholds are applied such that *(Referring to figure 2.15)* if the torque gradient, $\frac{dT}{dx}$ and the force gradient, $\frac{dF}{dx}$ satisfy the criteria shown in equation 2.9. In this instance typical values would be $T_{lim} = 0$

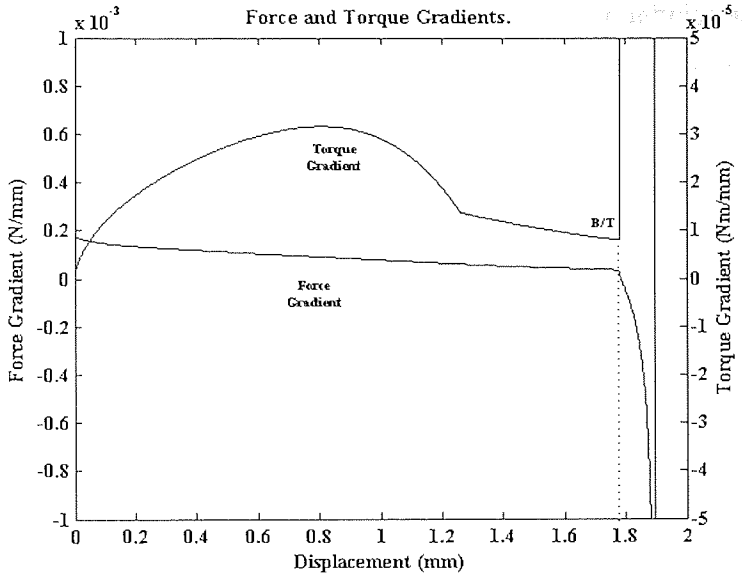

Figure 2.15: *Simulated Force and Torque Gradients.*

and $F_{lim} = 4 \times 10^{-5}$.

$$\frac{dF}{dx} < F_{lim} \quad AND \quad \frac{dT}{dx} > T_{lim} \tag{2.9}$$

Although this method is effective at identifying the breakthrough condition it suffers from a high false positive detection rate. This is primarily due to the effect of noise. In order to detect breakthrough as promptly as possible the magnitude of the force threshold is required to be as close to zero as possible. If the drill system was disturbed during the drilling process, for example the target was knocked, this would result in a sharp rise in the force as the target moves toward the drill and a corresponding spike in the torque transient. However as the target returns to it previous position there is a corresponding drop in the force. This may be falsely interpreted as the breakthrough condition.

The false detection rate can be reduced by increasing the thresholds however there is a trade off between sensitivity and detection delay. It may be further reduced by incorporating the rate of change of the gradients into the breakthrough criteria shown in equation 2.9. This provides four potential parameters that indi-

cate the state of the drilling process. This is particularly beneficial as fluctuations in the force and torque resulting from environmental noise or disturbance are in phase, the only conditions that result in the transient becoming out of phase are those that result from the breakthrough condition. The second differential provides a magnitude and direction of the force and torque signal and as such can be used to determine the rate and direction at which the threshold is being crossed. The new detection criteria is represented by equation 2.10.

$$\frac{dF}{dx} < F_{lim} \quad AND \quad \frac{dT}{dx} > T_{lim} \quad AND \quad \frac{d^2F}{dx^2} < 0 \quad AND \quad \frac{d^2T}{dx^2} > 0 \qquad (2.10)$$

The 3^{rd} and 4^{th} terms of equation 2.10 allow the system to differentiate between movement of the target and the breakthrough condition.

The use of filtering of the reference signal can further improve the false positive detection rate; however, the smoothing effect of the filter can delay breakthrough detection sufficiently to effect the accuracy of the technique.

Although the magnitude of the thresholds are more widely applicable than those of the force and torque alone, they are still absolute values and as such the same parameters may not be effective in all cases. What may be more effective is a threshold that is proportional to the amplitude of the signal.

2.3.3.2 Difference Method

The difference method builds on the gradient method described in the previous section. This approach is similar to that of the gradient method in that it looks primarily at the rate of change of the drilling transients, however it uses historical data in order to improve noise resistance. The algorithm looks at the variation between the current sample n, and the i^{th} sample typically 10 samples prior. This preferentially looks at low frequency changes, reducing the effect of high frequency fluctuations typically induced by environmental disturbance. Equations 2.11 and 2.12 are the force and torque difference functions.

$$\Delta F = (F_n - F_i)^3 \qquad (2.11)$$

$$\Delta T = (T_n - T_i)^3 \quad (2.12)$$

Where ΔF and ΔT represent the rate of change, F and T represent the force and torque when n is the current sample and $i = n - 10$. The cubed term is applied to retain the sign of the relative difference so the direction of the signal can be determined. This also makes the thresholds applied more sensitive to large, low frequency changes in the reference transients as low differences are effectively attenuated and larger changes are amplified. This allows the thresholds to be set lower making them more universally applicable.

The thresholds can be applied in the same manner described in the gradient method as shown in equation 2.13

$$\Delta F < F_{lim} \quad AND \quad \Delta T > T_{lim} \quad (2.13)$$

The same second derivative terms can also be applied to determine the magnitude and direction of the change.

This method takes the first steps to being truly independent of the magnitude of the reference signal and addresses the issue of high frequency noise. Although the false positive detection rate is lower than that of the gradient method it is still higher, typically 20%, than would be acceptable when deploying a technique such as this in the operating theatre. A more robust technique is desirable.

2.3.3.3 Mean Deviation Method

As noise in the operating theatre is unavoidable, particularly as clamping the patient down in any way is undesirable, a statistical approach can be used to reduce the effect of noise on the breakthrough detection. The use of averaging to create a baseline to which the reference signal can be compared reduces the need for filtering and improves detection performance.This method functions by comparing the variance of the current reference transient value with the mean of the n previous samples of the parent signal. This provides an approximate magnitude that represents the rate of change of the parent signal negating notice. Applying

the same technique again to the magnitude signal gives an approximation of the rate and direction of this variance.

The use of the mean of the previous n samples combined with a small degree of signal conditioning effectively eliminates the effect of rapid changes in the sensor transients. This method also increases the sensitivity of the detection method to low frequency fluctuations as the deviance from the mean is greater and more truly representative than that from prior samples. As such, large changes in the rate of change of the parent signal are magnified and small fluctuations as a result of noise are ignored. This not only allows the system to detect breakthrough, it enables it to differentiate between different types of contact that the drill may encounter, for example:

- target moving away from the drill;
- target moving toward the drill;
- drill crossing a tissue interface;
- drill crossing into free space;
- and the breakthrough condition.

The force and torque transient mean deviation magnitudes and rates of change are calculated using equations 2.14, 2.16, 2.14 and 2.17 respectively.

$$F_n^{'} = \bar{F}_n - \left(\frac{1}{n} \sum_{i=n-j}^{n} \bar{F}_i \right) \tag{2.14}$$

$$F_n^{''} = F_n^{'} - F_{n-1}^{'} \tag{2.15}$$

$$T_n^{'} = \bar{T}_n - \left(\frac{1}{n} \sum_{i=n-j}^{n} \bar{T}_i \right) \tag{2.16}$$

$$T_n'' = T_n' - T_{n-1}' \tag{2.17}$$

Where $\bar{F}$ and $\bar{F}$ are the filtered reference signals, F' and T' are the force and torque mean deviation magnitudes and F'' and T'' are the rate of change of the mean deviation magnitudes.

The start of breakthrough is detected when both of the following criteria are satisfied (Equations 2.18 and 2.19):

$$F_n' < F_{lim} \quad AND \quad F_n'' \leq 0 \tag{2.18}$$

$$T_n' > T_{lim} \quad AND \quad T_n'' \geq 0 \tag{2.19}$$

Where F_{lim} and T_{lim} are predetermined force and torque mean deviation thresholds based on the applications desired hole depth, minimum level of protrusion and the material properties. These values are empirically determined using laboratory results, this is discussed in more detail in section 7.3.1.

The primary conditions are $F_n' < F_{lim}$ and $T_n' > T_{lim}$. These terms indicate when the gradient of the force torque data exceeds a predefined value, i.e. it aims to identify the start of the rising torque feature that occurs at the start of breakthrough. Since there are fluctuations that can have similar characteristics to the breakthrough characteristics in both the force and the torque transients, using the force or torque alone would frequently result in premature *(false positive)* breakthrough detection. The use of the two signals combined drastically reduces the false positive detection rate to less than 10% using nominal thresholds *(refer to section 7.3)*. As breakthrough is approached the force mean deviation will tend to zero and then rapidly swing negative, satisfying the force criteria. This holds true for the torque mean deviation as this will also tend to zero as breakthrough is approached, it will then rapidly swing positive satisfying the torque criteria.

The $F_n'' \leq 0$ and $T_n'' \geq 0$ conditions are based on the fact that the force gradient reduces sharply and the torque gradient increases sharply following the onset of breakthrough. $F_n'' \leq 0$ is true and $T_n'' \geq 0$ is false from shortly after the start of drilling due to the slight decrease in gradient of both transients during drilling up to the start of breakthrough. These two conditions do not play a part in breakthrough detection as such, rather they are included to eliminate the occurrence of false positive detections and differentiate between alternative types of features that may be present. This means that if the force continues to rise for a short period after the start of breakthrough (e.g. if equilibrium drilling was not reached prior to the start of breakthrough) this condition does not delay the detection of breakthrough as identified by the $F_n'' \leq 0$ condition, as even though the force is increasing it will be at a falling rate such that the rate of change will be negative. Similar is true for the torque condition $T_n'' \geq 0$, if the torque increase is delayed for any reason and the signal falls, but at a reducing rate the torque condition will still be satisfied. This has the effect of reducing the likelihood of false positive breakthrough detection as opposite fluctuations such as this *(force decreasing and torque increasing)* in the force and torque data sets rarely coincide sufficiently to satisfy both conditions. For example, if the target was to move away from the drill, whether it be due to compliance or the sample physically moving backwards, both the force and torque would fall rapidly. However if the motion was to suddenly stop the torque would spike as the drill begins cutting again, the resulting jolt in the force would also produce a spike in the gradient which could be interpreted as breakthrough as both thresholds would be satisfied. However, the direction in which the thresholds would be crossed is opposite to that of breakthrough, so by taking into account the direction in which the transient is traveling it is possible to eliminate most false positive detections.

Once breakthrough has been detected it is necessary to control the remainder of the drilling process to prevent the drill protruding beyond the medial surface.

2.3.4 Breakthrough Control

At the point at which breakthrough is detected the burr is positioned on, or fractionally past the medial surface. The system can self-reference to the deflected tissue and thus has precise control over the remainder of the drilling sequence allowing hole completion to a high degree of accuracy and precision.

Having detected breakthrough it is necessary to cease drill feed and rotation as there is little tissue remaining ahead of the burr. This thin tissue will be partially deformed as a result of the concentration of the axial force due to the reduced surface area. It is for this reason that the cutting rate accelerates as breakthrough progresses resulting in the unique drilling characteristic described previously.

As well as ceasing drill rotation the drill must be retracted as quickly as safely possible to reduce the force concentration at the tip of the burr. This process must be executed immediately to prevent the burr deforming the tissue and protruding beyond the far surface.

At this point it is possible to calculate the thickness of the material being drilled. This can be done in one of two ways:

1. If the stiffness of the material is known the thickness can be calculated directly from the displacement at the point at which breakthrough was detected by rearranging equation 2.2.

2. The thickness can be measured directly by retracting drill until the force reaches zero, at which point the material will have returned to its neutral position. The thickness of the material is then calculated by subtracting the start position from the position at which breakthrough was detected.

Other parameters such as the cutting rate, hole depth, material thickness and stiffness can also be calculated.

Given that the system now has a precise reference position and all the associated drill parameters are known or can be calculated. These parameters can be used to model the tissue behavior for the remainder of the drilling process and adapt the drill control sequence to compensate during the hole completion.

2.3.5 Hole Completion

If required, the drilled hole can be completed to its full diameter and drill depth. The hole completion is perhaps the most precise part of the drilling process. Once the system has self-referenced to the deformed tissue and the drill has retracted the location of all interfaces relative to the drill tip are known. Using this information and the parameters determined at breakthrough the control parameters can be calculated. There are two possible methods that can be used to complete the hole.

1. Displacement Controlled Completion.
2. Force Controlled Completion

2.3.5.1 Displacement Controlled

Displacement controlled hole completion uses the absolute position of the drill unit and the reference points generated by the breakthrough detection algorithm. Using these it is possible to calculate, quite accurately, the location of the tissue interfaces and relative target positions for the drill.

After breakthrough is detected the drill is retracted until the axial force on the burr is approximately zero, the assumption is then made that the burr is positioned such that the cutting face is in contact with the remaining tissue at the base of the hole when the tissue has returned to its neutral position. Once this has been achieved the burr can be advanced forward a single burr radius to complete the hole to the full radius of the burr, alternatively this method allows a partial diameter hole to be drilled so that the full thickness of the tissue is not penetrated. In cases where a full diameter is desired the drilling process is very similar to the investigative drilling stage described earlier in this chapter. Drill rotation and feed are initiated and the burr advanced at a constant feed rate until the target position, the reference position plus the burr radius, is reached. During this process it is expected that a characteristic similar to that of the breakthrough characteristic will be generated, all be it at a lower amplitude due to the lower forces involved. If for any reason the breakthrough condition does not occur prior

to the drill reaching its target position, drill rotation is continued after the drill feed has ceased or until the feed force reaches zero. At this point the hole can be assumed to be complete and drilling can be stopped.

This method should provide the highest degree of accuracy given that once the onset of breakthrough has been detected the position of the medial interface is known to within a few microns depending on how quickly it was detected. The largest potential source of error occurs when the drill is retracted to find the neutral position of the tissue. The method works on the assumption that the drill is perpendicular to a planar surface and there is no side load on the burr. In cases where this is not true, the axial force will have both an F_x and although small, an F_y component. The drill operates along a single tool axis, as such the drill feed is in the x direction and can be considered to be rigid when a force is applied along this axis. In practice a side load results in a small deflection in the drill shaft so when the drill is retracted to find the neutral position of the tissue it has to be retracted further for the resultant force to fall to zero resulting in an error in the reference positions.

This can be compensated for by adjusting the trajectory of, and re-registering the drill to the surface of the tissue after breakthrough has been detected and drilling ceased, completion can then be commenced without complication. This has the added benefit that the drill can be retracted for inspection before the hole is completed without affecting the remainder of the process. Although this may be useful it would be a manual process requiring intervention by the operator.

Alternatively further force sensors could be integrated into any such system to measure the y component of the force and compensate for any deflection of the drill tip, however this would be a highly complicated solution.

Another possible solution would be the integration of force feedback into the control strategy.

2.3.5.2 Force Controlled

Force controlled hole completion, as the name suggests, uses the feed force to control the hole completion. This method makes the assumption that the target material behavior is entirely elastic and no plastic deformation occurs. The ac-

curacy and precision of this method is governed by the accuracy and precision to which the stiffness of the target tissue can be calculated, making the method used to determine the stiffness particularly important.

Rather than retracting the drill until the force is zero as with the displacement controlled hole completion; the position and force level at breakthrough can be used in conjunction with the tissue stiffness to calculate the position to which the drill must retract so that the force level would be equal to that if the material were deflected by a displacement equal to one burr radius. Once this position has been reached, drilling then commences until the breakthrough characteristic is detected, or the force level reaches zero indicating that the drilling process is complete.

This method does not suffer from the same geometric limitations as discussed when using the displacement controlled hole completion as at higher force levels the F_y component is less significant at small angles.

2.4 Conclusions

The process of drilling a compliant material can be broken down into five key stages and the drilling transients at each of these stages can be characterised and a model applied. By applying the model to real-time drilling data the relationship between the force and torque transients and the displacement can be used to accurately predict the current state of the drilling process.

Using these key points and their relationship with one another it is possible to achieve a high degree of precision when drilling. This lends itself well to micro surgical tasks as a technique for controlling drill penetration through compliant tissues.

The technique, like the compliant drilling model, is broken into a series of phases, each designed to detect a particular phase of the former. The first phase starts with the device registering the drill bit to the surface of the material and estimating the stiffness of the system.

The second phase is called investigative drilling during which the system advances, actively looking at the drilling transients in real-time for indications of

a change of state. Of the feed strategies discussed the force limited feed rate is perhaps the optimum offering the benefits of both the constant feed force and constant feed rate without the risk of applying excessive force.

The detection algorithms are all based on the gradient method in that they are looking for variations in the rate of change of the drilling transients however this method suffers from poor noise immunity resulting in a high false-positive detection rate. Two alternative algorithms were investigated; the difference and the mean deviation methods. The difference method look primarily for large changes in the transients of a period of approximately ten milliseconds, while this method was effective against normal drilling noise it was highly sensitive to disturbance.

The next step was to look at the potential of statistical methods to negate the noise which led to the mean deviation method. This method looked at the deviation of the n^{th} point from the mean of the previous i samples. The net effect of this was to reduce the sensitivity of the system to sudden changes. The inclusion of the second derivatives in the detection criterion meant that both the magnitude and direction of the deviation could be determined. This significantly reduced the false positive detection rate without affecting the detection of the actual breakthrough.

Upon detecting breakthrough the drilling process can be controlled to prevent breakthrough and the final hole completion phase can be initiated. The two methods for hole completion explored were force and displacement control strategies. While in theory the displacement controlled completion provides the most accurate method of hole completion, however, this is not always necessarily the case. The most reliable method is that of the force controlled strategy.

2.4.1 Technical Challenges

In this chapter the theory behind, and the methods employed, by the compliant drilling technique have been discussed in detail, along with the different ways in which they may be applied. As such, a platform must be developed capable of implementing the various stages.

Clinical requirements of any given application aside, at a basic level the primary functions to satisfy the requirements of the compliant drilling technique are as follows:

1. A means of rotating the cutting burr at a given velocity,
2. A means of advancing/retracting the burr to a given position/velocity,
3. A means of measuring position, force and torque at the burr tip,
4. A means of acquiring and analysing the data,
5. A means of programming sequenced control phases.

Obviously, drill rotation and linear actuation are key to the operation of the drilling system, but the use of different strategies across multiple phases also makes control over the velocity and/or position necessary. Previously typical drilling velocities have required rotational speeds as low as 2 Hz and linear velocities as low as 10 μm *per second*. However, to implement some of the strategies described in this chapter rotational velocities up to 25 Hz and linear velocities as high as 5 *mm per second* may be required.

To enable the state of drilling to be determined it is necessary to know the position of, and the force at the tool tip, as well as the torque developed as a result of drilling.

It is estimated that the nominal feed force level for the intended application should be approximately 1 N and should not exceed 2 N. This force level is sufficient to penetrate the target tissue in under the recommended time limit of three minutes without posing any undue risk to the patient through application of excessive force. Thus, a suitable force resolution would be 1 mN.

Using the mathematical model described in section 2.2, the peak torque expected with a nominal feed force of 1 N is in the order of 1 mNm with a nominal drilling torque of 0.1 mNm. As such, an suitable torque resolution would be 1 μNm.

While the system does not need to know the absolute position to detect and control breakthrough, it is required for calculation of both the stiffness and the

thickness of the tissue upon completion of the hole as such and estimated resolution of 1 μm is required.

With the motion and sensor requirements satisfied, a platform on to which the data acquisition and control algorithms can be implemented is needed. This may be computer based or embedded depending on the level of complexity, reliability and safety required; however, the control algorithms should be programmable to allow flexibility.

This represents the key building blocks of a system capable of implementing the compliant drilling technique. Now the system must be customised to meet the requirements of the application at hand.

Chapter 3

Robotics in surgery

3.1 Robotics in Surgery

Over the last two decades robotic surgery has made its mark as a precise means of tool deployment in surgical procedures. The majority of applications have focused on the control of tools on trajectories defined using pre-operative scan data. These pre-determined trajectories are appropriate where tissue movement between scanning and the surgical intervention can be considered insignificant or within acceptable limits. This level of assistance has its value in many procedures, however, more complex tool paths and variations in strategy are required in many other procedures that will benefit from the precise nature of robotic technologies.

To an extent this has been achieved by introducing the clinician into the control loop, where master-slave systems have attempted to harness the decisions on interpretation of state of tool-tissue interaction and the formulation of strategy by the surgeon and the response and accuracy of the robotic device.

There have been notable achievements up to the present day (38, 52, 54, 88) where the advantages of robotic technology have progressively been recognised and the types of application have been served through different configurations of robotic system to best harness capabilities of the machine and surgeon safely (50).

Most conventional surgical robots fall into one of three categories, Robot Assisted Surgery *(RAS)*, Computer Assisted Surgery *(CAS)* or Automated Robotic Surgery *(ARS)*. Most, if not all systems to date, despite their varying function share a common process that dictates the way in which they are used; the use of pre-operative planning. This is typically based on scan data taken prior to the surgical procedure, early systems used fiducial markers physically attached to the patient at the time of the pre-operative scans. The tool paths can then be defined and simulated based on the scan data taken. These markers, which remain in place up to, and during the procedure, are used to register the patient to the robot. More recent advances in computing technology allow the registration to anatomical features rather than fiducial markers but the principle remains the same (92).

This registration process poses several problems with adapting this technology for use in other procedures. It relies on tissue being immobile and thus is not suitable for soft tissue surgeries and it makes these procedures reliant on medical imaging technologies such as MRI and CT scanning, this increases both cost and introduces delays in treatment.

While devices like this perform their specific tasks effectively they still rely on the surgeon's perception of the interaction occurring at the tool point. This still poses a potential problem in the case of small scale MIS or micro-surgical tasks where visualisation may be obscured and tactile perception may be lost due to the reduced force levels involved.

It has long been established that one of the major ongoing concerns over robotic surgery is patient safety. Two ways of improving the level of safety and reducing the potential risks are the inclusion of the surgeon in the control loop and the custom design of a robotic system specific to the tasks being performed. Factor into this the current operating theatre environment and the cost and physical size of robotic systems available and it is possible to see why the uptake of robotic surgery has been slow. It would seem that a possible alternative is custom tools for specific tasks that combine both the skills of the clinician and the advantages that robotic technologies can offer.

Sensor guided robots can be used to control penetration through flexible tissues and to control relative motion to moving or deforming tissue targets and

interfaces in micro-surgical tasks. In these tasks precision would otherwise be compromised by deflection induced under the action of tool forces. In addition to the automatic and master-slave robotic systems in surgery, there is a need for sensor-guided robotic devices that can interpret and react to tissue motion in order to control the interaction between the tool and the target tissue. Thus a next logical step may be custom robotic tools that make use of advanced sensing and control strategies creating smart tools to assist the surgeon with specific tasks. These can be fully autonomous, automatic, or automatic as part of a master-slave system and can be used to enable precise operation of tool points with respect to compliant tissues and tissue interfaces.

3.1.1 Computer Assisted Surgery

Computer assisted surgery (CAS), as the name suggests, is the use of a computer to help the surgeon to perform the task at hand. Assistive systems are generally used to either position a tool accurately or to relay information about the tool position whilst relying on the surgeon to manipulate the tool tip and thus by definition act in a passive manner.

The earliest example of this is that of Kwoh *et al* (68) who used a Puma 200 six axis industrial robot used in conjunction with a computed tomography (CT) scanner for the positioning of a biopsy probe alongside a patients head at the correct trajectory for the biopsy of brain tumors. In the interest of safety the robot was used in a passive mode, that is, once in position the robot was powered down and the procedure was performed manually by the surgeon using the probe as a guide. Used in this fashion the system demonstrated significant improvements in the procedures duration and accuracy over conventional techniques using a stereotactic frame. Despite these encouraging initial results future trials were hampered due to the manufacturers of the robotic systems determining that the use of industrial robots that were not designed for use in close proximity to people was unsafe, and thus inappropriate and work was ceased. A number of similar systems were subsequently developed; one of the more successful was that developed by Lavallee *et al* (69) in which over three hundred operations were

performed. The system used intra-operative X-rays to register the patient to pre-operative CT scans to plan biopsy needle paths that avoided key structures and blood vessels. The robot was then used in the same passive manner but it was perhaps the first system to make use of a pre-operative planning phase.

The SpineAssist (Formerly MARS) robot from Mazor Surgical Technologies Limited (16) used for inserting pedicle screws into the spine is another example of an active robot used as a passive tool holder (86). The device is a miniature bone mounted system, unlike the MBARS robot discussed later in section 3.1.4, this device uses a pre-operative planning stage in which the surgeon uses CT scan data to define the desired screw location. Intra-operative X-rays are taken with the robot mount in place and are used to register the robot to the pre-operative scan data. The robot then positions a guide such that the surgeon can accurately position the pedicle screws. The robot was found to provide significant benefits over the conventional technique including shorter operating times, more accurate screw placement and fewer post-operative complications.

CAS also encompasses navigation systems that aid the surgeon by tracking the tool positions, one such system is that of Monahan (73) in which a series of encoder linkages are attached to arthroscopic probes for use in joint repair surgery. A reference pin is attached to the patient prior to surgery and a series of scan are performed. Encoder linkages are attached to the reference pin and thus register the instruments to the patients scan data. The instrument movements and tool point locations can then be tracked and are displayed on a monitor. The system also has the facility to warn the clinician if the tool moves outside of a safe region defined in the preoperative planning phase.

Other recent examples of assistive systems are the Pathfinder® (56), EndoAssist® (24) and the AESOP robots (95). The EndoAssist® and AESOP systems are camera holding robots for use in laparoscopic surgery. The Automated Endoscope System for Optimal Positioning or AESOP was the first commercially available surgical robot. Launched in 1994 by Computer Motion Inc., who have since merged with Intuitive Surgical (15), and was the first surgical robot approved by the US Food and Drug Administration (FDA) with over 100,000 procedures performed by the year 2000. The AESOP was used to hold and manipulate an endoscope that is operated by a clinician assisting in the pro-

cedure. The first generation instruments were adjusted using either a foot pedal or a remote control, but more recent models like the AESOP 3000 make use of voice recognition allowing the surgeon to control the unit directly.

The EndoAssist® from Prosurgics Limited (19) is a similar device that performs the same function, the main difference is the mode of operation. The system is operated via a foot pedal and a headset worn by the surgeon. When the foot pedal is depressed the robot position is adjusted by head movements detected by the headset. These systems do not require any pre-operative planning or scan data. In the case of EndoAssist®, the robot is registered to the patient by focusing two projected light beams on the entry port for the endoscope. This location then becomes a pivot point about which the robots movements are based, thus the risk of further trauma resulting from movement of the instrument is significantly reduced. This combined with the steady tool motion and stable mounting platform make these devices very effective. As such, both systems have been used extensively in the operating theatre and have demonstrated clear benefits over conventional laparoscopic techniques.

A more recent development is the FreeHand® (11), again from Prosurgics Limited (19). Although similar in function to the EndoAssist®, it is designed to be a small footprint, low cost device. The system is a good example of how custom design for a specific application can be used to reduce cost and improve the usability and performance of a surgical system.

The Pathfinder®, also from Prosurgics Limited (19), is designed for the accurate positioning of tools in neurosurgery similar to the system pioneered by Kwoh (68). Rather than an industrial robot, the system is comprised of a custom designed manipulator on a stable, mobile base. Prior to the procedure a number of fiducial markers are attached to the patient's skin. The use of a number of markers asymmetrically placed minimises any tracking error caused by tissue movement. Once in place, CT and MRI scans are performed and are used in a planning phase in which the surgeon can define the target location and the tool alignment. When in theatre the patients head is restrained in a Mayfield® head rest (14). The robot uses image guidance via video feedback to track the position of the fiducial markers and to calculate the tool path and position the tool holder required to reach the target. The surgeon then manually inserts the tool using

the guide in the tool holder. The system has demonstrated sub millimeter registration accuracies and very high levels of tool positioning accuracy and precision negating the need for a cumbersome stereotactic frame.

All of these systems are examples of active robots used as passive tool holders. None of these devices physically contact the patient and the clinicians are under complete control of the systems, and thus are examples of CAS. They make use of some, but not all of the benefits that robots can offer, these include:

- Precise and repeatable tool positioning;
- High degree of tool stability;
- Can maintain tool position for long periods.

These mitigate some of the human limitations by freeing the clinicians hands and eliminating the need to hold a device in the same position for long periods. In order to gain further benefits the robot must have an active part in the surgical procedure itself.

One of the few CAS systems developed for working on soft tissue was the NEUROMATE® (70), now marketed by Renishaw Mayfield, a subsidiary of Renishaw (20). While similar in function to the Pathfinder® described in section 3.1.1 in that it held a neuro-endoscope and provided an instrument guide so that tools could be used in the visual field of the endoscope; it combined the remote centre of motion strategy used in laparoscopic systems with a 3D ultrasound imaging system to track tissue movement and update the 3D MRI model used in the preoperative plan. This enabled the system to actively compensate for tissue movement to help avoid sensitive structures.

3.1.2 Robot Assisted Surgery

Robot assisted surgery (RAS), while still only assistive, uses a robot in an active capacity to help the surgeon perform the operation or to steady or limit the tool motions to predefined regions.

The concept of an assistive robotic system with active constraints was explored by Davies *et al* (49) with the Active Constraint Robot (ACROBOT®) from The

Acrobot Company Limited(4). The device is used in orthopedic surgery for knee replacement and mills the seat for the implant. The system consists of a robot arm to which a rotary cutter is attached. The arm is held by the surgeon who can back-drive the arm to move the cutter with all the motive force provided by the operator; encoders within the arm feed back the tool position to a computer.

A custom CT-based pre-operative planning system is used to optimally locate the prosthesis and define the region of bone to be removed and areas outside which the cutter must be constrained.

During the procedure the robot is registered to the patient, who is securely restrained, by using a probe which replaces the cutting tool which is then touched on key anatomical features enabling the system to map the patients knee and match it to the CT scan data. Once registered the surgeon is free to begin moving the robot and removing tissue. The robot prevents the cutter moving out of the predefined safe regions and as boundaries are approached more resistance is provided slowing the surgeons movements. As such, the surgeon can feel what the tool point is doing an has complete control of the device as long as the cutter remains within safe regions. ACROBOT® is termed a synergistic system due to the unique way in which the robot performs the procedure under complete control of the surgeon combining the benefits of both the skill, judgment and experience of the clinician with the accuracy and precision of a robotic device (51).

A more recent product development, due for release in 2009 pending clinical evaluation, is the ACROBOT Sculptor® (8) which integrates a tracking arm that is attached to the target tissue for intra-operative motion tracking eliminating the need for the more invasive rigid clamping.

Another example of RAS is the Passive Arm with Dynamic Constraints (PADYC) developed by Troccaz *et al* (93). This system, as the name suggests, is not an active robot, rather it uses a series of electro-mechanical brakes to impede the surgeons movements.

Further examples of RAS include 'steady hand' devices (91) and master-slave or tele-surgical systems.

3.1.3 Tele-Surgical Systems

To date the only surgical robots to be used on soft tissues in the operating theatre successfully on a large scale have been tele-surgical systems; given the safety implications of conventional robots and the requirements of MIS procedures this is unsurprising.

Tele-surgical systems are typically used in a master-slave configuration that consists of two separate devices. The slave is the robot that is in contact with the patient and performs the operation; the master is a separate remote terminal at which the operator sits. These devices can be located meters or even kilometers apart. The operator has a view of the operative field, typically relayed by cameras, and manipulates the slave via a control mechanism and console. The exact motions of the operator are filtered to remove tremor, scaled and are then translated to the slave manipulators.

The majority of MIS procedures are carried out on soft tissues located within the body using laparoscopic techniques. As such the surgeon is working in an extremely confined space that is often disorientating whilst trying to manipulate tools and delicate tissues with little or no tactile feedback. This makes MIS procedures difficult to perform at the best of times. While a robot may offer some advantages there are some fundamental challenges to be overcome before laparoscopic surgery can be performed autonomously or even be actively assisted by a robot. To achieve this a robotic system would require a means of tracking the tissue relative to the tool point and be aware of the state of the tool-tissue interaction. It is for this reason that the use of the master-slave configuration that takes advantage of the human ability to interpret visual information combined with limited tactile feedback, has made tele-surgical systems so successful.

As the slave robot is holding the surgical instruments, a camera and the manipulators themselves they are very stable, as is the view from the camera. The filtering and motion scaling aid delicate tasks because large movements at the master side translate to a small motion at the slave side, thus tremor is eliminated. In addition to this the manipulators themselves can have many more degrees of freedom than conventional laparoscopic instruments due to the additional control capability of the robots making working in confined spaces significantly

easier. The slow and controlled way in which a robot moves also significantly aids navigation.

A recent, although early stage, example of a tele-manipulator system is that of Westphal *et al* (98) in which a master-slave system was evaluated for use for femur shaft fracture reduction. The system uses an industrial clean room robot from Staubli (22) augmented with force and torque sensors that interfaces with a standard computer. In addition to this a separate support arm was used for affixing the proximal fracture segment to which a tracking quadrant is attached for use with an optical navigation system. The distal portion was attached to the robot, both segments were scanned prior to the procedure with fiducial plates in place. This enabled intra-operative registration of the bone segments. The position feedback from the robot tracks the distal segment and the optical system the proximal segment. The robot is then manipulated by the surgeon via joystick connected to the computer. A degree of force feedback was provided through the joystick from the force sensors in the robot. An X-ray imaging system provides intra-operative images of the bone segments to verify the procedure upon completion.

Two further examples of tele-surgical systems are the Da Vinci® system from Intuitive Surgical(15), and the Zeus system from Computer Motion Inc. (now also part of Intuitive Surgical) (90). Both systems are very similar and suffer from the same problem, the lack of tactile feedback. A basic force feedback system has been implemented in the Da Vinci® robot to provide some measure of tactile feedback but the system still relies heavily on its 3D visualisation system. For a true sense of 'touch' that can describe the tool-tissue interaction further information would be required directly from the tool point.

3.1.4 Automated Robotic Surgery

In the case of Automated Robotic Surgery (ARS), the robot performs the procedure automatically without the need for the surgeon's intervention, the surgeon is present only in a supervisory capacity in case of emergencies. Feedback is provided via various sensors enabling the computer or micro-controller to control the

procedure. Most, if not all ARS surgical devices are fully active.

There are a few robots that fall into this category; most existing systems sit between robot assisted surgery and automated robotic surgery. These systems operate about a fixed registration position, precisely defined with respect to pre-operative scan data. It is then assumed that the target area is rigid and unable to move in response to the tool action or movement of the patient.

Systems such as these are often only suitable for non-invasive procedures such as radio or laser therapy or where high degrees of accuracy are deemed unnecessary (97). The exception is orthopedic procedures where the bone can be clamped securely in position or where the tissue can be considered immobile. The robot is then registered to fiducial markers that were present during the pre-operative planning phase so their location is shown in the scan data. Small, repetitive motions are then required to complete the task which retains a very high level of accuracy making these systems ideally suited to these applications.

The first and only ARS system to have been successfully used in the operating theatre on unconstrained soft tissue is the PROBOT (48, 61). PROBOT was specifically designed for use in Trans-Urethral Resection of the Prostate (TURP). In this case the planning phase takes place at the beginning of the procedure when the robot is in position. A 3D ultrasound probe is inserted down the urethra and the robot moves the probe in such a way that a model of the prostate can be generated. The robot uses a diathermic resectoscope and moves it in a conical fashion to remove tissue from the prostate thus a plan is generated to remove a series of cones in sequence whilst avoiding sensitive structures. Once complete the resection can begin. In this case it is not the accuracy of the robot that is of most benefit it is the ability of the system to perform small, repetitive motions tirelessly in confined spaces. The prostate, although soft tissue, is held relatively immobile by the surrounding anatomy and the procedure does not require a high degree of accuracy. That said, the positional accuracy and steady motion make the system intrinsically safe. The PROBOT was the first example of ARS to be used in the operating theatre to actively remove tissue from a patient and demonstrated that not only was automated robotic surgery feasible but high quality clinical results could be achieved safely.

Another example is the ROBODOC® (88). The system, formerly marketed

by Integrated Surgical Limited, now owned by CUREXO Technology Corporation (21) was developed for cement-less total hip arthroplasty (hip replacement). The robot is a custom designed six axis manipulator that had integrated force sensing on each axis as well as in the wrist on which a high speed rotary cutter was located. The systems counter part, ORTHODOC®, was a pre-operative planning system that used 3D CT scan data to select the appropriate implant and define the tool path. The procedure could then be simulated and results verified prior to surgery. In theatre the patient is securely clamped in position and is considered immobile, the robot is then registered to 'ball and cup' fiducial markers placed during the pre-operative phase. The robot is moved under force control by the surgeon so a probe on the robot manipulator mates with the fiducial thus providing an accurate reference. After registration and the surgeon has opened, the robot is moved into position and milling is begun.

During the procedure the progress of the system was displayed on a monitor and force feedback is used as a safety feature such that if the force exceeds a predefined level the robot is halted. Although simple, this was the first example of sensory feedback from the tool point being used to control a surgical robot (66).

A further example is a Mini Bone Attached Robotic System (MBARS) for the milling of the bone cavity in joint arthroplasty developed by a group at Carnegie Mellon University, Pittsburgh (99). MBARS is a small robot that is rigidly affixed to the target bone tissue and acquires anatomical data using its own reference system in order to generate a surface model. Like the PROBOT this data is then used for intra-operative planning of the procedure. Once the intra-operative planning is complete, the robot then performs the procedure by following the tool path generated in the planning phase. Although not deployed in theatre yet, laboratory trials have shown reduced operating times and significantly improved implant placement.

The majority of existing ARS systems are intended for orthopedic application as registration and tracking of the tissue is significantly simpler. Soft and compliant tissues present far greater challenge as the position of the target area can be affected by tool action and other disturbances induced by functions of the body, for example respiration. This can result in the 'loss' of the target area; what is clearly needed is a method of either tracking the motion of the tissue or

an intelligent a smart tool that can react to the motion to compensate for target displacement.

3.2 Smart Surgical Tools

Given the limitations of conventional surgical robots, the cost of augmenting them with additional sensors and tracking systems to enable their use in soft tissue applications it is often prohibitive. Smart tools to assist surgeons by performing specific, particularly challenging tasks is an option being explored as an alternative to ARS to reduce the skill requirements while achieving high-quality results (41).

A new approach to surgical robotics is proposed that uses simple, custom designed mechatronic devices coupled with modern sensing technologies to create a new generation of smart surgical tools.

Smart tools are custom designed mechatronic devices that employ a multi-element sensing strategy to derive state information directly from the tool tip. Using this information as feedback to close the control loop enables such a device to control a process or navigate autonomously without the need for intervention from a clinician. This eliminates the need for external, intra-operative tracking and the pre-operative planning which are both costly and time consuming. This approach builds on the clinicians skills to improve the accuracy and repeatability of surgical tasks. Smart tools bring the additional benefits of lower cost of ownership and reduced operating costs in a small footprint. Owing to their custom design for specific tasks they are intrinsically safer than conventional robotic surgical systems.

Allota *et al* (25) successfully developed a technique for detecting breakthrough when drilling rigid bones using force transients derived from the tool tip. However the matter was complicated by the presence of compliance and/or inconsistencies in the bone structure. Other automated systems for detecting tool penetration of various tools through soft and flexible tissue interfaces have been presented for tissues with different deformation characteristics (39, 76, 96, 100). These systems can be distinguished from tools that are guided by preoperative scan data due

to the way that they use information directly from the tool point to actively control the system rather than just as a safety precaution or for feedback to the clinician (75).

In order to replace some of the more complicated tracking systems it is necessary for a smart tool to not only be able to measure the forces generated by the tool tissue interaction but to interpret them in real-time and react accordingly. In addition to this, to correctly describe the interaction, just quantitively measuring the forces is not sufficient; further information is required on the rate of change of forces and the motion of the tissue, as well as similar data for the tool point itself.

Employing multi-modal sensor schemes and using the relationship between them rather than absolute values enables a vast array of additional data to be derived which can be used to estimate the state at the tool tip.

An example of a smart tool point is the flexible digit with tactile feedback developed by Ma *et al* (72, 77, 78). This system was a master-slave device that employed a multi-element sensing strategy combined with the deformation characteristics of the digit itself enabling the system to determine the position, magnitude and load distribution with a high level of accuracy. This information could be used to make smart endoscopes that provide tactile information back to a clinician. A similar device developed for semi-autonomous colonoscopy has been developed by Chen *et al* (44) that uses a sensor guided approach for navigation.

The integration of smart tool points into active surgical robots presents a potential solution to many of the challenges surgical robots face, bringing to the forefront, a new generation of autonomous surgical tools.

3.3 Autonomous Surgical Robots

It is necessary to distinguish between the new category of Autonomous Robotic Surgery *(AuRS)* and ARS. Automated robots are active but follow a strict tool path defined during the pre-operative planning phase of the procedure. An autonomous robot is one that does not rely on a pre-operative planning phase, rather, it uses sensor feedback and a degree of autonomy to define its own tool

path and make any necessary changes in real-time in response to changing conditions at the tool tip.

The stapedotomy micro-drill developed by Baker *et al* (28) was the first system of its kind developed to integrarate a smart tool point and take advantage of such a strategy; leading the way for the next generation of smart robotic tools. The system was a sensor guided, robotic device that was capable of monitoring and compensating for target tissue displacement to ensure successful completion of the hole being drilled. Through automatic interpretation of the drilling transients it was able to control the break-through process and avoid penetration if required (38).

The proposed micro-drilling system is a further example of this new generation of surgical robotic devices and it will be the first of its kind deployed in the operating theatre.

Chapter 4

Background Work

4.1 The Stapedotomy Micro-drill

The first clinical prototype in which the compliant technique was applied was developed in 1995 for use in the stapedotomy procedure (38) (*Discussed in more detail in Chapter 5*). The stapedotomy was an ideal choice for this type of technology as the surgical requirements of the procedure are well suited to the benefits that the tool can provide. The primary benefits of smart mechatronic tools such as this present over conventional manual techniques include:

- high degree of tool precision,
- trajectory repeatability,
- steady, controlled tool motion,
- sensitive instrumentation,
- highly responsive.

Baker (27) explored the characteristics of compliant drilling and developed a drilling technique to control drill penetration. The technique was then success-

fully applied to a laboratory prototype capable of controlling drill penetration through a bone of unknown thickness with a resolution of 20 μm.

The prototype drill system, designed and built by Mechtron Design Limited (80), used a 0.6 mm diameter cutting burr and was actuated in the feed direction using a velocity servo-system that was controlled by the host computer. The drill unit itself occupied a slim envelope which aided visualisation of the working site, typically observed via a binocular surgical microscope. During drilling, the feed force and torque are measured. The sensory data is captured and analysed by the host computer running a detection algorithm that could determine the onset of the breakthrough condition. This information was then used to trigger an automatic breakthrough control sequence.

Results from initial laboratory and cadaveric trials showed promise however it was clear that issues regarding safety, sterility, interfacing and compatibility had to be addressed before further trials could be conducted. This led to the redesign of the prototype for use as a clinical demonstrator (29, 41).

The redesign primarily addressed issues regarding the improvement of drill performance, the addition of a rigid tool support and a head restraint. These modifications saw an improvement in the signal to noise ratio *(SNR)* and started to address the challenges faced when trying to deploy a device such as this in the operating theatre.

The clinical demonstrator went on to successfully demonstrate the compliant drilling technique and its potential for use in the stapedotomy procedure, however several issues still remained and had to be resolved prior to a research clinical trial. Baker identified three main areas that required improvement before the system would be suitable for use in surgery:

- Sensor sensitivity and resolution
- Tool presentation and positioning
- Adaptation to current safety guidelines

This chapter details the design, system architecture and control algorithms implemented in the clinical demonstrator system as described by Baker (27). However, the system was re-assembled and control interface re-written in order

to re-evaluate the system performance. All results shown in this chapter were generated as part of this research.

4.1.1 Clinical Prototypes

Two generations of clinical instrument were developed, the mechanical portion of the first clinical prototype is pictured in figure 4.1.

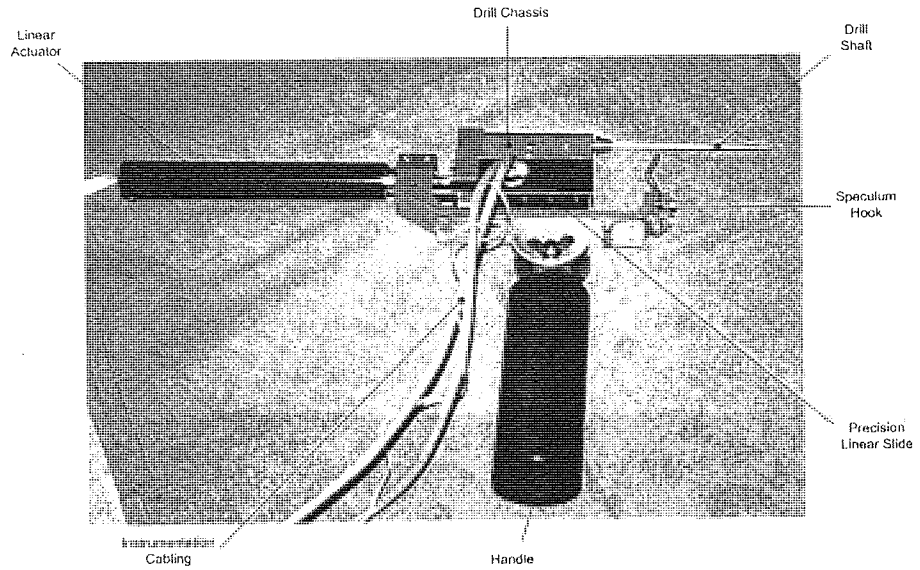

Figure 4.1: *The hand held micro-drill unit.*

4.1.1.1 Mechanical Design

Figure 4.1 shows the drilling tool which was a hand held device, the main mechanical components of which from left to right are the linear actuator *(left)*, Drill unit chassis *(top centre)*, Drill shaft *(top right)*, Speculum hook *(right)*, Drill cradle and precision slide *(centre)* and the handle *(bottom centre)*. The instrumentation and drive cabling can be seen coming from the centre and on the far left is the linear actuator.

The drill chassis was mounted on a precision linear guide attached to the drill cradle and was actuated by a precision ground lead screw. The cradle also housed

the linear actuator. Extension springs connected between the drill chassis and the cradle form an anti-backlash mechanism. The drill shaft passed through the top portion of the chassis through ball bearings at each end to ensure smooth operation. The rotational drive for the drill shaft was provided by a geared motor in the base of the chassis. The drive connected by a series of 1:1 ratio gears with an idler gear in between.

The unit itself was designed with clinical use in mind. The profile of the tool was kept to a minimum to maximise visualisation of the operative site. The drill shaft was also located as close to the top of the drill unit chassis as possible, this makes the tool easier to use in conjunction with a surgical microscope. The overall size of the hand held unit was sufficiently small to enable the surgeon to use the drill whilst observing the procedure without the unit encroaching on the microscope's visual field. This also provided a direct line of sight from behind the drill, down the ear canal to the stapes. Access to the operative site was gained via the ear canal aided by the use of a speculum. This necessitated the long drill shaft and the hook mounted on the handle of the device. The hook could be rested on the edge of the speculum to help the surgeon to steady the unit. Figure 4.2 shows the system being tested on a cadaveric temporal bone sample.

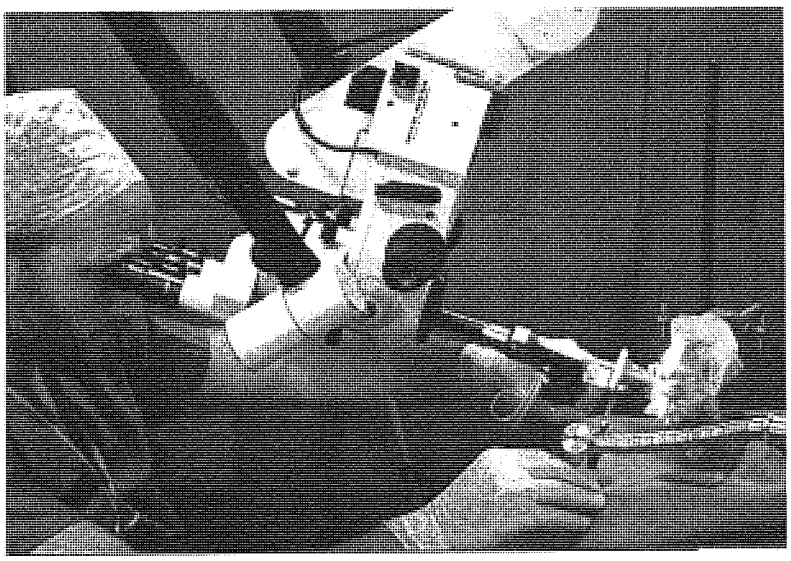

Figure 4.2: *The hand held micro-drill unit in the operating theatre.*

The drill bit used was a 0.6 *mm* spherical cutting burr and rotated at a

fixed velocity of 2 Hz. This was deliberately kept low to minimise local heating effects and to reduce the risk of acoustic trauma to the inner ear. Baker explored the characteristics of the most commonly available burr shapes such as conical, elliptical and cylindrical. Of all the drilling characteristics explored the spherical demonstrated the most effective, offering the highest degree of control. The burrs used were commonly available dental burrs fitted into a custom drill shaft, making the burrs easily interchangeable.

The redesign of the prototype drill saw the development of the clinical demonstrator depicted in figure 4.3.

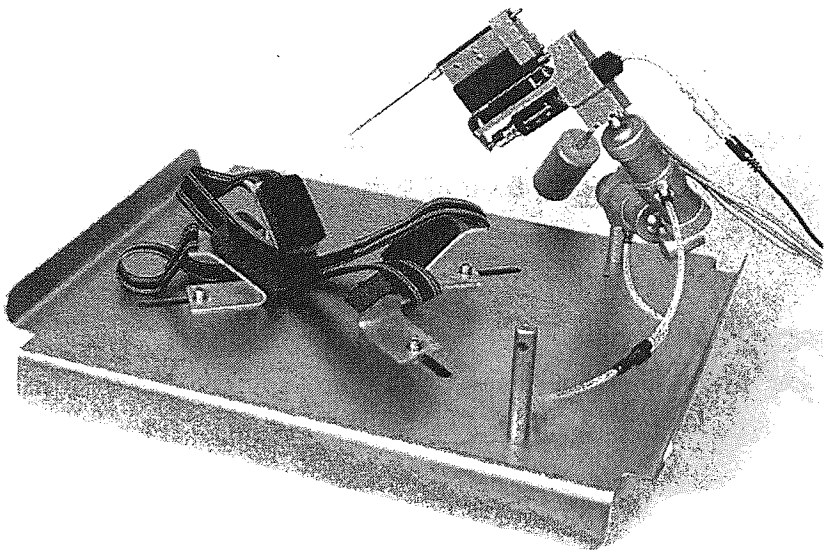

Figure 4.3: *The Stapedotomy drill clinical demonstrator.*

The drill unit itself remained largely unchanged, the main difference was the replacement of plastic gear elements with metal gears to reduce the meshing noise in the torque signal. The linear actuator was moved to the underside of the device to provide more clearance when used in conjunction with a surgical microscope. The most noticeable addition was the rigid tool support and baseplate instead of the pistol grip handle. This was added to improve tool stability and reduce sensitivity to environmental vibration which often resulted in false positive detections.

The tool support is a crude dual segment version of a flex and lock arm. The arm is air operated, as such the unit requires a 2100 kN/m^2 compressed air

supply. A foot pedal unlocked the device by cutting off the air supply and venting the air from the within the locking cylinders so that the unit could be moved into position. When the foot pedal was released the air supply was returned and the arm would lock with minimal backlash. This meant the default condition was locked. This was intentional as it was felt that this was safer. If air pressure was lost the support arm would remain locked and would not collapse possibly resulting in injury.

The baseplate provided a solid platform on which the drill system could be mounted, the cradle in the centre was added to prove support for the patients head and the straps to minimise the effect of movements of patient due to external sources such as breathing. The pillars located on the right hand side enabled the system to be used on either side of the patients head. The plate itself was shaped such that it would fit over the cushion at the head of the operating table and thus would replace the gel head rest that is used conventionally.

4.1.1.2 Sensing Scheme

The compliant drilling technique is based on using sensory feedback to predict and control drill breakthrough, therefore it was necessary to instrument the tool such that the force and torque from the tool point can be derived from sensor transients.

Torque measurement on this scale it not an easy task. This was done using the gear system between the drive motor and the drill shaft. The second gear of the train was an idler gear which was mounted on a cantilever as shown in figure 4.4. When torque was applied to the drill shaft the cantilever would deflect as the idler gear was linearly displaced.

Torque feedback was provided by a strain gauge affixed to the cantilever as shown in figue 4.5.

Force feedback was generated in a similar fashion, the drill unit chassis was hollow with a cantilever at each end on which strain gauges were attached forming a full bridge arrangement, this is also shown in figure 4.5.

The use of strain gauges required the use of high gain instrumentation amplifiers and signal conditioning units to achieve the necessary degree of resolution

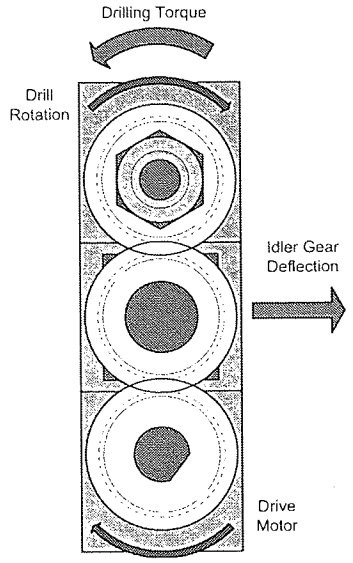

Figure 4.4: *Torque sensing mechanism.*

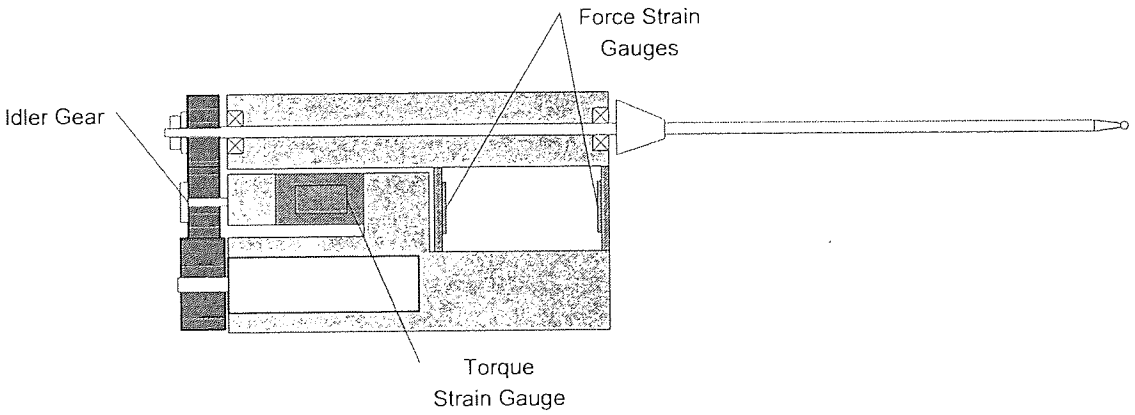

Figure 4.5: *Drill unit strain gauge configuration.*

and precision.

The final sensing element, although integrated into the linear actuator system, is a rotary encoder that provided velocity and position feedback to the servo controller in the host computer.

4.1.1.3 System Architecture

A schematic of the system architecture is shown in figure 4.6.

The system was operated via a host computer running a custom software interface. The device was controlled using multi-function data acquisition card and a servo interface card installed in the host. The servo interface was a complete integrated controller. Its mode of operation was independent of that of the host. The servo module used position feedback from a rotary quadrature encoder to control the linear actuator with the PID (Proportional, Integral and Derivative) running internally on a micro-controller. The interface card also incorporates an input/output module with multiple analogue and digital outputs, these were used to interface the drill drive motor and operate the remote control used by the operator.

Sensor transients were acquired using an external instrument amplifier and signal conditioning unit. Data was acquired by a multifunction data acquisition card at a rate of 1 kHz with a resolution of 10 bits (1/1024). The data was fed into the host software which operated a basic detection and control algorithm.

The principal functions of the controller are illustrated in figure 4.7. The controller consisted of a two tier hierarchy, a high level and a servo level controller. The high level controller in this instance was the host computer running the control software. The high level controller responded to key stages of the drilling process by selecting pre-defined strategies based on the interpreted state of the drilling process. In particular, the high level controller searched for the characteristics in the sensory transients indicating the onset of breakthrough. In addition, factors such as tissue stiffness and cutting coefficients could be evaluated to reflect how the system needed to respond on breakthrough. Progress of the procedure is relayed to the clinician who was able to override the process.

The servo controller was an independent device operating on a component

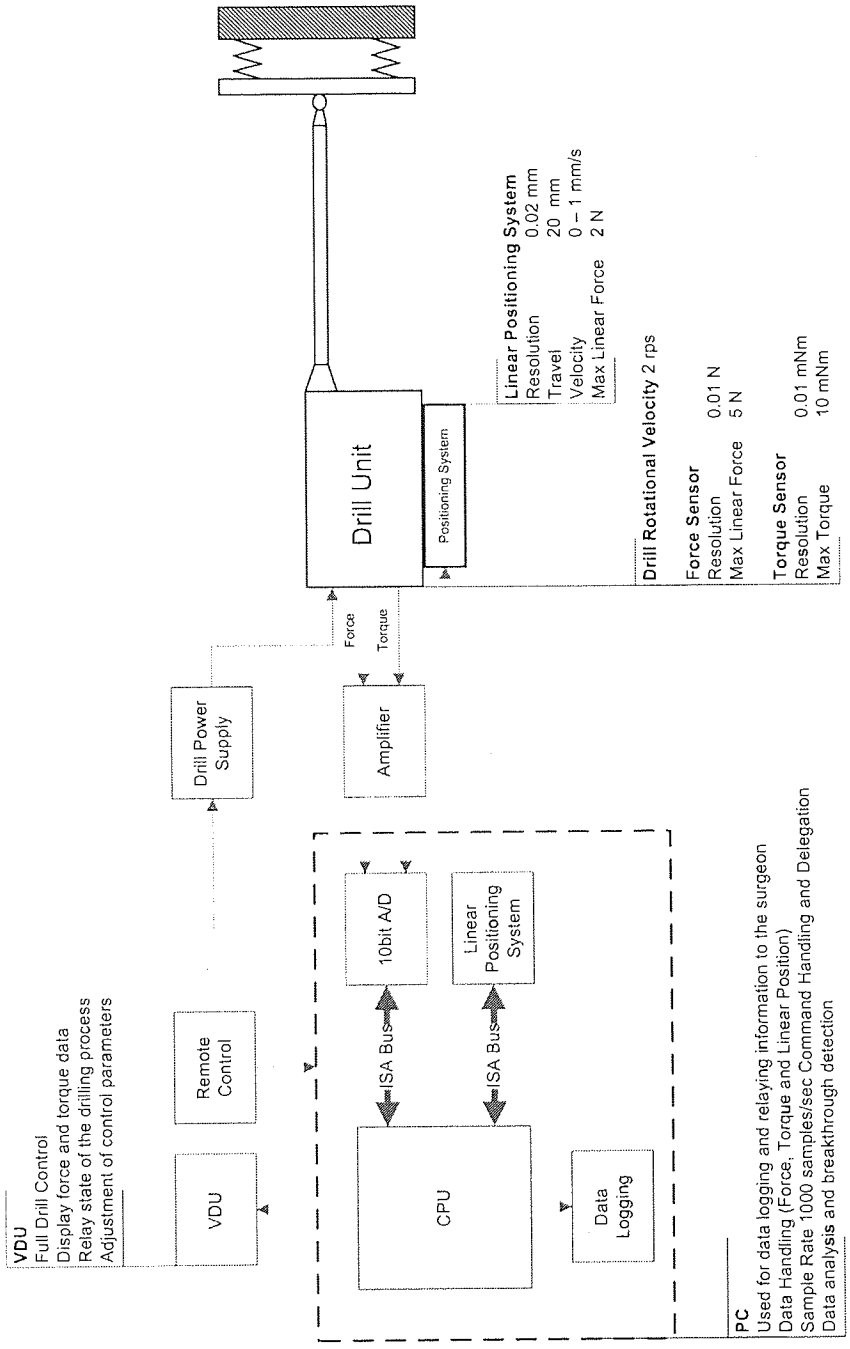

Figure 4.6: *Stapedotomy micro-drill system block diagram.*

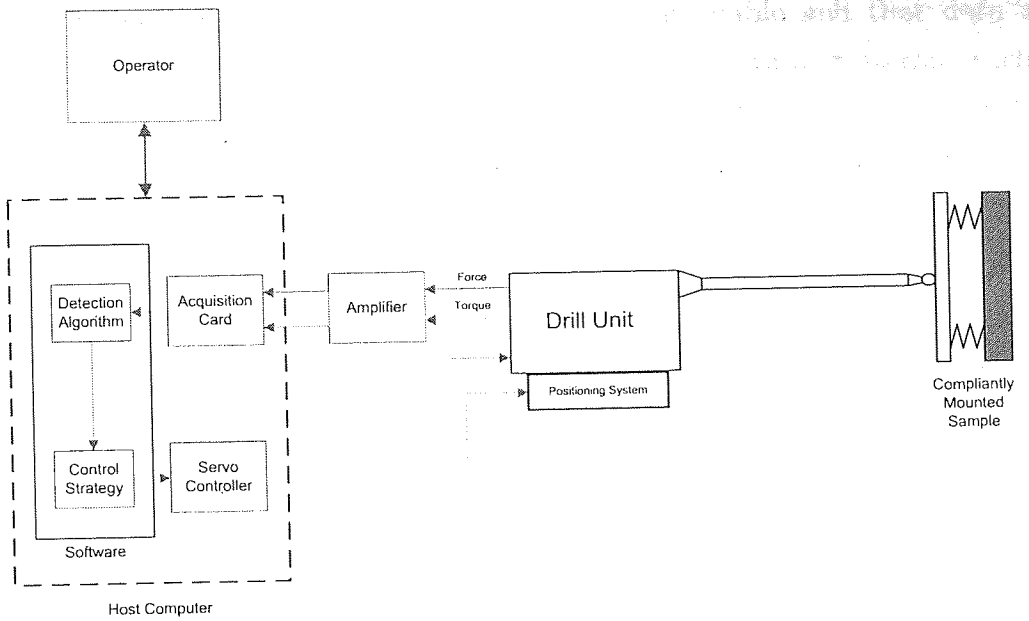

Figure 4.7: *Principal control functions of the drill system.*

level controlling the mechanical components of the drill. The servo controller was configured as a velocity servo from which position was determined by integration. The actuator was capable of sub-micron accuracy and could advance at velocities as low as 1 $\mu m/s$.

4.1.1.4 Breakthrough Detection

Baker (27) explored different schemes for detecting breakthrough, these methods aimed to reduce sensitivity to noise and attempted to identify the features indicating the commencement of the breakthrough process.

Monitoring the drilling data for sudden increases in the rate of change of the data gradients is a principal means of detecting the start of breakthrough. This method of breakthrough detection could be implemented in more than one way. Most simply it could be implemented by applying thresholds directly to the force and torque gradients, however it was found that sudden changes in breakthrough were not easily distinguishable from noise and breakthrough could occur without being detected. A further means was needed to discriminate between noise and the breakthrough features.

Given that noise in the drilling data was unavoidable and that data also included variations due to the non-uniform nature of natural materials such as bone, statistical methods could help to reduce the effect of these on the data. The technique employed was an extension of the gradient method that integrated linear regression to include historical data. The linear regression analysis, used within the breakthrough detection algorithm determines the best estimate of the straight-line segment through the current data point using the last n data points. This method has the added advantage that a high degree of filtering is not required due to its resilience to noise and it enables the calculation of the gradient and the y axis intersection point without the need to differentiate the sensor data. As a measure of the gradient, the axis intersection has the beneficial feature of becoming more sensitive to changes in the gradient as drilling progresses where as the gradient remains a true estimate.

The start of breakthrough was detected when criteria 4.1 was satisfied.

$$(ay > 0)\ AND\ (az < azLB)\ AND\ (\frac{\delta y}{\delta x} < 0) \tag{4.1}$$

$$azLB \quad = \quad Constant \times FeedDisplacement \tag{4.2}$$

Where ay is the axis intersect from the force data, az the axis intersect from the torque data and $\frac{\delta y}{\delta x}$ is the gradient from the force data. The primary condition is $(az < azLB)$. This term indicated when the gradient of the torque data exceeds a predefined threshold, *i.e.* it aimed to identify the start of the rising torque feature that occurs at the start of breakthrough. This condition was expressed in terms of the axis intersect value for two reasons:

1. Its increasing sensitivity to changes in the gradient as drilling progresses. This helps to minimise the impact of fluctuations in the data near the start of drilling when the fluctuations can be large compared to the torque magnitude;

2. the term $azLB$ is readily enumerated from a set of drilling sensory data

transients.

Since there are fluctuations that can have similar features to the breakthrough characteristics in both the force and the torque transients, using the torque alone frequently resulted in premature *(false positive)* breakthrough detection. Introducing the force-based conditions reduced the false positive detection rate. The $(ay > 0)$ condition was based on the fact that the force gradient reduces sharply following the start of breakthrough. Given ideal data $(ay > 0)$ would be true from shortly after the start of drilling due to the slight decrease in gradient during drilling up to the start of breakthrough. It means that if the force continues to rise for a short period after the start of breakthrough (e.g. if equilibrium drilling was not reached prior to the start of breakthrough) this condition does not delay the detection of breakthrough as it is identified by the $(az < azLB)$ condition. For real data sets however it had the important role of ensuring that if the $(az < azLB)$ condition was satisfied, breakthrough was only detected when the force was increasing slightly or falling. This has the effect of reducing the likelihood of false positive breakthrough detection as fluctuations in the force and torque data sets rarely coincided sufficiently to satisfy both conditions.

If the $(ay > 0)$ condition was not sufficiently strict for a particular type of drilling scenario then the $(\frac{\delta y}{\delta x} < 0)$ condition could be added. Whilst adding this condition may in principle delay breakthrough detection under some drilling conditions since it applied the force breakthrough characteristic more strictly than $(ay > 0)$, it can enable the $(az < azLB)$ condition to be set more sensitively and hence lead to a reduced likelihood of false positive breakthrough detection whilst having a negligible effect on the promptness of detection. To minimise the risk of breakthrough going undetected due to an anomaly in the drilling data the following conditions are also applied.

$$(ay > 3ayLB)\ OR\ (az < 2azLB) \tag{4.3}$$

$$ayLB = Constant \times FeedDisplacement \tag{4.4}$$

Both of these conditions were used to monitor the data for the rapidly falling force, or rapidly rising or falling torque that could occur during the later stages on the approach to drill bit break-breakthrough. Using this approach, the values for the constants $ayLB$ and $azLB$ were selected based on experimental evidence.

4.1.1.5 Control Strategy

The overall drilling strategy was separated into two discrete phases:

1. from the start of drilling to the start of breakthrough; and
2. from the start of breakthrough to the hole completion.

The compliant drilling technique requires that the system automatically identify the stage it was currently at and control the actions of the drill system accordingly. These key stages of the automatic drilling technique are illustrated in figure 4.8.

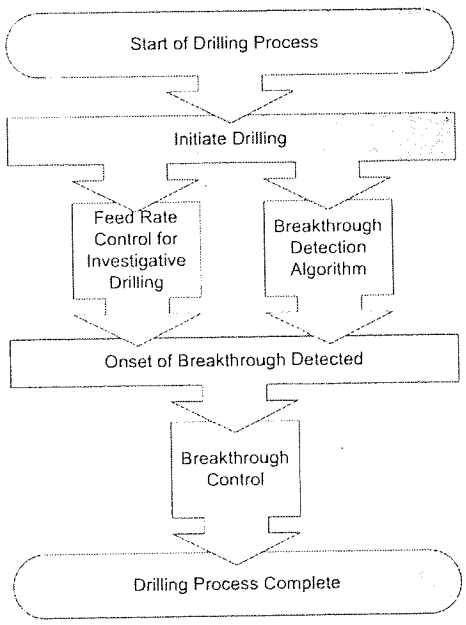

Figure 4.8: *Key stages in the drilling sequence.*

During the first stage of drilling, the breakthrough detection method uses the drilling force, torque and position feedback to monitor the state of the drilling pro-

cess and to identify the start of breakthrough. On identifying the start of breakthrough, the drilling process is promptly moved to the second stage of drilling. The control of the drill was then determined by the breakthrough control strategy and leads to the controlled completion of the hole.

The requirements of the drilling technique influence the selection of the breakthrough control strategy. For the stapedotomy procedure, typical requirements are are:

1. precise control of penetration and breakthrough given that:
   - the drilled material is mounted compliantly;
   - thickness is unknown;
   - material properties are unknown (but within a known range);
2. minimal protrusion beyond the far surface of the drilled material when forming a complete hole;
3. provision of feedback on the progress of drilling;
4. appropriate levels of intrinsic safety;
5. predictable structured actions.

The first three of these define the capabilities of the technique whilst the last two are underpinning requirements for surgical application. An example control strategy to precisely control penetration, breakthrough and minimise drill bit protrusion is shown in figure 4.9.

In the first phase, prior to breakthrough when the material thickness and stiffness are unknown, the system began the investigative drilling stage. Drilling was initiated and the unit was advanced slowly at a constant feed rate. The sensor transients are analysed in real-time for indications of the onset of breakthrough. On detecting breakthrough the drill unit was retracted until the feed force approached zero. At this point the burr would be positioned approximately on the distal surface of the hole and the target will have returned to its neutral position. The material thickness and stiffness could then be calculated and used

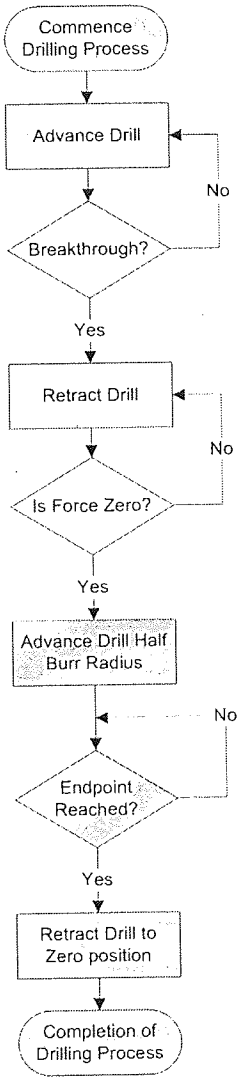

Figure 4.9: *Basic control strategy to minimise drill protrusion.*

to calculate the control parameters for the final phase. The next stage began by advancing the drill half a burr radius and commencing drilling. Given that the burr is spherical, half a radius is the minimum protrusion required. The force resulting from the deflection of the target tissue was then assumed to be sufficient to complete the hole.

4.1.2 Drill Performance

A series of laboratory trials were conducted in which samples of bone $0.5mm$ in thickness were compliantly mounted and drilled using the control strategy described in the previous section. An example set of drilling transients are shown in figure 4.10.

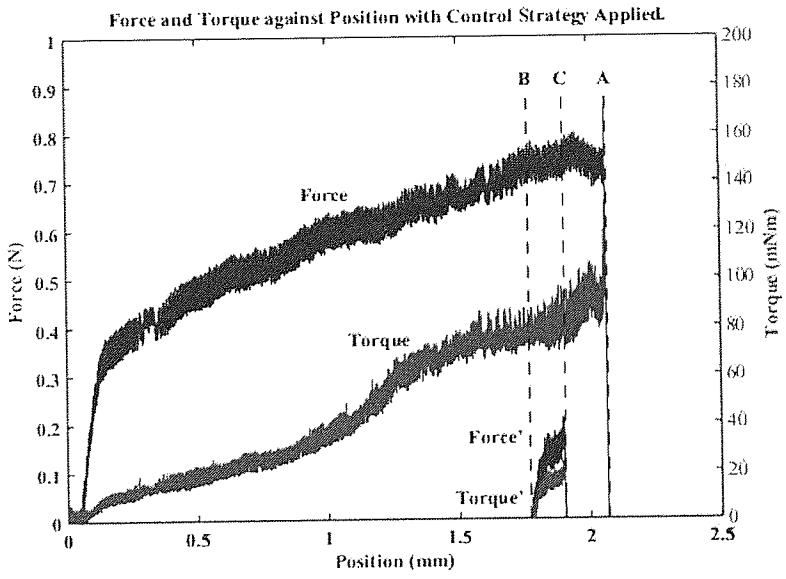

Figure 4.10: *Force and torque curves with the control strategy applied.*

After contacting the material surface the investigative drilling phase is initiated. The drill advances at a constant feedrate until the onset of breakthrough is detected by the analysis algorithm using data from both the force and torque curves. In this case the onset of breakthrough was detected at position **A**. The drill then retracts to reduce the applied force to zero which is achieved at position **B**. At this point the bone sample has adopted its neutral position with the

drill tip on the distal surface. The drill then advances at a constant feed rate to a displacement equal to one burr radius, position C. The drilling process is complete when the force and torque drop to zero. When using a spherical cutting burr this completes a full hole through the bone sample with the minimum value of protrusion achievable.

Drill protrusion was calculated by measuring the approximate diameter of the aperture at the base of the hole under a microscope when the onset of breakthrough was detected and drilling ceased. Assuming the cutting burr is perfectly spherical and knowing the burr radius, the depth of penetration can be calculated. Using this device with the described control strategy the drill position beyond distal surface was achieved to within a tolerance of ± 20 μm of the desired position.

Further experimental studies showed that there was a trade-off between the promptness of breakthrough detection and the likelihood of false positive detections. Detection to within ± 20 μm (7% of the drill bit radius) prior to the interface could be achieved with a high signal to noise ratio *(SNR)* in the force and torque transients, as was typical under controlled laborotory conditions. However, in the case of other trials where a low SNR was encountered, breakthrough was typically detected within ± 100 μm of the breakthrough point with a false positive detection rate of 20%.

4.1.3 Surgical Application

While the clinical prototype was designed with surgical use in mind, laboratory trials highlighted three main areas that require further development prior to surgical deployment. These primary areas requiring improvement were:

- Tool presentation and positioning,
- Tool Sterility,
- Operating theatre integration.

Operators of the system found the unit hard to position. Although the use of a foot pedal aided the operator as it was possible to have both hands free, aligning

the instrument was difficult making the precise location of the hole challenging. A means of adjusting the trajectory of the drilling axis is required to adjust the hole location once the support arm was locked.

Care had to be taken when handling and operating the device due to its sensitivity to disturbance. The use of a cantilever integrated into the chassis of the drill unit, while reducing size, caused problems particularly with the handling of the device. Any load applied to the drill chassis resulted in artifacts in the force transient, this included noise as a result of the rotating drill shaft and the meshing of gears in the torque system. Meshing of gears also showed up as noise in the torque transient.

Concern was expressed over the possibility of rotating components, namely the drill shaft, coming into contact with sensitive structures within the ear. This introduced artifacts in the torque transient unrelated to the drilling process that may affect breakthrough detection as well as posing unnecessary risk to the patient.

Due to the complexity of the drill unit it is not possible to sterilise the whole device using conventional techniques. One way around this is to drape the whole device in a sterile sheath and only sterilise exposed parts of the drill. However, fitting the drill shaft and sheath was not possible without the clinician coming into contact with both sterile and 'dirty' parts of the drill, potentially contaminating the sterile field. As such all exposed parts of the drilling system are required to be removable and sterilisable. These parts also need to be able to be fitted without handling the instrument or the use of tools.

Another large consideration when taking an advanced mechatronic device into the operating theatre is the integration with existing equipment and procedures. Some of these issues have been addressed, for example the slim profile of the drill unit to aid visualisation and the mounting system for the drill. There are however other potential problem areas.

The operating theatre is a small, enclosed environment that contains a vast array or electronic devices creating a lot of interference. The use of strain gauges requires a high degree of amplification and when used in an enclosed environment along side many electrical devices pick-up is unavoidable.

Other considerations include fast setup and removal in the case of emergency and the physical size and complexity of the equipment. Cables and ancillary components need to be kept to a minimum. The control interface and operating strategies need to kept as simple as possible. A move away from a computer based platform to faster and more stable one, such as an embedded system would also be beneficial.

4.2 Feasibility Studies

To begin to address the issues highlighted in the previous section, a series of feasibility studies were conducted in the laboratory using the re-assembled clinical demonstrator described in section 4.1 to identify potential solutions to some of the key technical issues surrounding the system performance. The areas explored were primarily focused on improving the signal to noise ratio, these areas included:

1. Sensing Technologies,

2. Tool Support.

Investigating different sensing technologies looked at ways of increasing the sensitivity and resolution of the measurements, such that more information could be extracted from the transient information while improving noise resistance. The tool support aids this by providing a stable base for the drill system to operate from, isolating it from environmental noise and vibration. However, while being highly stable, the tool support must be sufficiently manoeuvrable to enable precise positioning of the drill unit.

4.2.1 Sensing Technologies

4.2.1.1 Force Sensing

The simplest and perhaps the most cost effective method of force sensing is the use of a simple cantilever and measuring the deflection of the cantilever with some

form of sensor, whether it be optical, capacitive, inductive or a simple resistive element such as a strain gauge. This method can provide a very sensitive and accurate measurement which is proportional to the axial force applied to the cantilever.

The Simple Cantilever

A cantilever is a simple beam constrained at one end. The deflection of the beam is determined by its length, cross-section and material properties. A diagram of a simple cantilever is shown in figure 4.11.

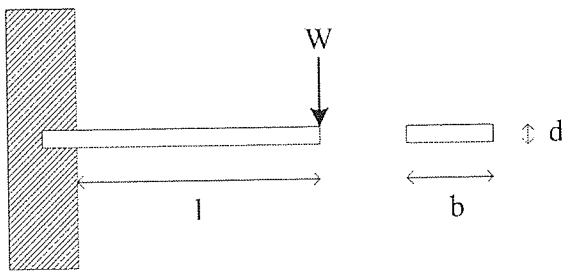

Figure 4.11: *Diagram of a simple cantilever.*

The deflection of a simple cantilever can be expressed using equation 4.5 (36).

$$\delta Y = \frac{Wl^3}{3EI} \tag{4.5}$$

Where W is the load, l is the distance of the load from the support, E is Young's Modulus of the material and I is the second moment of area given by 4.6 (36).

$$I = \frac{bd^3}{12} \tag{4.6}$$

Where b is the breadth and d is the depth as described in figure 4.11. An example of the load plot for an aluminium cantilever 1.5 mm under varying load is shown in figure 4.12. It can be seen that the force applied is directly proportional to

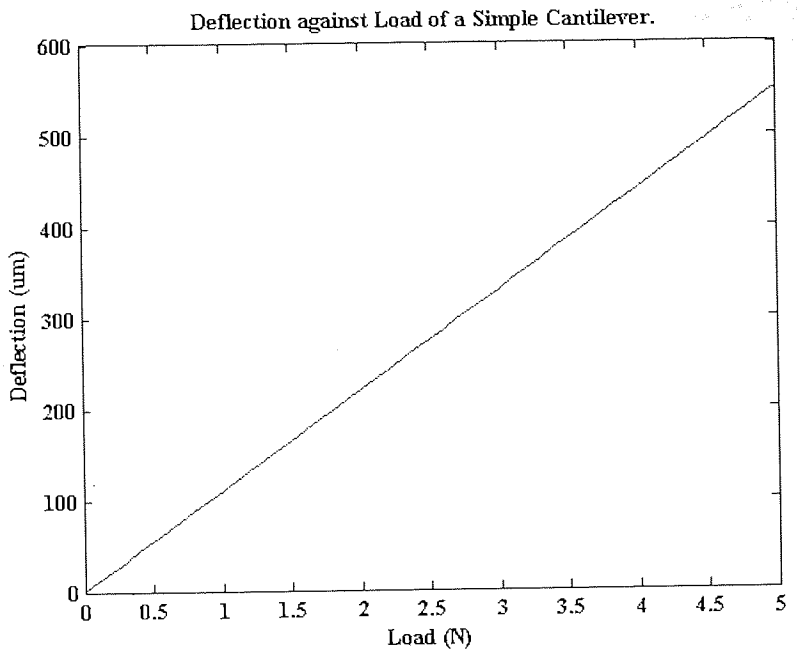

Figure 4.12: *Deflection - Force Characteristic of a* $40 \times 10 \times 1.5$ *mm aluminium cantilever.*

the deflection. If the dimensions and material of a cantilever are known and the material is not stressed beyond its proportional limit this linear relationship can be used to calculate the force applied by measuring the delflection. Young's modulus for a standard 1000 series aluminium alloy is in the order of 69 GPa and the yeild strength of 27.60 MN/m^2. Figures 4.13 and 4.14 show a finite element analysis *(FEA)* of the cantilever similar to that described above, under a load of 2 N. The only difference is that the load in this instance is distributed around the circumference of the aperture at the top of the cantilever as it would be in the intended application. Figures 4.14 shows the stress distribution throughout the material, the analysis shows that maximum stress occurs in a small region just above the support at the base of the cantilever. The maximum stress calculated was 14.81 MN/m^2, giving a safety factor of 1.87. The deformation analysis in figure 4.13 shows a maximum deformation of 85 μm.

This model can be used to design the cantilever for the intended application. Thickness, length and loading can be optimised to take into account the desired maximum deflection, load points and the sensing range of the measurement tech-

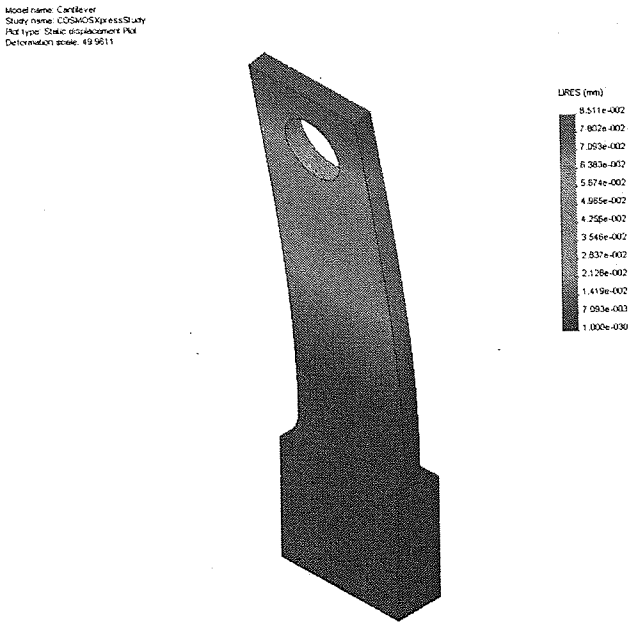

Figure 4.13: *Deflection of an aluminium cantilever under a load of* 2 N.

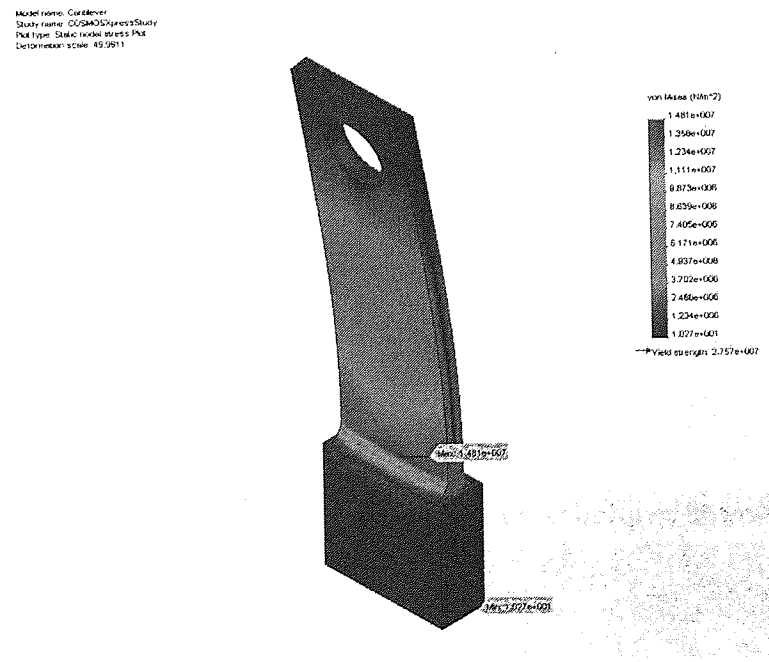

Figure 4.14: *Stress developed within an aluminium cantilever under a load of* 2 N.

nique employed. Figure 4.15 show how thickness of an aluminium cantilever can be used achieve this. For example if the desired maximum deflection at the tip was 100 μm at a maximum load of 2 N would correspond to a cantilever thickness of 1.5 mm.

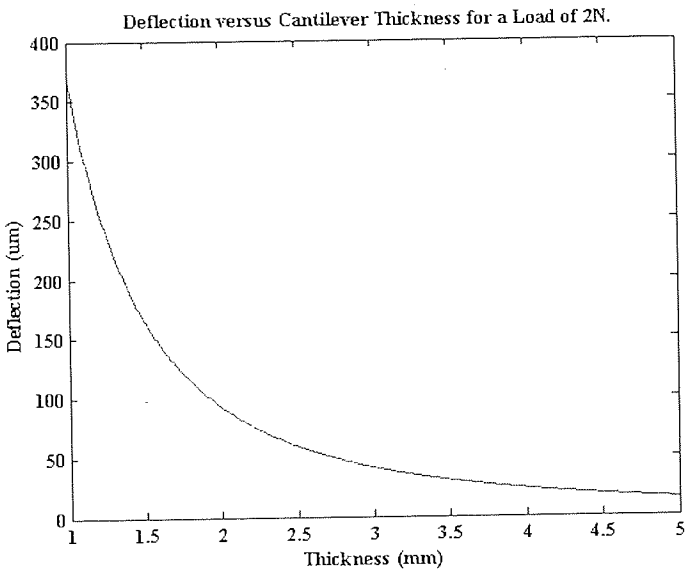

Figure 4.15: *Deflection of simple Aluminium cantilever of varying thickness under a load of* 2 N.

As such to design the cantilever system it is necessary to determine the most appropriate method for measuring the deflection of the cantilever. To achieve the desired resolution of the force measurement for the cantilever described above a sensor with a measurement resolution higher than 85 nm with sub-micron linearity would be required.

Strain Gauges

The initial prototypes employed this type sensing technique, however it was found that there were several drawbacks:

1. Poor noise immunity,

2. Instrument handling/Robustness,

3. Sensitivity and resolution.

Due to the high gain required, such a technique is susceptible to electromagnetic interference *(EMI)* from the surroundings, this is particularly true in the operating theatre due to the vast array of electronic equipment present.

As the gauges themselves are bonded to the cantilever they cannot be removed easily so that the sensitivity and peak output can be changed or adjusted. Given that the drill shaft must be in contact with the cantilever such that the axial force on the cutting burr can be measured, this creates a difficult design challenge. This was previously overcome by integrating the cantilever into the drill chassis, however problems handling the device were experienced.

Load Cells

A novel approach may be the use of a miniature piezo load cell or pressure sensor. These would provide an accurate measurement of the transient force, however these devices are unable to measure a static force, increasing the drive complexity.

Non-Contact sensor

Another approach may be to use a similar cantilever setup and employ a non-contact measurement device such as a capacitive or inductive sensor to measure deflection. This would mean a detachable cantilever could be used, allowing the cantilever to be changed to suit the application at hand, maximising both sensitivity and resolution. As the cantilever could then be integrated internally such that handling of the device does not affect the force measurement unless a force is applied directly to the drill tip.

Examples of non-contact deflection sensors include optical, capacitive and inductive. Each type has its own advantages and disadvantages, optical methods are very expensive and are particularly sensitive to alignment. Capacitive techniques are very accurate but also very expensive. Typically they have a very small working distance and can be susceptible to EMI. Inductive techniques however

are both lower cost and robust and are widely used in industrial applications. These techniques employ an eddy current sensor that detects changes in the surrounding magnetic field due to the proximity of any conductive material such as aluminium. Typical working distances are 1 to 5 mm and they provide sub-micron accuracy making it ideal for this application.

4.2.1.2 Torque Sensing

Torque sensing on such a small scale is extremely difficult. Previous prototypes employed the technique described in section 4.1.1.2 and suffered from a very poor signal to noise ratio. A large portion of the noise generated was from the meshing of the gears, and other mechanical components in the drive train. A geared motor rotated at 1 Hz and was coupled to the drive train at ratio of 2 : 1, hence the drill shaft rotated at a fixed velocity of 2 Hz via a series of metal gears. It was found that by replacing metal with plastic gears the noise was significantly reduced, but still present.

The optimum solution would not only eliminate the gearing but also allow the use of a variable speed drive system. Past experiments have found that mechanical techniques suffer from low sensitivity and introduce a high degree of noise into the system. An optimum solution given the design requirements may be the use of the drive motor current as a torque indicator.

Motor Current

As an initial test a current-voltage converter was constructed and integrated into the clinical demonstrator unit. An example force and torque profile is shown in 4.16.

It can be observed that while the signal still appears noisy, the characteristic torque transient is clearly present and the key features are similar, if not more prominent than in those shown in figure 4.10. Using the prior method it was observed that the noise frequency was dependent on the torque level, with lower frequencies being dominant at high torques. This often hampered breakthrough detection. Using the motor current requires no amplification, the torque output

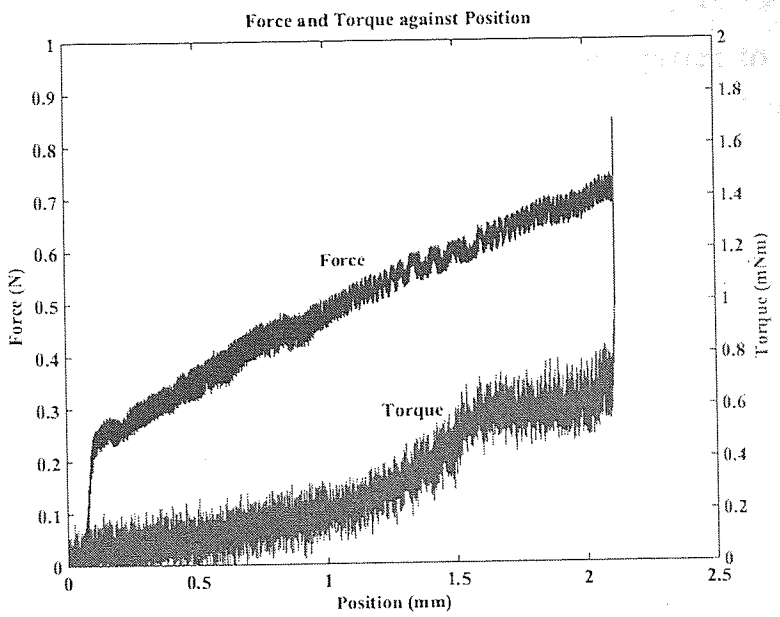

Figure 4.16: *Force and torque using the motor current to derive the torque.*

shown in figure 4.16 is in *Volts*. Although this is of great benefit there is still a high degree of noise in the torque signal. The most dominant frequencies in the signal were 2, 12 and 38 Hz which correspond to the rotational velocity, the number of cutting faces on the burr and the gear ratios of the drive train. Thus, not only does the meshing of gears generate noise in the signal, it also reduces sensitivity of the torque measurement.

Gearing systems act as a torque multiplier which increases the output torque of the system but also reduces the effect of changes in the micro-torques at the tool tip on the motor. It also means that the high torque is relied upon to keep the motor torque constant. This may well have safety implications for any intended medical application as there is no feedback from, or control over the motor.

The predictable noise frequencies present means that filtering in a possible solution to improve the signal to noise ratio, with the optimum being elimination of the source of the noise. For example one possibility is the removal of the gear train and use of a direct drive. Given that most typical DC motors operate most efficiently above 150 Hz and given the low operating velocity requirement of this application a motor controller would be required to provide the desired drilling

conditions.

A direct drive with a motor controller will allow the system to dictate the operating parameters such as maximum torque and velocity and monitor the motor output and it response to the changing torque requirement at the tool tip. The added benefit is that a higher level system can use this low-level response to determine the state at the tool tip and control the overall system accordingly.

Motor Control

A typical motor voltage characteristic is expressed in equation 4.7 (3).

$$V = K_v\omega + IR \tag{4.7}$$

Where V is the voltage, K_v is the motor voltage constant, ω is the angular velocity, I is the current and R is the resistance of the stator windings.

From 4.7, the velocity is dependent upon the voltage applied across the motor. It is for this reason that the use of the voltage is the most common method of velocity control. This provides two alternatives, pulse width modulation *(PWM)* or the use of a linear servo amplifier. Typically, at high speed, velocity is directly proportional to the voltage across the motor. However, at low velocities the current contribution exceeds the velocity term, making it more important to control the motor current.

A standard control algorithm is the proportional, integral and derivative *(PID)* controller.

PID controllers generally are concerned with controlling only one parameter and the gain values are tuned to provide optimum performance for that parameter, for example velocity. However, precise velocity control induces large fluctuations in the motor current, which in the case of the micro-drilling system, obscures the torque feedback. It is for this reason that analytical or manual tuning techniques cannot be used to attain optimal performance. This application is not only concerned with accurate velocity control but, more importantly, also with the sensitivity of the torque measurement.

Controller Parameters

A fundamental requirement for the successful design of a controller is the determination of the value of the controller parameters such as the PID and feed-forward gains. Bansal *et al* (32) developed a simulation model for use in the TuneLearn software application used for predictive maintenance in industrial applications.

Initially, the primary objective of TuneLearn was to generate training data for training the neural-network to be used in a real-time predictive maintenance system. The model generates the motor torque and velocity feedback characteristics based on the system parameters. Further work validated the simulation model and verified the use to simulate a real production machine (30).

An ideal solution would be to tune the micro-drill controller in an on-line environment, however this approach is impractical. Simulation modeling is a valuable alternative to conventional tuning techniques provided that the model is fully validated against a real controller (63). Bansal developed an algorithm based on this simulation model that effectively applied it in reverse, such that the input would be the desired motor torque and velocity profile, and the corresponding output would be the optimum controller parameters[1].

Simulation model

The simulation model employs a conventional PID controller in a closed loop form as shown in figure 4.17. The model supports a wide range of control applications and, therefore, uses position, velocity and current loops. However, the choice of the loops is based upon the type of control application, as indicated in table 4.1.

Given that of primary concern is constant drilling conditions for this application, the controller uses a velocity servo configuration as such the position loop in the model is not used. The PID loop begins with a velocity loop, the velocity loop calculates velocity error by subtracting the velocity feedback (obtained by differentiating the motor position) from the velocity command. The output of the velocity loop is the current command, which is calculated using the velocity loop

[1]The work in this section relating to TuneLearn and the simulation model was carried out in collaboration with Dheeraj Bansal (31, 32, 33)

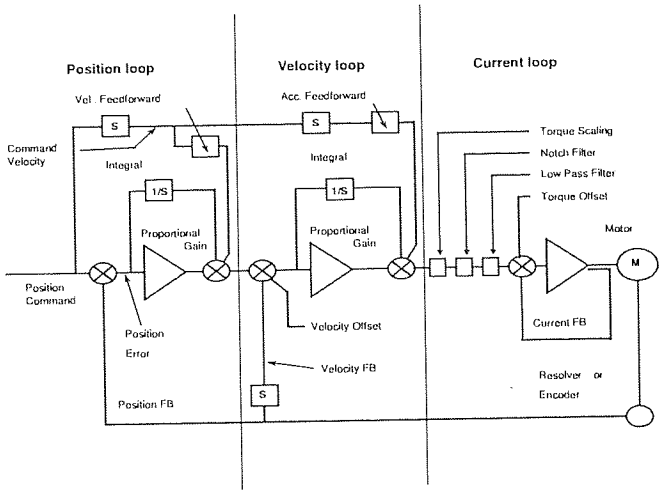

Figure 4.17: *TuneLearn simulation block diagram.*

Table 4.1: *Loop configurations of TuneLearn*

	Position Feedback Source	Velocity Feedback Source	Torque Offset	Velocity Loop	Position Loop
Position Servo	Motor	Motor	On	Yes	Yes
Velocity Servo	None	Motor	On	Yes	No
Torque Servo	None	None	On	No	No
Auxiliary Position Servo	Auxiliary	Auxiliary	On	Yes	Yes
Dual Position Servo	Auxiliary	Motor	On	Yes	Yes
Motor Dual Command Servo	Motor	Motor	Off	Yes	Yes
Auxiliary Dual Servo	Auxiliary	Auxiliary	Off	Yes	Yes

gains and the velocity error. The current command is carried forward as input to the current loop. The current command is filtered using a low pass filter within the current loop. The filtered current command is then used by the output stage to drive the motor.

Motor Model

The initial inputs to the model are a velocity profile and a variable load torque profile generated by the compliant model described in chapter 2. The profiles are shown in figures 4.18 and 4.19. This profile was added to the system parameters during the simulation of the micro-drill. The model uses a typical DC motor

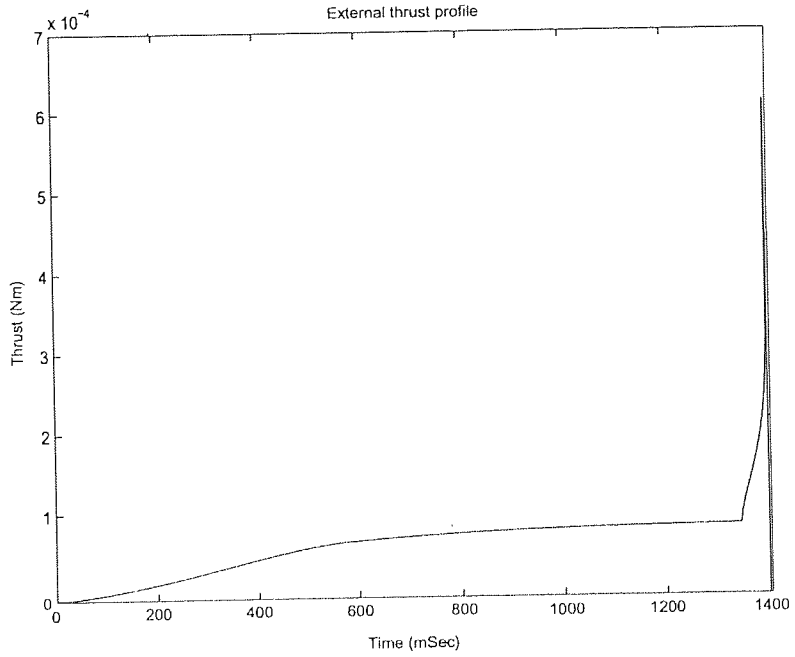

Figure 4.18: *Simulated torque profile.*

model taking into account motor and load inertia, friction torque.

The total inertia of the system J, is given by equation 4.8.

$$J = J_M + J_L \tag{4.8}$$

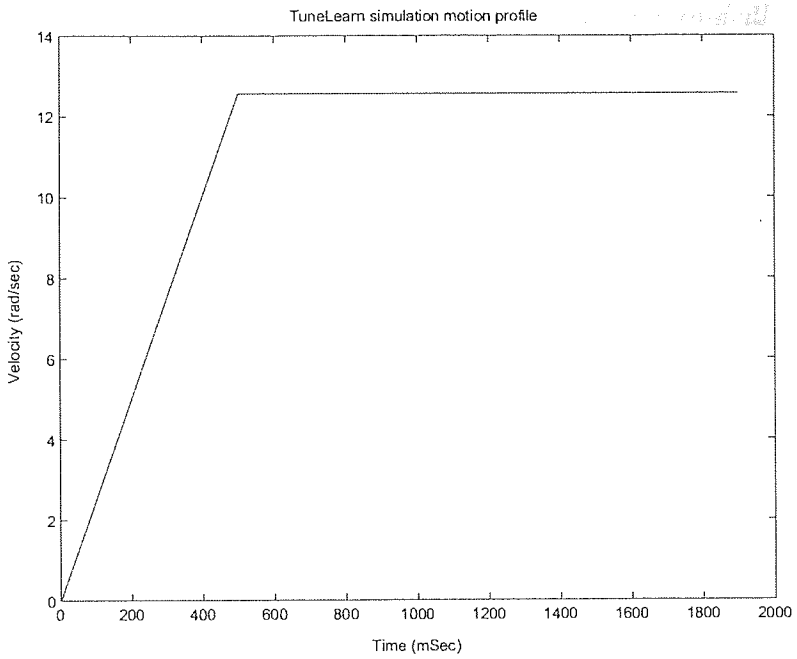

Figure 4.19: *Simulated velocity provifile.*

Where J_M and J_L denote the motor inertia and load inertia respectively. The total inertia is then used to calculate the acceleration torque, A_T, of the sub-profile using equation 4.9.

$$T_A = J \times \frac{d\omega}{dt} \tag{4.9}$$

Where ω is the angular velocity, dt is the sub-profile duration equal to the time interval and $\frac{d\omega}{dt}$ is the angular acceleration of the motor. The total torque of the system T, can be found using equation 4.10

$$T = (T_F + T_{Fm}) \times S \tag{4.10}$$

F_T represents friction torque of the sub-profile and F_{Tm} is motor friction torque. S is a constant determined by the rotational direction as shown below:

1. equal to 1, when the motion is in the clockwise direction;
2. equal to -1, when the motion is in the anti-clockwise direction;
3. equal to 0, when the motor shaft is stationary.

Table 4.2: *Motor parameters for the clinical micro-drill.*

Parameter Name	Value	Units
Motor Type	Maxon RE-10	-
Motor Inertia	10^{-8}	kgm^2
Motor torque constant	0.009	Nm-A
Motor peak torque	0.00324	Nm
Motor rms torque	0.00159	Nm
Motor friction torque	0.00005274	Nm
Motor maximum speed	19000	rpm

Summing acceleration torque, T_A, gravitational torque, T_G, friction torque, T_{Fm}, and instantaneous load torque, T_L^t, we obtain equation 4.11.

$$T = T_G + T_A + F + T_L^t \tag{4.11}$$

There T is the total torque.

Based on the torque requirement of the micro-drilling application a suitably sized motor was selected, the parameter of which are shown in table 4.2.

Velocity loop

As the position loop is not used in this application, the output of this stage is simply differentiated to determione the velocity for input into the velocity loop. Within the loop, the actual velocity V_A^t, is subtracted from the velocity command, V_{cmd}^t, as shown in equation 4.12.

$$V_{err}^t = V_{cmd}^t - V_A^t \tag{4.12}$$

Where V_{err}^t is the velocity error. Subtracting the velocity error of the previous time interval(V_{err}^{t-1}) from the current velocity error (V_{err}^t) gives the differential velocity error 4.13

$$V_{errdiff}^t = V_{err}^t - V_{err}^{t-1} \tag{4.13}$$

Similarly, the integral velocity error, V^t_{errint}, is calculated using equation 4.14.

$$V^t_{errint} = V^{t-1}_{errint} + V^t_{err} \tag{4.14}$$

Taking the values of the velocity error, V^t_{err}, the differential velocity error, $V^t_{errdiff}$, and the integral velocity error, V^t_{errint}, from 4.12, 4.13 and 4.14 to form a PID equation gives equation 4.15.

$$I^t_{cmd} = (V^t_{err} \times K_p) + (V^t_{errint} \times K_i) + (V^t_{errdiff} \times K_d) + (\frac{V^t_{ff}}{t} \times K_{ffa}) \tag{4.15}$$

The acceleration feed-forward gain, K_{ffa}, generates a current command, I^t_{cmd}, proportional to the derivative of the velocity command. The current command from 4.15 is passed as an input to the current loop.

Current loop

The current command, I^t_{cmd}, is scaled and filtered using a low pass filter. The filtered value of current command is converted to a voltage command using equation 4.7 and is output to an amplifier to drive the motor. Finally, a quadrature encoder on the motor provides position feedback for the analysis of the next time increment, thereby closing the loop.

Simulation Results

The remaining parameters to enable the simulation to run are shown in table 4.3, these include the controller update rate and encoder resolution.

The simulation results are shown in figure 4.20.

Figure 4.20 shows the theoretical input torque profile generated using the model presented in section 2.2 overlaid with the output torque profile from the TuneLearn simulation model. It can be seen that the output torque, derived from the motor current, matches the input profile very closely. The wider spread of

Table 4.3: *Configuration parameters for simulating the clinical micro-drill.*

Parameter Name	Value	Units
Coarse Update Rate	1	mSec
Sercos Rate	1	mSec
Motor Cycles	1024	per rev
Motor Interpolation	8	-
Fine Update Rate	125	μS
Current Loop Bandwidth	1000	Hz
Drive Resolution	4096	counts/motor rev
Loop Configuration	Velocity Servo	-

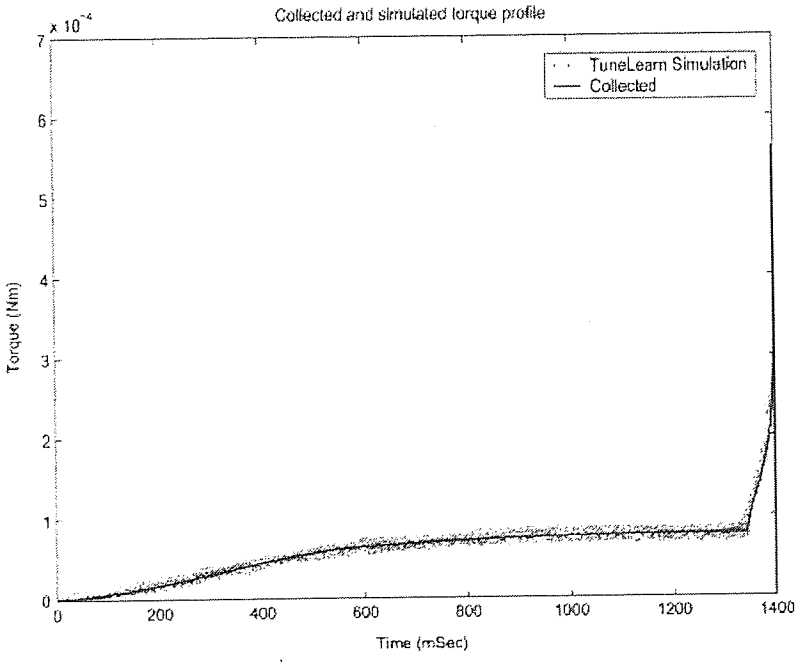

Figure 4.20: *Simulation results with the input load profile.*

Table 4.4: *Controller determined by simulating the clinical micro-drill.*

Parameter Name	Value
Velocity Proportional Gain	100
Velocity Integral Gain	20
Velocity Differential Gain	100
Velocity Feed-forward gain	0
Current Proportional Gain	1

points is representative of noise introduced to the motor current signal by the control system. The model uses the controller configuration and a model of the physical system to generate the controller response taking into to account factors such as the update rate, motor time constant and the resolution of the encoder feedback.

In addition to generating the output torque profile, the simulation model generates the optimum control parameters for the PID loop. These control parameters are shown in table 4.4.

Controller Implementation

The test setup for the controller was designed to reflect the capability of the system to be implemented in the surgical micro-drill. The system block diagram is shown in figure 4.21.

A prototype board was developed to explore the motor control and sensory feedback solutions. The controller was based around the Microchip PIC18F2320 micro-controller (7). The board has a dedicated PID motor controller that provides current and velocity feedback to a computer via the serial port, allowing discrete velocity control of the motor. The board also featured external analogue to digital channels allowing force data to be channeled through the card, thus removing the need for an external analogue to digital converter card within the computer. A circuit diagram for the test rig controller can be found in the appendix in figure A.1.

A suitable motor was sized to correctly supply sufficient torque to drill whilst providing sufficient bandwidth. The drilling of hard bone in this application typically requires a maximum torque of approximately 1.5 mNm, the Maxon

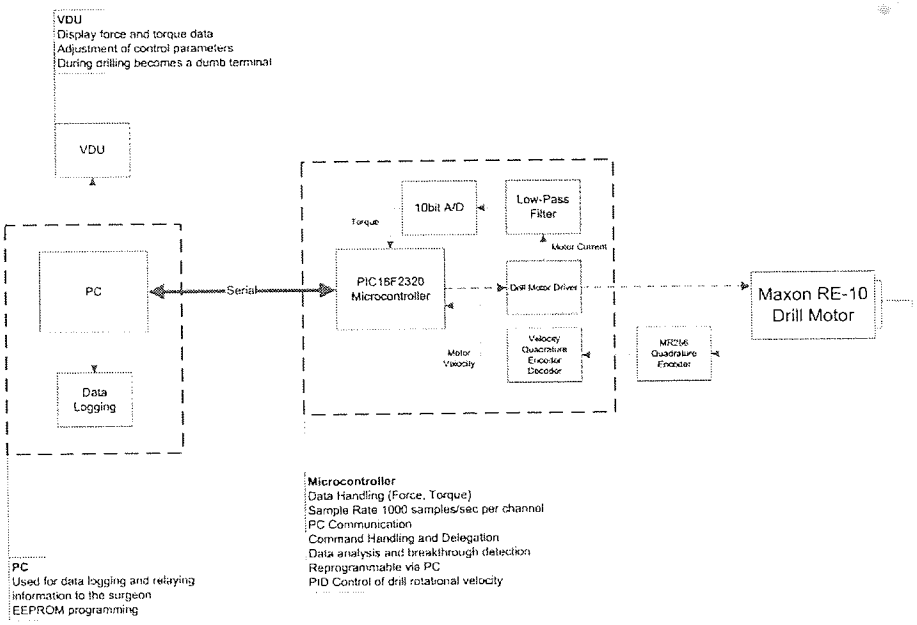

Figure 4.21: *Prototype controller schematic.*

RE10 motor (3) was chosen as it can deliver a maximum continuous torque of 1.59 mNm when running at its rated voltage. The motor was fitted with a MR256 quadrature encoder, the output of which was passed to a dedicated quadrature decoder providing an interpolation factor of four.

The motor current was monitored via a current sensing resistor incorporated within the motor driver. The signal was passed through a low pass filter to an analogue to digital converter within the micro-controller. The motor is driven directly from the micro-controller using pulse width modulation at 45 kHz via a full bridge driver rated up to 12 $Volts$. The process parameters were set via the computer and it logged all data sent from the board.

The micro-controller operates at 40 MHz, with a sampling and PID update rate of 1000 samples per second. A flow diagram of the software loop is shown in figure 4.22.

The PID loop operated using a velocity set point, the velocity error was calculated based on this point. The units of the gains are changed and scaled to provide a current command in mA for input into the current loop. The current loop then calculated a suitable output level to achieve the desired velocity output. This ensures that the motor delivers maximum torque when required, and

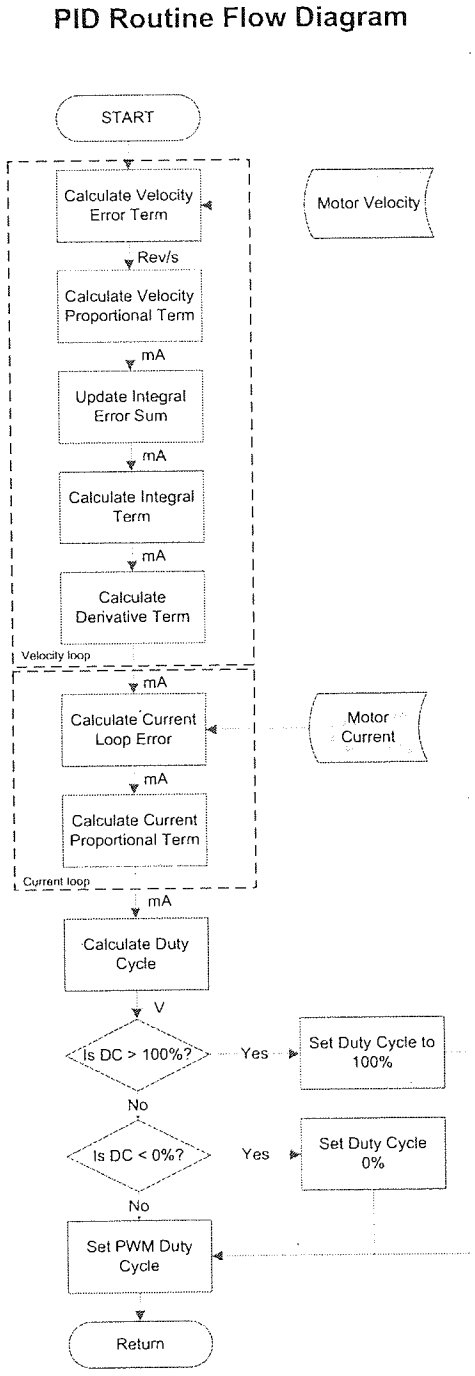

Figure 4.22: *PID algorithm flow diagram.*

maintains motor velocity.

The algorithm is identical to that described earlier in this chapter. The calculations performed inside the PID loop are optimised to reduce the software overhead for faster execution, as such, the units of the gains are calculated and scaled outside the loop.

Within the PID loop, the velocity error term is calculated using equation 4.16.

$$V_{err} = V^t_{cmd} - V^t_A. \tag{4.16}$$

Where V_{err}, V^t_{cmd} and V^t_A denote the velocity error, the set point and the encoder count respectively. The velocity error is then used to calculate the proportional, integral and derivative terms for the velocity PID loop using equations 4.18 to 4.19.

$$V^t_{errint} = V^{t-1}_{errint} + V^t_{err} \tag{4.17}$$

$$V^t_{errdiff} = V^t_{err} - V^{t-1}_{err} \tag{4.18}$$

Where V_{err} is the proportional term, V^t_{errint} is the integral term, V^t_{errint} is the differential term. The output of the loop is then calculated by summing the terms multiplied by their respective gains as shown in equation 4.19.

$$I^t_{cmd} = (V^t_{err} \times K_p) + (V^t_{errint} \times K_i) + (V^t_{errdiff} \times K_d) + (\frac{V^t_{ff}}{t} \times K_{ffa}) \tag{4.19}$$

Where K_p is the proportional gain, K_i is the integral gain and K_d is the differential gain.

Multiplying the current command of the velocity loop with the current loop proportional gain, K_{pc} gives equation 4.20.

$$V^t_{cmd} = I^t_{cmd} \times K_{pc}. \tag{4.20}$$

K_{pc} is scaled to give a value directly proportional to the corresponding duty cycle of the pulse width modulation *(PWM)* module.[1]

It is worth noting that K_{ffa} is 0 thus this term is not included in the calculation.

Drilling tests were performed using the motor test rig shown in Figure 4.23. This rig provided a constant force to be applied to the drill tip allowing direct calculation of the torque.

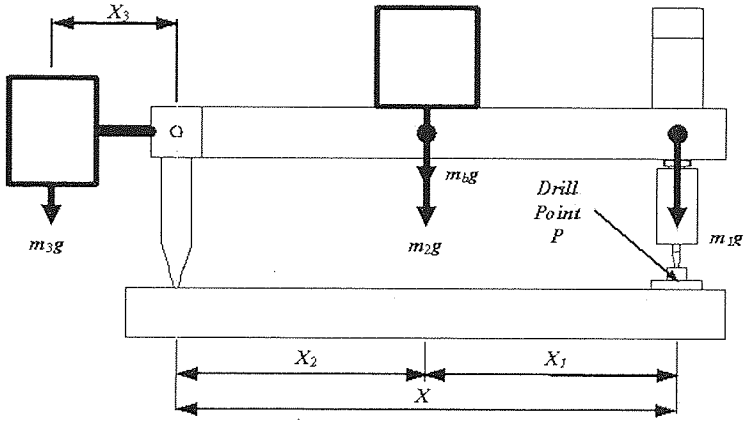

Figure 4.23: *Constant feed force test rig.*

The force at the drll tip is given by equation 4.21.

$$F_p = \frac{m_2 \times g \times X_2}{X} \tag{4.21}$$

Where F_p is the force at the drill point, m_2 is the mass of the counter balance, m_1 is the load and X and X_2 denote the load position.

The force applied at the drill point was adjusted by adjusting the load and length of X_2, very fine adjustments down to approximately 0.001N could be made. Although the motion of the rig is rotational, the angle through which the arm moves is very small and can be considered to be negligible. This is also beneficial

[1]The duty cycle is the ratio of the on voltage time to off voltage time. For example, 50% duty cycle would be equivalent to 6 $Volts$, ie half of the maximum voltage.

as breakthrough could be considered friction free.

This allowed the analysis of each motor torque profile for each set of PID parameters. The rig was designed to provide a constant axial force and friction free breakthrough, the upper section of the rig is counter balanced such that the force applied by mass m_2 is the only force exerted on the drill tip. Given that the axial force is a known constant, the torque can be calculated using the drilling model described in chapter 2.1.

Controller Performance

The initial set point for all tests was 2 Hz. The test configuration shown in the implementation section was used with a load of 100 g (This equates to an axial force of 0.5 N). The test sample was a piece of high density card of thickness 0.25 mm. The drill bit used was a standard 0.6 mm dental cutting burr.

Initially, the motor velocity set point of 2 Hz was used to assess the motor performance. The drive voltage was determined using equation 4.7 and the proportional gain was set to 1, all other terms were set to 0. The desired velocity was so far outside the normal operating range of the motor it was found that the system did not have sufficient torque to achieve the set velocity or drill successfully. The set velocity was increased until the system provided sufficient torque to complete the drilling process. The minimum sustainable velocity found with this process was approximately 7 Hz. An example of the current and velocity characteristics of the motor operating in an open loop configuration are shown in figures 4.24 and 4.25.

This clearly demonstrates that the system cannot function without a control loop. Note the reduced drilling time due to the higher drilling speed.

Velocity PID loop: The system was manually tuned using the decreasing velocity error algorithm (30). This should provide optimum velocity control. The results from the tuned velocity PID loop are shown in figures 4.26 and 4.27.

While it can be observed that velocity control is now approaching an optimum and the system can now maintain the set velocity, there are sizable fluctuations in torque characteristic that may mask changes due to micro-torques experienced at the tool tip. Due to the extreme operating range, the motor did not conform

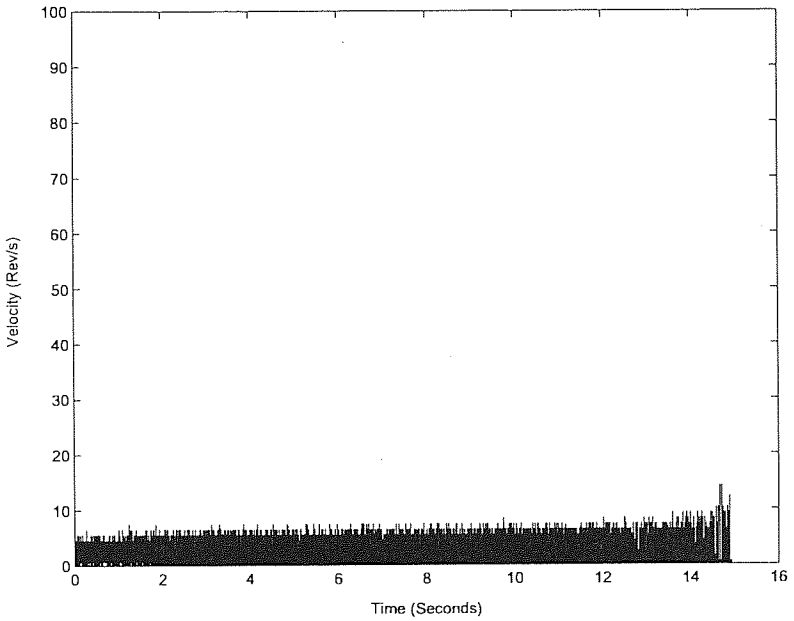

Figure 4.24: *Motor velocity without the controller enabled.*

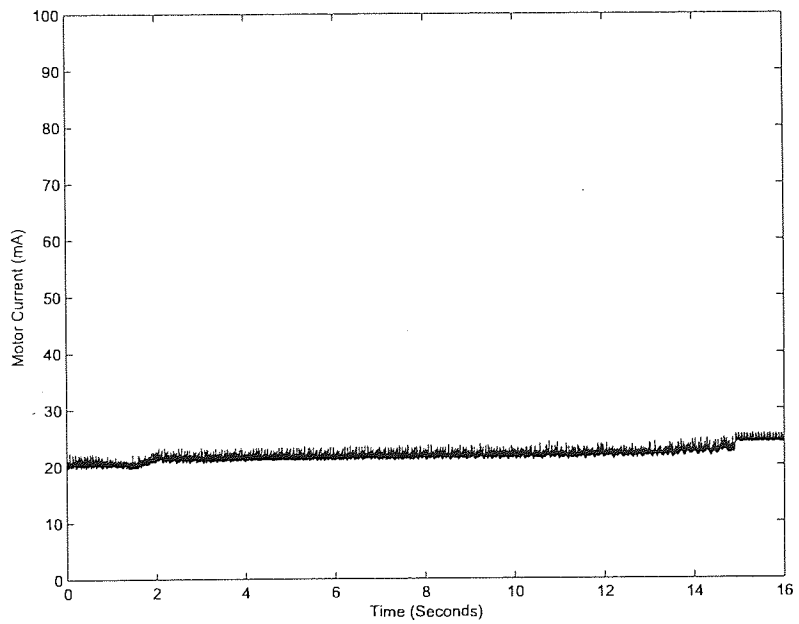

Figure 4.25: *Motor current without the controller enabled.*

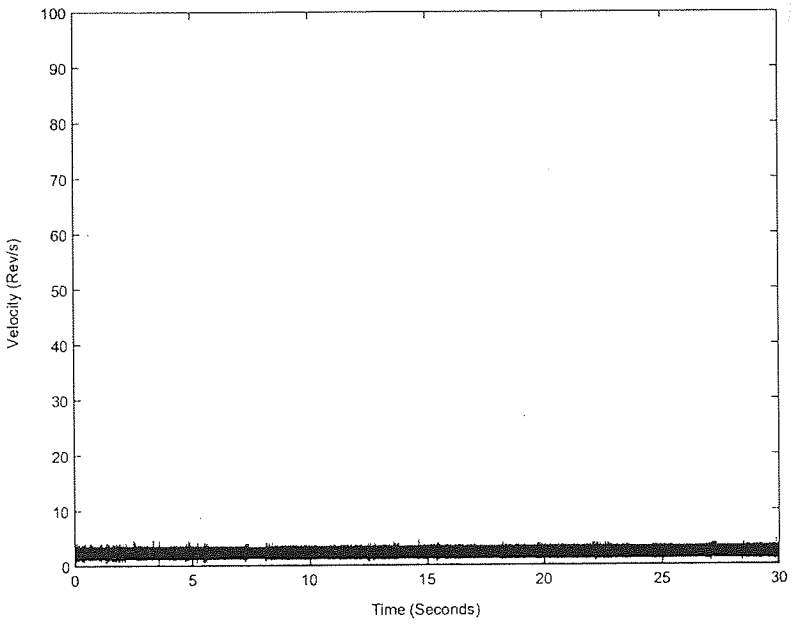

Figure 4.26: *Motor velocity with only velocity control enabled.*

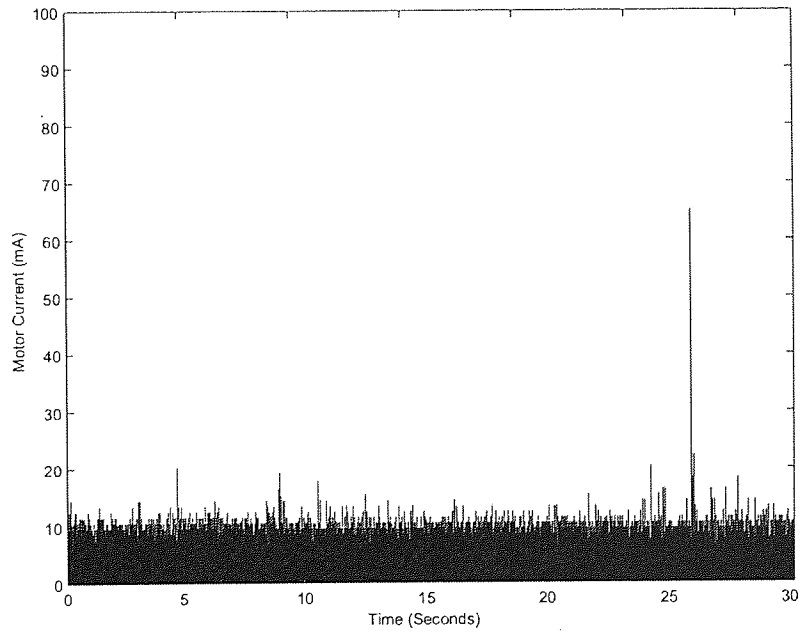

Figure 4.27: *Motor current with only velocity control enabled.*

to the documented characteristics, as such, the fluctuations in motor current required to maintain velocity while loaded were as high as 25%. This indicates that it is not only necessary to control the velocity, but the system also needs a current control component.

Velocity and current PID loop: The velocity and the current loop in sequence represent a velocity servo configuration, which was easily simulated using the TuneLearn application (33). Figures 4.28 and 4.29 show the velocity and motor current results obtained by implementing the velocity servo-control parameters generated.

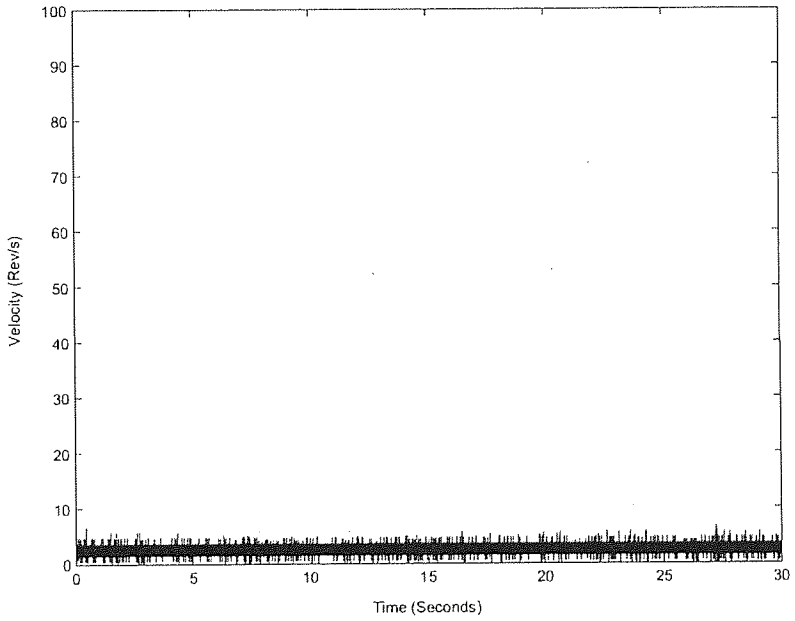

Figure 4.28: *Motor velocity with both velocity and current control enabled*

Tests were performed at the lower operating limit of 2 Hz. The mean velocity was 1.98 Hz with a standard deviation of 0.27 Hz and torque fluctuations of less than 5% were observed. The current loop ensures there is sufficient torque to maintain velocity whilst still retaining the finer detail in the motor current transient. This illustrates that the velocity servo control configuration, i.e. velocity and current PID loop in sequence, can be used effectively for the micro-drilling application.

Although successful, this system is still not ideal. A higher degree of control

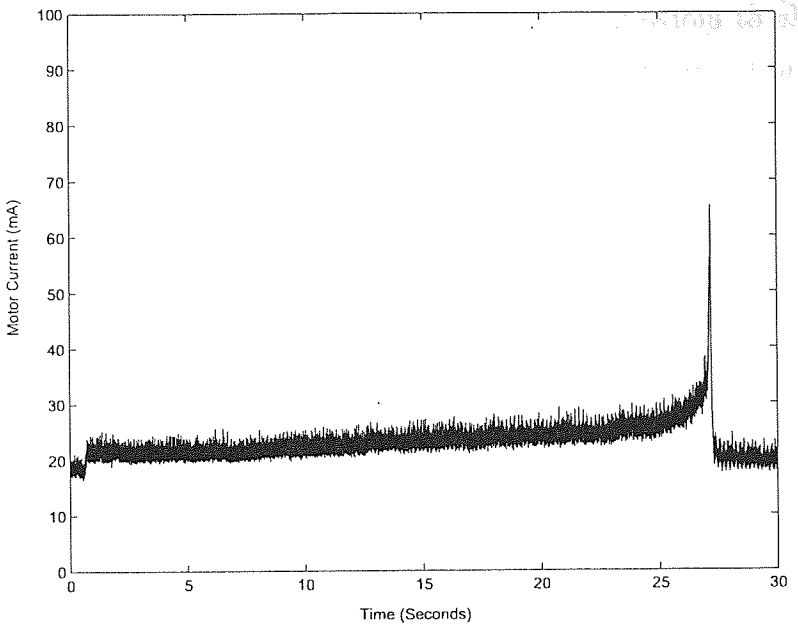

Figure 4.29: *Motor current with both velocity and current control enabled.*

was not achievable due to mechanical and electronic limitations of the test system. The MR256 (3) is the highest resolution quadrature encoder that can be used on a such a small scale. When operating with a PID update rate of 1 ms, at 2 Hz, the micro-controller can only receive a maximum of 8 pulses in the time between updates. This limits the accuracy of the velocity measurement to 0.25 Hz, at the lower operating limit of the motor. Hence, this increases likelihood of fluctuations at low velocities. The analogue to digital converter used for current measurement is also limited to a 10 *bit* conversion, providing a maximum resolution of 5 mV. These factors significantly increase the noise present in the signal, despite this, and bearing in mind there is no signal conditioning implemented, the performance of the controller and torque feedback is sufficient for the micro-drilling application.

4.2.2 Tool Support

The tool support has two main functions:

1. To support the weight of the drill unit such that is can be positioned easily,
2. to provide a rigid support when drilling is commenced.

As such the support must have sufficient degrees of freedom to allow enough movement so the drill can be positioned in the correct position prior to drilling. Once in position the support must lock rigid, with no backlash to maintain the correct position.

The initial clinical prototype employed two segment arm with ball joints at the end of each section. While the ball joints allowed a large degree of movement at each joint, they were unable to support the weight of the drill unit when unlocked, thus had to be held in position until the pneumatic locking mechanism was engaged, although was partly due to consideration of the safety factors. The use of two sections severely limited the level of macro alignment that could be achieved.

The Operational Field

Given that one of the main functions of the tool support is to provide a rigid base to operate the drill from, a solid mounting point is required. Most operating tables come fitted will mounting bars along each side especially for this purpose.

A typical operating arrangement is shown in figure 4.30.

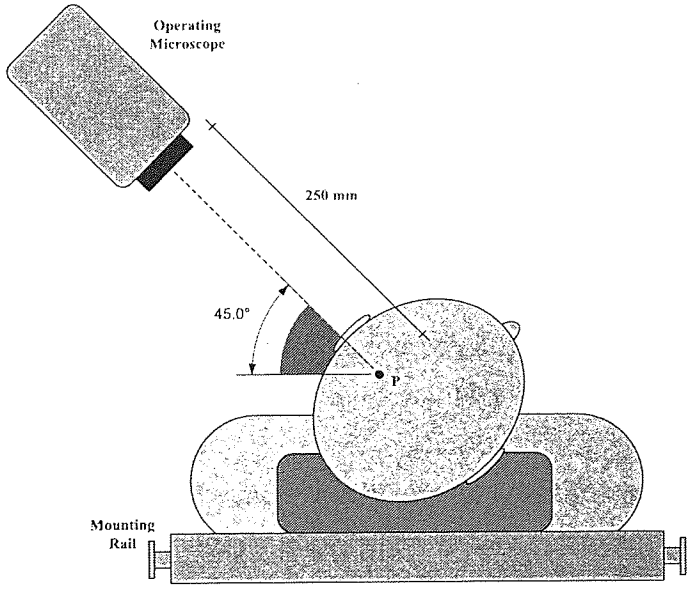

Figure 4.30: *Angle of approch and distance to the operative site.*

The patients head is orientated at approximately 45° so that the surgeon can use an operating microscope. The focal length of a typical binocular scope is between 150 *to* 250 *mm*. The position of the microscope, the patient and the operating table effectively define the area in which the drilling system must be fitted and operated. This is shown in figure 4.30 by the light grey shaded area. The dark grey segment shows the acceptance angles for access to operative site which the drill unit must be able to achieve. This angle is typically between between 0° and 45°, nominally 30°.

In the redesign of the system, the three segment support provided significantly more freedom. Based on the angles described in figure 4.30 this design can be positioned in the correct orientation as depicted in figure 4.31.

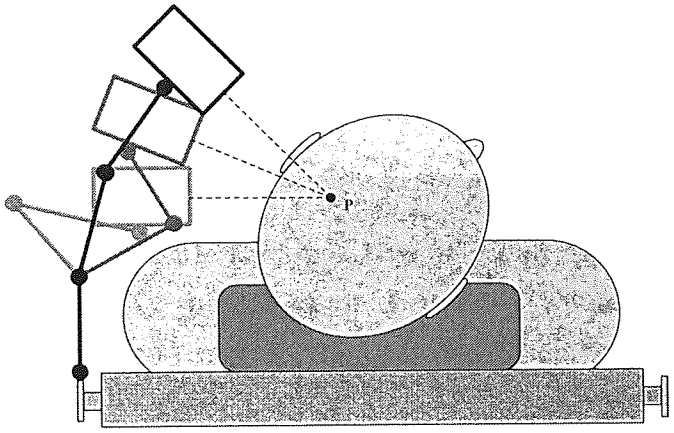

Figure 4.31: *Drill positioning required to reach to the operative site.*

While the use of ball joints allow for more flexibility this may lead to movement as the system is locked or if an external load is applied to the drill unit during the procedure. This is particularly true of joints located farthest from the drill unit as the arm acts as a lever.

Single axis rotary joints are more constrained and thus are more stable, particularly at high load points. During locking a force can be applied perpendicular to the rotational axis and no movement is induced.

The support arm consists of two horizontal axis, two vertical axis and a single ball joint connected to the drill unit mount. Given the short distance from the

drill unit this joint is not affected by severe loading and thus is sufficiently stable.

The detail design of the are arm will be discussed in more detail in the next chapter, a concept design of the locking arm is shown in figure 4.32.

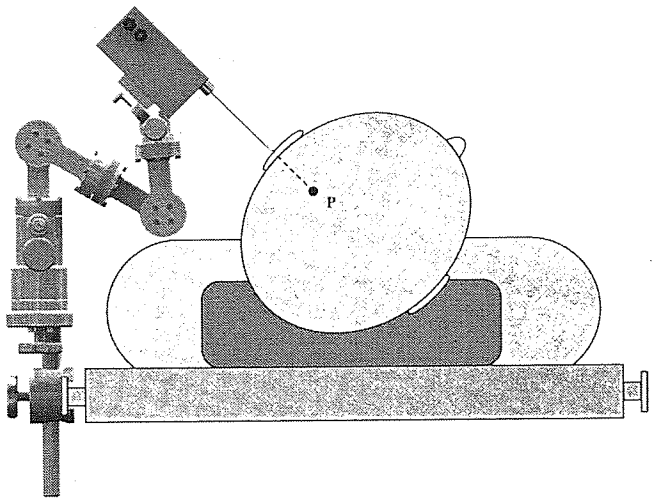

Figure 4.32: *Position of the actual drill as it may be used.*

The design clearly fits inside the operative field and can achieve the desired angles. To test the usability, and to assess if this design had sufficient freedom, a model was prototyped and tested in the operating theatre.

Rapid Prototyping and Evaluation

3D modeling and rapid prototyping are invaluable tools that can save a significant amount of time and money when developing new products. In this project the initial design of the support and drilling unit were prototyped and assessed for usability and suitability for use in the operating theatre.

The 3D model shown in 4.33, was drawn in SolidWorks® and was manufactured on a Dimension 3D printer in ABS plastic.

The completed model was tested in the operating threatre to ensure that it would not interfere with the surgeons tasks during the rest of the procedure. It also allowed the freedom of movement to be assessed to ensure it is easy to operate

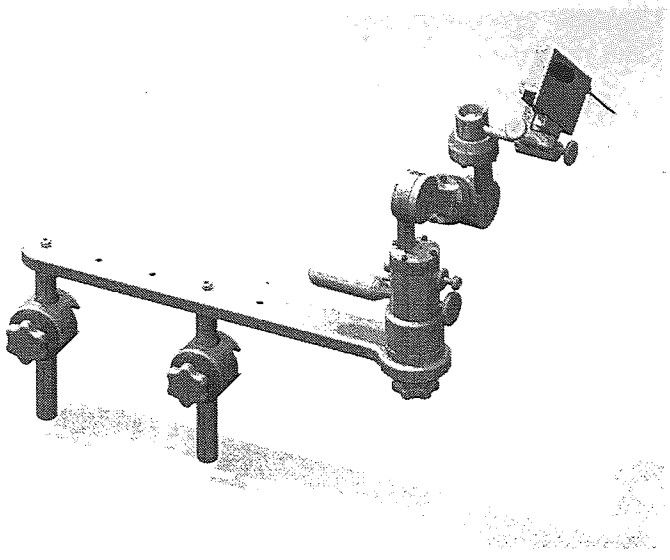

Figure 4.33: *A 3D rendering of the final drill design.*

and that access to the operative site could be achieved. Figure 4.34 shows the model being assessed in theatre.

The outcome of the tests were positive, the clinicians found the support arm easy to operate and manouvre. The model also demonstrated that the design would be able to reach the operative site with ample clearance. While in theatre the model was also successfully draped for sterilisation.

4.3 Conclusions

The compliant drilling technique was effectively applied to a clinical prototype. The ability to precisely control a drill bit up to the distal interface in a flexible tissue and then penetrate the medial surface in a controlled fashion, minimising protrusion was successfully demonstrated. To achieve this, the drill self-referenced to the deflecting tissue. The technique consisted of three elements:

- Controlled investigative drilling (up to the start of breakthrough);
- breakthrough detection (establishes the reference);
- breakthrough control.

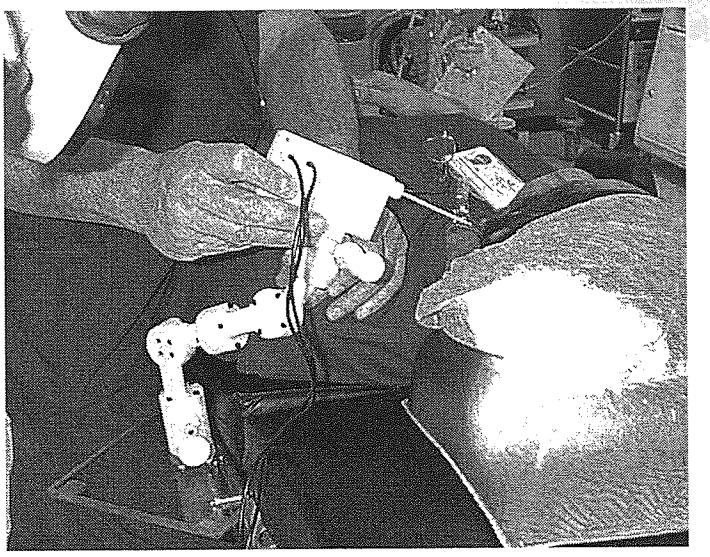

Figure 4.34: *The 3D model being tested in the operating theatre.*

The solutions developed for these three elements enabled the drilling technique to control drill penetration and breakthrough, with a resolution of$\pm 20\ \mu m$. This is under the conditions where the drilled material was mounted compliantly and the stiffness, thickness and material properties were unknown. .

The method used ensured that protrusion beyond the far surface of the drilled material was minimised, taking variations in the drilled medium and data characteristics into consideration. The drilling system also provided feedback on the progress of drilling and could be used to automatically identify the critical states of the process.

A series of laboratory tests using this method showed the need to match sensor ranges to the typical force and torque levels of the application in order to maximise the signal to noise ratio. A strong signal to noise ratio increases performance in the detection of breakthrough. With lower SNR's, detection was less precise and the rate of false positive detection was higher.

All previous versions of the clinical micro-drill have relied on the compliance of the material to generate the typical drilling characteristic that enables the detection of the onset of breakthrough. When drilling stiffer materials the breakthrough characteristic is far more abrupt and the onset of breakthrough is significantly faster making detection difficult. This is due to the lack of compli-

ance. This may be negated my the introduction of compliance within the drilling unit itself.

The reduction in performance with lower SNR values was shown to lead to a fail-safe mode through false positive detection of the onset of breakthrough rather than failed detection. For this reason the system can be said to be intrinsically safe. The structured and predictable nature of the control strategy make this drilling technique suitable for surgical application.

Trials on cadaveric temporal bone samples proved successful in the laboratory environment but suffered as a result of low force levels and suceptability to external vibrations in an uncontrolled environment. For further clinical trials to be conducted it was clear that not only the sensor sensitivity and resolution required increasing to improve the SNR, the sensitivity to external influences requires reduction.

Although designed as a clinical demonstrator, the prototype drill is not suitable for clinical deployment. Feedback from clinicians operating the device indicated that improvements needed to be be made to the way in which the device was positioned and operated and issues regarding sterility needed to be addressed.

When looking to redesign the system the following considerations need to be taken into account:

1. tool manouvrebility and stability,
2. sensor sensitivity and resolution,
3. tool sterility,
4. tool support,
5. operating theatre integration.

A series of studies were conducted to investigate some of the technical challenges presented by the surgical drilling procedure.

To address the issue of force and torque sensor precision and resolution alternative sensing strategies were investigated and potential solutions were evaluated.

The system is well suited to the use of a cantilever arrangement for force measurement however a more appropriate method of deflection measurement is

required. The most appropriate method found employed a non-contact eddy current sensor, the working distance, measurement resolution and form factor allow maximum flexibility within the system. This combined with detailed cantilever design means the system can be easily adapted to the task at hand to optimise performance.

Torque measurement to any degree of accuracy at this level is difficult to achieve and there are few, if any, off the shelf solutions. The most effective method of toque measurement available is to derive it from the motor current, however this has technical challenges to overcome in itself. A novel approach for the design and optimisation of a PID controller for use in a clinical micro-drilling system was described. The use of the TuneLearn simulation model, not only reduced the time to achieve the optimum performance, it also allowed an acceptable compromise between the two desired parameters, which ordinarily would be very difficult to achieve. The motor velocity was held to within 1% of the set point and the current fluctuations of less than 5% were observed when the system was operating under load. The current system has no form of signal conditioning other than a simple RC low pass filter designed to remove noise induced by the PWM signal, however if this was to be implemented, a degree of filtering may be required. It may be preferable to use a linear amplifier rather than a PWM drive, to reduce the high frequency component of the noise.

With the aid of a 3D model the suitability of the initial designs of the tool support were assessed. It was found that there was sufficient movement and the operative site was easily reached. Clinicians also found that the arm was easy to operate. The main observations were summarised as:

1. The system was easy to manouvre into the correct position,
2. The system will fit comfortably into the available space in the operating theatre,
3. Some of the thumb screws were difficult to use, especially with gloves on,
4. The field of view over the top of the drill unit when using the microscope was acceptable.

5. The support arm and drill unit can be easily draped in theatre for sterility.

Chapter 5

Clinical Applications

5.1 ENT

Ear Nose and Throat (ENT) is one area of surgery to which the use of smart mechatronic tools are particularly applicable (47). This area of surgery is primarily concerned with the skull and the surrounding tissues. The skull is one of the most complicated and thus fragile bones in the human body containing sensitive structures such as the hearing and balance system. Ear surgery is particularly suitable as there are many procedures that require drilling up to or through thin sections of compliant tissue without penetrating or damaging sensitive structures that may lie beyond the distal surface. While many procedures present similar challenges, this research will focus on the drilling of the stapedotomy, for which the original clinical demonstrator was developed; and the cochleostomy as part of the cochlea implant procedure. This chapter will present the conventional techniques and the clinical challenges they represent.

Table 5.1: *Deafness levels as defined by the RNID. http://www.rnid.org.uk*

Level	Description	Typical Audible Range
Mild deafness	People with mild deafness who have some difficulty following speech, mainly in noisy situations.	$25dB$ and $39dB$
Moderate deafness	People with moderate deafness who have difficulty in following speech without a hearing aid.	$40dB$ and $69dB$
Severe deafness	People with severe deafness who rely on lipreading, even with a hearing aid.	$70dB$ and $94dB$
Profound deafness	People who are profoundly deaf and communicate solely by lipreading.	$95dB$ or More

5.2 Hearing Loss and Deafness

Deafness is the most common of all disabilities. It is estimated that 10% of the world population have some degree of hearing impairment and one third of the population over 65 years of age have noticeable hearing loss. The latest RNID statistics show there are about 9 million deaf or hard of hearing people in the UK alone. Approximately 10% of these are profoundly deaf.

5.2.1 Definition of deafness

Levels of hearing loss vary greatly between sufferers and as such to identify the cause and suitable treatments, the level has to be classified against a predefined criteria. Table 5.1 shows differing deafness levels as defined by the RNID.

Hearing loss and deafness is usually measured by varying the amplitude and frequencies of sounds as they are listened to. The person being tested responds when they can hear a particular tone, the level of the tone is then adjusted until

they can only just hear it. This level is termed the *threshold*. Individuals with thresholds between $0dB$ and $20dB$ across all the frequencies are considered to have *normal* hearing. The greater the threshold level the higher the degree of hearing loss. The typical guidelines for identifying the level of deafness as laid out by the RNID are shown in table 5.1.

There are two principal types of hearing loss that can occur, conductive and sensorineural.

5.2.2 Conductive Deafness

Conductive deafness is a result of disruption to the ossicular chain affecting the mechanical transfer of sound through the middle ear to the inner ear. This results in dampening of the oscillations being transferred to the cochlea so the amplitude of the stimuli at the nerve receptors is severely diminished making sounds appear muffled. Typical causes are shown below:

- middle ear infections;
- fluid build up in the middle ear;
- obstruction of the outer ear;
- damage to the eardrum;
- otosclerosis;
- rheumatoid arthritis.

Most cases of conductive deafness are caused by infections, collectively known as otitis media which is typically treated with medication. Deafness can also be caused by perforation or rupture of the tympanic membrane by a sudden loud noise or physical puncture. In some such cases the eardrum can be repaired by grafting. The predominant cause of conductive deafness, particularly in adults is otosclerosis. This is a chronic hereditary condition in which ossification of the

annular ligament results in the fixation of the stapes footplate to the surrounding bone tissue restricting its movement (71). Rarely rheumatoid arthritis can stiffen the cartilaginous joints between the bones of the ossicles dampening sound transmission. This is treated in the same manor as otosclerosis.

Advances in modern surgical techniques have led to successful treatment of otosclerosis by replacing the stapes with a plastic piston prosthesis through a hole drilled in the stapes footplate, this procedure is known as the stapedotomy. Though effective, the stapedotomy is not a permanent solution as the ossification may continue, eventually fixing the prosthesis in place resulting in a similar degree of hearing loss that was experienced initially. Surgeons are beginning to look toward other means of restoring the lost hearing, for example in the use of Bone Anchored Hearing Aids (BAHA) (43, 83). BAHA's are an increasingly common form of treatment for conductive hearing loss. These devices are well proven, showing significant success (65), and can be upgraded as improvements are made in the future. The fact that they can be implanted under local anesthetic is a huge advantage.

5.2.3 Sensorineural Deafness

Sensorineural deafness is a result of damage to the neural receptors of the inner ear *(the hair cells, located in the organ of Corti)*, the nerve pathways to the brain *(more notably the auditory nerve)*, or the area of the brain that receives and processes auditory nerve impulses. Deafness of this type is usually permanent and it can be congenital or induced by external influences. There are many potential causes, including the following:

- age-related hearing loss
- acoustic trauma to the hair cells
- infections of the inner ear
- Mnire's disease

Aging is the most common cause of sensorineural hearing loss. Over time, as with any part of the body, cell death occurs causing a natural degradation of the neural receptors and pathways. This process can be accelerated by illness or conditions such as Mnire's disease or by continued exposure to loud noise. Unfortunately this damage is permanent, causing irreversible hearing loss.

There are few treatments for sensorineural deafness, for moderate cases treatment involves using a hearing aid amplifying sound to a level that the person can perceive. BAHA's are also being explored for more severe cases (62). For profound sensorineural deafness there is only one possible treatment, cochlea implantation. Cochlea implantation involves implanting a sub-dermal micro-electronic device with an electrode array that is inserted directly into the cochlea. This electrode array directly stimulates the remaining nerve cells using electric impulses that, with time can be perceived allowing a good degree of auditory function.

5.3 Review of current surgical practice

Deploying a new device for a specific application not only requires customisation of the hardware but it is necessary to understand the surgical procedure in detail so that the use of such a device can be integrated as effectively as possible so as to not prolong the time required in theatre or cause the patient undue stress. In addition the benefits that such a device offer can be identified and matched to the specific requirements of the task, potentially improving on current surgical practice and bringing to light potential new applications of the technology. For example, the use of an autonomous clinical micro-drill may significantly reduce the level of access required to reach the operative site when compared to manual techniques, or a different sequence of tasks may reduce risks involved to the patient. When designing a new surgical technique it is necessary to understand how and why the conventional procedure is performed in a specific way to correctly identify the design requirements of a new tool. This includes the surgical sequence, preparation and location of access to the operative site, the surrounding tissues and structures that may need to be avoided and the requirements specific to the task. As such, the descriptions include a number of specific terms that

also include the surrounding structures, thus to appreciate the significance of the steps of the techniques a basic understanding of the aural anatomy is required.

5.3.1 Ear Anatomy

The ear is responsible for both hearing and balance and as such it is a very complicated system. The ear consists of three main regions as shown in figure 5.1.

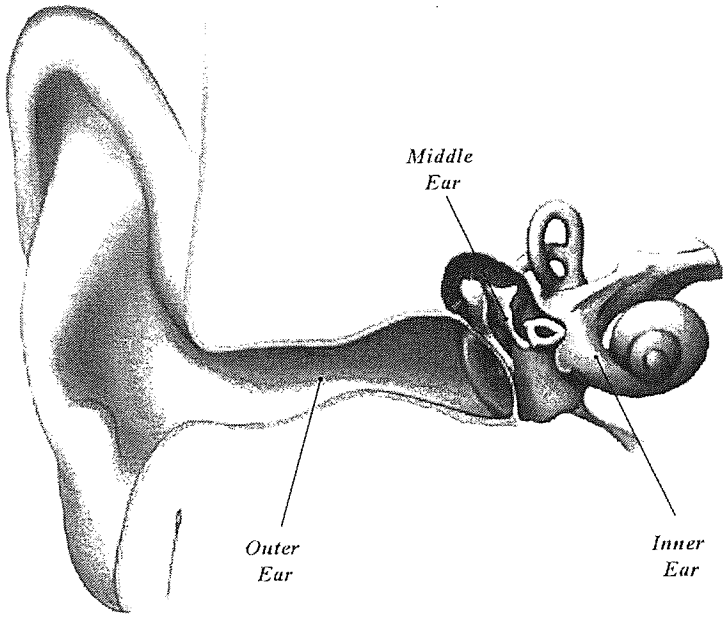

Figure 5.1: *Ear anatomy: The three main regions of the ear (1).*

5.3.1.1 Outer Ear

Figure 5.2 shows the outer ear region. The outer ear consists of the pinna (also called the auricle) and is the visible part of the ear composed of folds of skin and cartilage. The pinna directs sound waves along the external auditory canal to the tympanic membrane. This membrane acts like a drum, hence the term

'eardrum', converting the compressions and rarefactions of the sound waves into a mechanical motion that can be transferred to the inner ear via the middle ear.

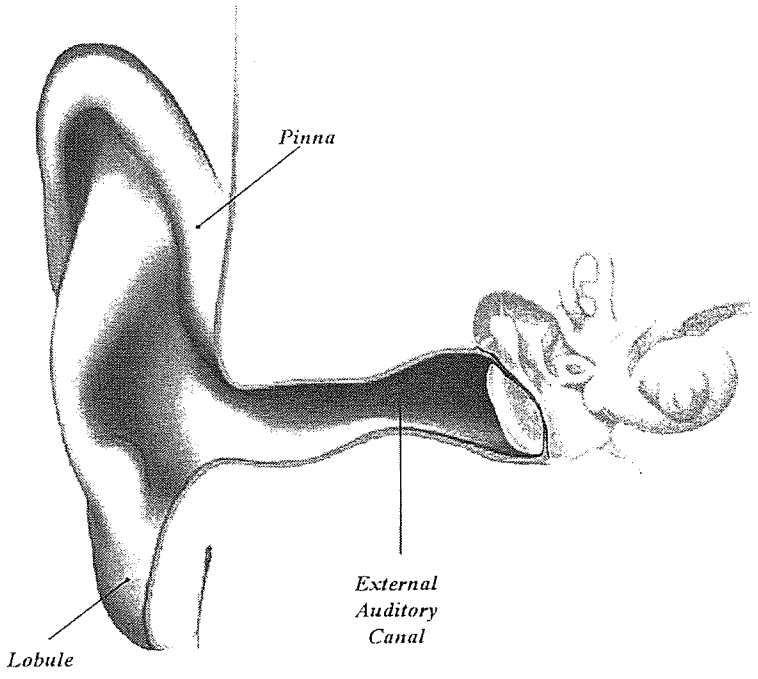

Figure 5.2: *Ear anatomy: The outer ear (1).*

5.3.1.2 Middle Ear

The middle ear space is a small cavity located between the tympanic membrane and the inner ear regions. The posterior wall of the middle ear space leads into the antrum via the middle ear attic *(Epitympanic recess)* which is the largest air cell at the top of the mastoid air system. The anterior wall contains the eustachian tube, its primary function is to equalise the pressure between the middle ear space and the environment to respond to changes in the external pressure. The lateral wall opens into the external auditory canal and is covered by the tympanic membrane. This oscillates in sympathy with sound waves traveling along the auditory canal. Sound is conducted to the inner ear via a chain of small bones known collectively as the ossicles. The ossicles provide a mechanical link between the tympanic

membrane and the oval window, over which the stapes footplate sits. The oval window is located on the medial wall of the middle ear space superior to the round window niche and the promontory. The promontory is actually an exposed section of the basal turn of the cochlea.

The ossicles are shown in figure 5.3. The Malleus*(left)*, Incus*(center)* and the Stapes*(right)*.

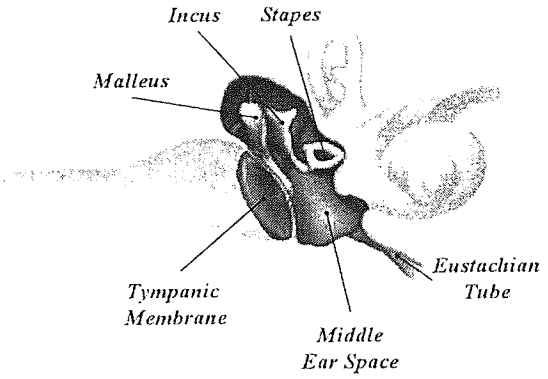

Figure 5.3: *Ear anatomy: The middle ear (1).*

The manubrium of the malleus is attached to the tympanic membrane, the head of which protrudes up into the attic and is connected to the short process of the incus. The long process of the incus extends downwards and connects to the crura of the stapes completing the ossicular chain. The ossicles are thought to act as a mechanical amplifier increasing the amplitude of the sound oscillations to approximately three hundred times their previous level. This can be adjusted by a series of tendons that dampen and hence attenuate high amplitude oscillations that could be potentially damaging, these muscles also serve to pretension the tympanic membrane. The main two tendons are the stapedius and the tensor

tympani. The stapedius emerges from a conical bone cavity in the wall of middle ear space and connects to the crura of the stapes. The tensor tympani is located in the small bony canal and is attached to the manubrium of the malleus.

The mechanical motion of the ossicles is transferred to the inner ear fluid via the oval window. The stapes footplate is attached to the surrounding bone tissue by a flexible ligament *(Annular Ligament)* and is free to oscillate. This oscillation sets up pressure waves that travel up the cochlea spiral located in the inner ear. Beyond the stapes is a small volume of perilymph which acts as a buffer between the stapes foot plate and the membranous chamber of the vestibule. The vestibule is also filled with fluid, however this portion is filled with endolymph.

5.3.1.3 Inner Ear

The inner ear is the most complex part of the ear. It is an extremely intricate series of structures contained deep within a region of the skull known as the petrous portion of the temporal bone. Figure 5.4 illustrates the basic anatomy of the inner ear.

The inner ear consists of two parts, the fragile soft tissue *(Membranous Labyrinth)* is enclosed in a bony protective shell *(Bony Labyrinth)*. The membranous labyrinth is made up of fluid filled channels and compartments. This region contains the both the auditory and the vestibular system. The vestibular system is responsible for equilibrium and balance and the auditory system is primarily for hearing. Both systems are highly integrated sharing much of the same fluid network.

The posterior portion of the labyrinth contains the vestibular system which comprises of the vestibule (which contains the saccule and ultricle), the three semi-circular canals *(anterior, posterior and lateral)* and the vestibular nerve. The semicircular canals are responsible for the detection of angular acceleration. The semicircular canals are set at right angles to each other so as to provide the angular acceleration in each of the three axes. The saccule and ultricle are responsible for the detection of linear acceleration and gravity respectively. The vestibular nerve connects the labyrinth with its paired organ on the opposite side of the skull and the brain stem.

The anterior portion of the bony labyrinth contains the cochlea, the final part

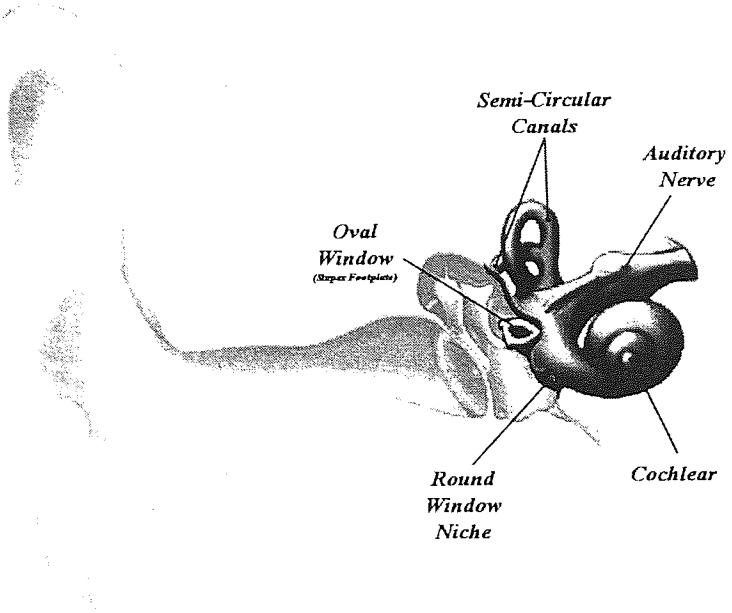

Figure 5.4: *Ear anatomy: The inner ear (1).*

of the auditory system. The cochlea is a hollow spiral structure that decreases in diameter as it approaches the apex approximately $2\frac{3}{4}$ turns from the basal cavity. The wall thickness of this structure varies form $0.3mm$ to $3.0mm$ in severely ossified cases, but it is typically in the region of $0.5mm$. The cochlea coils around a central pillar of bone called the modiolus. The modiolus houses the spiral ganglion and the cochlea nerve. Projecting from the modiolus is a partial shelf of bone know as the osseous spiral lamina.

The bony cochlea is divided into three channels by the osseous spiral lamina and membranous cochlea. These channels: the scala tympani, scala media and the scala vestibula are depicted in 5.5.

The scala media runs along the centre of the bony cochlea joining the osseous spiral lamina running along the lateral cochlea wall to divide cochlea into the additional two channels scala tympani and the scala vestibula. It is the scala vestibular into which the oval window opens. The scala tympani and the scala vestibla are connected in the apex of the cochlea via an opening called the *heli-*

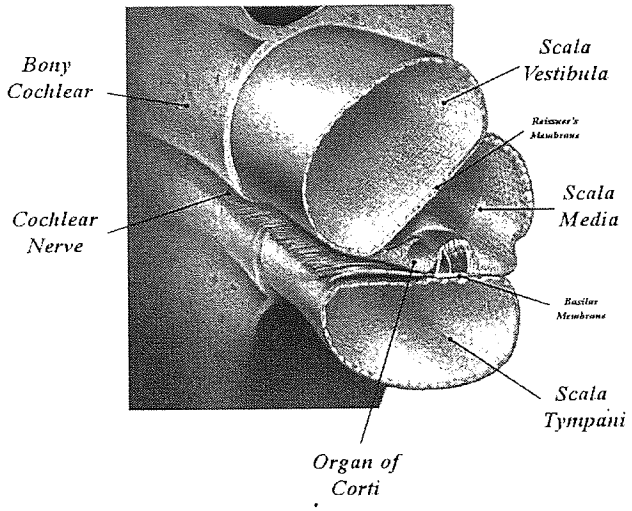

Figure 5.5: *Ear Anatomy: Cochlea cross section (1).*

cotrema. These spaces are therefore continuous with one another and are filled with the cochlea fluid, perilymph. Pressure waves induced by the oscillation of the stapes footplate travel up the scala vestibula and then back down the scala tympani where the energy is dissipated by the round window. The scala media *(also known as the cochlea duct)* is connected to the cerebral spinal fluid *(CSF)* system via the cochlea aqueduct and is filled with endolymph. The scala media also contains the organ of corti, this is perhaps the most delicate part of the cochlea and is responsible for converting the pressure wave conducted through the fluid filled space into electrical impulses which are sent to the brain via the cochlea nerve *(The 8^{th} Cranial Nerve)*.

The labyrinth is very unique as it is the only organ that is fully formed at birth and does not develop further with age. This means that the bony labyrinth is not active tissue, that is it does not grow and heal in the same way normal tissue does. If damaged fibrosis occurs. As already mentioned the membranous labyrinth is made up of fluid-filled compartments (endolymphatic fluid in the endolymphatic space) contained within the fluid-filled bony labyrinth (perilymphatic fluid in the perilymphatic space). To function correctly the system relies

on the correct balance of fluid between these spaces. If the bony labyrinth is perforated then perilymph is driven out by the hydrostatic pressure of the cerebral spinal fluid *(CSF)* system. The escaping fluid is replaced by CSF entering the cochlea through the cochlea aqueduct disrupting the balance of the system. This can be complicated further by the fibrous growth as it can often invade these spaces. If this occurs it can permanently impair the organ by affecting the fluid flow and, in the case of the cochlea, change the acoustic properties.

5.3.2 The Stapedotomy

The stapedotomy is a procedure to alleviate the effects of conductive deafness due to the fixation of the stapes footplate. The anatomy of the stapes is shown in figure 5.6.

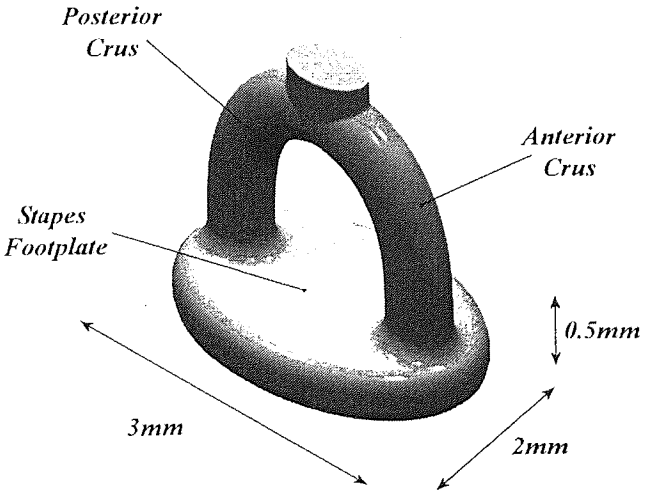

Figure 5.6: *Anatomy of the stapes (1).*

The Stapedotomy procedure involves the removal of the crura (*posterior and anterior crus*) of the stapes and the creation of a $0.8mm$ hole through the stapes footplate. A small piston prosthesis is placed in the hole so the base of the piston sits against the membrane surrounding the vestibule. The opposite end of the

prosthesis is crimped around the long process of the incus. When in place the piston prosthesis moves in sympathy with the oscillations transferred from the tympanic membrane via the ossiclular chain. The oscillations are then passed into the scala vestibular through the surrounding membrane as it would have been prior to the stapes fixation, restoring the patients hearing.

5.3.2.1 Surgical Technique

The stapedotomy itself is a relatively simple procedure, however it is difficult to perform effectively. The scale of the procedure and the available access require that it be performed via an operating microscope and as such it is considered to be a micro-surgical task. Although the way in which the procedure is performed may vary depending on the preferences of the surgeon, it can be broken down into a series of general procedural steps (55) as shown below:

1. Patient preparation,
2. Elevation of the tympanomeatal flap,
3. Removal or meatal bone and reflection of the chorda tympani,
4. Section of the stapedius tendon,
5. Fracture of the stapedial crura and removal of the stapes superstructure,
6. Penetration of the stapes footplate,
7. Insertion of the piston prosthesis,
8. Sealing of the oval window,
9. Closure of the operative site.

This operation is performed under a general anesthetic and the patient is placed in a hypotensive state to minimise bleeding. The procedure begins with the anesthitised patient being brought into theatre. The patient is then draped and the local area is sterilised.

The surgeon begins by preparing the approach to the middle ear via a perimeatal tympanotomy. An incision is made approximately $5mm$ anterior to the tympanic membrane from the 6 o'clock to the 12 o'clock position *(approximately 180 degrees)* and the skin is elevated from the underlying bone. The fibro-cartilaginous annulus that surrounds the tympanic membrane is also elevated and moved to one side allowing access into the middle ear cavity. At this point it is possible to visualise the long process of the incus and tip of the crura of the stapes, however the stapes footplate is not yet visible.

To expose the footplate it is necessary to remove some bone tissue from the wall of the canal, this is done by hand with a curette. Bone is slowly scooped out until the footplate becomes visible. This process exposes the chorda tympani, if it is possible the nerve is lifted from its bony canal, however, more often than not the nerve is severed.

The stapedius tendon is then severed and the mobility of the ossicles is checked. The surgeon then proceeds to sever the incustapedial joint, separating the stapes and the long process of the incus. With the stapes free from the rest of the ossicular chain, the crura are fractured and the superstructure of the stapes is removed.

The perforation of the stapes footplate is the most delicate part of the procedure, and often is the cause of any complications that arise as a result of the intervention.

There are three general techniques for the formation of the hole through the footplate, the first, and what was perhaps the most common, is manual fenestration. This involves the use of a sharp needle and using it to crack the thin blue area located in the centre of the footplate without the crack propagating across its full width. Once cracked, approximately one third of the material in the centre of the footplate is removed to create the aperture for the prosthesis.

The second method is the use of a hand-held, low speed micro-drill known as a Skeeter®, from Medtronic (6), to drill through the footplate until the membrane is visible, and then manual fenestration is used to complete the hole. Drilling is the most widely used technique in Europe.

The third and final method is laser ablation, this is rapidly becoming the method of choice in the United States. Each of these methods carry a similar

level of risk and their use is largely down to preference.

In an ideal situation the hole is located in the supero-posterior portion of the stapes footplate, maximising the fluid gap between the distal surface and underlying membrane. This minimises the risk of perforation, however, this is not always possible due to the size of the footplate. The stapes after the formation of the hole for the piston prosthesis is shown in figure 5.7.

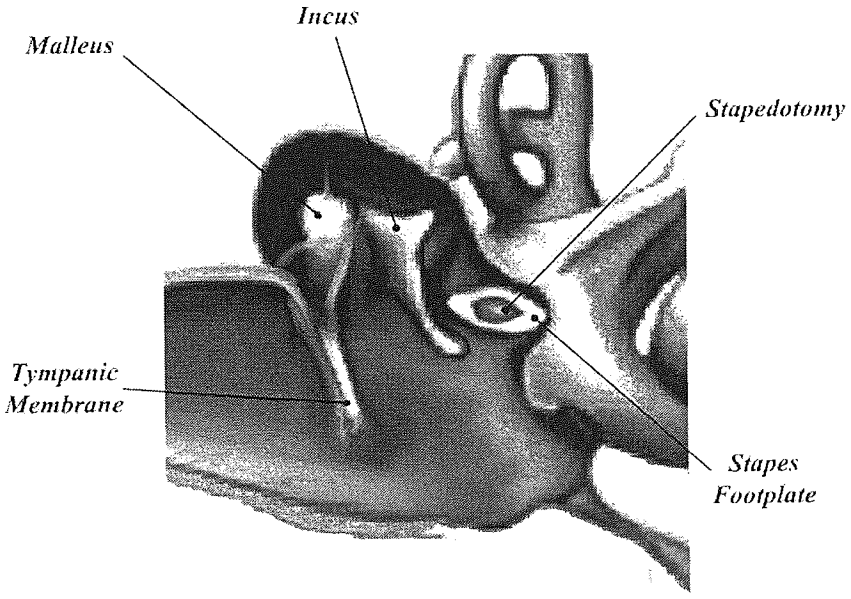

Figure 5.7: *Middle ear after resection of the stapes (1).*

The hole diameter is approximately 0.8 mm which is sufficient to fit the prosthesis into without interfering with its oscillation. The piston is then inserted such that the base is in contact with the membrane that surrounds the saccule. The opposite end, which comprises a wire hook, is crimped around the long process of the incus. Care is taken to insert the piston so the open hook slips simultaneously over the incus and into the prepared hole minimising trauma to the remaining ossicles. When in position the hook is crimped around the incus re-connecting the ossicular chain.

The final stages of the procedure consist of packing the base of the piston prosthesis with fatty tissue to prevent the leakage of perilymph from the opening. The ear drum is then moved back into position and the incisions closed completing the procedure. The middle ear after the stapedotomy procedure is shown in in

figure 5.8.

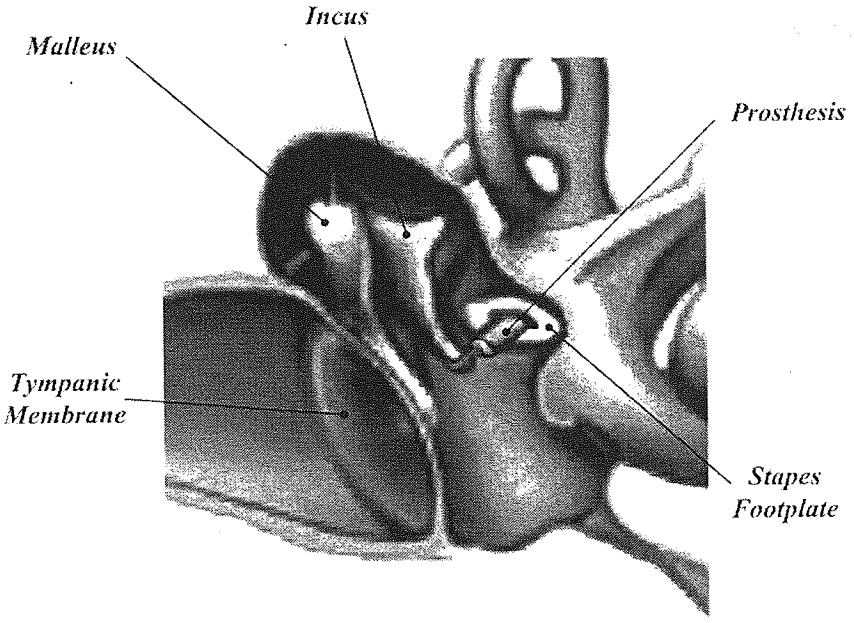

Figure 5.8: *The middle ear with prosthesis in position (1).*

5.3.2.2 Complications

The stapedotomy can lead to complications common to most surgical procedures performed under general anesthetic, as well as complications unique to this particular procedure due to the individual's anatomy and the surgical technique employed.

The majority of the complications, particularly those of a more serious nature are as a direct result of the formation of the hole through the stapes footplate.

As mentioned in the previous section, there are three primary techniques for the formation of the hole.

Manual fenestration, by nature produces a very poor quality and an irregular shaped hole. The hole geometry is largely determined by the way the initial fracture of the footplate occurs. This technique carries the highest risk of complete fracture and/or mobilisation of the footplate due to the application of excessive force.

Drilling, which is now the preferred technique in the UK, over comes these problems by removing the need for the surgeon to manually form the hole thus creating a higher quality circular hole. However, there is a larger risk of displacing the footplate due to the high cutting rate and rotational torque supplied by the drill.

Laser ablation, whilst being non-contact, thus eliminating the risk of mechanical trauma to the tissue, poses the highest risk, as overshoot cannot be controlled. The surgeon has to rely on the fluid space beyond the surface being sufficient to absorb the energy from the laser thus preventing damage the the membrane of the saccule. It is worth noting that recent advances in laser and scanning technology have allowed much safer deployment of the technique (64) and improved hole quality however the technique still caries with it a high risk of thermal shock to the structures of the inner ear.

These techniques, though very different, all share one major contributing factor to severe complications. It is not possible to control the degree of overshoot as a result of unexpectedly penetrating the medial surface of the stapes footplate, hence damage to the underlying saccule membrane is highly probable. The membrane separates the two fluids contained within the inner ear and damage to this membrane is likely to result in cross contamination, severely disrupting auditory and vestibular function. Damage such as this usually results in profound sensorineural hearing loss.

Although hole position is not a complication in itsef, poor hole postioning can considerably contribute to post operative complications. Studies have shown that correct hole position can greatly improve high frequency hearing by as much as 7 dB (26).

Although rare, another possible complication is damage to the facial nerve. The nerve runs through a thin bony canal that follows the superior aspect of the oval window. It is not uncommon for the canal wall to be very thin and/or the nerve itself to be exposed. In severe otoscleritic cases malformation of the bone structure surrounding the oval window is common, often obscuring the stapes footplate making positioning the hole difficult and in severe cases impossible. This can be overcome by the removal of boney tissue covering the window. This can also lead to exposure of the nerve itself, any trauma to which can lead to

facial paralysis (67).

Despite these intra-operative complications, the procedure is generally successful with some degree of hearing improvement in approximately 80% of cases. Unfortunately post-operative complications are more common. When manual fenestration or laser techniques are used to form the hole, the quality and position is often poor resulting in deterioration of hearing.

Although it is possible to say that generally complications are rare, it is inevitably down to the skills and experience of the surgeon performing the operation. This procedure, as with all micro-surgical techniques, requires the surgeon to work at the limits of human perception and dexterity, studies have shown clear differences in performance levels between differing experience levels during critical steps of the stapedotomy (82).

5.3.3 Cochlea Implantation

Cochlea implantation is one of the greatest advancements in recent years for the sensorineural deaf (101). A cochlea implant consists of a receiver and amplifier unit implanted behind the ear, connected to an electrode that passes through the mastoid into the middle ear where it enters the cochlea via the cochleostomy. An external microphone and signal processing unit is worn externally by the patient. The transmitter is placed over the implanted receiver and is held in place by a magnet, sound is then transferred to the implant via an inductive loop. The implant electrode delivers electronic impulses that directly stimulate the remaining nerve cells allowing the patient to regain a basic level of auditory function.

5.3.3.1 Surgical Technique

As the number of suitable candidates for cochlea implantation is increasing, cochlea implant surgery is now a standardised procedure which consists of the following surgical steps:

1. Patient preparation,

2. Post aural incision,
3. Complete mastoidectomy,
4. Posterior tympanotomy,
5. Cochleostomy,
6. Milling of the implant well,
7. Insertion of the implant and electrode array,
8. Closing the post aural incision.

Prior to surgery the area surrounding the implant site and the mastoid is shaved. As with the stapedotomy the implantation procedure is performed under a general anesthetic and the patient is placed in a hypotensive state. The procedure begins with the anaesthetised patient being brought into theatre and the local area is sterilised. The electrodes for the facial nerve monitor are inserted into the patients cheek and forehead and the area is then covered. After the patient is draped the line for the incision and the desired implant site are marked on the skin.

Access to the mastoid process is gained via an s-shaped post aural incision. The incision is made well posterior to the mastoid tip and is then extended superiorly. Tissue is then elevated to expose the tip of the mastoid and the mastoid cortex. A region of bone superior to the mastoid is also exposed to allow for milling of the implant well into which the receiver is placed.

The middle ear cavity is reached by performing a complete mastoidectomy, followed by a posterior tympanotomy. Due to the delicate nature or the structures within the ear a slow approach is taken in preparing the access to maximise visualisation of the anatomical landmarks that enable the correct positioning of the posterior tympanotomy. The mastoid air cells are excavated completely until the antrum is exposed at which point the horizontal semi-circular canal can be identified. At this point the facial nerve monitor is switched on to alert the surgeon if the cutting tool is approaching the facial nerve. Tissue is then slowly removed thinning the posterior canal wall, widening the access so the long

process of the incus can be seen through the fossa incudis. The visualisation of these two features enable the posterior tympanotomy to be placed between the facial nerve and the semi-circular canal, avoiding damage to both structures. A hole is formed superior to the semi-circular canal wall, in-line with the long process of the incus exposing the incudostapedial joint. The surgical microscope is brought in at this point, and the remainder of the tissue removal is performed via the microscope. From this point the tympanotomy can be widened laterally to reveal the promontory portion of the cochlea. Extending further, the stapedius tendon and round window niche become visible, thus revealing the cochleostomy site.

The cochleostomy is a small hole (approximately $1.0mm$ in diameter) drilled through the wall of the cochlea into which the electrode of the cochlea implant is inserted. This is perhaps the most delicate and critical step in the cochlea implant procedure, demands on the surgeon are high. The drilling of the cochleostomy, even when performed perfectly, is extremely traumatic to the cochlea and care must be taken when penetrating the cochlea wall. The correct positioning of the cochleostomy is also critical to the successful outcome of the procedure.

The cochleostomy site is located anterior and inferior to the round window, and anterior to the oval window. As with the tympanotomy the use of these anatomical landmarks enable the hole to be drilled in the correct position (89). The correct location for the cochleostomy should enter into the basal turn of the cochlea, opening into the scala tympani. This approach avoids the '*hook*' portion of the cochlea allowing direct insertion of the electrode and the path of least resistance. This ensures minimal trauma to the membranous cochlea upon insertion.

Once the posterior tympanotomy has been sufficiently widened for visualisation of the round window niche, the mucosa covering the promontory is moved aside to reduce bleeding. This serves two purposes, firstly it aids the surgeon as it is easier to see the cochleostomy site, thus less irrigation and suctioning is required. Secondly, it minimises contamination of the perilymph.

The cochleostomy is drilled using a Skeeter® hand drill (6) with 0.6 mm diamond burr. Pressure is applied gently as the burr begins to cut, pausing occasionally to remove debris to aid visibility. Drilling is continued until the

endosteum can be seen at the centre of the hole as a dark blue circle. The applied pressure is then reduced and the burr is moved in small circular motions to increase the diameter of the hole. When the hole is sufficiently widened there is a hole approximately $1.0 - 1.2\ mm$ in diameter drilled down to the membrane beneath. Bone debris is removed and then the posterior tympanotomy is packed with swabs to prevent any debris entering the middle ear while the implant well is milled.

The implant well, located in the cortical bone, is milled with a large diameter burr and an array of shaped burrs for cutting the correct recess to fit the receiver part of the implant. This is tested with a blank to ensure the correct fit before the device is implanted. The receiver portion of the electrode is then inserted under the scalp flap and is secured in place with sutures. The ball electrode is also tucked up under the flap.

The final part pf the procedure is the electrode insertion. Like the cochleostomy this is a critical part of the procedure as rough electrode insertion can also cause severe damage to the sensitive structures within the cochlea. The packing in the posterior tympanotomy is removed and a globule of Healon® (18) *(hyaluronic acid)* is placed over the cochleostomy site. The Healon® gel helps to protect the cochlea from contamination, prevents leakage of the perilymph and acts as a lubricant when the electrode is inserted. The cochlea endosteum is then incised and the electrode inserted immediately to minimise the risk of contamination and the loss of perilymph. The electrode is inserted slowly if any resistance is felt it is withdrawn slightly, rotated medially and re-advanced. Full insertion of the array represents an insertion depth of approximately 25 mm which is indicated by three rings, the first of which should be inserted so that the electrode is held in position. The lead of the electrode array is placed in the mastoidectomy such that the natural stiffness of the cable holds the electrode in position. The cochleostomy site is then packed with a small muscle graft to prevent any further loss of perilymph. Lastly, the excess electrode wire is coiled and packed into the mastoid cavity and the operative site closed while an implant technician performs a diagnostic on the implant.

5.3.3.2 Complications

Like the stapedotomy, the cochlea implant procedure can lead to complications common to most surgical procedures performed under general anesthetic as well as complications unique to this particular procedure due to the individuals anatomy and the surgical technique employed.

The most common complication, which is now considered to be a result of the procedure rather than a complication, is the deterioration or loss of any residual hearing the patient had prior to the operation. This has been generally associated with trauma to the cochlea which primarily occurs as a result of the formation of the cochleostomy and the electrode insertion. Roland *et al* (81) summated the causes, effects and possible solutions to complcations that may affect post-operative residual hearing retention in table 5.2.

The formation of the cochleostomy, by its very nature is a massive assault on the cochlea. The cochlea is a very complex and delicate structure buried deep within the temporal bone. The bone of the cochlea is unique, it is much harder and more brittle than that of other bone tissue. The cochlea is fully formed at birth and as such cannot heal in the same way normal bone tissue does, rather a fibrous growth forms over any fracture. This can cause severe complications as the fibrous growth can invade healthy tissue, not only permanently changing the acoustic properties of the cochlea but also damaging any remaining nerve cells (45). This often results in permanent loss of any residual hearing and can adversely affect the operation of the implant.

A common occurrence is overshoot when drilling through the cochlea wall. Due to the scale of the procedure it is very difficult for the surgeon to prevent the drill suddenly advancing forward upon breakthrough of the medial surface, into the cochlea space. This can often result in fracture of the spiral lamina and tearing of the membranous cochlea, often damaging the basilar membrane(Shown in figure 5.5). If any of the membranes separating the individual channels within the cochlea are breached, it can result in the contamination of the fluid contained within. This can also cause hydraulic shock. The cochlea is a sealed, fluid filled space and as such when the drill bit penetrates the inner wall it acts like a piston. The resulting pressure increase within the cochlea can cause severe trauma to the

remaining nerve structures.

Another common occurrence is the formation of an over-sized, irregular shaped hole resulting in a poor electrode fit. This causes two problems, the first is leakage of perilymph from the cochleostomy and the second is electrode extrusion because the electrode is not held in place sufficiently. The gap surrounding the electrode also increases the risk of post-operative infection.

Several techniques have been put forward to reduce the likelihood of these complications, for example, delaying of the formation of the cochleostomy until the end of the procedure and immediate electrode insertion (46). This reduces perilymph leakage intra-operatively. The technique described in the previous section is used to minimise trauma when drilling the cochleostomy, however it is worth noting that these techniques are not widely used.

Although the anatomical 'landmarks' are used to identify the correct site for the cochleostomy, variations in anatomy and the experience level of the surgeon often result in incorrect positioning of the cochleostomy and thus poor implant performance.

Fortunately the complications are rare, however, implant effectiveness can often be improved as could retention of residual hearing. This is particularly relevant at present as candidates with higher degrees of residual hearing that fall into the lower end of the moderate deafness category are being considered for implantation. Previously only those with profound deafness would be considered, however, there is much evidence to support that patients with both a degree of acoustic hearing coupled with an implant perform very well and have exceptionally good speech perception (94).

This is particularly true for patients with only high frequency hearing loss. This aside, these patients generally have acceptable levels of hearing, however, this results in very poor speech perception. Unfortunately hearing aids do not help with this type of hearing loss so the only real solution is cochlea implantation. As such, it is possible to use electro-stimulation combined with the residual acoustic stimulation resulting in a much higher hearing performance (81). Therefore, it is vital that as much or the residual hearing as possible is preserved. These candidates are often suitable for implantation with the new 'short' electrode designed to only stimulate the high frequency regions. The shorter insertion reduces

Table 5.2: *Factors contributing to residual hearing loss intra/post cochlea implantation (81).*

Mechanism	Cause	Solution
Necrosis	Surgical or electrode issues.	Surgical technique, electrode design
Apical cochlea trauma	Electrode dislocations	Electrode design
Basal cochlea trauma	Basal surgical trauma	Cochleostomy size, location, angle
Scala vestibuli insertions	Location and angle of the cochleostomy	Use of anatomical landmarks
Electrode dislocations	Electrode stiffness	Electrode design
Apoptosis	Intraoperative trauma	Soft surgical techniques
Post-op hair cell loss	Intraoperative trauma	Corticosteroid application
Disturbance of cochlea mechanics	Electrode lies against the basilar membrane	Free fitting arrays
Perilymphatic fluid loss	Large cochleostomy, early opening	Late cochleostomy opening, sealing
Cochlea contamination	Blood influx during surgery	Late opening, clean surgical situs

the possibility of damage to the intact low frequency regions.

5.4 The Surgical Environment

The operating theatre is often a small, crowded space full of both theatre staff and medical equipment to support both the patient and the surgeon. For any given operation there are typically five staff present: the surgeon, a scrub nurse, an anaesthetist and two supporting nurses. A typical theatre layout for the conventional cochlea implant procedure is shown in figure 5.9.

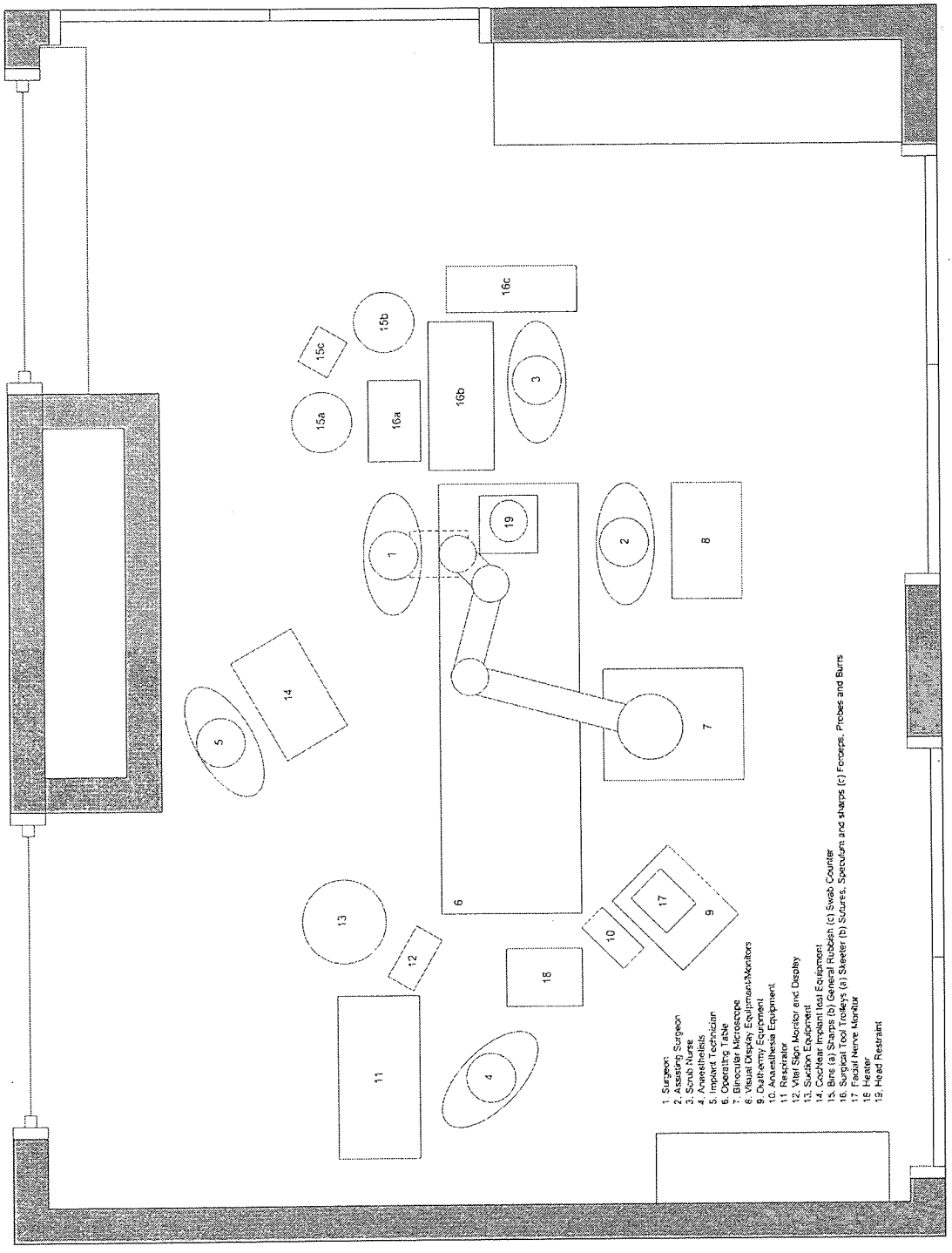

Figure 5.9: *Typical theatre layout for the cochlea implant procedure.*

5.4.1 Sterility

Sterility is of the utmost importance in a surgical environment. Everything in an operating theatre is designed such that the risks of contamination and/or infection are minimised. There are predefined paths for theatre staff such that sterile and non-sterile team members do not come into contact. Contaminated equipment and instruments are removed in such a way that they are not in the vicinity of freshly sterilised ones (58). Typically only the surgeon and the scrub nurse will 'scrub in'. This is where they first clean their hands and forearms with an antiseptic agent, from this point on they are considered sterile. They are then handed sterile packed gowns and gloves. The gowns are put on and tied behind and then the gloves are put on.

All equipment that comes into direct contact with the patient has to be cleaned and then sterilised in an autoclave. These instruments are double packaged in sterile bags prior to autoclaving. This is so that a non-sterile team member can handle them prior to surgery. When they are to be used the outer packaging can be opened and handed to a sterile team member. They can then open the inner packaging and handle the instrument without fear of contamination. The same goes for the patient themselves, they are considered non-sterile and as such they are covered in sterile drapes after the operative site has been sterilised. Great care is taken to ensure that all possible sources of contamination are covered, this include areas where non-sterile team members have come into contact with any exposed areas on the patients body that have not been sterilised.

Most, if not all theatre equipment that is used in the vicinity of the operative site can be sterilised, if not, it will typically be covered in a sterile polythene drape along with all their ancillary components and/or cables. Examples of this are camera equipment, surgical microscopes and instruments such as powered drills and cutting tools. This can make the setting up of complicated equipment difficult as it requires co-ordination of both sterile and non-sterile team members. Prior to draping, the equipment is non-sterile and after the drape is applied only sterile team members may handle it. This can be complicated further, for example if the equipment is to be mounted on the side operating table as this is also considered non-sterile. In these instances the equipment is held by a sterile team

member and is then attached by a non-sterile team member, the contaminated area is then draped by the sterile team member to prevent cross-contamination. It is for this reason that all surgical equipment has a specific sterilisation, setup and draping procedure.

5.4.2 Integration

Any system under development for clinical deployment must integrate into the operating theatre seamlessly. The theatre itself is a small, confined space filled with a multitude of equipment. The environment is precisely controlled and a sterile field around the patient must be maintained. The clinician must also be able to perform their tasks unhindered by the surrounding equipment.

A device such as the micro-drill will not be used on its own, it has to be used in conjunction with the other equipment. The operating table, binocular microscope and surgical instrumentation to name but a few. In the case of the surgical microscope, the device must not interfere with the clinician's visual field so that the operative site can be observed at all times. This affects the profile as well as the overall length of the device as microscopes typically have a focal length of 250 *mm*, leaving approximately 200 *mm* between the patient and the microscope.

This means the size and location of the instrument is extremely important, as is how it is located in the proximity of the patient. Fast setup and removal procedures are vital to enable smooth operation of the surgical tasks at hand; especially in the case of an emergency when the clinician may require immediate access to the patient.

Consideration must also be given to the power up and power-down modes of the device and their implications on safety.

Construction and material selection is also important as handling and cleaning of the device must integrate with existing operating practice such as cleaning, draping and sterilisation.

The environment is also a busy place, with multiple staff performing multiple tasks simultaneously. This makes it noisy, not only sound but vibration and

electromagnetic interference as well. As such, any device must be resilient to disturbance from the surroundings.

5.5 Conclusions

In this chapter two potential applications for the micro-drilling system have been reviewed:

1. the stapedotomy,
2. and the cochleostomy.

Both present similar requirements and challenges as well as suffering from the same limitation. The general requirement is the drilling of a small diameter hole through tissue that can vary in both thickness and compliance. In both applications the placement of the hole is key to a successful outcome of the procedure.

When drilling there is a need to limit penetration to prevent damage to the underlying membrane. This is particularly true of the stapedotomy as the prosthesis that is to be inserted has to sit on the membrane where as in the cochleostomy the membrane will be incised anyway. In the latter case, the emphasis is on limiting trauma to the surrounding structures. Another key factor is the hole quality, as in both cases a poorly formed hole will cause issues with implantation and increase the risk of post-operative complications.

5.5.1 Clinical Challenges

Both precise penetration and hole quality are entirely dependent on the skills of the surgeon and it is here that the procedures are limited. Due to the magnitude of the forces involved it is virtually impossible for the surgeon to have a sufficient perception to control the breakthrough process to any degree of accuracy, and preservation of the underlying membrane is very difficult whilst maintaining hole

quality. While some clinicians may be able to do this on occasion, it is a laborious and lengthy process that is rarely achieved.

The clinical challenges facing a robotic surgical system include:

1. reaching the operative site and working through tight access;
2. drill through bone tissue of varying thickness and compliance;
3. account for tissue deflection and/or deformation;
4. detect and control the breakthrough process and prevent drill penetration;
5. where appropriate, completion of the hole with minimal drill protrusion;
6. minimise trauma, thus reducing the risk of membrane penetration;
7. integrate with existing procedures.

5.5.2 Environmental Challenges

When taking a new device into the operating theatre there are a number of things to consider; namely system integration, sterility and patient and operator safety. In summary the general challenges of working in the surgical environments are as follows, the system must be:

1. safe;
2. simple to setup, operate and remove;
3. suitable for use in a sterile environment;
4. mounted on the operating table and be used in conjunction with a binocular microscope;
5. integrate with existing theatre equipment and procedures;
6. robust and thus immune to EMC/EMI from surrounding equipment as well as physical disturbances.

5.5.3 The Intended Application

The two procedures reviewed present very similar challenges however the drilling system will be deployed for one application only. The number of stapedotomy procedures is falling due to alternative, less invasive therapies (43, 83) making recruitment of patients for a research clinical trial difficult. However, the number of cochlea implants is increasing as a result of lowering costs and less stringent selection criterion (47). As such the focus of this research is to be on the cochlea implant procedure and thus the cochleostomy.

Chapter 6

System Design and Architecture

6.1 System Specification

By taking into account the procedures and processes described in the previous chapters a specification for the new drilling system can be derived. There are three key areas into which the specification can be broken down. Firstly the clinical specification which details the requirement from a surgical point of view, relating to the use of the device, its function and operating procedure. Secondly, the environmental specification which outlines where it will be used and how it will integrate into the operating theatre environment. Lastly the technical, or detail specification. This describes the technical requirements to enable implementation of the compliant drilling technique. The technical specification is derived from the requirements of the compliant drilling technique and from knowledge gained from previous prototype devices.

6.1.1 Clinical

- The drilling system is to be designed for use in a surgical environment by a surgical team performing the stapedotomy or cochleostomy procedures.

- The system is required to drill a 0.6 to 1.2 mm diameter hole through bone tissue. This bone can be anywhere between 0.5 and 2.5 mm in thickness and can be considered to be compliant or compliantly mounted.
- The system stiffness must be the same order of magnitude as the expected tissue stiffness, typically in the region of $0.5 - 5\ N/mm$.
- The device must be sufficiently small to be used in conjunction with a binocular microscope with an effective focal length *(EFL)* of 250 mm allowing sufficient clearance to manoeuvre the device.
- The device must be able to reach the operative site located between 40 to 60 mm within the skull and is accessible via a narrow aperture no more than 8 mm in diameter without obstructing the view of the operative site.
- The drill shaft be located as close to the top of the unit as possible and all materials are to have a matte finish wherever possible.
- The drill is to be supported by a *'flex and lock'* arm that will, when unlocked support the weight of the drilling unit allowing for easy location of the drill shaft within the vicinity of the patients ear.
- The arm can then be locked with no movement *(back-lash)*, and fixed in position such that it is rigid and cannot move throughout the drilling process.
- The support is to be mounted on the mounting rails located on the side of the operating table and as such must use standard fittings.
- The device must be able to be used on either side of the operating table.
- From a safety point of view the device must be optimised for quick removal in the event of an emergency.
- The clinician requires basic feedback on the state of the drilling process with a visual representation of the force and torque transients.

- Prior to drilling the clinician has control over the positioning of the unit at the desired location, and the initiation of the drilling procedure.
- Once initiated, control of the device is in a purely supervisory capacity.
- The drill shaft is to be made to accept standard 1.6 mm diameter, by 19 mm long, friction grip dental cutting burrs.

6.1.2 Environmental

- Sterility is key in the surgical environment and as such all exposed parts of the drilling system must be sterilisable and as such must be unaffected by cleansing agents.
- All portions that may come into contact with the patient must be either autoclaved or covered in a sterile drape. Drill bits must be disposable and assembled drill shafts must be sterilised in an autoclave.
- Given that the operating theatre is a small, confined space and it is filled with electronic equipment the device must be resilient to electromagnetic interference.
- The device will also be handled roughly and it is unlikely that any extra care will be taken when setting up or removing the device. Therefore it must be sufficiently robust to withstand any such handling without affecting the performance.

6.1.3 Technical

A graphical representation of the technical requirements of the compliant drilling technique is shown in figure 6.1.

The key system points are as follows:

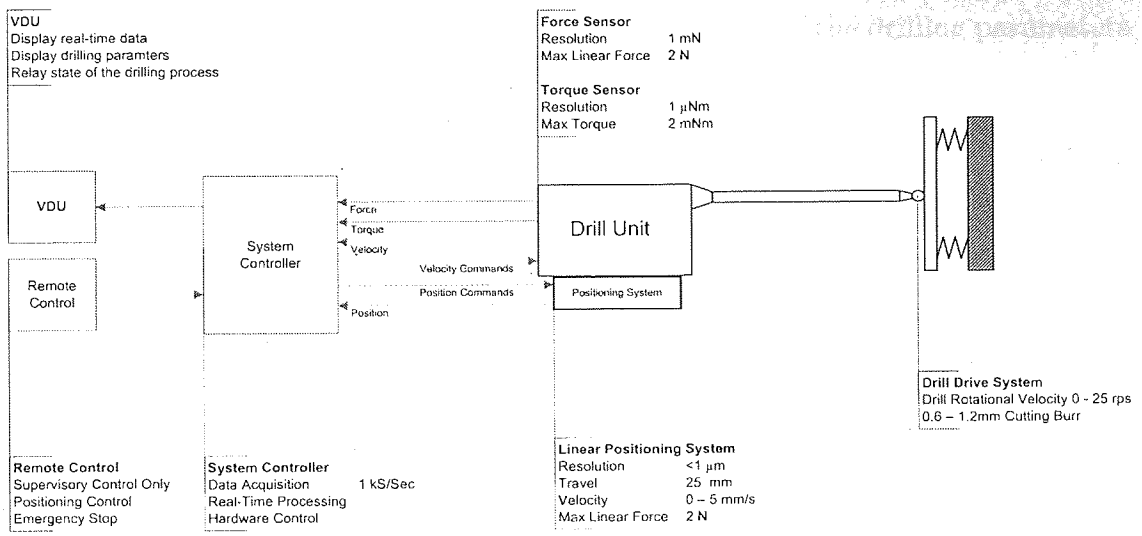

Figure 6.1: *Primary functions of the drilling system.*

- Feedback from drill is required to enable the determination of the state of the drilling process via force and torque data from the drill tip. Respective minimum resolutions of 1 mN and 1 μNm.
- The drill unit itself will be linearly actuated to provide approximately 25 mm of travel at velocities as low as 10 $\mu m/s$.
- Drill rotation must be controllable up to 25 Hz.
- The system controller is a standalone unit capable of operating the entire system without a computer.
- The user interface will consist of the simple hand held remote control and a visual display unit *(VDU)* that will display the force and torque transients and the estimated drilling parameters, such as, estimated bone thickness, drill penetration and state of the drilling process.
- Once the drilling process is initiated the procedure is handled solely by the system controller, with the clinician having supervisory control only.
- The telemetry from the drill is displayed on the VDU such that it can be monitored and if at any point the surgeon is unhappy with the progress, it can be paused or aborted and the drill retracted.

- The host interface will provide off line adjustment of the drilling parameters and real-time data logging.

It is also worth noting that for an electronic device for use in a hospital the device must conform to the electrical specifications as defined by the medical device standard.

6.2 Mechanical Design

The mechanical system described in this chapter was developed based on the specification in section 6.1. The system was designed in collaboration, however, the detail design and manufacture was carried out by Mechtron Design Limited (80).

6.2.1 Locking Arm

The locking arm is not only a solid base from which the drill unit can operate, it is a tool to assist the clinician to position it along the correct trajectory.

The design uses a number of single axis rotary joints and a single ball joint. The arm segment of the support is shown in figure 6.2.

The arm is comprised of four segments with a joint between each segment. The base segment is connected to the valve assembly located at the bottom via a horizontal rotary joint. The central segment has a vertical rotary joint at each end with another horizontal joint in between. The third segment connects the top vertical rotary joint to the ball joint at the base of the top section. The horizontal joints have a full 360° of motion, and the vertical joints have approximately 270°.

The ball joint at the tip has a 60° cone angle with a slot located on one side allowing the final segment to move through a full 90° and lock into position. The whole ball assembly can then be rotated horizontally through a full 360°. This allows the final segment 360° about all three axes. This combination of joints allow a unique level of freedom whilst retaining its rigidity which is difficult to achieve with other solutions. Most notable, is the ability to move the top segment

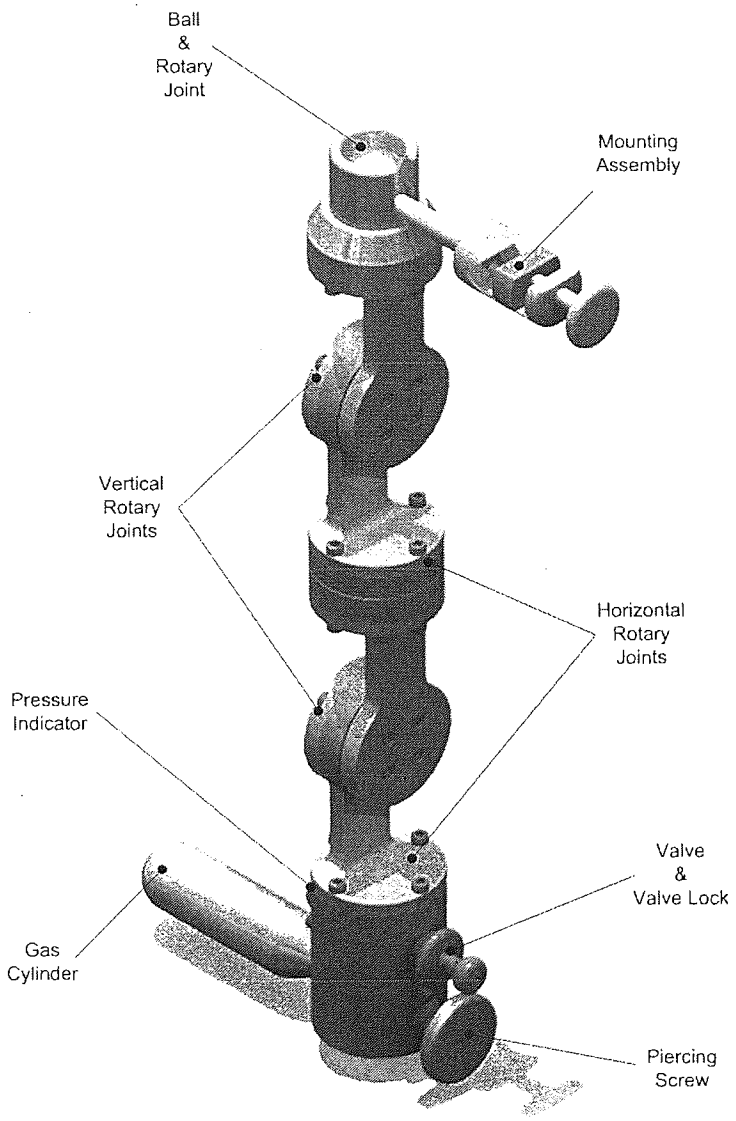

Figure 6.2: *Flex and Lock arm assembly.*

linearly by moving two of the rotary joints simultaneously which aids positioning the drilling system down long and narrow access routes.

The mounting assembly comprises a simple clamp and 'V' groove, the mating section has a square cross section with chamfered edges to allow the drilling unit to be easily and repeatably located. If, for any reason, during a procedure the drill unit itself has to be removed, it can be replaced without having to realign the system.

The locking mechanism is powered via a miniature 12 g CO_2 cartridge which when fully charged supplies a back pressure of approximately 350 kN/m^2. The gas pathways in the arm have been kept to a minimum, as such, the arm has an operating volume of approximately 1 cm^3. A single cartridge can be used for up to forty lock and unlock cycles before the rigidity of the system is affected significantly due to low pressure. When unlocked, each rotary joint has sufficient friction force to support the weight of the assembly above. This allows the device to be positioned unaided and it will remain in position while the trajectory is inspected; the arm can then be locked without movement.

The cylinder screws into the base of the valve assembly, a piercing pin is screwed in from the opposite side to open the cartridge. Once pierced a small chamber within the assembly fills and a spring mounted pressure indicator is forced outwards. As the pressure drops the indicator moves back into the body of the valve assembly.

The locking system is operated via a sliding valve at the base of the arm, when it is in the locked position a locking disc can be rotated to prevent accidental unlocking of the arm. The arm locks and unlocks instantly upon activation of the valve. When unlocking the gas is vented at the base of the arm away from the patient.

6.2.1.1 Anti-Backlash

For the support arm to flex when unlocked, and then lock without any backlash a simple piston arrangement is used. A section through one of the vertical rotary joints is shown in figure 6.3.

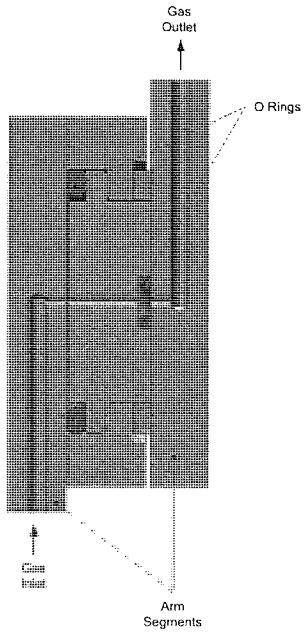

Figure 6.3: *A section through a rotary joint of the flex and lock arm.*

Each joint consist of two halves with an overlapping flange attached to each arm segment. A large O-ring occupies the gap between the two rotary sections forcing the mating surfaces of the flanges together. This serves two purposes, firstly it seals the expansion chamber on the left hand segment. Secondly the force provided by the O-ring generates sufficient friction to enable the joint to support the weight of the arm above, while still allowing the joint to be rotated by the operator. In the lower segments where a higher moment may be experienced when the arm is outstretched; either a larger O-ring or a wave spring was incorporated to increase the friction force.

When the valve on the base is moved to the lock position, gas from a CO_2 cylinder under high pressure is passed through the arm segments into the rotary joint.

When the arm is pressurised the small expansion chamber fills with gas, forcing the O-ring outwards sealing the chamber. This significantly increases the friction force between the two segments. Although the volume is small, the gas acts over a large area in the expansion chamber and acts as a piston effectively locking the joint rigid. A small hole through the centre of the right-hand segment allows gas to pass through to the upper segments.

As the two mating surfaces are already in contact when the arm is pressurised the movement in each joint is negligible providing an almost zero back lash mechanism. It was found that backlash could be produced if the valve was opened too quickly, however this was negated by reducing the size of the venturi between the valve and the cylinder to slow the flow rate of gas from the cylinder reducing the shock experienced by the arm.

The spherical joint at the tip of the arm works in much the same way only the final rotary segment has no vent through the centre, sealing the system. It also acts as a piston forcing the ball against the casing preventing movement. Although a ball joint would require a significantly greater force due to the reduced contact area, given the position of the joint on the arm the loading is greatly reduced and thus the locking force is sufficient.

The cross section of the arm was kept small so that it could be used with conventional camera drapes.

6.2.1.2 Material Selection

A number metal alloys were considered when selecting one suitable for this application, these included high grade aluminium, stainless steel and titanium. The arm, and indeed the majority of the mechanical parts of the system were manufactured in titanium. Although titanium is expensive and difficult to machine it offers many benefits including very high corrosion resistance, high strength to weight ratio and good wear resistance. Its inert nature also lends itself well to medical applications. While steel or aluminum alloys may have been suitable for some parts and would have reduced costs, it would have significantly increased the size and weight of the device and would not offer the same level of corrosion resistance.

Titanium offers comparable tensile strengths to that of some high grade stainless steels, but offers up to a 45% weight saving (34). The high corrosion resistance also means parts can be cleaned with aggressive cleansing agents and will be unaffected by most, if not all, sterilisation procedures.

The reduced weight has a large impact on the self-supporting nature of the locking arm. A greater weight would induce a larger moment on the lower joints.

When unlocked, the force required to support its own weight would be much greater. This will also have a knock on effect on the operating life of the joints owing to the fact that the locking mechanism relies on friction and the contact surfaces of the joints will be prone to wear over time. As such the wear resistance of titanium is of particular benefit.

All parts of the system were blasted with fine glass beads. This process removes all burrs, blemishes, and contaminants creating a very smooth, matte finish without affecting the dimensions of the part as minimum surface material is removed. The peening action of the glass spheres further acts to create a layer of compressive stresses on the surface of the part. This effectively work-hardens the surface increasing corrosion and wear resistance (74). The removal of all burrs and surface blemishes is beneficial as it ensures there are no sharp edges and there are no indentations into which detritus can get trapped. The bead blasted finish is particularly beneficial as it satisfies the need to minimise the amount of reflective surfaces that can be seen via the surgical microscope.

6.2.1.3 Theatre Mounting System

The operating table is designed for mounting surgical equipment on; most have a standard 32 *mm* x 6 *mm* stainless steel mounting rail that runs the length of the table on each side designed specifically for this purpose. This also makes an ideal platform for the mounting of the drilling system. Standard clamps are used in conjunction with mounting rods 18 *mm* in diameter with a flat on one side. The clamp hooks over the rail and the rods fit through the centre, a hand screw is then tightened which pushes the rods against the mounting rail, locking it in position.

A similar arrangement is used for the drill mounting system shown in figure 6.4.

The design was optimised for stability, fast setup, removal, and sterility. The mount is completely reversible so it may be used on either side of the operating table; though, the mount has to be disassembled and re-assembled in reverse to do this. However this can be performed prior to the procedure.

Only when the system is to be used, is it mounted on the rail directly in-

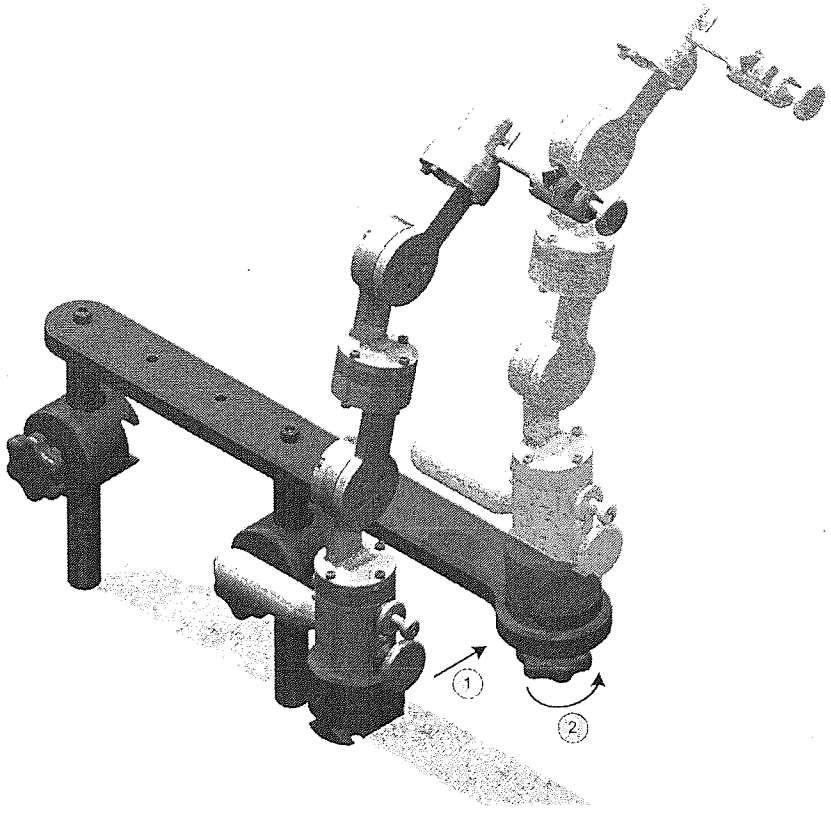

Figure 6.4: *Operating table mount for the support arm.*

front of the clinician. As a result, it would have to be setup midway through the procedure and removed shortly after. For this reason the profile of that base portion of the mount is reduced to a minimum so it can be attached to the operating table prior to the procedure then simply slid into position when required. This significantly reduces the setup time and reduces the risk of cross contamination as the base of the mount is outside the sterile field and is covered with drapes.

For quick removal of the locking arm a simple dove-tail joint and clamp is used, this provides a very stable base. While the lower portion of the mount is not required to be sterile, the upper portion and the arm does. This joint allows the arm to be draped separately and attached once draped.

As the mount is a fixture it was made entirely of stainless steel rather than titanium and the individual parts were also bead blasted to give the optimum surface finish.

6.2.2 Drill Unit

The drill unit is perhaps the most complex mechanical part of the drilling system. It houses the linear actuator, drill drive system and the sensors. The complete unit is show in figure 6.5. The unit itself is $99 \times 55 \times 16$ *mm* and is made predominantly of titanium for the reasons described previously. The profile of the device was kept to a minimum to aid visualisation of the operative site via the operating microscope. The shaft itself is 80 *mm* long, giving an overall length of 179 *mm* providing ample clearance between both the drill unit and the patient and the microscope and the drill unit to allow positioning of the device.

The drill shaft is inserted at the top of the device and rotates in static sheath which is screwed into the drill chassis. The position of the drill shaft is optimised to ensure a minimum viewing angle of 5° between the drill tip and the microscope as shown in figure 6.6. A PTFE bearing at the end of the sheath supports the drill shaft 10 *mm* from the burr tip. This ensures that the patient does not come into contact with the rotating portion of the shaft beyond the tip and prevents the torque transient being affected by contact along the shafts length. Both the

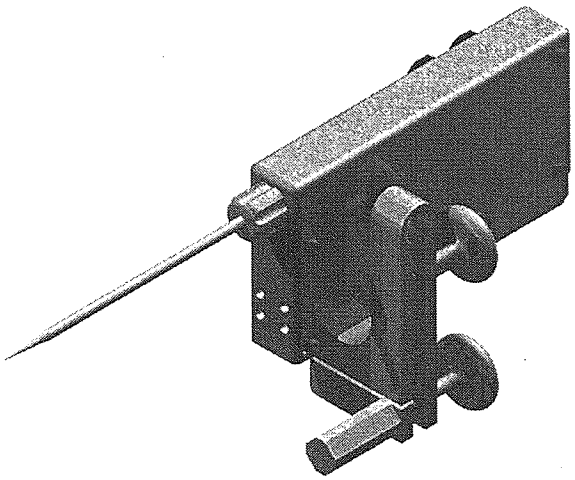

Figure 6.5: *Complete drill unit.*

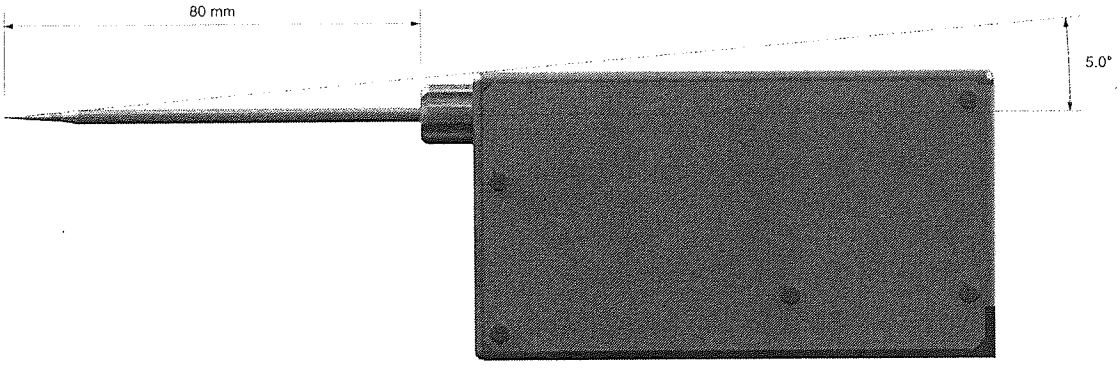

Figure 6.6: *Complete drill unit.*

drill shaft and sheath are removable and can be sterilised in an autoclave.

The slim profile of the device fits comfortably inside a standard large, sterile polythene camera drape. The unit has no sharp edges to prevent piercing of the drape and contamination of the sterile field.

The unit is mounted from below on a simple adjustment assembly to allow fine control over the trajectory of the drill tip. The assembly then locates in the 'V' groove on the locking arm and can then be clamped on securely.

Located inside the chassis are the force, torque, position and velocity sensors as well as the rotational and linear drive systems. The sensor and drive portions are sealed within the chassis by the cover plate; the associated cables exit the chassis via two cable glands on the left had side of the device. The adjustment assembly is located on the right. The internal configuration of drill unit is shown in figure 6.7.

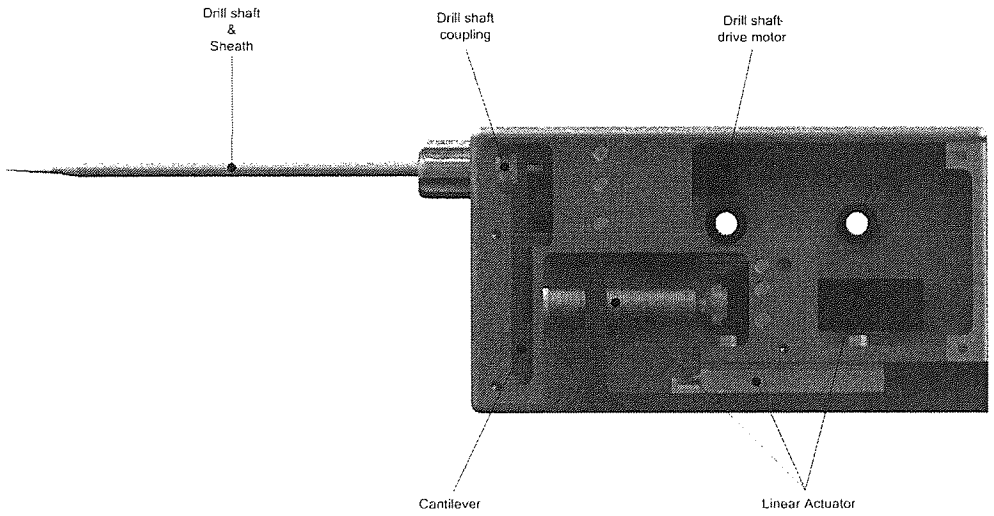

Figure 6.7: *Drill unit internal components.*

6.2.2.1 Linear Actuator System

In order for the drilling system to operate autonomously the drill unit is linearly actuated along the drilling axis. The actuation is achieved using the lead screw and motor assembly shown in figure 6.8.

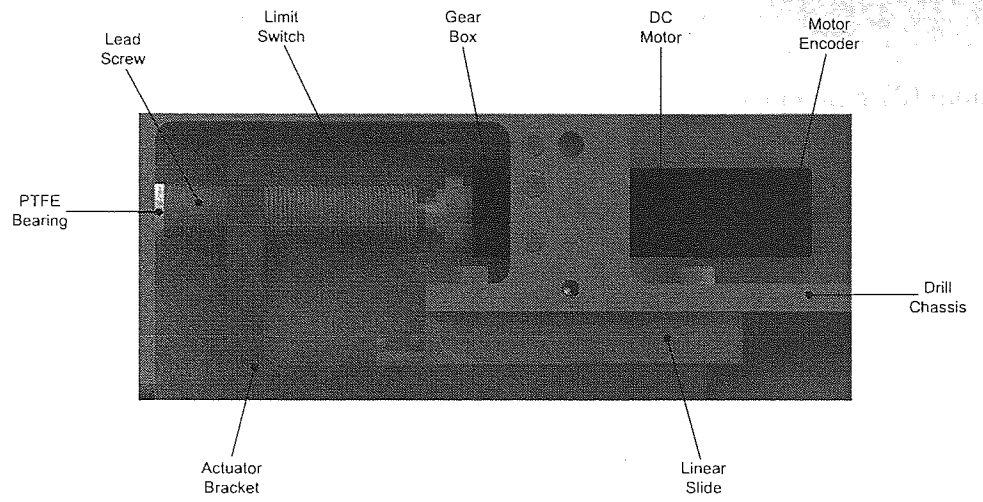

Figure 6.8: *Linear actuator mechanics.*

Mechanics

The drill unit is mounted on the actuator bracket using a high precision linear slide. The motor, mounted within the drill chassis, is coupled to the actuator bracket via a 29 mm hardened stainless steel, precision lead screw with an M6 fine pitch thread, giving 0.75 mm of travel per revolution. The opposite end of the lead screw is located in a PTFE bearing also mounted on the drill chassis. The motor is mounted with a 5 N preload to minimise backlash in the motor bearing.

Drive System

The actuator is driven by a Maxon RE10, 0.75 W DC motor, combined with a rotary encoder and a 64 : 1 planetary gearbox (3). The motor has a maximum permissible speed of 300 Hz, when combined with the gearbox and the lead screw pitch this equates to a maximum linear velocity of 3.5 mm/s. The motor is driven by a linear amplifier controlled by a PID loop running on the low level controller. This will be described in more detail later in section 6.3.1.3.

Position and Velocity Feedback

Position feed back is generated by a Maxon MR256 magnetic encoder (3) mounted on the rear of the motor. This encoder has a quadrature output and thus position and direction can be derived. The quadrature signal is generated by two channels, 90° degrees out of phase. A single encoder count is clocked on each rising and falling edge of each channel giving an effective resolution of 1024 counts per revolution. The gearbox multiplies this resolution to give 65536 counts per revolution of the output shaft. Thus the theoretical linear resolution, neglecting backlash, is 0.01 μm. The gearbox backlash is rated at 2° at the input shaft. This is equivalent to 7 encoder counts, or 0.7 μm linear precision providing a sufficient level of accuracy for this application. An inductive limit switch is used to define a reference position, these sensors are non-contact and have a very repeatable trigger position. In this application absolute position accuracy relative to a datum is not necessary, this only needs to be used when the drilling system is initialised to define the start position and travel range.

6.2.2.2 Sensing Elements

The sensing elements are the most critical part of the drilling unit, they are responsible for relaying information about the state of the drilling process at the tool tip. A section through the drill unit showing the sensor configuration is shown in figure 6.9. To ensure that the sensing elements are as robust as possible, both are mounted inside the instrument and are decoupled from the chassis to prevent disturbance due to handling or environmental noise.

Force Sensing

Force sensing is achieved using a basic cantilever arrangement. The cantilever itself is mounted at the front of the drill unit, secured by four sets screws at its base. This makes it possible to change the cantilever to suit the force requirements of different applications.

A thrust bearing is located at the top of the cantilever in which the drill shaft rotates, a flange at the end of the drill shaft rests against the bearing surface.

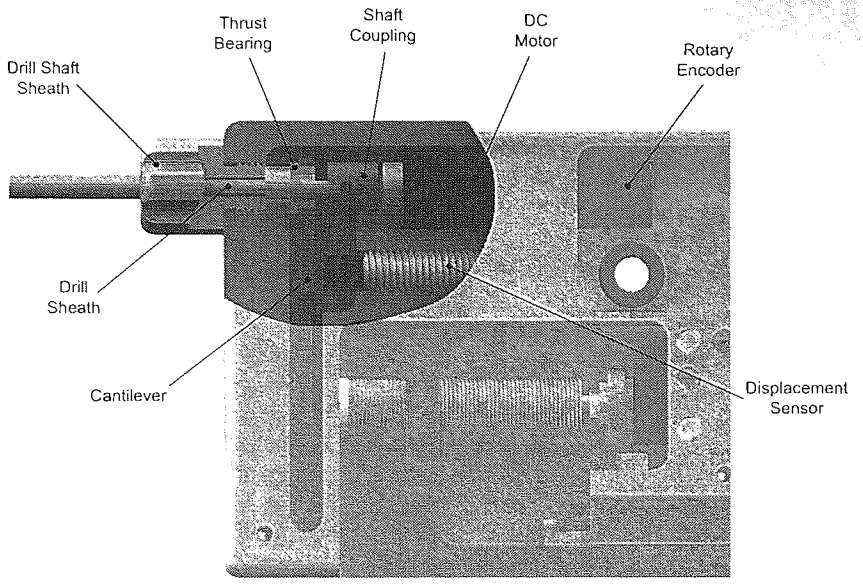

Figure 6.9: *Drill drive system and sensors.*

Any axial force applied to the drill tip is translated along the drill shaft deflecting the cantilever.

Initially PTFE bearings were used, however problems occurred with the bearing sticking under load introducing noise in the torque signal. Ball bearings were considered as a potential replacement however their rigid nature introduces further noise into the torque signal as the cantilever deflects. A suitable replacement was found in Drylin® polymer bearings from IGUS UK (13). The low friction, hard wearing nature of the material significantly reduced noise in the torque signal. Polymer bushes are also very compact.

The cantilever design was optimised for a peak force of 3 N, approximately twice of that required by the cochleostomy procedure. When the cantilever deflects it affects the alignment of the drill shaft bearing, as such the cantilever deflection has to be designed to use the minimum deflection required to achieve the desired force resolution. The stress and displacement plots for the chosen cantilever design are shown in figures 6.10 and 6.11. The peak deflection of this cantilever at maximum load (3 N) is 140 μm at the tip, the sensor is located 10 mm below the loading point at which the deflection is estimated as 60 μm. Assuming the deflection is linear this equates to 20 $\mu m/N$, giving a minimum

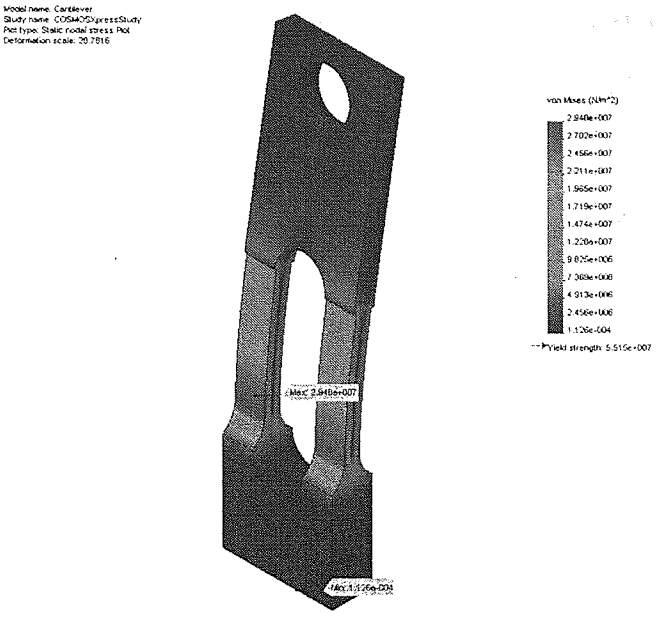

Figure 6.10: *Cantilever stresses at maximum load.*

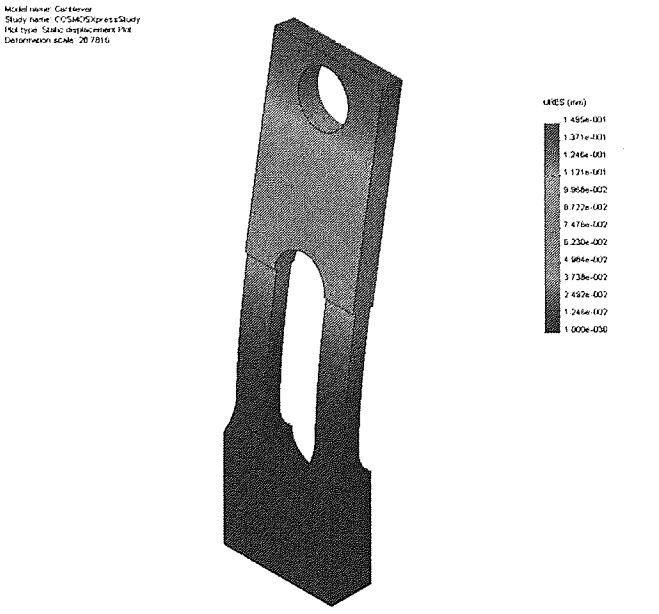

Figure 6.11: *Cantilever displacement at maximum load.*

required sensor resolution of 20 nm. At maximum load the safety factor of this design is 1.86 indicating that it operates well within both the elastic limit and the yield strength of the material therefore hysteresis and plastic deformation are avoided.

Deflection of the cantilever is measured using an eddy current sensor from Micro-Epsilon. This range of sensors is optimised for displacement measurements of non-ferromagnetic elements and is capable of sub-nanometer dynamic resolution. The eddyNCDT 3701-U1 from Micro-Epsilon (17) has a minimum working distance of 0.1 mm and a nominal range of 1 mm with a maximum resolution of 1.3 nm. The sensor is supplied with an integrated power supply and conditioning unit that gives a voltage output proportional to the displacement of the measurement target. Taking into account the data acquisition range and scaling this gives an effective force resolution of 0.25 mN.

6.2.2.3 Drive System

The drill shaft is driven by a Maxon RE10 1.5W DC motor, similar to that used in the linear actuator, however, no gearbox is used on this motor to maximise torque sensitivity. In order to do this the velocity control loop described earlier has been implemented. Velocity feedback is generated by differentiating the position information from a Maxon MR256 rotary encoder.

Torque Sensing

The torque sensing uses the motor current method described in section 4.2.1.2. This sensing method is electronic based and as such has no specific design requirements, that said, correct alignment of the cantilever in which the drill shaft bearing is held is critical. Misalignment of the cantilever induces cyclic noise in the torque transient.This was eliminated by using an alignment tool which screws into the front of the device where the drill shaft sheath normally sits. This tool, when screwed in, has a stud protruding where the drill shaft would normally locate, this is fixed and mates with both the drilling (motor) axis and the bearing axis of the cantilever. This ensures the correct alignment when fitting the

cantilever.

Drill Shaft Coupling

The drill shaft coupling consists of two parts, a blade and slot as shown in figure 6.12. The drill shaft can be seen connected in the left hand view, with the drill shaft-motor coupling located directly behind. The blade is located on the drill shaft flange that sits within the cantilever bearing. The slot portion is mounted on the motor shaft. This arrangement efficiently transfers the rotary motion without interfering with the linear displacement of the drill shaft along the drilling axis due to a load at the tool tip. The inset view shows an alignment

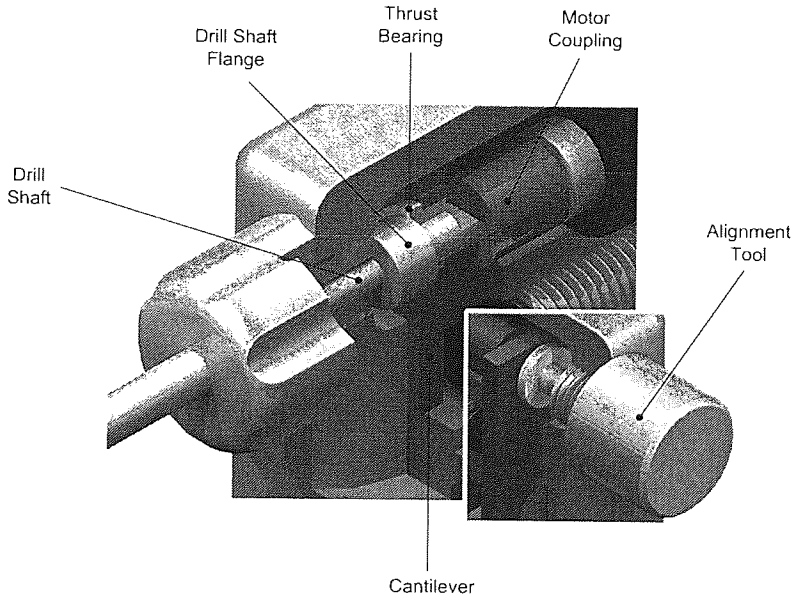

Figure 6.12: *Drill shaft coupling and cantilever alignment tool (inset).*

tool in place of the drill shaft that is used to align the cantilever bearing prior to drill shaft insertion.

6.2.2.4 Drill Shaft

The drill shaft and sheath are the only parts of the system that should come into contact with the patient, thus sterility is crucial. The drill shaft assembly has

been designed to be completely removable and can be sterilised by any method including autoclave. A section view of the assembly is shown in figure 6.13. The drill shaft is made of $\varnothing 2.2\ mm$ stainless steel hypodermic tubing, this has an

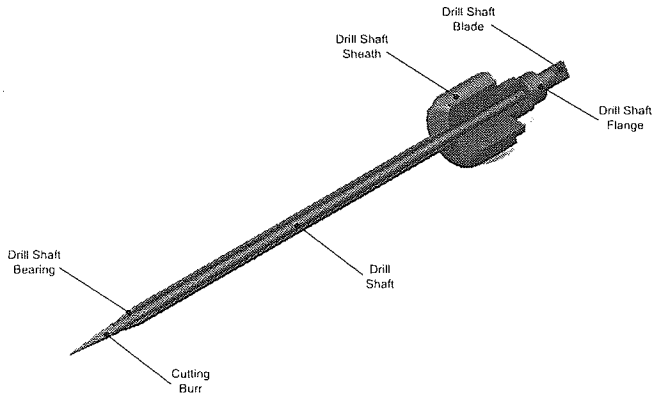

Figure 6.13: *Drill shaft assembly.*

internal diameter of 1.6 *mm* which will accept standard friction grip dental burrs. The overall shaft length from blade to tip is 100 *mm*. Additional support to give the shaft more rigidity is added by inserting an 80 *mm*, $\varnothing 1.6\ m$ stainless steel rod, this leaves a 10 *mm* recess at the end of the tube to insert the burr. The drill shaft sheath is also made from hypodermic tubing 3.3 *mm* in diameter which is affixed to a titanium thumb screw which locates on the drill chassis. The opposite end of the tube has a polymer bearing to reduce the friction force experienced by the rotating drill shaft and it also provides extra support close to the drill tip. All parts in the assembly are bonded together with the exception of the cutting burr which uses a friction grip so it can be changed, making the burrs disposable. The drill shaft is inserted into the sheath from behind which, in turn, is inserted into the drill chassis. The drill shaft flange locates in the cantilever thrust bearing, the blade in the motor coupling and the sheath is screwed in tightly completing the assembly.

6.2.2.5 Adjustment Mechanism

The macro positioning of the instrument is achieved by manipulation of the locking arm and the drill unit manually by the clinician. The arm, being self supporting, allows the drill unit to be placed in the vicinity of the subject along an approximate trajectory to within a few millimeters of the operative site. At this point the support arm is locked and the clinician begins using the surgical microscope. As described in Chapter 4, selection of the hole location is critical to a successful outcome, as such a method of easily fine tuning the drilling trajectory, that can be used in conjunction with the microscope is required.

This has been achieved through the use of the dual axis rotational adjustment assembly shown in figure 6.14.

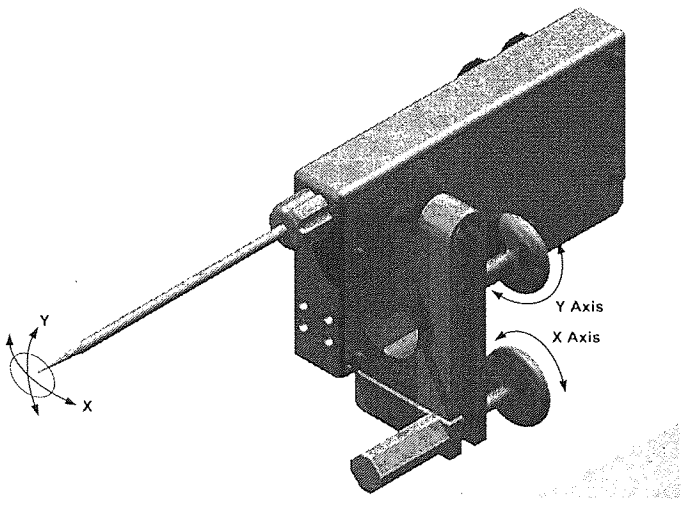

Figure 6.14: *Drill trajectory adjustment assembly.*

The adjustment assembly consists of three components, two thumb screws and the adjustment bracket. The bracket is made from a single piece of titanium; wire erosion was used to create the complex geometry of the part enabling the mechanism to be as compact as possible. After machining, a pre-load was applied across each pivot arc to allow motion in both directions.

The pivot arc on each axis acts as a sprung hinge at the centre of rotation. The assembly has two rotational axes which intersect the drilling axis at the same point, denoted as the fulcrum in figure 6.15.

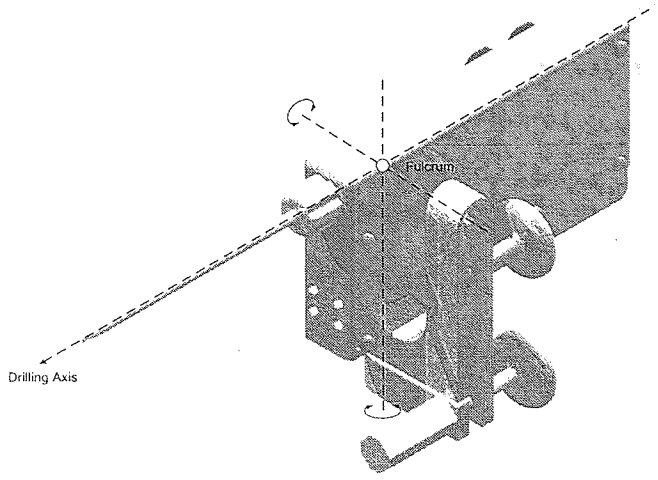

Figure 6.15: *Rotation axis of the adjustment assembly.*

This provides a centre of rotation coincident on the drilling axis eliminating lever affects making the travel symmetrical about all axis. The drill tip rotates about the fulcrum at a radius of 117 mm, each thumbscrew is offset by 18 mm thus a single turn of one of the thumbscrews equates to approximately 4 mm of linear motion at the drill tip. The mechanism allows the drill tip to be positioned anywhere within a 25 mm^2 area. Although the motion is rotational rather than linear, the large radius minimises the angular deviation between the drilling axis and the target to an absolute maximum of 2° which is insufficient to have any impact on drilling performance.

6.2.3 Drill Controller

The drill controller contains all the drive and control electronics including the power supply and the embedded controller itself. It is the central hub of the system, housing all the sockets that enable the three sub-systems to be plugged together: the drill unit, the host PC and the hand-held remote control.

6.2.3.1 Controller Enclosure

The specific design of the controller enclosure for a device at this stage of development is not critical, it has to be functional rather than be optimised for manufacture with commercial requirements in mind. That said, this is something that must be considered for the future.

The functional requirements of the enclosure are:

1. to contain and protect internal electronics from environmental noise, contaminants and rough handling;
2. prevent accidental contact with sensitive or potentially harmful parts of the system;
3. provide a platform to which the other subsystems can be connected.

With these requirements in mind a suitable enclosure was chosen. Made entirely from metal the enclosure acts as a Faraday cage minimising electromagnetic interference from external sources as well as reducing emissions. This is particularly important in the operating theatre due to the amount of high power equipment contained within a very small space. This is especially true when highly sensitive analogue signals are used. Fully screened cables are also used between sub-systems for the same reasons.

The connectors are industrial standard, key polarised, multi-pole connectors with locking rings. This makes sure the system is easy to assemble; the rugged nature of the plugs combined with the key polarisation mean that it is not possible to incorrectly connect the sub-systems and once in place they lock preventing them from accidentally being dislodged. The drill controller enclosure along with the host computer and the remote control are shown in figure 6.16.

6.2.3.2 Hand-held Remote

The hand-held remote control was designed to be as simple to operate as possible. The unit is small and fits in the palm of the hand, additional weight was added so that it sits comfortably. The unit, shown in figure 6.17, is water resistant and the keypad is a four button, class IP67 rubberised keypad. The pad has a

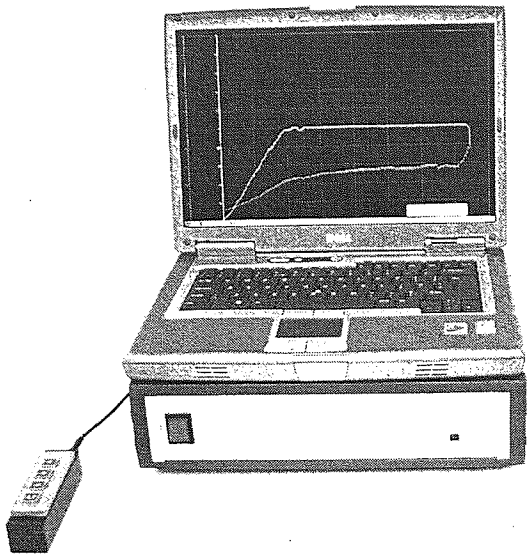

Figure 6.16: *The drill controller, host PC and remote control.*

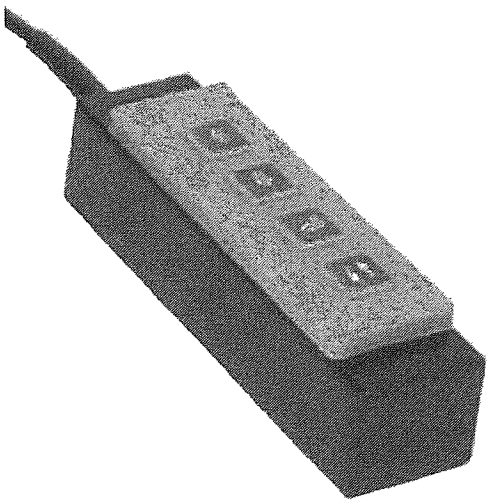

Figure 6.17: *Hand-held remote.*

very tactile feel and provides a click that can be felt when the button is pressed ensuring that the user is aware when a button is pressed. The remote provides four basic functions, advance, retract, start and stop.

6.3 Electronic Design

When considering the electronic design and architecture of any system there are three key considerations:

1. Stability,
2. Reliability,
3. Robustness.

These factors become even more important in the context of the surgical environment as they also have a significant influence over safety and performance of a device operating under those conditions.

In the case of the surgical micro-drill this is especially true; the device operates in an autonomous capacity. That is, it interprets sensor data in real-time and makes decisions based on a set of predefined conditions without the need of intervention from the clinician. As such it is vital that the data is as accurate and up to date as possible and free from interference from the environment in which the device is operating. This is also true of the control aspects of the system as one of the key principles behind robotic surgery is that a system can perceive, interpret and respond immediately to situations that could not be detected and controlled by a clinician.

It is for these reasons that a two tier embedded architecture was chosen for the implementation of this device.

An embedded system is inherently more stable than one running on a computer. It removes the reliance of the device on the host computer that may be running several applications simultaneously, all competing for resources. The hardware of the embedded system is designed around the application and the firmware is significantly less complex and specific to the task at hand.

Such a system can be broken down further into levels dictated by the function of the device. In this application two tiers provide a sufficient platform to operate the device from. A high level controller, or system supervisor, operates the high level functions such as data handling, processing and interpretation while a low level, or hardware controller takes care of all of the basic control and I/O functions of the device. This approach ensures that the higher functions of the system are not affected by the simpler, but more intensive control functions.

The electronic design described in this section is based on the system level specification shown in figure 6.18, part of which was derived form the low level controller design described in section 4.2.1.2. The detail electronic design, PCB layout and assembly was carried out by Shand Systems Limited (85).

6.3.1 Controller Hardware Architecture

Figure 6.18 shows a schematic of the drill controller hardware architecture.

Detailed circuit diagrams can be found in figures A.2, A.3, A.4 in the appendix.

6.3.1.1 Host Computer

Although the system makes use of a host computer, it is not necessary to operate the device. The host software running on the computer provides a means of altering configuration parameters if necessary, visualising and logging drilling data received from the drill controller.

6.3.1.2 High Level Controller

The high level controller performs all the data handling, pattern recognition, instruction processing and PC communications. The breakthrough detection and control strategies are all hardware coded within the controller as well as all control functions. The micro-controller selected for this function was the Cypress EZ-USB® FX2 (10). This device is based on the widely used 8051 core and has a fully integrated USB 2.0 transceiver. It also has the additional benefit of an external 16-bit interface allowing additional memory and peripherals to be addressed

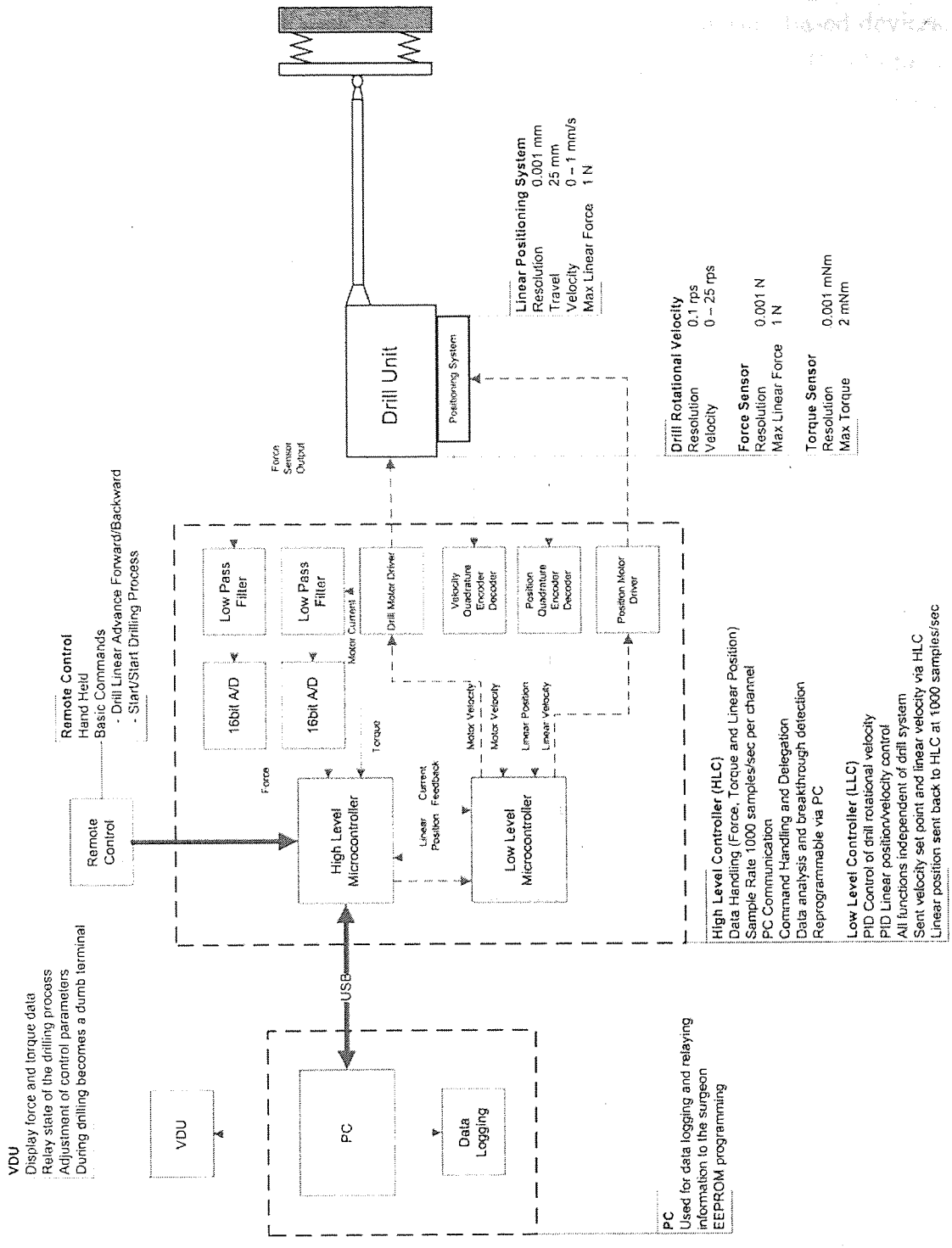

Figure 6.18: *Drill hardware architecture overview.*

directly via a high speed bus. The hardware integrated peripherals significantly reduce the operating overhead when compared to similar firmware based devices. This is also true of the USB transceiver, the device has integrated FIFO buffers, clock timings and control registers implemented in hardware so the use of the USB communications has little or no processor overhead leaving the core free to process data and significantly reducing the complexity of the firmware. The 16-bit architecture of this device enables high speed data processing and lends itself well to application development in the C programming language.

This device was coupled with a 256kb SRAM memory chip via an inbuilt 16-bit parallel data bus and the 8-bit parallel address bus to provide additional memory for buffering data. Using the device in this way meant it could be addressed internally at high speed by the cypress micro-controller as if it were an extension of the internal RAM.

Due to the lack of internal non-volatile memory in the Cypress device a 2kb EEPROM chip was connected via the I2C bus to provide storage for configuration data and the USB device descriptors.

6.3.1.3 Low Level Controller

The low level controller subsystem is based on the test rig controller described in section 4.2.1.2; it is a dedicated hardware controller responsible for handling all the principal mechanical functions of the drill; the controller receives parameters from the high level controller and uses a PID algorithm to maintain the unit position and angular velocity of the drill bit. These functions are completely autonomous and are independent of the operation of the high level controller. The device chosen for this task was the Microchip PIC18F4620 (7), this is an 8-bit RISC based micro-controller capable of up to 10 million instructions per second *(MIPS)*. It has 64kb of flash memory, 4kb of RAM, 1k of EEPROM and an extended 16-bit instruction set with programmable interrupts. The fast operation and large memory enable the device to perform a multitude of tasks simultaneously. These devices are low cost, very stable and ideally suited to control applications. Programming of this device is also performed in the C programming language.

6.3.1.4 Peripheral Devices

There are a number of peripheral devices in the drill controller that perform various functions within the system. The key functions are:

1. Analog data acquisition,
2. Quadrature encoder decoding,
3. Analog output,
4. and data Buffering.

Analog Data Acquisition

Analog data acquisition is performed by ADS7807 single channel 16-bit analog to digital converter from Texas Instruments (23). The chip is capable of doing an analog conversion in less than $26\mu s$ with a maximum error of 1.5 LSB. This is also a low cost, low power device that uses a standard 8-bit parallel bus interface.

Quadrature Encoder Decoding

Quadrature decoding is performed by an HCTL-2032 quadrature decoder from Avago Technologies (5). The linear actuator and the drill drive system each use a single chip to provide position feedback. This device has a built in filter to remove noise from the encoder signal and have internal shift registers that track position. Again, they are interfaced via an 8-bit parallel bus but they also provide a clock and direction output which is more appropriate for velocity control.

Analog Output

The motor drive subsystem uses a dual channel digital to analog converter *(DAC)* from Analog Devices (9). The device is a 12-bit DAC capable of outputting $\pm 10\ V\ DC$. Again an 8-bit parallel interface is used so this device also has register select lines to allow for its dual capability. The second stage of the analog output

stages is a linear amplifier and relay for controlling the DC motors. Given that this is the only high power part for the device, this is current limited for safety reasons.

Data Buffering

Data buffering is performed by two (one upstream and one down stream) asynchronous FIFO buffers from IDT (12), the IDT7200L. This device is a 256 byte by 9-bit buffer which can be read and written to simultaneously, it also has built in empty, half full and full flags combined with a very high read and write speed making it ideal for use as a high speed buffer.

6.3.1.5 Internal Hardware Communication

In order for the controller to function correctly, communications between the various devices have to be as efficient as possible and steps must be taken to avoid data loss or corruption. The most efficient way to achieve this is implement a bus architecture. A bus is a communication pathway that connects all the devices in a subsystem and there are two main types of bus, data and address. Each bus has master and a number of peripherals or slave devices. The master is connected to the address decoder via the address bus. The address decoder is then connected to the control lines of all the peripheral devices.

All buses are routed via the programmable logic device *(PLD)* as its primary function is as an address decoder. An address decoder is typically a logic device that has a high number of I/O pins and can perform basic logic functions extremely quickly. When the master wishes to talk to a peripheral it sends the associated address to the decoder, this in turn toggles the appropriate control lines depending on what the master wishes to do. The I/O pins of the devices on the bus are what is known as tristate, this means they can be configured as an input, output or put in a high-impedance state in which the bus is unaffected by the presence of the device whether it be active or not. This means that communication between different devices is possible along the same pathway without interference.

A PLD such as the Altera MAX 3000A (2) is ideal for this task, it is a low cost, low power, high pin count device that can be programmed to perform multiple tasks simultaneously as though they were implemented in hardware. This is a single chip, re-programmable solution that offers maximum flexibility. The use of a PLD as a dedicated address decoder also means that I/O pins on the master do not have to be used as control lines which also eliminates the processor overhead that would be required to implement this at a such a high level.

The drill controller has four main communication pathways; a single 16-bit data bus with an 8-bit address bus, two 8-bit data buses each with a 4-bit address bus and the universal serial bus. A block diagram of the communication pathways is shown in figure 6.19. The only peripheral located on the HLC's 16-bit bus is external memory. Each of the controllers (the HLC and LLC) have their own individual data bus which is connected to each of its peripherals. In the case of the LLC, the peripherals are:

- HLC write FIFO,
- LLC read FIFO,
- Dual channel digital to analog converter,
- Linear actuator position decoder,
- Drill velocity decoder,
- PLD.

The HLC peripherals are:

- LLC write FIFO,
- HLC read FIFO,
- Force analog to digital converter,
- Torque analog to digital converter,
- PLD.

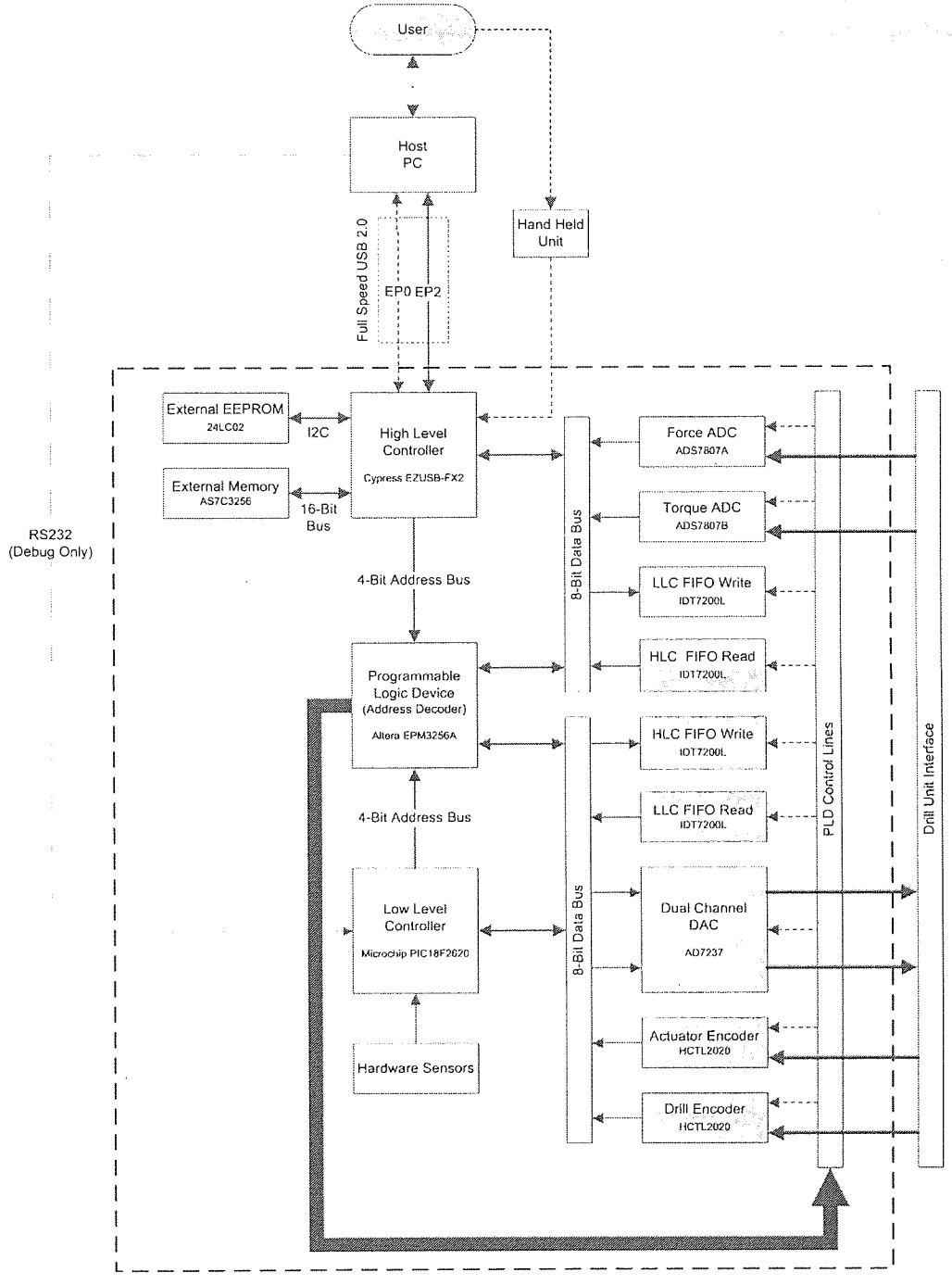

Figure 6.19: *Drill hardware communication schematic.*

The two buses are bridged by a pair of first-in-first-out *(FIFO)* buffers, one upstream and one down stream. This allows the two controllers to communicate without the risk of cross-talk between the buses which may cause corruption of other, higher priority traffic. As the name suggests, the buffer works on a first in, first out principle and as such data sent, but waiting to be retrieved is queued in sequence so no commands or data are lost. While this protocol works for most traffic, in this application there are two exceptions. To enable the drill rotation control loop to function effectively the LLC requires the motor current. This is acquired by the analog to digital converter located on the HLC bus and communication via the FIFO buffer would be two slow. The same goes for the HLC as it requires the position of the linear actuator each time it acquires a force and torque sample. To get around this the PLD is also located on both buses and provides an addressable register on both buses from which the values can be read. This will be described in more detail in the next section as it is implemented in the firmware.

6.3.1.6 External Communication

The universal serial bus, or USB, is used for communications between the host computer and the drill controller. This differs from the internal bus because it uses serial communication rather than parallel, as the name suggests. USB is a low-cost, high speed interface capable of sustained transfer rates of up to 480 $MBit/s$. It is a widely used platform and almost every modern computer now has USB ports available. The interface fully supports Plug'n'Play meaning the user simply plugs the device into a computer and it is automatically recognised and configured. These reasons make it a good choice when interfacing any device with a computer.

USB communications are conducted via a series of channels called endpoints. A USB device can have up to 32 endpoints, 16 upstream and 16 down stream. Endpoints are uni-directional with the exception of endpoint zero *(EP0)* which is used for control transfers which consists of commands and status information and up to 64 bytes of additional data. Control transfers are hardware timed and

are continuous where as all other transfers across other endpoints can be asynchronous depending how the device is configured. Each individual USB transfer is called a frame, when using USB 2.0 in high speed mode the frame interval is 125 μs.

This device makes use of EP0 for command and status information and EP2 in bulk transfer mode for the transmission of data to the host computer.

6.3.2 Sensing Elements

The force and torque measurement is performed by the 16 *bit* dual channel analog to digital converter described in the previous section.

The deflection of the cantilever is measured using the eddyNCDT 3701-U1 eddy current sensor (17) which generates a voltage proportional to the displacement of the cantilever. This voltage is input directly into the analogue to digital converter via a simple unity gain op-amp buffer. Any further signal conditioning is unnecessary as this is performed by drive electronics of the sensor.

The deflection of the cantilever is designed to be approximately 1 mm at a load of 2 N, this is matched with the active sensing range of the eddy current sensor giving an effective maximum resolution of 0.1 mN, this is a factor of 10 higher than the required force resolution. A simple experiment was conducted to calibrate the force measurement system. The drill unit was mounted vertically and a mass was mounted on the drill shaft such that a known force was applied to the cantilever. The mass was increased in 10 g increments and the voltage output recorded. The calibration curve is shown in figure 6.20. During testing it was found that the system suffers from a degree of hysteresis and the zero point can shift by up to 0.3 V. To account for this a force offset was added to compensate for the shift, a force offset is performed prior to each procedure. The force is calculated using equation 6.1.

$$F = (V_{adc} - V_{off}) \times M \tag{6.1}$$

Where M if the gradient of the linear approximation, 0.612 V/N, and V_{off} is the

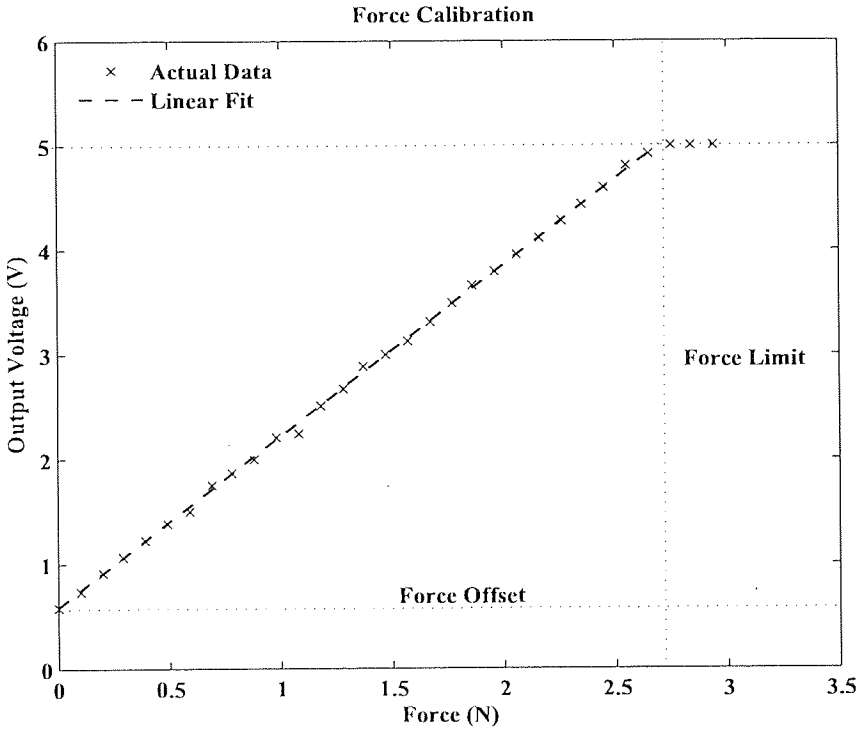

Figure 6.20: *Force calibration curve.*

voltage offset.

Using this force calibration the stiffness of the complete drilling system was evaluated using the conact routine described in section 2.3.1.1. Contact was initiated against a rigid, non-compliant surface and the stiffness was estimimated as 2.818 N/mm with a typical measurement error of ± 6 mN/mm.

The torque measurement is derived from the motor current. A low value potentiometer placed between the output of the motor and ground and is used to generate a voltage. This voltage is passed through a low gain amplifier and filter, into the analogue to digital converter. The value of the potentiometer is adjusted such that the output voltage of the amplifier and filter peaks at $+5$ V when the motor current is at its maximum. The use of the amplifier has several benefits, firstly the bandwidth can be set to act as a low pass filter, secondly the additional gain enables the use of a very low value resistor thus motor performance is unaffected and finally it acts as a high impedance buffer protecting the rest of the circuit.

The torque characteristics of DC motors are well characterised and highly repeatable, more so than is possible to measure in the laboratory; therefore the torque calibration uses a different approach. The gain of the amplifier is adjusted to output 5 V at the peak current and the maximum current is defined in the manufacturers data for the motor as is the torque constant. Subtracting the no-load current and using these values the motor torque can be derived directly. This provides sufficient accuracy; precision is more important as the compliant drilling technique looks at changes in the drilling torque rather than absolute values. As such the precision is derived by the acquisition electronics. The peak motor current is given as 360 mA, which equates to a peak torque of 3.24 mNm, this is scaled to give a voltage output of 5 V to match the maximum differential voltage of the analog to digital converter. At 16 *bit* resolution, this gives a theoretical torque resolution of 0.05 μNm. The peak to peak noise of this signal when operating a constant load is approximately 3 units which equates to an equivalent of 0.15 μNm actual resolution. Although this is out of specification the use of digital filtering of the signal brings the performance up to the specified level.

6.4 Firmware Architecture

Firmware is the name given to the program that operates within an embedded device. Like software, firmware is written using a programming language for example assembler or C. Once compiled firmware is downloaded to the read only memory of a programmable device like one of the Microchip PIC series devices. Once there the code cannot be altered and is executed by the processor core within the device, it can only be changed by reprogramming the device.

The firmware architecture describes how the programmable devices within the controller operate and interact to enable the drilling system to function. These devices are all programmed via a computer using an external programmer that interfaces with the control board via a socket. The drill controller has three flash based, programmable devices:

1. High level controller,
2. Low level controller,
3. and the programmable logic device.

Each have specific tasks, the top level functions of which were briefly described in the previous section.

6.4.1 High Level Controller

The high level controller uses a combination of software timed loops for low priority tasks and hardware driven interrupts for high priority, timing critical tasks. The main program loop is shown in figure 6.21. The main program loop starts on power up with the initialisation routine. This routine configures the device and its peripherals as well as performing some basic power-on-self-tests *(POST)* to ensure the device is operating correctly, this includes the configuration and initialisation of the USB port and timing interrupts.

Upon completion of the POST and device configuration the main program continuously loops every 2 μs. The main loop has three key tasks each carried out by a subroutine:

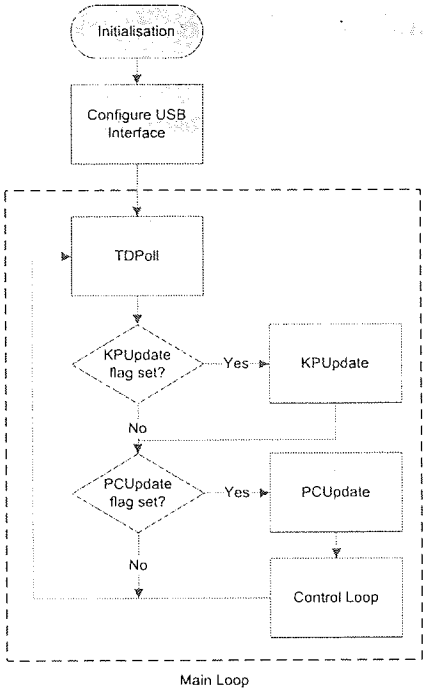

Figure 6.21: *Main program loop of the HLC.*

1. Hardware Communication,
2. Data acquisition and processing,
3. Execution of control sequences.

6.4.1.1 Hardware Communication

Further to the hardware communication protocols described in the previous section the bus master devices require a means to transfer data between each other and the host PC in such a way that the data can be received and interpreted correctly.

Internal Hardware Communication

Communication between devices within the drill controller is handled almost entirely by the hardware to improve efficiency, this minimises the processing overhead for the bus master device when requesting data from a peripheral. In the

case of communication between the controllers within the device this is a little more complicated. These two devices communicate directly by a pair of FIFO buffers and as such the devices themselves have to be able to verify and interpret data coming from the buffer. This is done by packetising the data prior to sending it, and then acknowledging it upon receipt. This ensures that no data is lost or corrupted, and if it is, it is detected and handled appropriately. Figure 6.22 shows the typical structure of a FIFO packet. The packet consists of a header

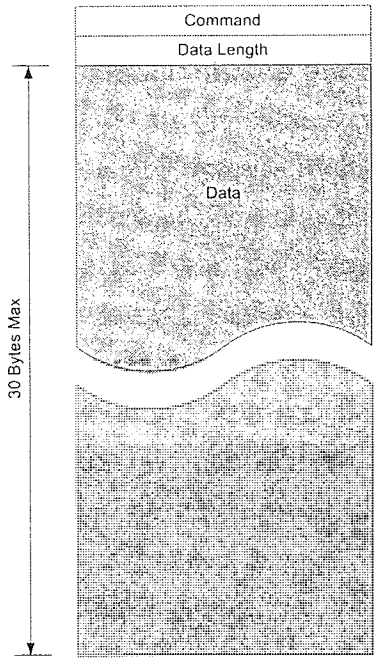

Figure 6.22: *Internal communication packet.*

that contains details of the command and the length of any data sent, for example if the linear velocity was to be set the command would be PC_DVEL with which two bytes of data would be sent, thus the Data Length would be 2.

Upon receipt of the command the LLC would save the data into its EEPROM, if that was successful it would return the command value to the HLC along with the new value of the velocity. The HLC then checks the received value against the command issued, if they match the error flag is cleared other wise the command is issued again. If a command fails more than once the error flag is set and the drill is halted and the operator alerted.

Host Communication

Communication between the host PC and the high level controller is conducted over the universal serial bus. Although all transfers across the USB are handled by the hardware the data has to be arranged in the USB frames in such a way that it can be decoded at the host end. This is dictated by the way in which the data is put into the buffer by the firmware of the USB device.

Each communication transaction requires acknowledgment and verification, also known as handshaking, as such it is again necessary to packetise the data to be transferred. This means that the data is put into the buffer in a specific sequence, the data is then extracted in the same sequence upon receipt. Along with each USB transfer the number of bytes is included along with a checksum and is used to verify that the data has been transmitted successfully, if this is not the case an error code is generated and the system is halted.

Command and status information is transfered between the HLC and the host via the bi-directional endpoint 0. Data is transfered from the HLC to the host by endpoint 2 which is a uni-directional, bulk transfer pipe.

Commands and the associated data can be sent from the host PC via EP0 where they are executed immediately due to the interrupt configuration on the USB device. Endpoint 0 is a hardware timed transfer that occurs every 125 μs and is triggered by the host PC. A transfer is initiated even if there are no commands in the command queue, in the event that a command is issued the command as well as the number of bytes received is echoed by the device accompanied by the status information and configuration parameters of the controller. If a command is not echoed or is echoed incorrectly the host knows an error has occurred and can take appropriate action. This ensures that no commands go astray and that no false commands are issued; the host always displays the correct configuration data even if communication is interrupted. EP0 is 64 *bytes* wide and each transfer contains a single packet. Figure 6.23 shows a typical EP0 data packet. Endpoint 2 operates in a similar fashion, it uses a software trigger to transmit the data contained within the buffer. The firmware running on the device starts a transfer once the FIFO buffer has been filled with data. The FIFO is 512 *Bytes* wide, each data packet is 16 *bytes* long, thus once 16 data packets have been written to the

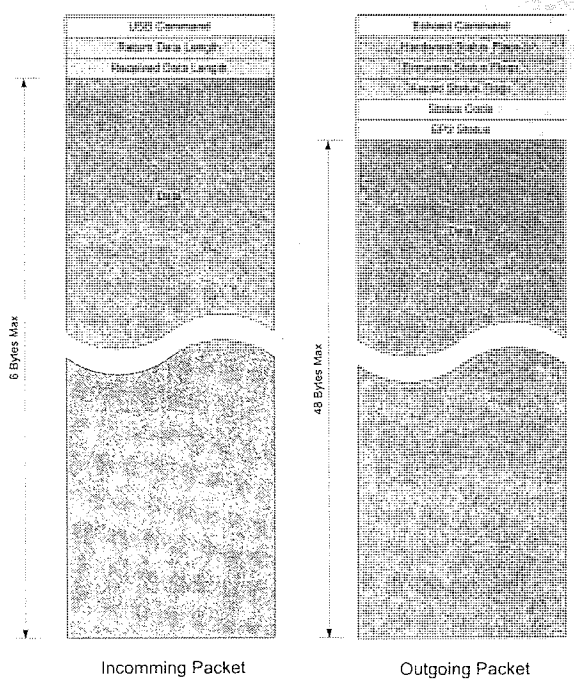

Figure 6.23: *Endpoint 0 outbound and inbound control transfer packets.*

buffer a transfer is automatically initiated. As such transfers occur approximately at 16 ms intervals. Figure 6.24 shows a typical EP2 data packet.

Remote Keypad Control Interface

The remote keypad is interfaced directly with the HLC and provides a means for the clinician to directly control the system.

The keypad uses a parallel interface and is continuously monitored. When a key is pressed a software interrupt is triggered and the keypad decode routine is initiated. The flow diagram for this routine is shown in figure 6.25. The firmware uses software de-bouncing to prevent extraneous button presses being detected. This is done via the use of a PRESSED flag, this is set as soon a button press is detected and it remains set until both the action has been executed and the button has been released by the operator.

Given that the operator only requires supervisory control the remote provides four functions:

1. Advance drill unit,

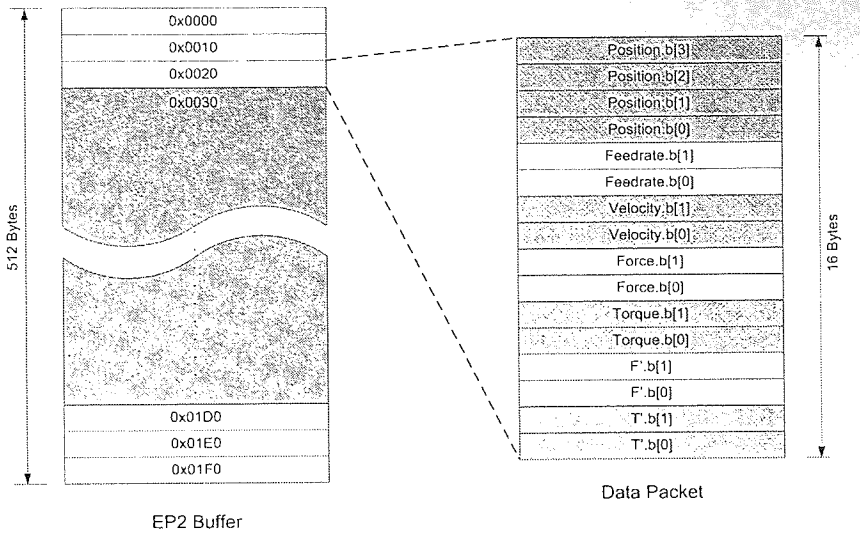

Figure 6.24: *Endpoint 2 data packet.*

2. Retract drill unit,

3. Start next control sequence,

4. Pause/Stop and reset.

The advance and retract button move the drill unit back and forth along the drilling axis a single 0.1 *mm* increment per button press.

The start button initiates the next control sequence in line, if no sequences have been executed previously, the contact sequence is started. This button also functions as a resume button. If the PAUSED flag is set and the start button is pressed the system continues any action it was performing prior to being paused.

The control functions are only available to the user when the drill is performing an action. If the drill unit is executing a command the PBUSY flag is set. While this is the case the only available button is stop. In this situation when stop is pressed and released the system is paused, if stop is pressed again the unit is retracted slowly to the home position.

If the stop button is pressed twice in quick succession an emergency stop is executed. This ceases any action the drill is currently performing, for example drill rotation, and retracts the drill at maximum velocity. Once reached, a full system reset is performed.

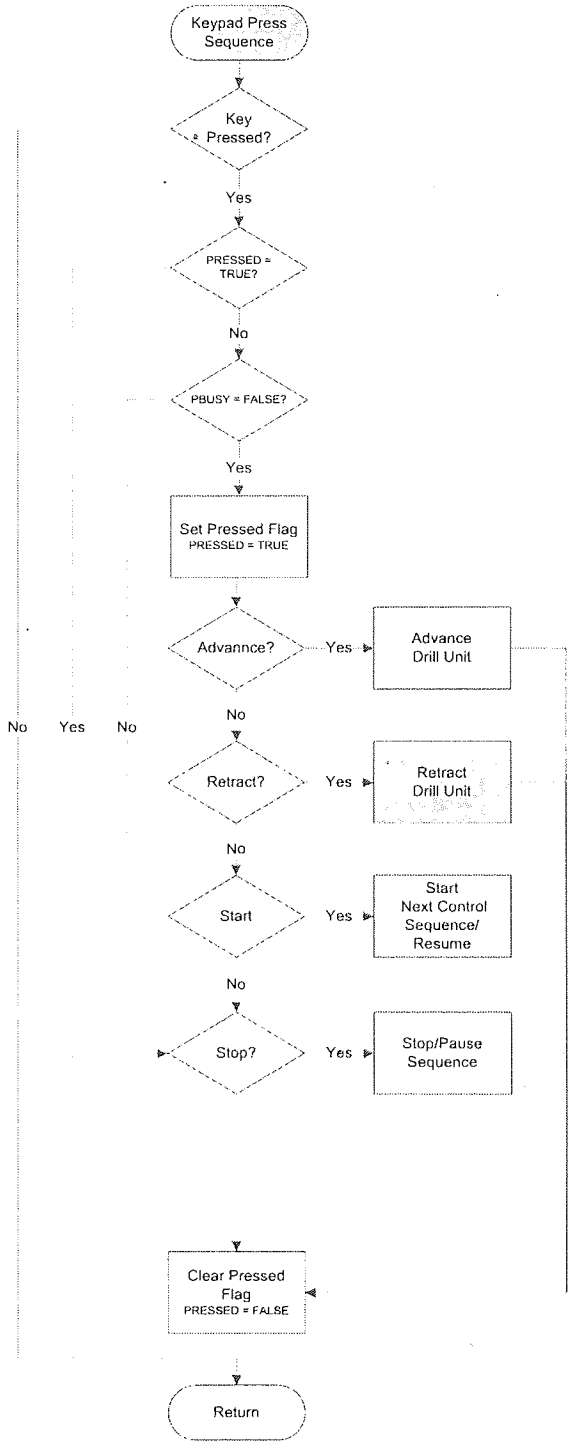

Figure 6.25: *Keypad routine flow diagram.*

The individual control sequences for each button are shown in figure A.9 in the Appendix.

6.4.1.2 Control Sequences

The overall control strategy dictates how the system handles the drilling process from start to completion. The control strategy is broken down into a series of sequential steps, each governed by an individual control sequence or subset of sequences.

Given that the firmware works on an iterative basis, calculating new values on each pass, the control sequences must also be executed in this fashion. The main loop is shown in figure 6.26. The sequences are controlled by what is called

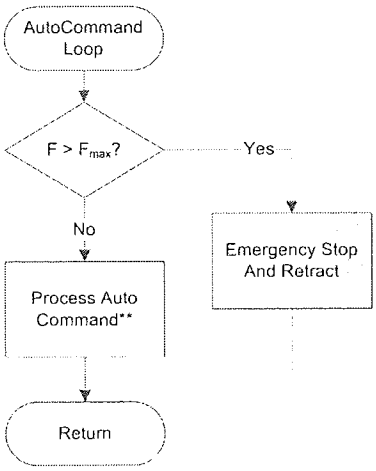

Figure 6.26: *AutoCommand Loop (** See figure 6.27).*

the AUTO_COMMAND routine, each sequence is initiated by either the host computer or the by the clinician using the had held remote. The routine are controlled using the *AutoCommand* parameter which indicates the current sequence being executed, and the *StatusCode* parameter which indicates the current status within that sequence. These parameters are updated on each pass through the control loop and dictate what happens on the next pass. All events within the AUTO_COMMAND routine occur in series and upon completion pass onto the next event in the chain.

A flow diagram for the command sequences is shown in figure 6.27. The

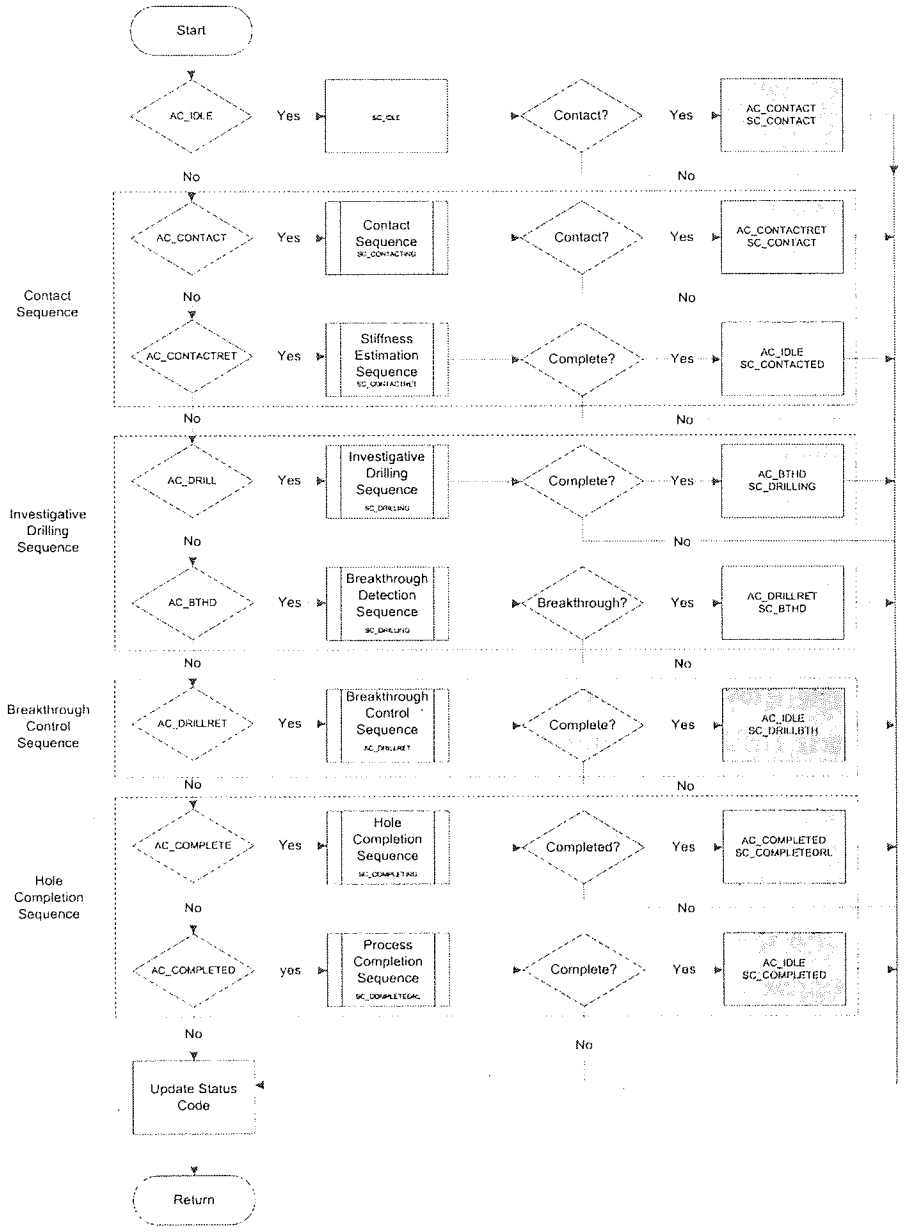

Figure 6.27: *AutoCommand subroutine flow diagram.*

sequences are divided into phases, each phase corresponds to a stage in the control strategy. The individual AutoCommand sequences can be found in the Appendix in figures A.5, A.6, A.7 and A.8.

Control Timing

Although the main program loop is a software timed loop, it is driven by control flags that are set via hardware driven interrupts. The only exception to this is the TDPoll routine which checks to see if any data has been received from the LLC and is awaiting retrieval from the FIFO buffer. This occurs on every loop of the main program. This ensures the HLC retrieves data from the FIFO extremely quickly and the computational routines always have up-to-date data. The only transfers from the LLC other than the position data transfer are echoed commands that indicate that a command from the HLC has been successfully received and executed.

For data sycronisation the hardware timed loop that handles the USB transfers is used as the timing source for the control loops. This interrupt occurs every 125 μs. On each event the KPUpdate flag is set, and every eight loops the PCUpdate flag is set. Although this interrupt initiates a USB transfer, this is handled by the hardware and has no impact on the software loop timing, the complete interrupt routine is executed in less than 1 μs.

Once the appropriate flags have been set and the device has returned from the interrupt routine the tasks within the main program loop are executed on the next cycle. As such the tasks are executed in the correct sequence and well within time. The timing intervals for the sequences listed above are 2 μs, 125 μs, 125 μs, and 1 ms respectively.

The high priority interrupts over and above these processes are the receipt of commands from the host computer, the pressing of the stop button on the remote and the generation of an error command.

Each of the key subroutines described above performs a primary task and a series of sub-tasks to achieve the former.

6.4.1.3 Data Acquisition and Processing

The data processing routine is called every millisecond and follows the process flow shown in figure 6.28. The routine starts with the acquisition of a sample

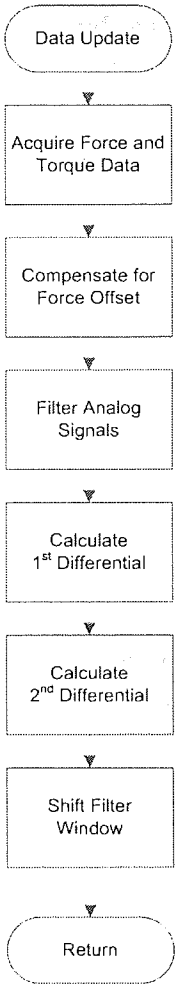

Figure 6.28: *Data processing subroutine stages.*

from each of the analog sensor channels.

Due to hysteresis in the cantilever each time the system is initialised a force calibration is performed and a force offset calculated, this offset is applied to each force sample as it is acquired. After the data acquisition is complete, the data is filtered to remove high frequency noise. It is then differentiated twice; this provides all the parameters necessary for the detection of breakthrough. The calculated values are stored in memory for use by the control algorithms. There

are up to 256 samples from each dataset resident in memory at any one moment in time, as such this represents the maximum possible window size for a digital filter.

Each time the processing routine is run a packet of data is created consisting of the position, velocity, force, torque and gradient data. Each packet consists of 16 bytes of data and the EP2 buffer holds 512 bytes of data and the packet is saved directly to the buffer. The Cypress micro-controller uses an auto pointer that increments the buffer address automatically after each write. When the byte count in the buffer reaches 512 the data is automatically transmitted to the host and the buffer cleared ready to accept more data. As such there is a USB data transfer every 16 *ms* which is ample time for the host to process each frame. As mentioned earlier the USB transfers are handled entirely by the hardware and as such the routine timings are unaffected.

The final task in the routine is to shift the window of the filter.

Data Filtering

By the very nature of the application and given the scale of the features that are key to successful detection a low signal to noise ratio reduces the effectiveness of any method used. Different noise reduction schemes were explored. Several factors had to be considered when looking at improving the signal to noise ration:

- computational efficiency;
- memory footprint;
- feature attenuation;
- phase shift;

The first two items are a result of limitations of the hardware controller, the later two are design limitations of the filters themselves. The filter has to be implemented in the firmware of the device and as such a faster, more computationally efficient algorithm is desirable. High frequency noise is the biggest problem, most of which is generated by three main sources.

The torque is derived from the drive motor current, which is in turn driven by a PID velocity loop. This has the effect of introducing noise due to the PID loop refresh rate at approximately 1 kHz. This is exaggerated by the control function. To achieve optimum velocity control large swings in motor current are generated as the control loop maintains the desired velocity. As such the PID loop is tuned to give an acceptable level of velocity control, while still maintaining the signal integrity.

The second source of noise is mechanically induced by the cutting faces of the burr interacting with the tissue. This occurs at approximately six times the rotational velocity of the drill bit.

The third source is a quantisation effect due to the use of an analogue to digital conversion combined with the effect of the sampling frequency. Other sources include noise from bearings and ambient noise. Breakthrough occurs at sufficiently low frequency that it can be considered a DC signal and as such is not affected greatly by the attenuation introduced by heavy filtering, however, phase shift presents a problem.

Simple 1^{st} and 2^{nd} order low pass recursive filters *(e.g. Butterworth and Chebychev)* proved effective at reducing noise however the computational efficiency of these algorithms was very low due to the number of floating point calculations required. The most efficient method explored was a recursive n-sample moving average filter, however, this introduced a high degree of phase shift. A non-recursive n-sample moving average filter was chosen, despite having a larger memory footprint than the recursive algorithm, the algorithm is also very computationally efficient. A side benefit from having a large memory footprint is that the historic data is always available for use by other algorithms. The use of this type of algorithm enables breakthrough detection to function in real-time and the use of a non-recursive filter means there is minimal phase shift. The algorithm is represented by equations 6.2 and 6.3, where F is the input data, $\bar{F}$ is filtered output value, n is the current sample, i is the i^{th} sample in the filter window and k is the filter window width.

$$\bar{F}_n = \frac{1}{n}\left(\left[\sum_{i=n-k}^{n} F_i\right] - F_{n-k} + F_n\right) \tag{6.2}$$

$$\bar{T}_n = \frac{1}{n}\left(\left[\sum_{i=n-k}^{n} T_i\right] - T_{n-k} + T_n\right) \tag{6.3}$$

Mean Deviation Implementation

The mean deviation calculation is implemented in a similar fashion to the filter algorithm. The mean deviation is defined as the rate at which the transient deviates from the mean of the last n samples. The formula for which is expressed in Chapter 2 in equation 2.14. Like the filtering algorithms, a running sum is used from which the first sample within the averaging window is subtracted and the latest sample is added. Clever use of memory pointers ensures that this process is executed within a few instruction cycles and the new sum is divided by the mean window width. The deviation is calculated by subtracting the current value from the mean.

Differentials

The differential calculation is a very simple one. The mean deviation is in effect a measure of the rate of change of the sensor transient and as such can be approximated as the gradient or first differential. Given that the signal is a time based capture with a fixed period between samples, the second differential can be calculated by simply looking at the difference between the current and previous first differential as shown in equation 2.15.

Memory Management

Handling this amount of data quickly and efficiently is difficult especially when operating inside an embedded system where resources are extremely limited. A large portion of the time taken for a function to execute is taken up by the manipulation of memory and movement of data; as such it is vital that any algorithms operating on such a device have as small a memory footprint as possible and are required to move large amount of data as little as possible.

One implementation of an averaging algorithm may individually sum each

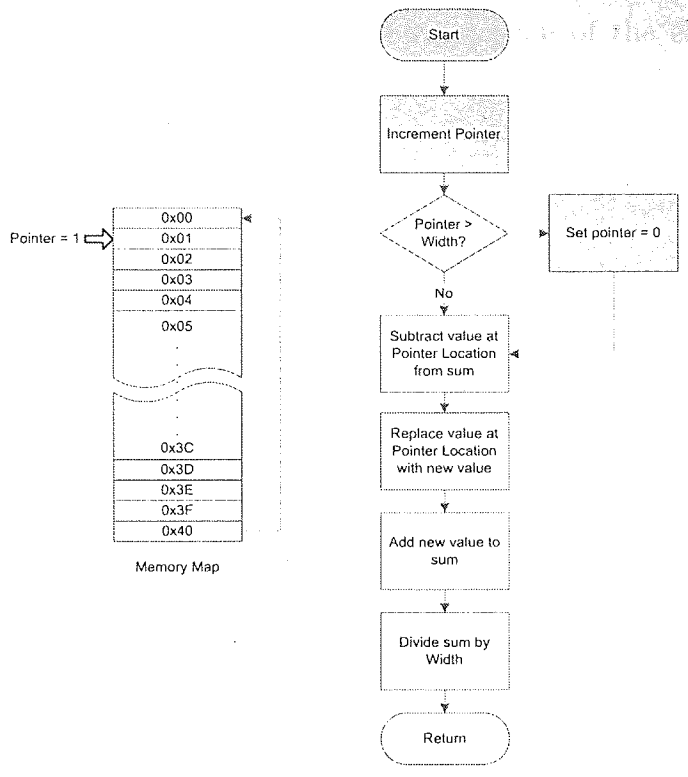

Figure 6.29: *Window shift subroutine and local memory map.*

value and then divide by the number of samples, after each operation the entire averaging window is moved one point to the left and the new value added on the end. This is very inefficient, a better approach is to use a running average.

The algorithms maintain a sum resident in memory and simply subtracts the first value in the filter window from the sum and then adds the new value. The sum is them divided by the window width. The most complicated portion of this algorithm is in fact calculation of the pointer value. To minimise the memory usage the amount of data kept resident in memory is equal to the window width, as such there is no space available to write new values. The new value must be written over the oldest value within the window and several counters are employed to ensure that the position of these values is kept track of. Figure 6.29 shows the instruction flow and memory map. Memory footprint is also aided by the use of temporary variables, and passing them from function to function, however, there is a degree of processing overhead involved in this.

The values are kept as integers to reduce the processing overhead, but it must

be noted that this has a knock on effect on precision of the estimation when compared to the use of floating point values.

Breakthrough Detection

Breakthrough detection operates using a set of empirically determined thresholds. The drilling system makes decisions on the current state at the tool tip by taking into account the following parameters:

1. Force and torque magnitude,
2. Force and torque mean deviation,
3. Force and torque rate of mean deviation,
4. Duration over which each each threshold is met.

Notice that all of these criteria are independent of position as is necessary when drilling under compliant conditions. Each of these criteria, or combinations there of, relate to specific conditions; the key states for these combinations relate to patient movement relative to the drill and obviously the breakthrough condition. Thus the states between which the current system is able to differentiate are:

1. Target moving away from the drill,
2. Target moving toward from the drill,
3. Target moving laterally,
4. External disturbance,
5. and the breakthrough condition.

The decision flow that the device goes through is shown in figure 6.30. So if the patient moving toward the drill is taken as an example; this is characterised by an increase in both the force and torque magnitudes over and above that which would be expected as a result of the drill feed rate. Thus the force and torque deviation magnitudes, $F^{'}$ and $T^{'}$, exceed the set thresholds and the force and

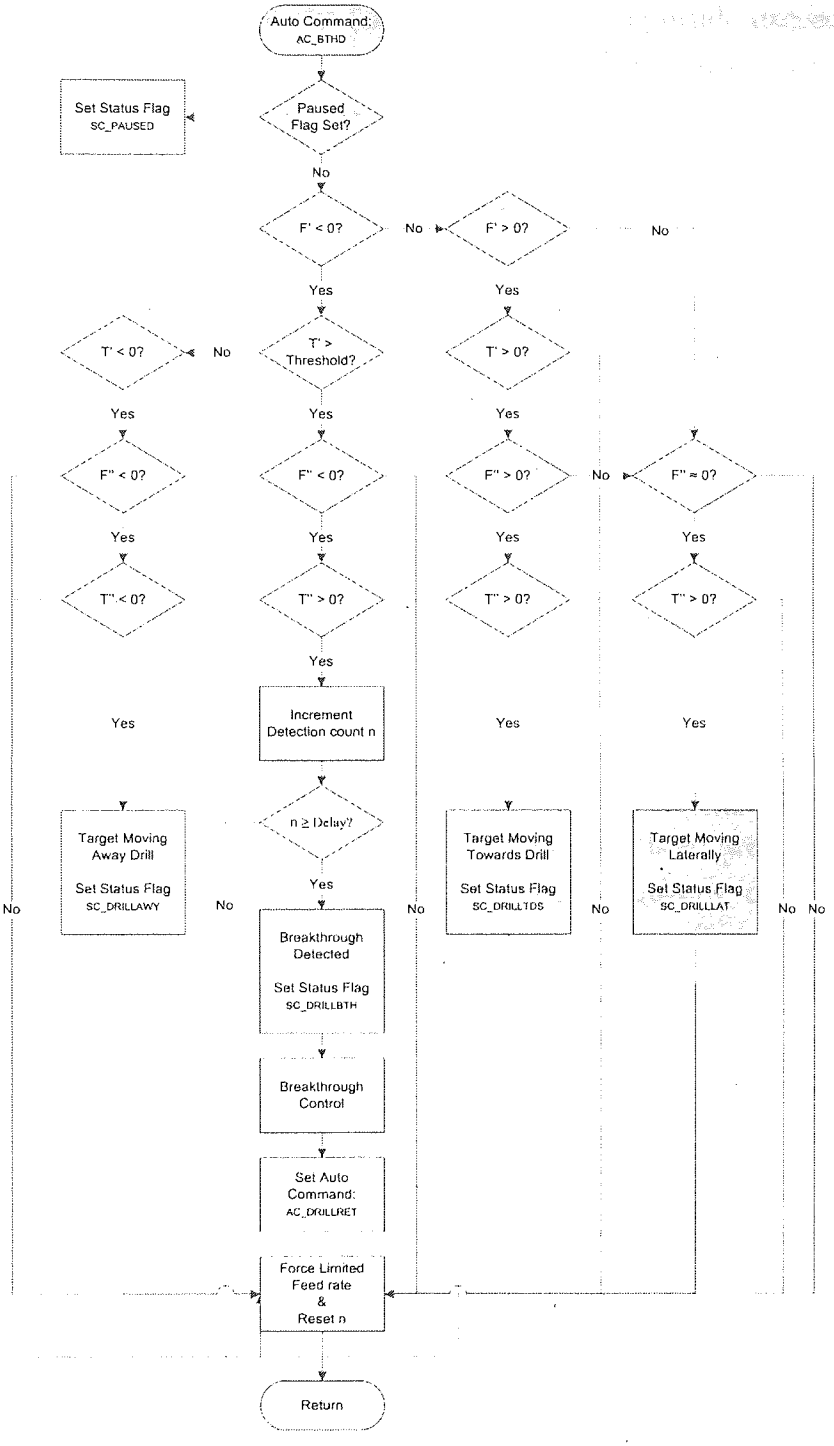

Figure 6.30: *Drilling state decision process.*

torque deviation rates, F'' and T'', are both positive. In contrast, the breakthrough condition is met when the force and torque magnitude exceed also the set threshold, but in opposite directions, so F' and T' exceed the set threshold but F'' is negative and T'' is positive.

At this stage, to determine the state of the drilling process the firmware takes the values calculated by the processing algorithms described above and uses them within the series of conditional statements shown in figure 6.30.

The only exceptions to these rules are unexpected, sudden external disturbances, for example someone bumping into the operating table. In this case a variety of conditions can occur. This can make characterising the response to sudden disturbance very difficult, however, these events occur very quickly and the transients tend to stay in phase. When compared to the duration over which drilling events occur, it is a very short period of time. As such rather than try to catagorise disturbances like this it is possible to negate them by making the system take into account the duration of any feature that occurs.

A typical example of this is when drilling is initiated. At this stage the burr is in contact with the surface of the target, when rotation is started there are large fluctuations in the drilling transients which can manifest as breakthrough due to the conditions at the tip and the surface geometry. As these are caused by the burr cutting into the target, the oscillations are high frequency, once the burr is bedded in, the oscillations cease.

The firmware takes this into account by counting the number of times the routine loops while the condition is satisfied, if at any point the criterion is no longer met the count is reset to zero. If the count reaches the duration threshold *(loop count threshold)* the condition is determined to be true and the system takes the appropriate action.

This set of conditions can be expanded further to encompass a much wider variety of conditions using more parameters, however due to code size limitations it was not possible to implement at this stage, this may well be a necessary future development.

In the case of the detection of breakthrough, the breakthrough control strategy is initiated. The flow diagram for this subroutine can be found in the appendix in figure A.7.

6.4.2 Low Level Controller

The operation of the low level controller is almost entirely independent of the higher level functions of the drilling system. It was specifically engineered this way to ensure that the timing critical control functions of the LLC would be unaffected by the more processor intensive functions of the HLC. The core tasks of the controller are:

1. Position and velocity control of the linear actuator,
2. and velocity control of the drill drive motor.

The architecture builds on the prototype controller described in section 6.3.1.3, incorporating not only the control loop optimised for providing torque feedback, but a separate velocity and position controller for the linear actuator and command interface through which the device can be controlled.

6.4.2.1 Command Interface

Command Handling

All commands are received directly from the HLC via the FIFO buffer. When a byte is put into the buffer a flag is set that indicates that there is data waiting to be retrieved. This flag triggers an interrupt on the LLC which retrieves any data from the buffer and processes it. The FIFO interrupt is the lowest priority interrupt after the PID update timer and the limit switch. As such, upon completion of the update routine any awaiting commands are executed immediately.

When a command is received and executed the parameters are echoed back to the HLC to acknowledge the command. This is vital as it ensures that no commands go astray, or more importantly, no incorrect commands are received. For example, the setting of one of the controller gains. In this case the command is received along with an identifier and a value of the gain. When executed the gain value is written to the device's non-volatile EEPROM at the location specified by the identifier. Once written, the value is then read back from the memory and both the command and the retrieved gain are returned. The HLC then checks

what was received against what was sent, if an error has occurred a flag is set, the operator is notified and the system is halted.

Interrupt Handling

Given the timing critical nature of the hardware control, the LLC is entirely interrupt driven. Three primary, high priority interrupts operate the main sub-routines, each of which is assigned a priority level with higher priority routines being executed first. The interrupt priorities are as follows:

1. Actuator limit switch,
2. Timer interrupt,
3. Command interrupt.

The highest priority is assigned to the actuator limit switch. The limit switch should only be triggered during the initialisation sequence, however, in the unlikely event that this does occur under general use, it is vital that the controller reacts to prevent damage to the system.

The PID control loops are driven by an internally timed interrupt which occurs every millisecond. This is the second highest priority. The timing of this routine is critical as the interval is used in the velocity calculation for both the drill and the linear actuator, as such it is critical that timing remains unaffected.

The lowest of the three high priority interrupts is the command interface. Although the command interface has the lowest interrupt priority which may pose the greater risk from a safety point of view by introducing potential latency between the HLC issuing a command an the LLC responding; the largest delay that can occur is equal to the length of time over which the PID loops are executed. This is approximately 500 μs which has minimal impact on the overall system performance.

The priority structure ensures that system critical tasks are performed at the correct time, if a lower priority interrupt is triggered while a high priority event is taking place the lower priority events are queued. Once the higher of the

queued events has been carried out, the next in the queue is executed. When programming, care had to be taken to ensure that these events cannot overlap.

When the LLC is not busy, that is not processing an interrupt, the main program loop writes current parameters to the non-volatile memory region and verifies data located there. This is so that in the event of a power failure, the system can perform a 'warm' start allowing it to resume from where it left off rather than having re-initialise the whole system.

6.4.2.2 Drill Velocity Control Loop

The drill velocity PID loop was also based on the prototype described in chapter 3. The flow diagram is shown in figure 6.31 The implementation is very similar to that described in chapter 3 however as two separate loops have to be executed in the same time frame some improvements in efficiency had to be achieved.

This was done in a number of ways, firstly all the values were scaled so that integers could be used throughout rather than floating point numbers. Secondly the gains, scale factors and units are used to calculate constants outside the main loop by which the error terms are multiplied reducing the calculation of each PID component to a simple multiplication. This also allows the use of cumulative sums for the current command and integral terms.

The calculation of the error terms carried out within the loop are expressed by equations 6.4, 6.5 and 6.6.

$$V_{err}^{t} = V_{cmd}^{t} - V_{A}^{t} \tag{6.4}$$

$$V_{errint}^{t} = V_{errint}^{t-1} + V_{err}^{t} \tag{6.5}$$

$$V_{errdiff}^{t} = V_{err}^{t} - V_{err}^{t-1} \tag{6.6}$$

Where V_{cmd} is the velocity command, V_{err} is the velocity error, $V_{errdiff}$ is the differential velocity term and the integral error sum, V_{errint}^{t-1}, is a cumulative sum

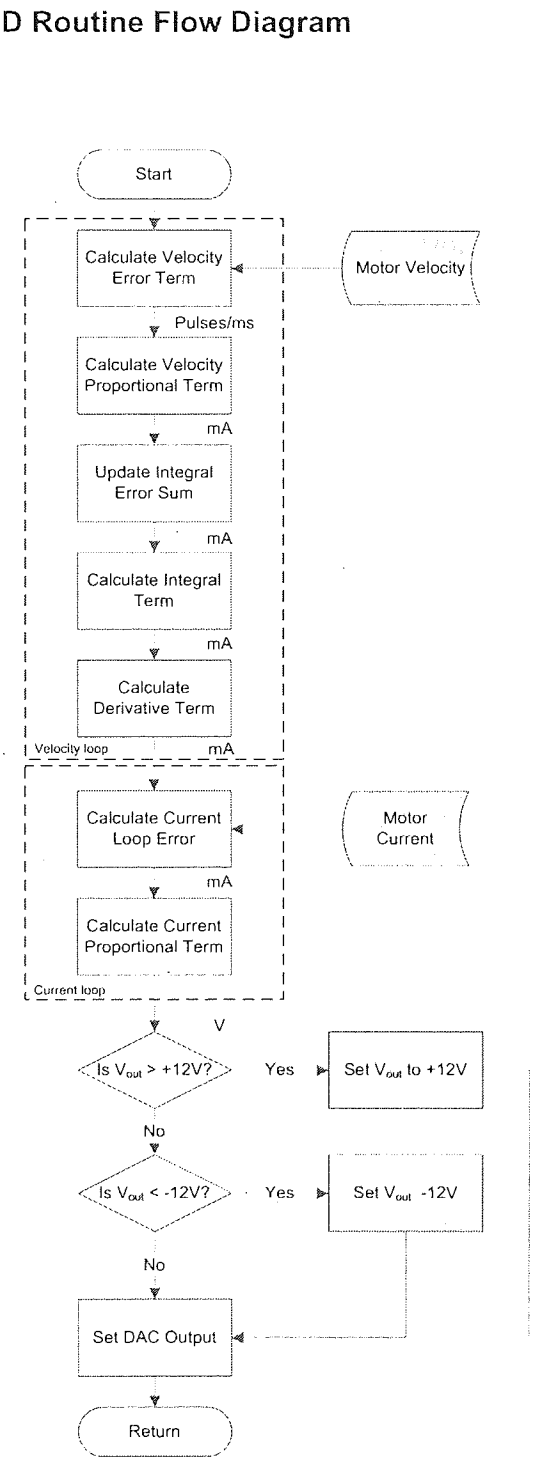

Figure 6.31: *LLC PID Loop.*

that can be expressed by equation 6.7.

$$V_{errint}^{t-1} = \sum_{0}^{t-1} V_{err}^{t} \tag{6.7}$$

The current command, I_{cmd} is calculated using equations 6.8, 6.9 and 6.10.

$$I_{cmd}^{t} = V_{err}^{t} \times K_p \tag{6.8}$$

$$I_{cmd}^{t} = I_{cmd}^{t} + (V_{errint}^{t} \times K_i) \tag{6.9}$$

$$I_{cmd}^{t} = I_{cmd}^{t} + (V_{errdiff}^{t} \times K_d) \tag{6.10}$$

Where K_p, K_i and K_d are the proportional, integral and derivative gains respectively. The voltage output, V_out, to the motor is given by multiplying the current command by the current proportional gain, K_c as shown in equation 6.11.

$$V_{out}^{t} = I_{cmd}^{t} \times K_c \tag{6.11}$$

The scaled gain parameters used in the controller are shown in table 6.1.

Gain	Value
K_p	10
K_i	0.2
K_d	1
K_c	0.01

Table 6.1: *Drill velocity PID Parameters.*

Drill Performance

Figures 6.32 and 6.33 show the drill drive motor velocity control performance. Figure 6.32 shows sixty second capture of velocity data with a constant friction

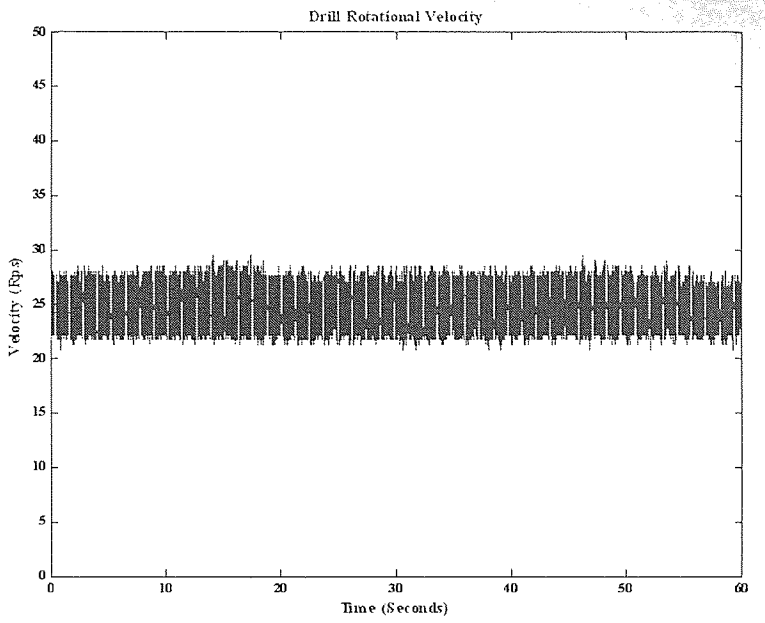

Figure 6.32: *Drill rotational velocity performance, 60 second capture.*

force applied to the drill shaft rotating with a set velocity of 25 *rps*. It can be observed that the velocity is controlled to within two revolutions per second. Figure 6.33 show the velocity sample distribution over the sixty second capture. The data set shows a mean velocity, $\overline{V}$ of 24.71 *revolutions per second* and has a standard deviation, of $\sigma = 1.32$.

6.4.2.3 Actuator Position and Velocity Control Loop

The linear actuator uses the same DC motor as the drill drive subsystem and again, the key requirement for the linear drive is provision of a constant linear velocity although a degree of position control is required. As such, the velocity loop described above was also used for this controller although the gain parameters are slightly different. The use of the gearbox means that the typical operating velocities are significantly higher and as torque feedback is not required and greater integral and current terms are used to improve the control performance.

These values were empirically determined using the drill drive motor parameters as a reference point.

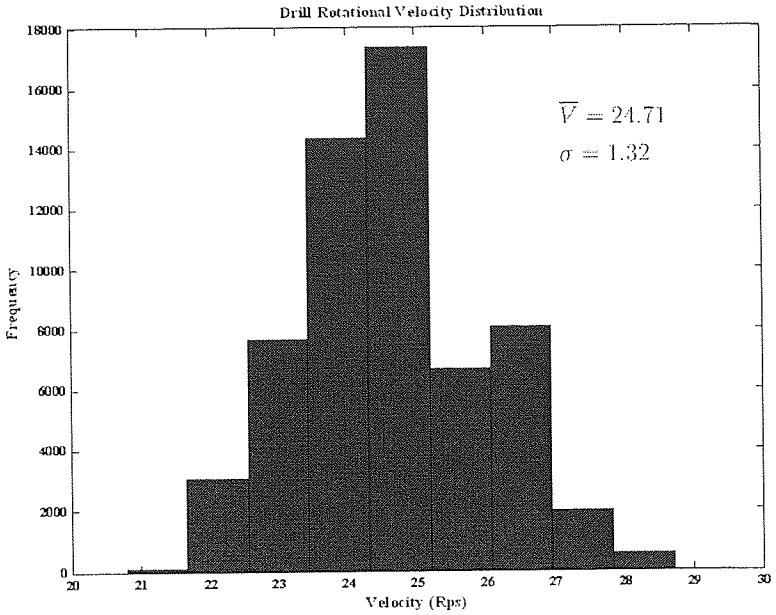

Figure 6.33: *Drill velocity distribution.*

Gain	Value
K_p	10
K_i	2
K_d	1
K_c	0.1

Table 6.2: *Linear actuator PID Parameters.*

The position control uses a simple proportional algorithm that reduces the velocity as the target position is reached however due to the very low velocities involved the position control is very tolerant with no overshoot and does not compromise performance.

Initialisation and Positional Accuracy

To achieve a high level of accuracy and precision involves not only the control loop, but the way in which the system creates and uses a reference point. This system uses an inductive limit switch with a very repeatable trigger position to define the start position for the actuator system.

The instrument performs intialisation sequence to define this reference position when the device is turned on. The sequence follows the following steps:

1. Set linear velocity to 1 mm/s,
2. Retract until limit switch is triggered,
3. Set linear velocity to 0.01 mm/s,
4. Advance until the limit switch goes low,
5. Stop and set reference position.

A series of 30 tests were conducted in which the actuator was initialised and the reference *(home)* position defined. The target position was then set to 12.5 mm and the actuator moved back and forth between the target and home position. On each oscillation the position reached and the trigger position were measured using a 1 μm digital dial gauge mounted against the drill chassis. Figure 6.34 shows the target position error as measured via the dial gauge. Figure 6.35 shows the distribution of the limit switch trigger position. It can be seen that both distributions centre on zero and have standard deviations of 1.2 μm and 1.4 μm respectively.

The velocity performance is shown in figures 6.36 and 6.37. The data was acquired over a period of sixty seconds with a set velocity of 0.01 mm/s and a sample rate of 1 kHz. It can be observed that even at minimum velocity the

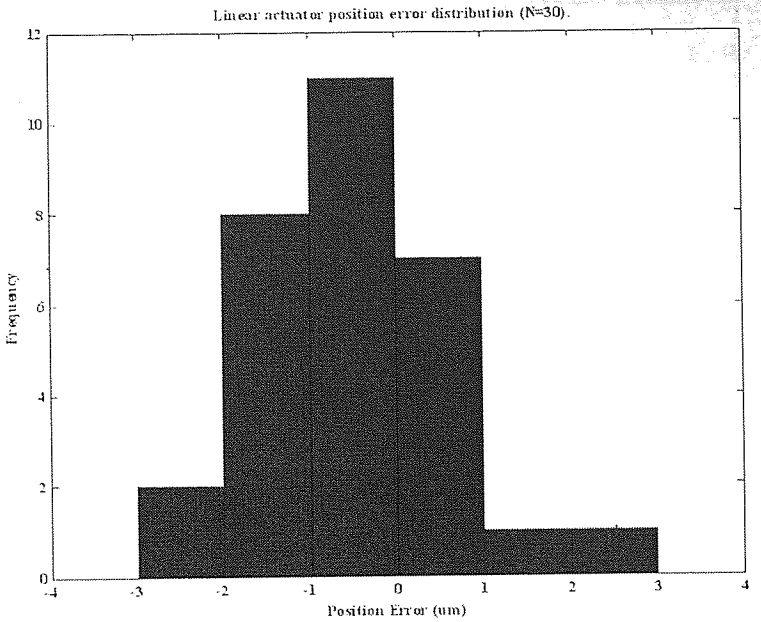

Figure 6.34: *Linear actuator position error distribution.*

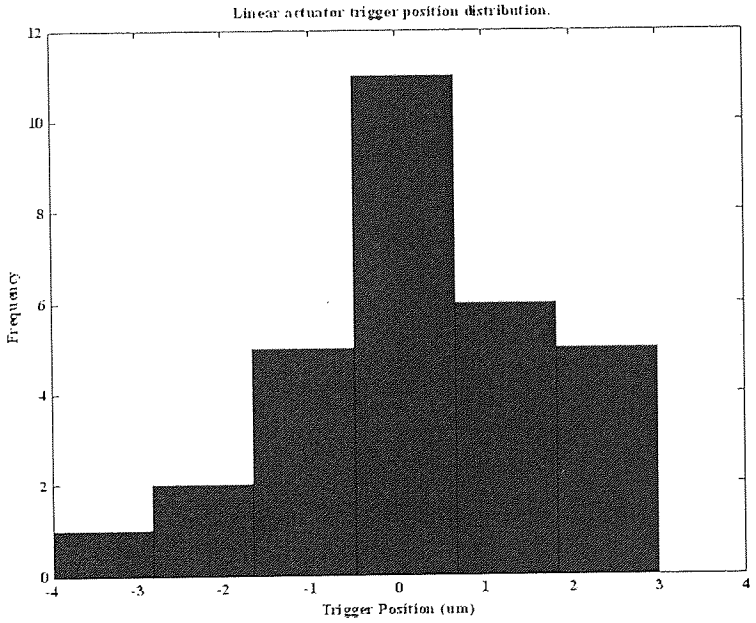

Figure 6.35: *Limit switch trigger position distribution.*

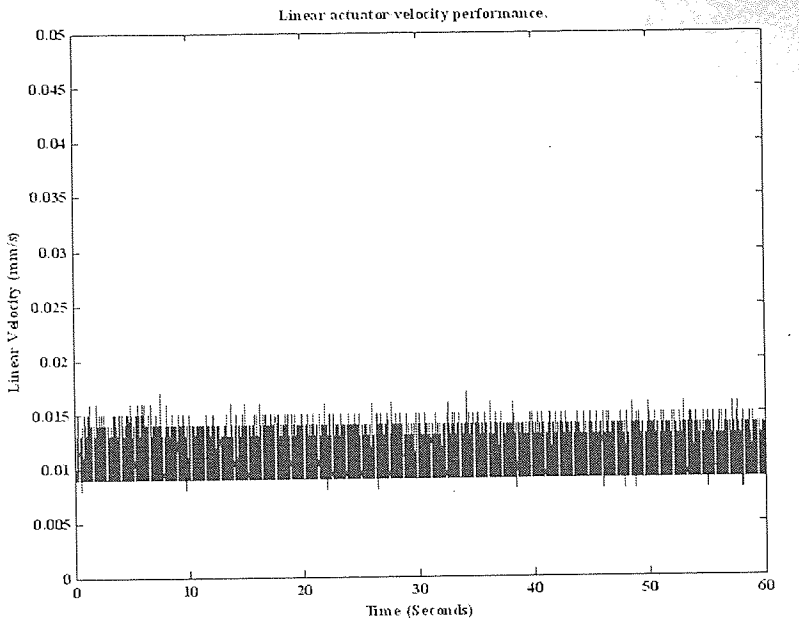

Figure 6.36: *Linear actuator velocity performance, 60 second capture.*

velocity error is less than 10%. The large error is mainly due to the small number of encoder pulses generated at this veocity. Even with the high ratio gearbox only 4 pulses are generated per sample period thus a fluctuation of 1 pulse could lead to as much as a 25% error. The distribution of the velocity samples is shown in figure 6.37. Despite the large error the mean velocity $\overline{V}$ is 0.01 mm/s and the standard deviation σ is 0.0013 mm/s. This is a worst case scenario as this is the minimum acheivable velocity, hence the lop-sided distribution, at higher velocities the error reduces significantly. It should be noted that this does not affect the drill performance as constant velocity is not assumed, position feedback is provided directly to the controller and each sample has a position index.

6.5 Host Software Architecture

The host software provides a visual interface from which the drill unit can be configured and its progress through the drilling process monitored. Its three core functions are as follows:

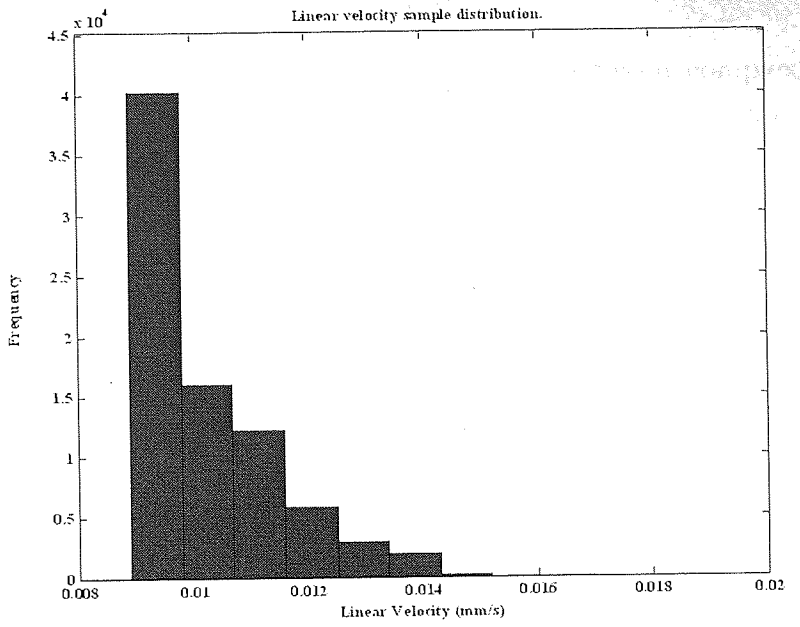

Figure 6.37: *Linear actuator velocity sample distribution.*

1. Provide an interface from which the drill system can be configured,
2. Give a visual representation of the status of drilling,
3. Monitor and log status and data from the drilling system.

The software was written entirely in Visual C++ and was a stand alone package that runs on the Microsoft Windows XP platform. The software communicates with the drill controller via the USB interface sending commands and receiving status information through EP0 and receiving data through EP2. The software is multi-threaded with separate threads controlling the data and control transfers, This ensures there is never any delay in sending commands to the device due to processing data coming from the drilling system.

Once configured via the host software, the drill system is primarily controlled via the hand held remote control and the computer is simply used as a display terminal to monitor the progress of the drilling process. Secondary to this a control interface is provided that mimics that of the remote allowing the device to be controlled from both.

6.5.1 Graphical User Interface

The user interface is required to strike a balance between complexity and the level of information that is conveyed to the operator. Enough information must be displayed to provide the operator with a sufficient understanding of what the system is doing without causing confusion, yet the interface must be simple to operate and and as robust as possible to prevent mistakes from occurring.

As this is a research orientated device it typically displays more information than would normally be required in a surgical environment, however, steps were taken to convey the necessary information in such a way that it could be easily interpreted and understood.

Referring to figure A.10 which can be found in the Appendix, the top left hand corner displays all the current drilling parameters, both set and actual values are displayed. The control buttons are located below these readouts, also on the left. The majority of the screen is taken up with a graphs of the drilling transients with active bar graphs on the right that indicate when the drilling characteristics approach the breakthrough condition. These visual representations dominate the screen and are easy to see from a distance as it is unlikely that the clinician will be seated at the host computer. The graphical display can also be maximised to fill the entire screen, hiding all the additional information as shown in figure 6.38. These displays convey most, if not all of the information required by the operator during the drilling process. Small anomalies that may go unseen are detected by the system and if necessary the operator is alerted; larger fluctuations that could be an indication of a problem are clearly visible on the display. In the unlikely event that system does not respond the clinician can react.

Whenever an event occurs the operator is notified with both a visual and audible alerts which have to be acknowledged by the operator for the process to continue. This can be done either by pressing the Start button on the remote or clicking Start in the user interface. The same process is used upon the completion of drilling phases. It must be noted that the host computer is not within the sterile operating field and as such the clinician can not approach or touch the host computer during the procedure. This is performed by a non sterile member of staff, alternatively the entire system can be controlled from the hand held

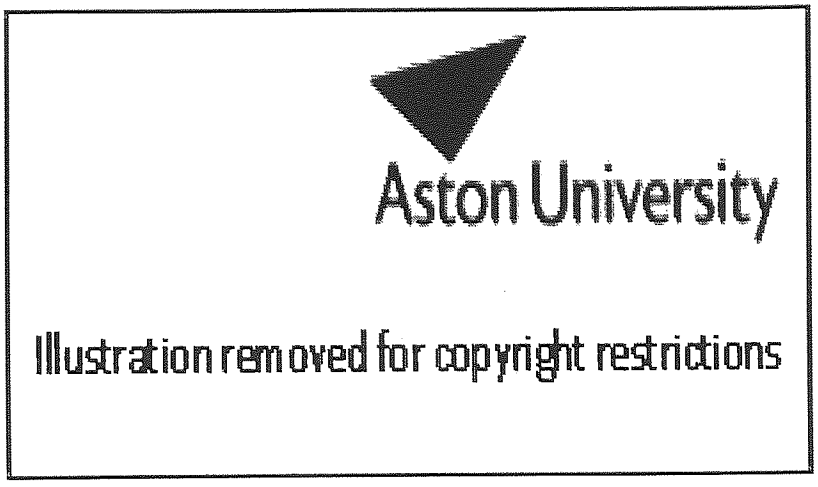

Figure 6.38: *The host computer in full screen mode.*

remote which is within a sterile sheath. The computer simply provides a backup interface.

In addition to this a video capture device was incorporated into the host computer and the software can display the feed next to the drilling transients. This enables the operating microscope to be connected such that the drill point and the drilling transients can be imaged side by side aiding further visualisation. The facility is also available to capture the video directly to the laptop

The drilling system does not only provide a user interface, it is responsible for logging every data transaction between the device and the host and any events that occur or commands sent to and from the device are logged. These events are recorded in chronological order along with the date, time, commands and status information. This provides complete traceability from the initialisation of the drilling system to the completion of the procedure.

Events and commands are stored in a separate log file, while data is stored in individual data files specific to the procedure being performed. These data files also contain the drilling configuration parameters and any relevant patient information entered by the clinician in an anonymous format via the patient information dialog.

The software also provides the ability to reload and examine previously cap-

tured data.

Figure 6.39 shows how the user interface may be typically arranged in the operating theatre. The video preview window displaying the feed from the tool tip is overlaid next to the drilling transient. The status window which displays the current stage and state of drilling is located in the top left corner. Lastly the main GUI window located in the centre so the clinician has a clear view of the drilling transients and the threshold bars located on the right. A complete

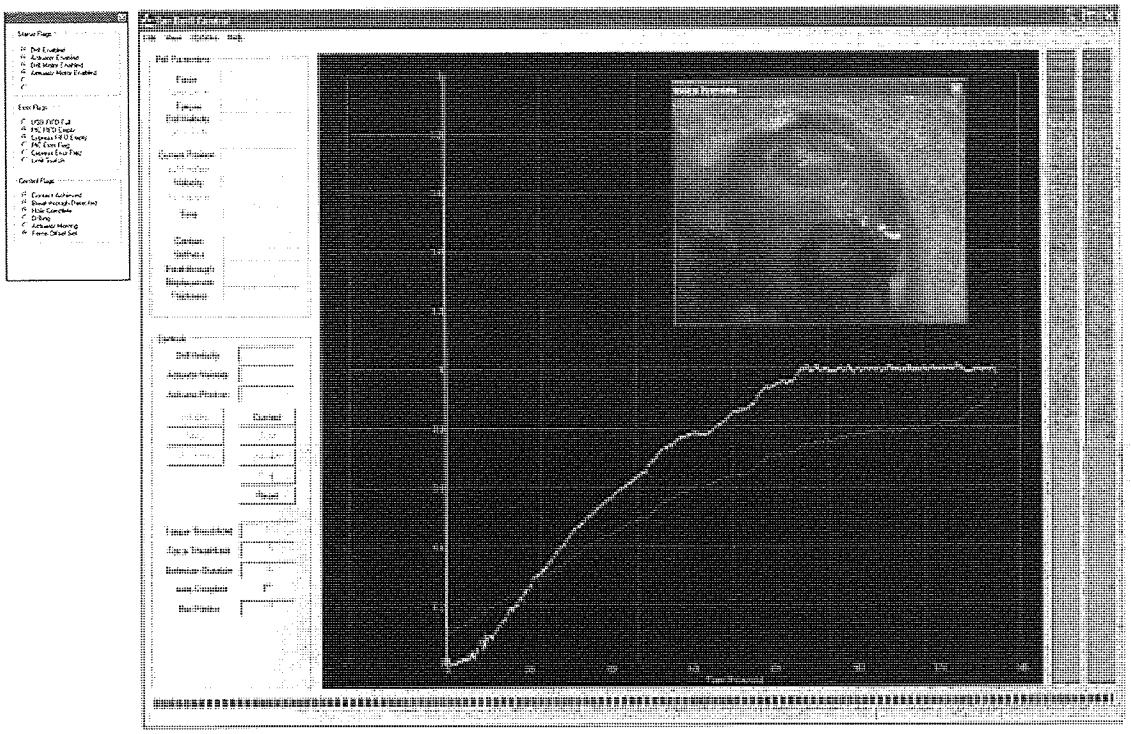

Figure 6.39: *The drill system GUI as it may be viewed in the operating theatre.*

list of functions available within the software can be found in the Appendix in section A.3. While all of these controls and configuration options are available to the operator, they are seldom used. These options are primarily for optimising the drill performance in the laboratory, at this time the drill system defaults are set and stored in the internal memory of the controller so the system is pre-configured out of the box. That said, if something needs to be adjusted during the procedure the facility is available.

6.6 System Overview

This chapter has described the design and development of a complete system, from specification to a working prototype of an autonomous mechatronic tool for the controlled drilling of tissues under compliant conditions. The tool has been designed to be used in the operating theatre by a clinician as part of either the stapedotomy or the cochleostomy as part of the cochlea implant procedure. The key mechanical, electronic and software components and their interaction have been described in detail and these together form the complete surgical drilling system.

A picture of the completed surgical micro-drilling system, setup as it would be in the operating theatre is shown in figure 6.40 The figure shows the key system

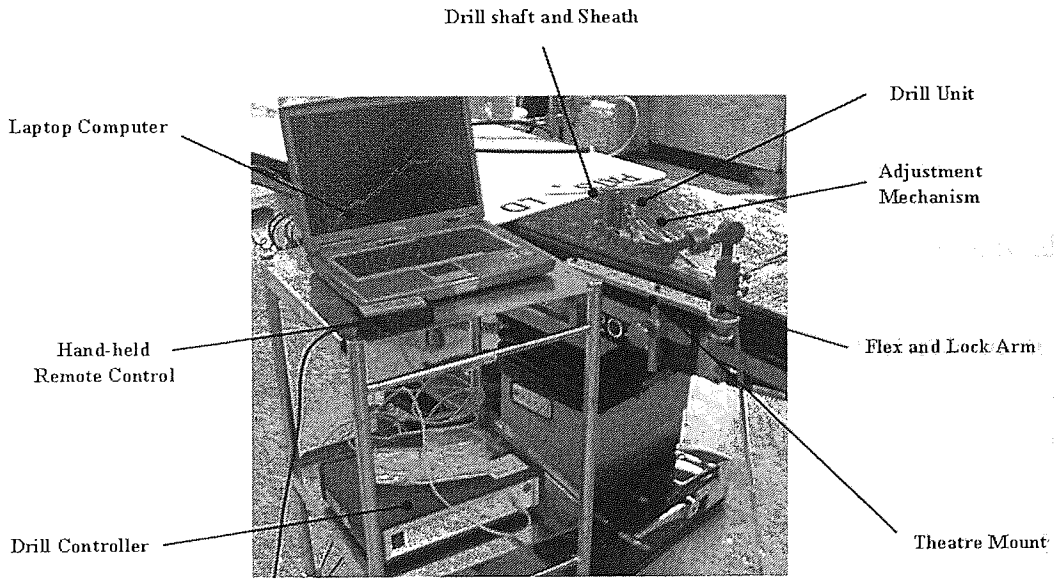

Figure 6.40: *The complete surgical drilling system.*

components that make up the drilling system:

1. The drill unit, drill shaft and sheath and the adjustment mechanism,
2. Drill controller and remote control,
3. Flex and lock arm supported by the theatre mount,
4. and lastly a laptop computer.

The theatre mount is located at the head of the operating table and is attached to the mounting rail that runs along its length. It is secured in position by two clamps that, when loosened allow the complete drill unit assembly to be slid along the rail as well as providing height adjustment. The mount is reversible such that it can be located on either side of the operating table and provides a solid base to which the locking arm can be secured.

The locking arm locates in a dove tail joint at the far end of the mount and is also secured with a clamp. The arm is removed by turning the clamp anticlockwise and then slides away from the table enabling fast setup and removal. The arm has sufficient degrees of freedom to be moved into any required position and orientation to reach the operative site. The arm is free to move when unlocked and has sufficient friction force to support its own weight unaided, significantly simplifying the alignment process. When in position the arm locks with zero backlash. It is operated by a simple sliding valve located on its base which incorperates a locking wheel that prevents the arm from being accidentally unlocked. The arm is self powered from an integated CO_2 cylinder so it does not have to rely on an external gas supply.

The drill unit fits into a 'V' clamp at the end of the locking arm, again to allow easy setup and removal as well as repeatable positioning. The unit integrates all sensing and drive elements into a slim titanium chassis with a minimum height and width profile to aid visualisation of the operative site. The unit itself is actuated along a single tool axis with micron level precision and accuracy over a range of 25 mm. The drill shaft is located at the top of the drill unit giving a 5° viewing angle to the tool tip. The drill shaft rotates in a protective sheath that can be removed from the drill unit and uses standard 1.6 mm dental cutting burrs. The shaft and sheath have a length of 80 mm and a profile of 3.5 mm allowing the operative site to be reached via long, narrow access ways. To provide a fine adjustment of the drilling trajectory the drill unit is mounted on an adjustment assembly.

The theatre mount is made from stainless steel and the locking arm and drill unit are made from titanium. All parts have a bead blasted finish that creates a very smooth matte finish that eliminates any reflective surfaces. This combined with the slim profile and long drill shaft enable the device to be used effectively

in conjunction with an operating microscope.

The system is controlled by the Drill Controller which integrates all of the system electronics. The operation of the device is entirely embedded, thus is independent of the operation the the computer. However a laptop computer is required as a platform from which the system can be configured and monitored prior to, and during the procedure. The device is supervised by the clinician at all times who has overriding control via a hand held remote, interfaced directly with the drill controller. A degree of secondary control is also available through the computer, however, its main function is to relay information about the progress of drilling to the clinician.

The control of the drill system is broken down into a series of control sequences that make up the overall control strategy.

6.6.1 Control Strategy

The concept behind the automated drilling technique is to build on the surgeons skills to enable them to achieve what was previously extremely challenging, if not impossible. The device itself is capable of detecting minute changes in the force and torque undetectable by the clinician. These changes carry a significant amount of information relating to what is occurring at the tool tip. The control strategy dictates the way in which this information is used and in turn, determines how the drilling process is carried out.

While the fundamental requirements, and hence the key stages of the drilling technique remain unchanged, issues regarding safety had to be addressed for surgical deployment. Device design changes aside, the main ways of improving tool safety are through operational protocol and the control strategy. From the perspective of the clinician, the device operator, the three main areas that impact tool safety are:

1. Operator awareness and visibility of what is occurring at the tool tip,
2. control complexity,
3. level of interaction required by the system,

As the clinician is present only in a supervisory capacity it is vital that they have maximum visibility of the entire process from start to finish. This is not only achieved by displaying the correct information, but by reducing the control complexity and minimising the level of interaction required to the key stages of the procedure. Thus the clinicians attention need not be drawn away from what is happening at the tool tip.

The control strategy implemented in the drilling system builds on that described in section 4.1.1.5 and encompasses the entire drilling process from target registration to hole completion. The strategy is broken down in to a series of control sequences; different solutions for each control sequence were presented in Chapter 2. The key sequences are:

1. Target registration,
2. investigative drilling,
3. breakthrough control and
4. hole completion.

A graphical representation of the control strategy flow is shown in figure 6.41. The

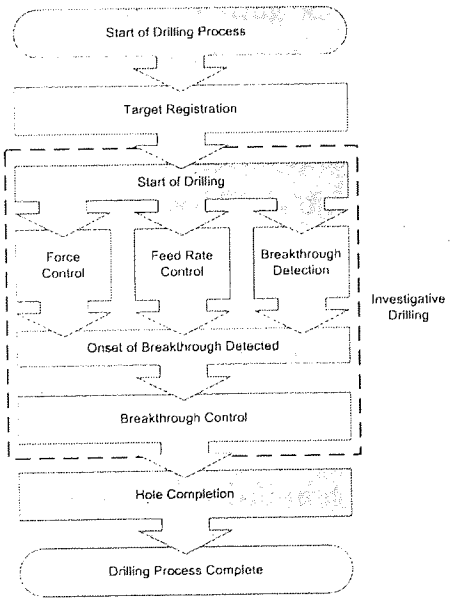

Figure 6.41: *Implemented control strategy.*

drilling procedure is carried out in three phases, each consisting of one or more control sequences. Three of the main independent control sequences are shown in figure 6.42. There are three operator initiated, independent control sequences, one of which can be initiated automatically and a further two autonomous sequences. The first phase consists of only the contact or target registration sequence. This is the first sequence initiated by the operator, however, if at any point in the setting up or positioning of the drill a small force is experienced by the drill tip, for example if the clinician accidentally advances the drill unit too far forward when positioning the system, the contact sequence is started automatically. This sequence advances the drill unit forward at a moderate speed until a force is detected at the drill tip. When this occurs the system continues forward until a force threshold is reached at which point the drill pauses and the retracts slowly until the force approaches zero. At this point the system waits and alerts the clinician that the drill tip is located at the surface of the target. The device then uses the force and displacement information to estimate the stiffness of the system which is used later in the configuration of the hole completion sequence.

The second phase consists of the investigative drilling, breakthrough detection and breakthrough control sequences. This is an operator initiated sequence and can only be started once contact has been achieved in phase one. The sequence begins with the the cutting burr rotating at a set velocity, typically 25 Hz, and the drill unit advancing again at a set velocity typically in the region of 0.01 mm/s. The feed strategy employed is the force limited feed rate described in section 2.3.2.3, this provides a close to optimal drilling characteristics while providing the benefits of constant feed force drilling without any additional risks to patient safety. The drilling transients are monitored for indications of the onset of breakthrough using the mean deviation method described in section 2.3.3.3, the progress of which can be monitored by the real-time display on the computer. On detection of the onset of breakthrough the first of the autonomous sequences is initiated, the breakthrough control sequence. When breakthrough is detected the drilling is ceased immediately and the drill unit begins retracting until the force drops below the zero threshold. The clinician is then notified that breakthrough has occurred and that the target is at its neutral position and the burr located on the medial surface.

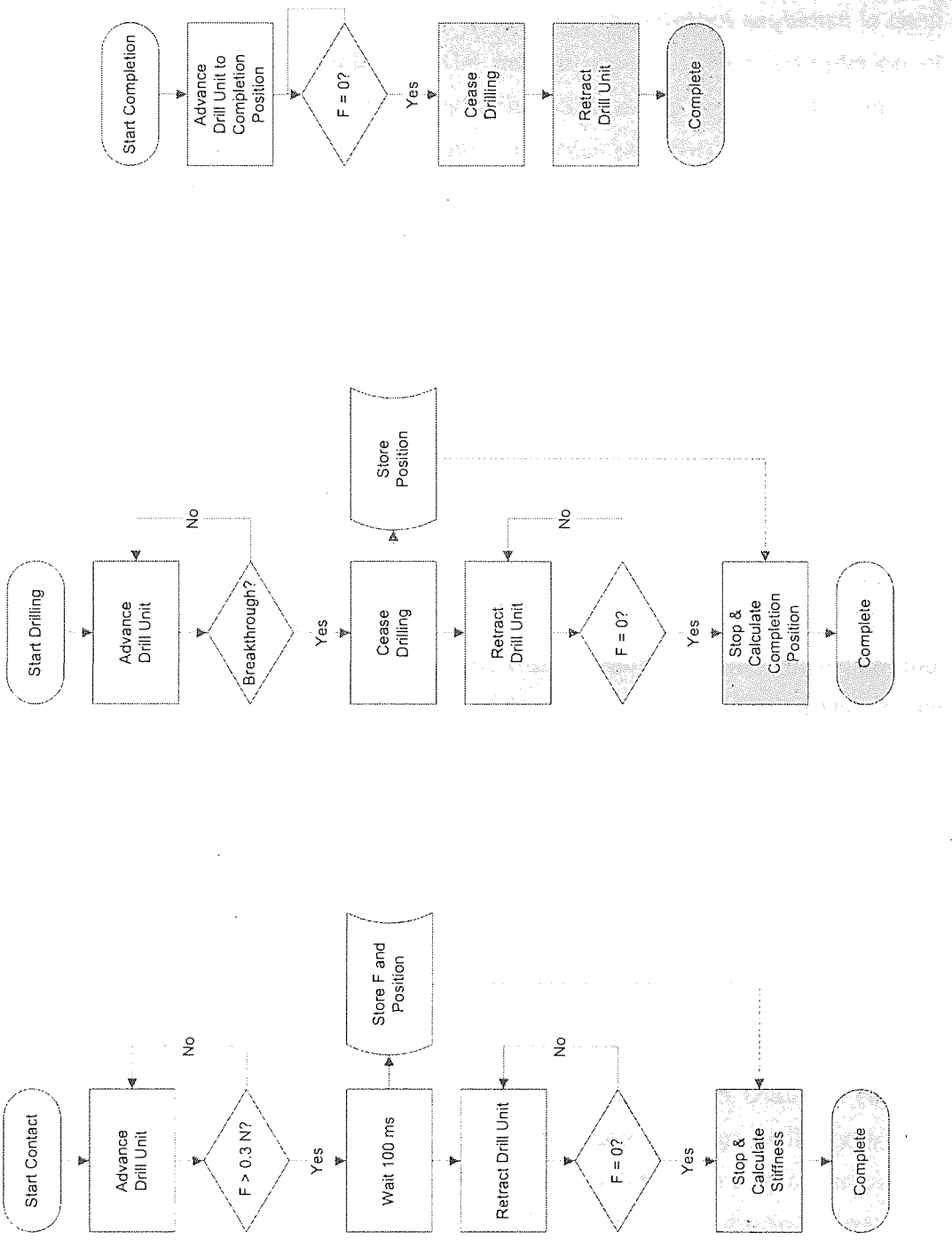

Figure 6.42: *Control sequences, (top) Hole Completion, (Centre)Investigative Drilling, (Bottom) Target Registration.*

At this point the clinician may retract the drill unit further to inspect the drill hole more closely. If they are happy to proceed the contact sequence is used again to ensure the burr is located on the medial surface. Upon completion of the contact routine the clinician may begin the final phase, hole completion.

The hole completion sequence calculates a target position using the stiffness of the system calculated by the contact routine as detailed in section 2.3.5.2. The drill then advances to this position slowly whilst drilling and the force level is monitored, the drilling process can be considered complete as the force approaches zero.

The second autonomous sequence is that of the emergency retract which is initiated if the force exceeds a maximum threshold, typically 2 N. If triggered, all processes are ceased and the drill is retracted at maximum velocity and an alert is sounded.

The control of the system has been reduced to a simple sequence of button presses, with any one action requiring a maximum of two consecutive button presses at the most. The control sequences themselves are strictly defined with only certain control actions being permitted during each sequence ensuring that a minimal level of interaction is required and the risk of mal-control of the device is minimal. The clinician is then free to concentrate on the task at hand rather than the control of the device.

The individual sequences combine to make up the overall control strategy implemented within the drilling system. An important feature of this strategy is that although the system is capable of performing the entire process independently. This approach ensures the clinician is aware of what is happening at every stage and the procedure does not progress without the clinicians acknowledgment. Only elements that are truly beyond a clinician's ability to control have been automated. This also ensures that clinician does not feel that the control of the procedure has been taken out of their hands and they are still free to use their judgment to override the system. This plays a large part in reducing the risks associated with robotic surgery and this is key if smart, autonomous tools are to be successfully adopted into general surgical practice.

6.6.2 Device Operation

The operation of the drilling system is a very simple process. Figure 6.43 is a flow digram that shows the stages and sequence of drilling process. The procedure starts with the clinician positioning the drill unit in close proximity to the operative site an approximately the right trajectory. This is done by manually manipulating the joints of the locking arm. The self supporting nature of the arm means this is simple to do; when in approximately the correct position the clinician can let go of the unit, inspect it position and adjust it if necessary.

Once in the correct position with the drill tip approximately 10 *mm* from the target, the supporting arm is locked by sliding the valve located on the arm base. Located on the valve stem is a locking wheel, that when turned prevents the support arm being accidentally unlocked.

The drill unit can then be moved into the exact drilling position using the the linear actuator and the adjustment mechanism. The linear actuator provides motion along the drilling axis; the adjustment mechanism provides horizontal and vertical motion. This process can be performed while viewing the drill tip via a microscope allowing very accurate hole positioning.

The linear actuator is controlled using the hand held remote advance and retract buttons. The remote is pictured in figure 6.44. Double pressing the stop button at any stage returns the drill system to its home position. The adjustment mechanism employs a pair of thumb wheels to provide the actuation across the horizontal and vertical axis.

The remainder of the drilling process is controlled via the remote pictured above.

Now the correct position and trajectory has been reached, contact mode is initiated by a single press of the Start button. Once contact has been achieved the operator is notified. A dialog is displayed on the computer along with a visual and audible alert that has to be acknowledged by a button press on the remote.

The drilling phase, like the contact phase is initiated by a single press of the start button. When breakthrough occurs the system automatically manages the event and takes the appropriate action. Again on completion of this phase a visual and audible alert is generated which has to be acknowledged by the

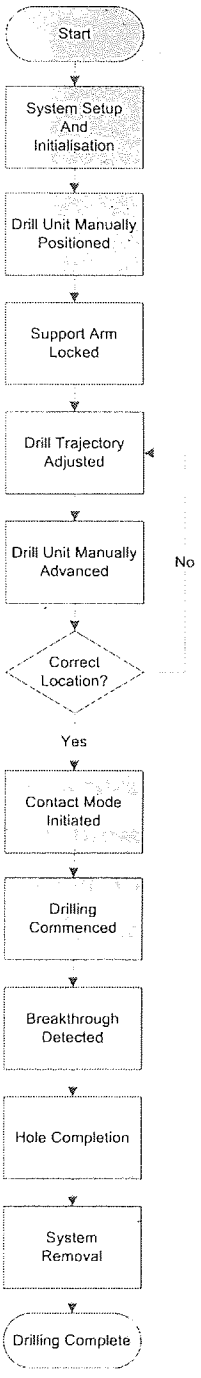

Figure 6.43: *Drilling process flow diagram.*

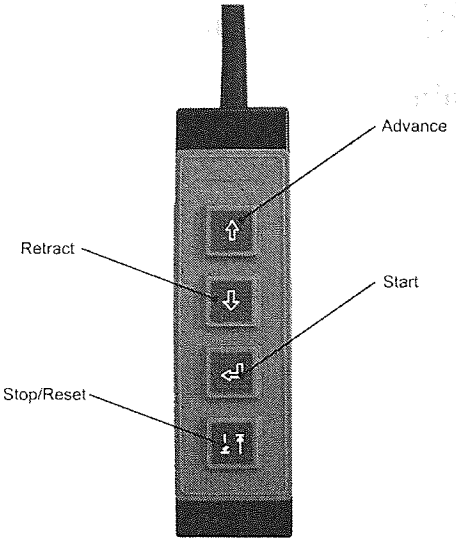

Figure 6.44: *Hand-held remote.*

operator before any further action can be taken.

At any point during this process the clinician can press the Stop button to pause the process in order to inspect the progress of the system more closely. When paused, the drill can be retracted for a closer view of the hole. A second press of the stop button resets the system and returns the drill to the home position. The process is resumed by pressing the Start button, at which point the drill returns to its previous position and commences drilling. If the drill has been retracted the contact sequence is executed prior to the commencement of drilling.

Upon completion of the breakthrough control routine and acknowledgment by the clinician, they can take one of two courses of action.

The drilling process can be terminated and the drill system removed or the hole completion sequence can be initiated. In the case of the former, the drill simply retracts to the home position, saves all data and then shuts itself down. In case of the latter, the hole completion sequence is executed.

When the hole is complete a notification is sent and then the drill completes its shut down sequence. This concludes the drilling process, the system is then retracted and removed from the vicinity of the patient.

6.6.3 Sterility Considerations

Given that sterility is of utmost important in the operating theatre it is vital that this be taken into account in the design and operating procedure of the drilling system, for example, the drill shaft and sheath.

These issues were addressed by making all parts of the drill that will come into direct contact with the patient removable and suitable for sterilisation in an autoclave or by any other conventional method.

All parts of the system that may come into contact with the patient, objects within the sterile field, or be handled by the clinicical staff must be sterile. Due to the fact that the drill unit contains sensitive electronic components it cannot be submersed in fluid or sterilised in an autoclave. The slim profile of the drilling unit means that it can be draped in a sterile polythene camera sheath relatively easily. Further to this the entire system was made from titanium with a very smooth surface finish with few recesses and sharp edges. The inert nature of the materials mean that the system can be cleaned with most cleansing agents, including those that are alcohol based. The smooth surface finish and rounded geometry mean that there are few places in which contaminants can become trapped.

The final method for addressing these issues is part of the setup and draping procedure for the system, this will be discussed in Chapter 8.

6.6.4 Safety Considerations

Operating protocol and sterility considerations to one side, there were many measures taken to ensure that the system was as safe as possible for both the operator and the patient.

Firstly a point of general safety, it is generally accepted that designs of robotic systems that use custom manipulators with sufficient force and motion for the task at hand represent the safest approach (53). As such, the micro-drilling system was designed with this in mind by reducing the range of motion to the minimum required to perform the cochleostomy successfully with appropriate force limits.

There are two main risks involved in the usage of the drilling system that

may pose a threat to patient safety. Firstly is the application of excessive force resulting in injury and the second is the patient moving against the drill, again resulting in injury. Both of these effectively amount to the same thing however the second carries a greater risk due to the the effect of relative velocities as the patient can move significantly faster than the drill and the drill is rigidly mounted. Fortunately, the likelihood of this occurring is very small as the patient is paralysed, anaesthetised and ventilated during the procedure. The addition of head restraints can further reduce the risk.

In the case of the application of excessive force, the system is force limited. While the drill is advancing it uses a force limited feed rate strategy. If the lower force threshold, 1 N by default, is crossed the system ceases advancing, if the high force is maintained it will retract. If the drill unit is stationary and a force is experienced, the unit automatically retracts until the force is zero and notifies the operator.

If at any time the upper force limit of 2 N is exceeded an emergency reset is performed. This ceases drilling (if the drill was drilling at the time) and retracts the drill unit at maximum velocity and generates an alert to notify the operator. The system operates on a very stable embedded platform with an internal control process that cycles 1000 times a second meaning that any event occurring at the tool tip is registered extremely quickly and the system can take action far quicker than a clinician can. Should the system not react, given the rate at which drilling progresses the clinician has a significant amount of time to manually stop the system. The force control algorithms are in the base level firmware of the device and the force is monitored continuously regardless of the current operation.

The same is true for breakthrough detection failure. In the unlikely event that this occurs the clinician will see what is occurring at the tool tip on the computer display long before the burr penetration exceeds that of the conventional procedure thus making the system intrinsically safe. That said, the detection parameters are set in such a way that a false-positive detection is far more likely than a detection failure because a false-positive detection is in itself fail-safe.

During the drilling process the designed-in level of user interaction ensures that at key stages the drilling process are observed and the system cannot progress without the clinicians approval.

In the event of power failure the system is again fail-safe. If the drill is powered down and then switched on again, the system remembers its previous task and the operator can continue or reset the drill system. If the system is reset, it will retract to its home position and await further commands. Even then the procedure can be recommenced. If for any reason the internal memory fails an internal flag is set and the system will only allow the operator to reset the device.

In the case of the locking arm, the gas supply is integrated and a new cylinder is used for each procedure. There is also a visual indicator that indicates there is sufficient pressure present. In the event that the gas supply does fail the locking arm is self supporting and thus cannot fall and injure the patient. Should the arm move while the system is drilling it will be detected and the operator notified.

Most, if not all, remaining risks will be down to the actual manipulation and operation of the device by the clinician. These issues are primarily addressed through training and operating protocol. These will be discussed in more detail in Chapter 8.

Chapter 7

The Route to Theatre

7.1 Surgical Deployment

This body of work so far has seen the development of a technique capable of controlling the penetration of a drill through a compliant material. It has also been demonstrated that there are many surgical procedures that will benefit from the use of such a system. Based on the requirements of both the technique and the possible applications, combined with prior learning, a specification for a clinical micro-drilling system suitable for surgical deployment was derived. Using this specification a complete system was designed, manufactured and a complete functioning system built.

To take this completed system and deploy it in the operating theatre a number of further steps must be taken:

1. the device has to be validated and verified through a series of trials;
2. a surgical protocol for the use of the device in the operating theatre must be defined;
3. and a research clinical trial must be designed and suitable candidates identified;

4. the clinical staff must be familiarised with, and trained on how to use the device.

7.2 Testing Protocol

The verification and validation is a vital part in the development of any device, but particularly for medical devices (57). Verification is the process of ensuring that a device meets its intended specification and any regulatory requirements dictated by its intended use. In the case of the micro-drilling system this means that it meets the specification outlined in section 6.1. Validation is the process through which documented evidence is generated to show that a device is fit for its intended purpose.

For the micro-drilling system this means ensuring that:

1. the device is suitable for use in the operating theatre,
2. that the device is capable of controlling the penetration of the drill to an acceptable level,
3. that the device minimises any risk and does not compromise patient safety.

A large part of the verification and validation processes was covered in Chapter 6, in particular ensuring that the device meets its intended specification and that the steps have been taken to address concerns over patient safety. Individual mechanical and electronic subsystems have been tested and software algorithms have been modeled to ensure that they perform their individual tasks. The testing protocol aims to validate the device performance as a complete system, that is, all subsystems working in unison to carry out the intended purpose of the clinical micro-drilling system. The trials are broken down into three discrete phases:

1. Laboratory trials,
2. cadaver trial,
3. and a research clinical trial on one or more live subjects.

The laboratory trials are used to assess the device performance under controlled conditions. Factors assessed include optimal detection thresholds, drill penetration, detection rate, drilling time and overall system performance can be assessed. A statistical body of data can be generated that can be used as a direct measure of the device performance.

Once the system performance has been proven to be satisfactory, cadaver trials are to be used to evaluate the performance in a situation that is as close to the intended application as possible. Factors evaluated will include ergonomic considerations relating to the use and positioning of the system and anatomical factors affecting reaching the operative site. Due to the restrictions on the use of cadaveric tissues, few trials can be performed, but even a qualitative assessment can highlight some of the potential issues that may be experienced in the operating theatre.

The final phase of the testing protocol is a full research clinical trial on one or more live patients as part of the normal surgical procedure, and it is this that is the chief aim of the work.

7.3 Laboratory Trials

The aim of the laboratory trials was to verify the system performance under controlled conditions. Given that the primary requirements of the device are to detect and control breakthrough the first task is to define the optimal detection parameters.

Initial tests were carried out on compliantly mounted egg shells. Egg shell provided a good test medium due to its similarity in structure and thickness to the cochlea as well as its availability and low cost. It is, however, harder than the cochlea which results in more noise in the drilling transients.

The laboratory tests were carried out using the full micro-drilling system setup. The egg shell was mounted compliantly using a flexible putty with a nominal stiffness of approximately 2.5 N/mm, thus the overall system stiffness was typically in the region of $1.5 - 3.0$ N/mm. The drill was positioned using the locking arm; a typical setup is shown in figure 7.1. Figure 7.2 shows a typical

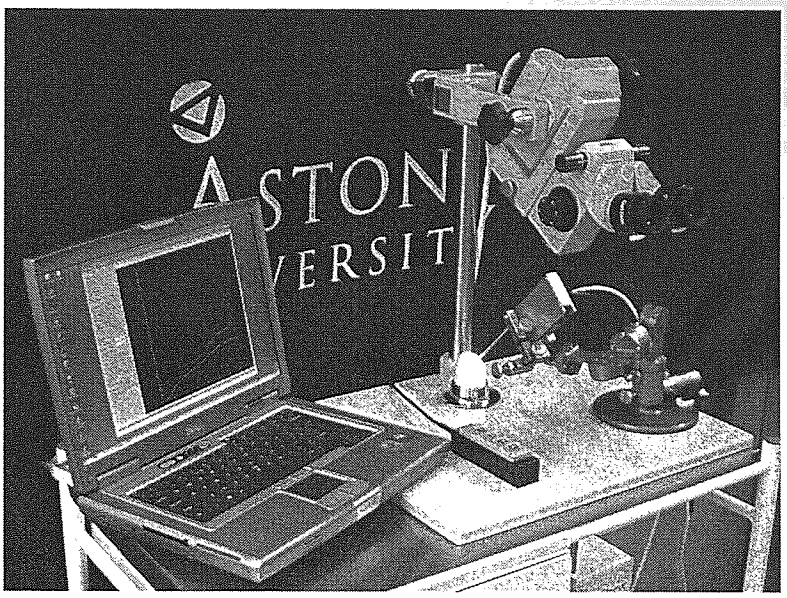

Figure 7.1: *Typical laboratory setup.*

set of transients from the drilling of a 1.2 *mm* hole through an egg shell with a diamond burr. In this instance the egg shell was 0.43 *mm* thick, the drilling axis was approximately normal to the surface of the egg and the total drilling time was 80 seconds.

Figure 7.3 shows the corresponding mean deviation magnitudes for the force and torque transients calculated using equations 2.14 and 2.16 in section 2.3.3.3. Firstly it can be observed that the breakthrough characteristic in figure 7.2 is clearly distinguishable from the rest of the signal and that the corresponding features in figure 7.3 are considerably more pronounced. Further more, the earlier fluctuations in the torque signal do not manifest themselves in the mean deviation plot. The two dashed lines represent force and torque thresholds of -5 and 5 respectively, by inspection it can be seen that if the detection thresholds were set at this level breakthrough would be easily detected. It should be noted that within normal operating ranges the breakthrough delay introduced in section 7.3.1 has negligible effect on figure 7.3 due to the controlled progression of the drilling process.

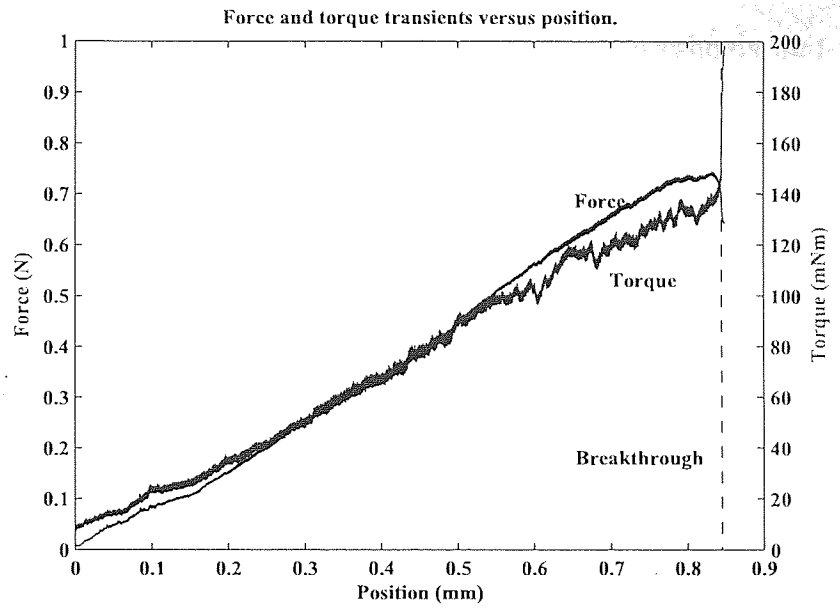

Figure 7.2: *Typical drilling transients from drilling egg shell.*

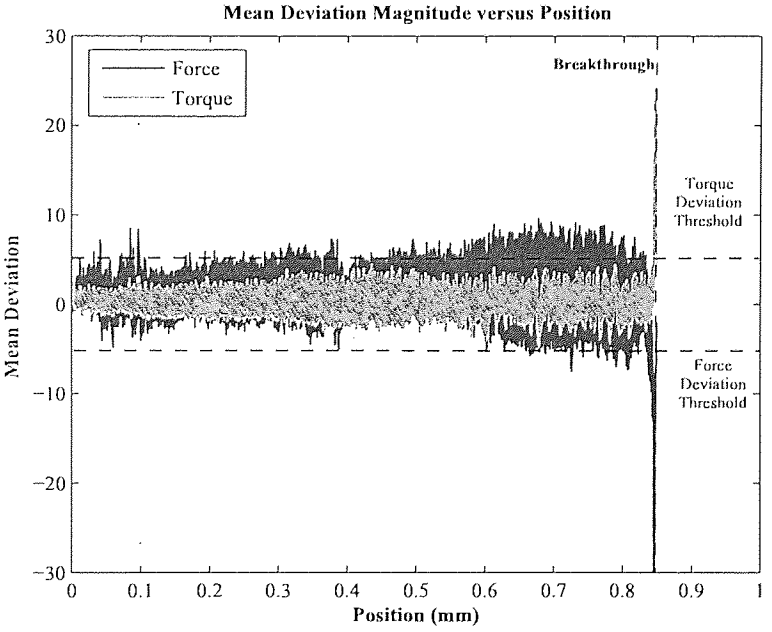

Figure 7.3: *Typical mean deviation magnitude plots.*

7.3.1 Threshold Evaluation

A series of further tests were conducted, varying the thresholds and performing repeated drilling's in order to asses the relationship between false positive detections and failures. The breakthrough detection delay was set to zero for this experiment and ten tests were carried out for each threshold. The results are shown in figure 7.4. The figure shows the number of false (false positive)

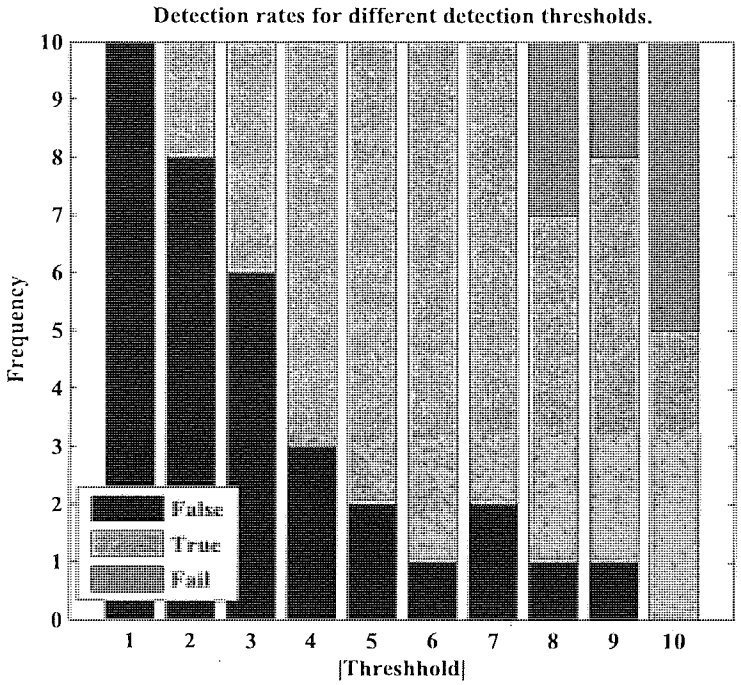

Figure 7.4: *Detection rates for varying thresholds.*

along with the number of successes and failures. It clearly demonstrates that for low thresholds the false positive detection rate is very high. As the magnitude of thresholds is increased the number of false positives decreases until approximately 8 when detection failures begin to occur. It should be noted that the lower thresholds were particularly sensitive to disturbance from the surroundings while the higher thresholds were equally insensitive to disturbance as well as breakthrough detection. When the thresholds were set below 3 the process rarely progressed past the first few seconds of drilling. This was primarily due to large fluctuations

in the torque caused by the burr initially bedding into the target material.

Clearly a false positive detection poses significantly lower risk than a failure therefore it is better to have the instrument too sensitive rather than not enough, thus the base level setting for the force and torque detection threshold should be at most -5 and 5 respectively.

Although a false positive poses little risk to the patient and the procedure can just be re-initiated, it is undesirable due to the time penalty involved as this may cause the patient undue stress. It was for this reason that in addition to the detection thresholds there is also a breakthrough detection delay parameter. This parameter determines the length of time that the breakthrough condition must be true in order for breakthrough to be detected. The idea behind this parameter is that it enables the thresholds to be set lower because disturbances that may cause a false positive detection act over a very short period of time. The experiment described above was repeated with the breakthrough detection delay set to 10 *ms*, the results are shown in figure 7.5. It can be seen that the

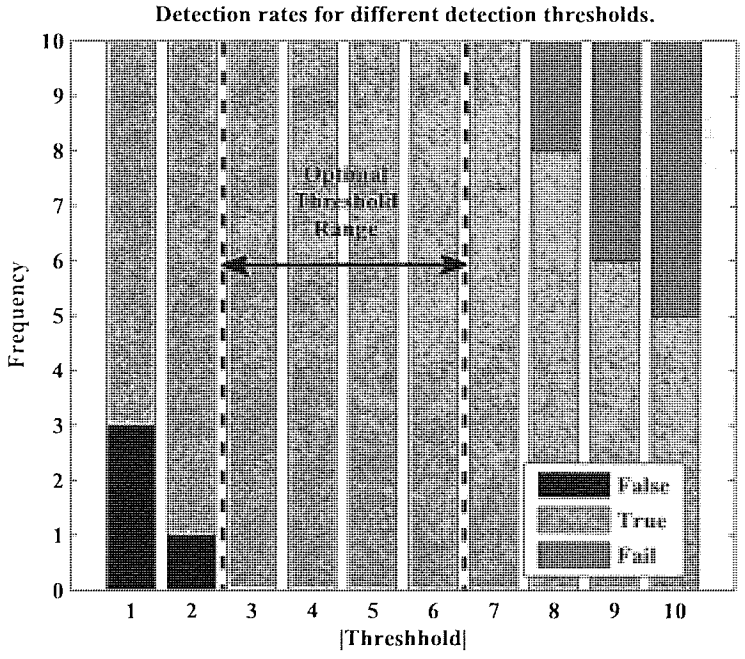

Figure 7.5: *Detection rates for varying thresholds with the detection delay of* 10 *ms.*

introduction of the delay has significantly improved the false positive detection

rate without affecting the failure rate. The false positive detections that did occur were also well into the drilling process and the response to disturbance was significantly improved.

While the breakthrough detection delay improved the detection rates there was a knock-on effect on the rapidity with which the system reacts when breakthrough does occur and thus, the level of drill penetration prior to hole completion. To assess this effect a method of estimating the drill penetration was needed.

7.3.2 Drill Penetration Estimation

Estimation of the burr penetration is a difficult task, the measurement can be in the order of a few tens of microns. The method chosen uses a visual inspection of the hole via a microscope or camera and measurement of the size of the aperture at the base of the hole through which the burr has penetrated. Figure 7.6 shows a confocal Z stack consisting of 250 images superimposed on top of one another to create a three dimensional image. The microscope software was then used to

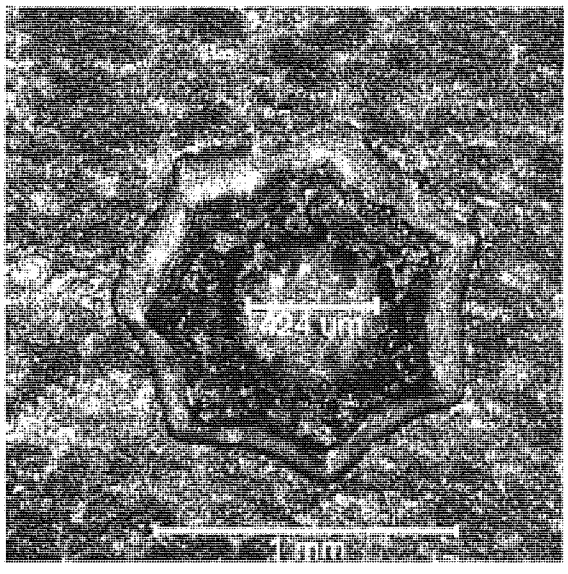

Figure 7.6: *Confocal Z scan of a hole drilled in egg shell.*

make an accurate measurement of the hole diameter. Using this measurement

and the geometric relationship of the hole and the burr shown in figure 7.7, trigonometry can be used to calculate the burr penetration. The relationship

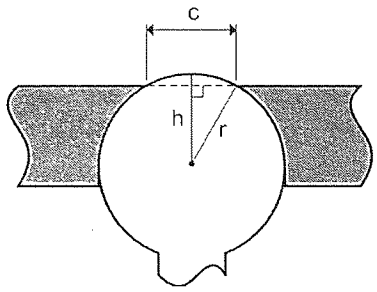

Figure 7.7: *Using the drill aperture for drill penetration estimation.*

between the aperture diameter and the penetration is expressed in equation 7.1.

$$h_{dp} = \sqrt{(r^2 - \frac{c^2}{2})} \tag{7.1}$$

Where h_{dp} is the drill penetration, r is the burr radius and c is the hole aperture. The evaluated function is shown in figure 7.8. By inspection, the burr penetration in figure 7.6 is estimated as 35 μm.

This method does rely on several assumptions; the burr is perfectly spherical and the actual burr diameter is the same as the specified diameter; the aperture at the base of the hole is flat and circular. This method is not an exact measurement and should not be treated as such, it is at best an estimation, however, this is sufficient for the requirements of this study.

7.3.3 Drill Penetration Evaluation

To evaluate the effect on the breakthrough delay on the burr penetration prior to detection a series of experiments was conducted. The same system setup described earlier for use with eggs was used and the breakthrough threshold magnitude was fixed at 5. The breakthrough delay was varied between 0 and 50 ms and each test was conducted three times. The remaining drilling parameters were left at the default values. Rotational and linear velocities were 25 rps and

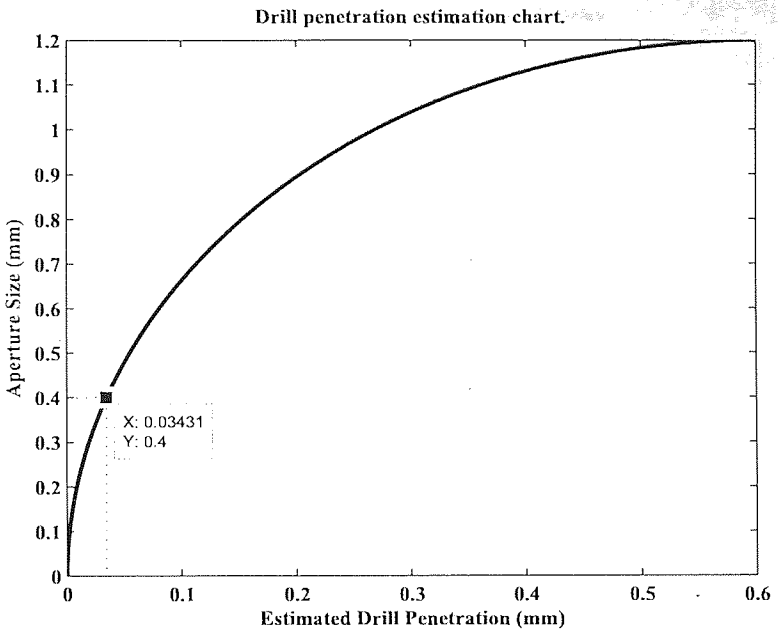

Figure 7.8: *Chart for the estimation of drill penetration.*

0.01 mm/s respectively and the force limit was set to 1 N. Using the method described in section 7.3.2 the hole apertures were estimated to the nearest 10 μm by visual inspection using the operating microscope shown in figure 7.1 and a set of digital calipers. The results are shown in figure 7.9. The figure shows that the relationship between the hole parameter could be approximated as linear between delays of 10 ms and 20 ms, values below this will not be considered due to the occurrence of false positive detections. For the lowest and highest delays there were instances of false positive and failed detections, in these cases the tests were repeated until three valid results were collected. After 30 ms there is a marked increase in both the variability and the size of the aperture indicating a marked drop in performance; detection failures occurred at delay greater than 45 ms. Over the linear range the drill performance was unaltered in this trial; the larger delays make the system far more resilient to disturbance thus further reducing the likelihood of false positive detections. This is at the cost of greater degree of burr penetration, approximately 20 μm across the linear range. The main objective of this system is to form a hole with minimum protrusion while causing minimal damage to the underlying soft tissue. This means that to form a full hole with

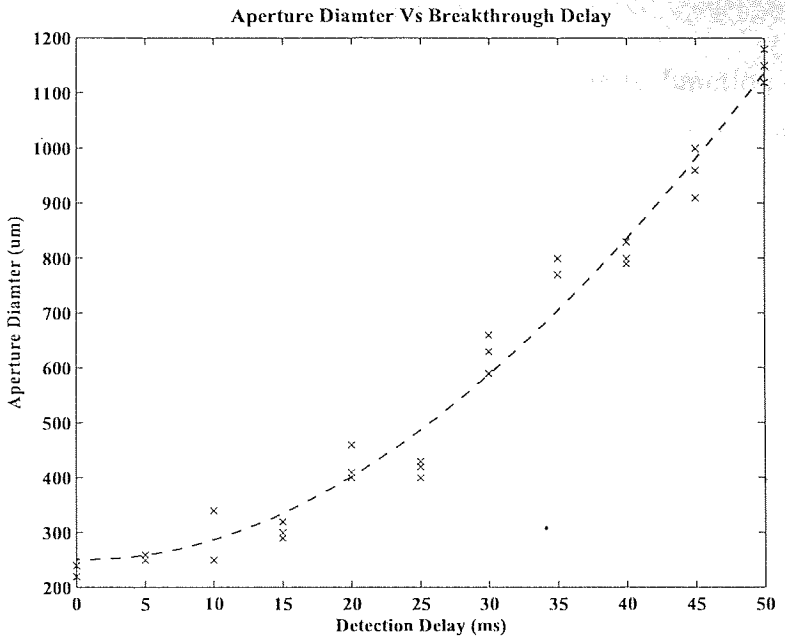

Figure 7.9: *Relationship between aperture diameter and breakthrough delay.*

a 1.2 *mm* burr the minimum level of protrusion is 0.6 *mm*. When compared to this the additional initial protrusion will have negligible impact on the outcome of the procedure. The only time this may become a significant factor would if a smaller burr were to be used. As such this relationship may be co-dependent on a number of factors including:

1. burr diameter,
2. material properties,
3. axial force,
4. linear velocity,
5. and rotational velocity.

With this in mind the optimal delay is toward the higher end of the linear range, providing the best compromise between performance and robustness. Therefore, the default value for the detection delay is set at 25 *ms*. A summary of the associated drilling parameters are shown in in table 7.1.

7.3.4 Response to Disturbance

Figure 7.10 shows an example of the system continuing to function correctly and going on to successfully detect breakthrough when experiencing a high degree of disturbance. In this example the target was oscillated to simulate the effect

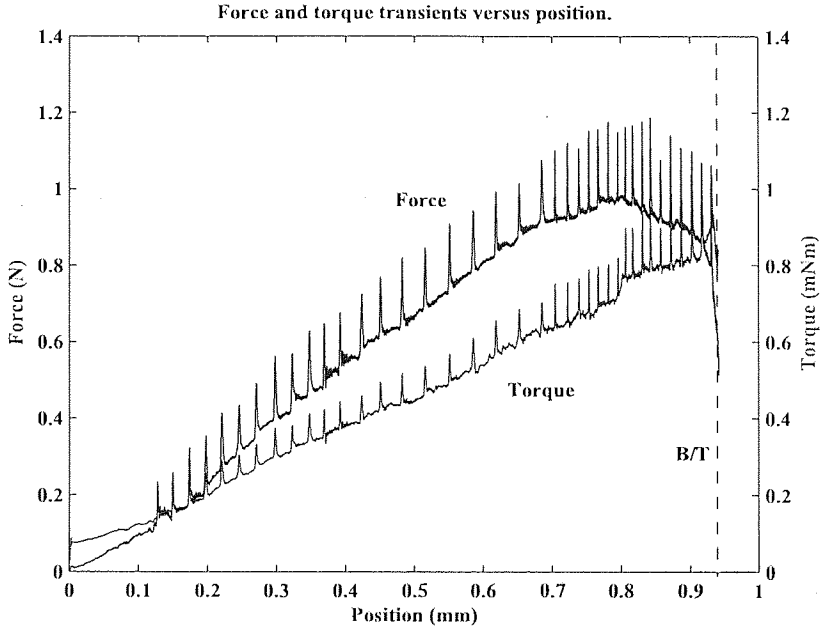

Figure 7.10: *An example of the systems response to disturbance.*

that a patients breathing may have on the drilling system. The target was oscillated at approximately 0.5 Hz for the duration of the drilling process using an electro-mechanical oscillator attached to the mounting platform. The oscillation amplitude was set to induce force spikes of approximately 0.15 N, which equates to 10% of the feed force limit of 1.5 N.

Breakthrough was achieved in 81 seconds with an estimated burr penetration of 39 μm. It can be seen that the oscillation had little or no effect on the system performance.

The force limit on this occasion was set to 1 N and the force can be seen to be dropping as the breakthrough point is approached, however, this is due to the force periodically crossing the force limit threshold and the system is responding accordingly. Each event was detected and logged by the device as the target

moving toward the drill. This clearly demonstrates the systems robustness as well as the ability to determine between different states at the tool tip.

7.3.5 Overall Performance

Using the parameters defined in sections 7.3.1 and 7.3.3 thirty tests were carried on a compliantly mounted egg. The drilling parameters are listed in table 7.1.

Parameter	Value	Units
Drill Velocity	25	Hz
Linear Velocity	0.01	mm/s
Force Threshold	−5	mN/ms
Torque Threshold	5	mNm/ms
Breakthrough Delay	25	ms
Burr Radius	1.2	mm

Table 7.1: *Laborotory trial drilling parampeters.*

For each test the drilling duration, breakthrough burr penetration and thickness was recorded. Figure 7.11 shows and typical set of drilling transients representative of all thirty tests.

Figure 7.12 shows the distribution of the burr penetration.

It can be seen that the distribution can be approximated as normal; the mean burr penetration was 37 μm with a standard deviation of 18 μm. The average drilling time was 84 seconds through an average thickness of 450 μm. There were no false positive or failed breakthrough detections.

This demonstrates that, in the case of compliantly mounted egg shell, breakthrough burr penetration can be controlled to within 45 μm of the distal surface in 95% of all cases. Although this value may appear high, the rate at which breakthrough occurs when drilling egg shell is significantly faster than when drilling softer materials and thus, is harder to control. These drilling paramters should now be evaluated against a medium analagous to the human cochlea.

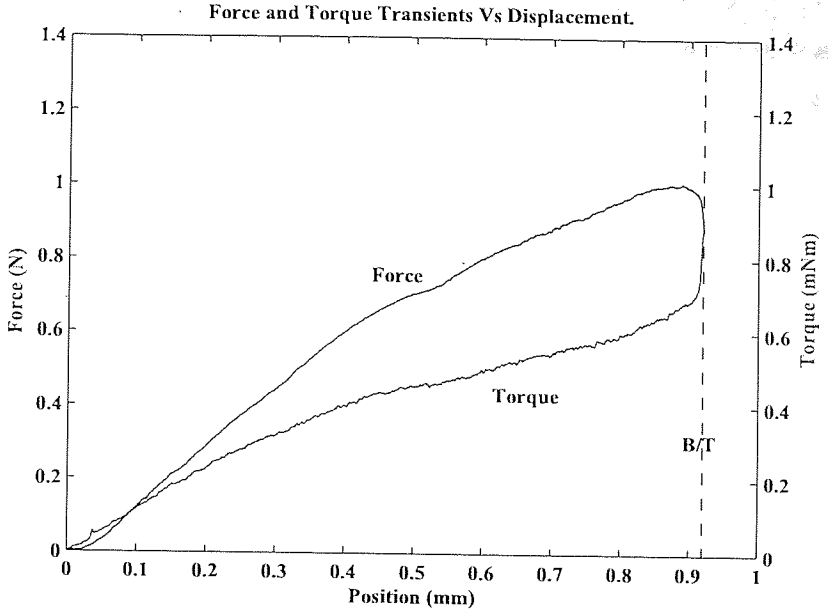

Figure 7.11: *Example set of drilling transients.*

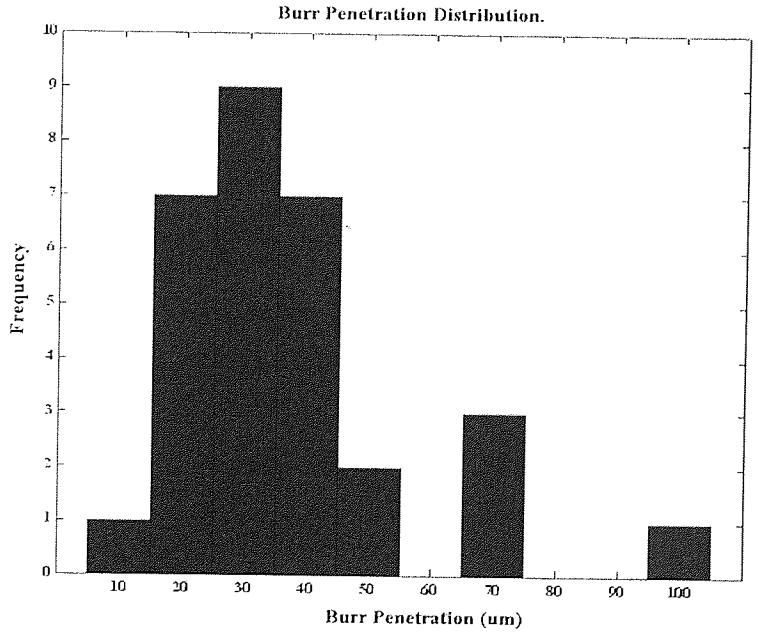

Figure 7.12: *Breakthrough burr penetration distribution.*

7.4 Porcine Trials

The next stage is to investigate the device performance under a lesser controlled environment. This was carried out by drilling fresh porcine cochleae. The drilling of porcine cochleae is the closest approximation of the human cochlea that can be used for laboratory trials. Studies have shown that it closely resembles human tissue in both density and thickness (84). This, its availability and ease of extraction make it an ideal test medium. The cochleae were harvested from fresh middle white pig carcasses and stored in saline solution and refrigerated until drilling.

The drilling setup used was similar to the configuration to be used in the operating theatre, with the porcine cochlea mounted compliantly *(See table 7.2 for the mounting compliance)*. They were not rigidly constrained thus free to move under the tool action. The drilling speed was set to 25 Hz using a 1.2 mm diamond burr. The linear feed rate of 0.01 mm/s and maximum linear force 1 N were used. The default detection thresholds were used. The hole drilled was located just above the round window, anterior to the oval window to mimic that of the real procedure.

Figure 7.13 shows the results of five test drillings on fresh porcine cochlea (47).

All figures share common features when compared to that of the constant feed rate strategy shown in figure 2.5. While demonstrating the same key features it can be seen that each set of drilling transients are significantly different. The differences between each transient may be explained by variations in bone tissue stiffness and thickness, mounting compliance and angle of drilling. All these factors are unknown and affect the way in which drilling progresses, yet in each case breakthrough detection was successful. The drilling parameters estimated by the system on completion of the drilling process are shown in table 7.2. Where x is the feed displacement, x_t is the tissue thickness, x_d is the deflection, k the material thickness, γ is the average cutting and h_{dp} is the burr penetration upon breakthrough.

It should be noted that the accuracies stated in table 7.2 are relative to the deformed tissue.

Referring to figure 7.13 (a) it can be seen that that the maximum force level

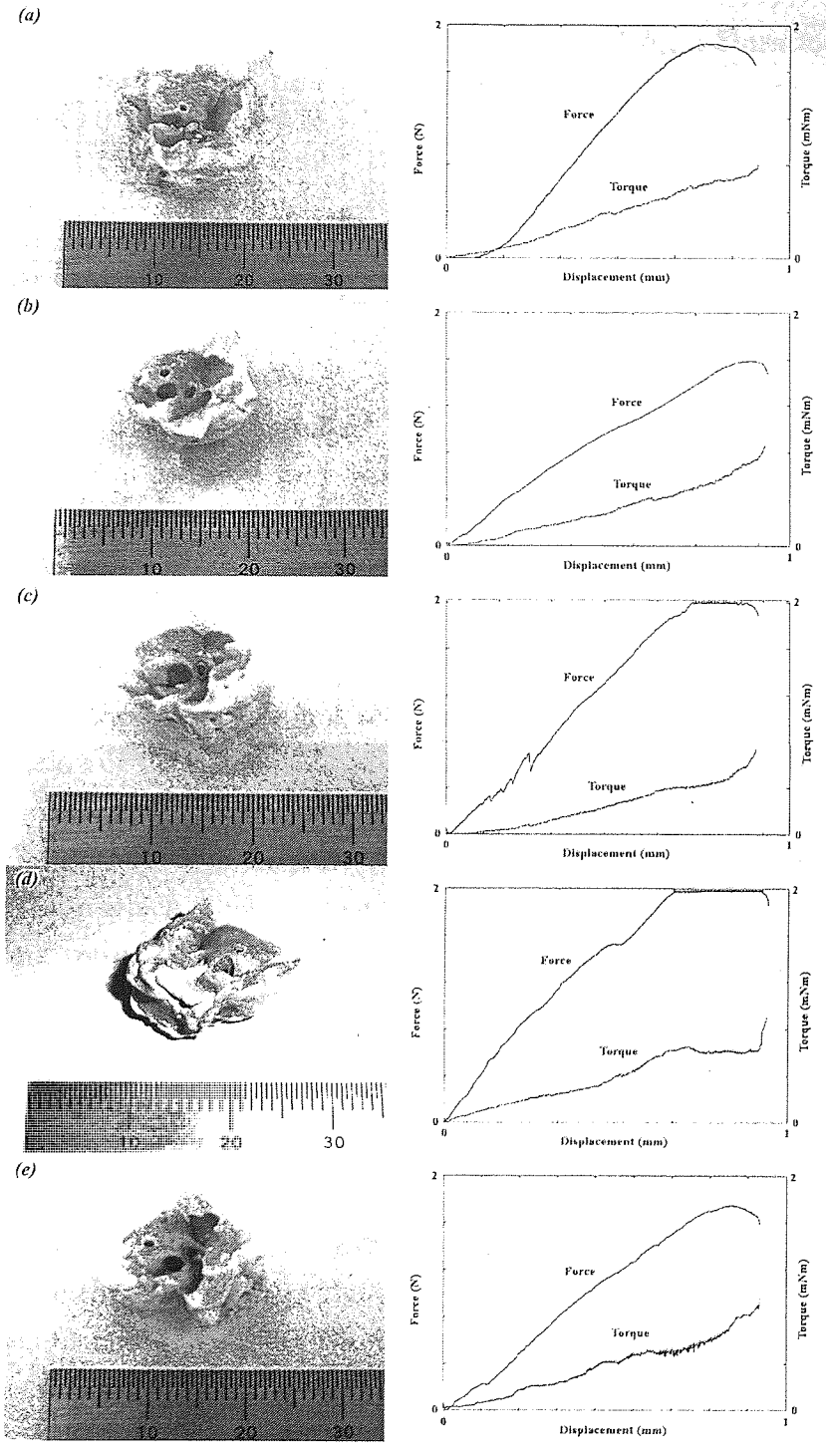

Figure 7.13: *Result of five tests on porcine cochlea.*

Table 7.2: *Estimated drilling parameters based on porcine cochlea tests.*

Test	x	x_t	x_d	k	γ	h_{dp}	Duration
	mm	mm	mm	N/m	mm/sN^{-1}	μm	s.
a	0.57	0.33	0.24	3332	0.023	26	84
b	1.03	0.54	0.49	1700	0.008	19	105
c	1.23	0.73	0.50	2010	0.005	14	122
d	1.41	0.74	0.67	1499	0.008	12	135
e	0.83	0.41	0.42	2143	0.012	20	81

achieved was approximately 0.9 N. As the maximum force level was set to 1 N the force control was never initiated. This generates the very gradual force roll off that is typical in constant feed rate drilling. The section of bone being drilled in this instance is very thin at 0.33 mm and the stiffness is relatively high such that a high force level is achieved quickly resulting in a higher cutting efficiency. As the start of breakthrough occurs the cutting rate increases, leading to a rise in the reactive torque. The low level of compliance accentuates the shallow force roll off because the material is not returning to its natural position and there is less deformation of the material ahead of the drill. As a result the cutting rate is also lower.

Figure 7.13 (c) also demonstrates similar characteristics; when compared with figure 7.13 (b) in which a high degree of compliance is present it can bee seen that the force and torque gradients are much higher as breakthrough is approached. Another interesting observation is that (a) and (c) are also the thinnest specimens and both have a higher cutting rate than the others. This is due, in part to the surface area of the burr in contact with the bone tissue. The smaller area creates higher localised forces at the cutting face resulting in a higher cutting rate. This accelerates the breakthrough process thus resulting in greater burr penetration.

Figures 7.13 (c) and 7.13 (d) again share the same key features however there is considerable contrast between the transients themselves. Figure 7.13(d) bears a great resemblance to the hybrid control strategy shown in 2.11; the fast roll off in the force signal indicative of the constant feed force control due to the force limitation occurring prior to the equilibrium drilling point.

Figure 7.13 (c) is also a good example of where the drilling system distinguishes between noise due to disturbance and the key drilling features. In this

instance the hole was drilled at approximately 30° to the normal due to the geometry of the specimen. As a result, a degree of oscillation was present in the signal until the cutting burr had bedded into the bone tissue. This disturbance can be seen in the first section of the force transient; note that the disturbance in the torque signal is significantly smaller in amplitude.

Each of these holes was completed to its full diameter after breakthrough was detected and in each case the membranous cochlea remained intact upon completion.

7.5 Cadaver Trial

The laboratory trials conducted on both eggs and porcine cochlea have proven the drilling system's ability to detect and control breakthrough under varying conditions. The final stage prior to conducting a full research clinical trial is a cadaver trial. The main aims of a cadaver trial are:

1. To evaluate the ease with which the drill can be correctly positioned,
2. ensure that the cutting burr can reach the operative site with sufficient clearance,
3. to perform a full test drilling on a human cochlea;
4. evaluate the system performance.

If successful, the drilling characteristics may also be used as a comparison with the porcine data. If the data is comparable it will further validate the use of porcine cochlea as a model for evaluating the drilling performance.

7.5.1 Surgical Access

After a suitable cadaveric specimen was chosen the operative site was prepared by a clinician in the same way that it would be in the normal cochlea implant procedure. A complete mastoidectomy was perfromed, followed by the creation

of a posterior tympanotomy to gain access to the cochlea. Figure 7.14 shows the prepared access clearly showing the cochlea. The top of the round window

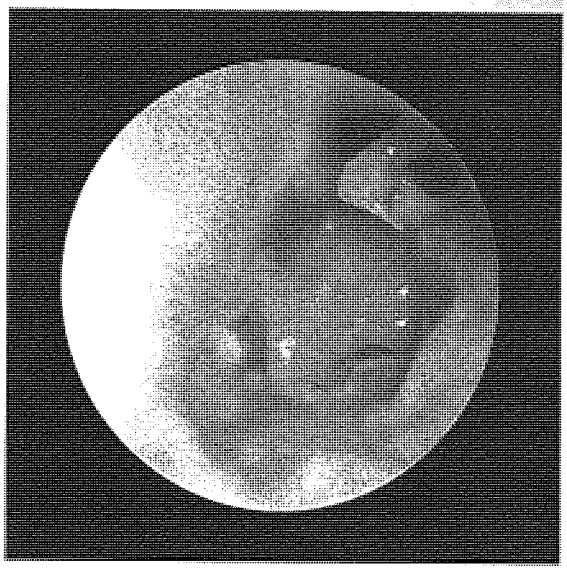

Figure 7.14: *Prepared access to the cochlea via a posterior tympanotomy.*

can be seen as a dark crescent, slightly down and right of the centre. The long process of the incus and the crura of the stapes can be seen in the top right hand corner. It is these two landmarks that are used to determine the position of the cochleostomy.

7.5.2 Drill Positioning

After the access has been prepared the drilling system was moved into position and put along the correct trajectory. The unit was then advanced and the trajectory corrected using the hand held remote and the adjustment mechanism. Figure 7.15 shows the drill unit in position, with the drill shaft passing into the mastoidectomy, through the posterior tympanotomy into the middle ear space. Figure 7.16 shows a view along the surgical access via a surgical microscope. The drill tip and operative site can be clearly seen and the trajectory extrapolated to the optimal cochleostomy location. The clinician reported that the drill unit was simple to position and had sufficient degrees of freedom for the shaft to be located

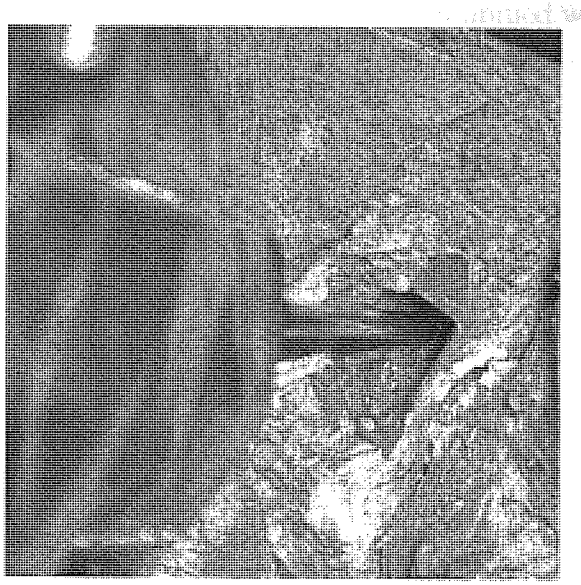

Figure 7.15: *Drill unit placed at the operative site via the surgical access way.*

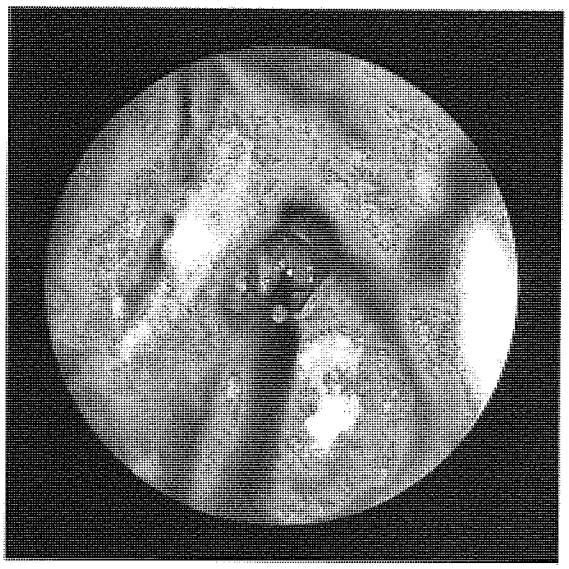

Figure 7.16: *Cutting burr in position above the oval window.*

within the access site and then moved forward into the middle ear without contacting the patient. The use of the linear actuator combined with the adjustment mechanism proved successful at precisely positioning the drill tip close to the cochleostomy site. It was found that these controls could be used effectively in conjunction with the surgical microscope. However, it was observed that in setting the drill trajectory approximately normal to the cochleostomy site the drill shaft sheath was in close proximity to the lateral wall of the mastoidectomy. To allow sufficient clearance to complete the drilling procedure the drill trajectory was estimated as approximately 10° off normal.

7.5.3 Drilling Procedure

As with the setup, the drilling procedure was performed in the same way it would be in the operating theatre. Once the burr was positioned close enough to the surface of the cochlea and the precise cochleostomy location could be determined, the contact sequence was initiated. The contact sequence was completed and estimated the system stiffness as 1.64 N/mm. The drilling sequence was then initiated. The drilling transients are shown in figure 7.17. Due to the angle of drilling a high degree of noise can be seen during the first half a millimeter of travel at which point the burr finally bedded into the bony tissue. There is a low initial force despite there being a measurable torque signal present. This is an indication that the burr is cutting on its side rather than the front. The force is generated by deflection of the drill tip which acts perpendicularly to the measurement axis and thus does not register. This is due to the curved geometry of the cochlea; as the drilling progresses more of the front portion of the burr comes into contact with the bone tissue. The point at which the gradients become steeper indicates that the front of the burr is fully engaged with the bone tissue and normal drilling is resumed. As the bone thickness was less than the burr diameter equilibrium drilling was never achieved hence the continually increasing torque which can also be approximated as linear.

As breakthrough is approached both the force and torque steadily roll off indicating that the tissue in front of the burr is deflecting and the cutting rate is

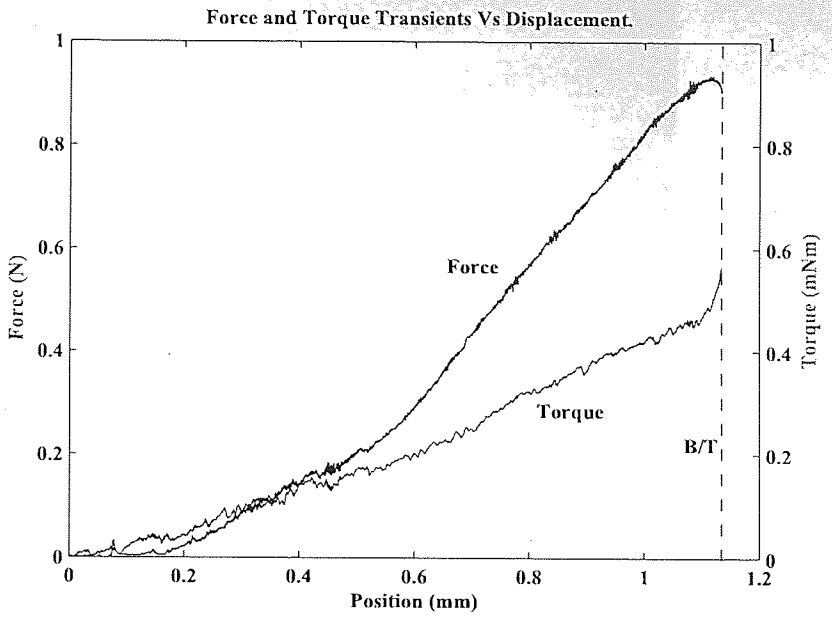

Figure 7.17: *Force and torque transients from a cadaver trial.*

accelerating as breakthrough commences. The drilling process took 111 *seconds* and the estimated cochlea wall thickness was 0.54 *mm*. The partially complete cochleostomy is shown in figure 7.18. The breakthrough aperture can be seen in the centre of the image, surrounded by white. The white is a very thin section of bone surrounding the aperture that has started to fracture as a result of deflection under the drilling forces. The aperture at the centre was estimated at 240 μm in diameter which equates to a breakthrough penetration of 12 μm. Upon removal of the cutting burr the endosteal membrane was still intact and undamaged, there was also no visible leakage of perilymph.

7.6 Conclusion

A series of trials was conducted, designed to verify and validate the drilling system performance to ensure that the design specification was met and that the system was fit for its intended purpose. All the subsystems that make up the drilling system were tested independently in isolation to ensure that they all met their

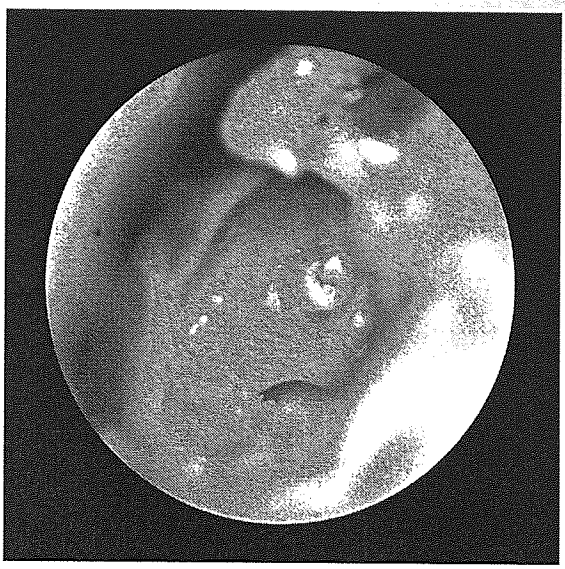

Figure 7.18: *Cochleostomy after breakthrough detection and control.*

design specification. In each case their performance met, if not surpassed the defined specification. The aim of the laboratory trials was to test the performance of the device as a complete system.

The first stage trials saw the empirical determination of the parameters that control the systems ability to detect breakthrough and in doing so it was found that a large number of false positive detections occurred. Despite a false-positive being a fail-safe condition it may induce unnecessary delays during the operating procedure causing the patient undue stress. This led to the inclusion of an additional parameter, breakthrough detection delay, that enables the system to differentiate between noise and the onset of breakthrough. The knock-on effect of this is the possibility of a small delay between breakthrough being detected and any controlling action to be taken. To evaluate the affect of this on burr penetration it was necessary to devise a means of determining the breakthrough penetration.

The method employed uses the diameter of the aperture at the base of the burr hole and the burr geometry to estimate the penetration beyond the distal surface. Using this method it was estimated that the average burr penetration upon breakthrough when drilling through the shell of egg was found to be less than 40 μm. The average drilling time was 81 *seconds* through a mean thickness

of 0.43 *mm*. The results of these investigations were used to define default values of the detection parameters force and torque mean deviation thresholds and the breakthrough delay. There were -5, 5 and 25 *ms* respectively.

A qualitative investigation was conducted into the systems response to noise induced by movement and vibration and the detection performance was unaffected.

Using these laboratory trial it is possible to conclude that under controlled conditions the system complies with its design specification and is suitable for its intended use.

A number of porcine trials were conducted, of which the results of five are shown in figure 7.13. A false positive detection rate of less than 1% was observed. There were no detection failures, however, in some cases where the angle of drilling was greater than 30°, flexure in the drill shaft prevented the burr reaching the medial surface and drilling was ceased by the clinician.

The remaining tests had an average drilling time of 105 *seconds* through an average thickness of 0.55 *mm*. The average burr penetration upon breakthrough was 18 μm. In all cases the angle of approach was kept as close to normal as possible, however, this could not always be achieved. In instances where this was not possible the following observations were made:

1. drilling duration was increased due to greater apparent thickness;
2. breakthrough detection was successful, although the aperture was generally located to the side of the burr;
3. in cases where the drilling angle was greater than 30° the burr would struggle to gain purchase and begin drilling;
4. a high degree of noise was present in the early stages of the drilling transients;
5. flexure of the drill shaft occurred as a result of any lateral component, F_y, of the feed force;
6. the resulting aperture upon breakthrough was elliptical.

At this stage it is not possible to account for this so for future trials the drilling angle should be no more than 30°. An additional improvement to the system was the stiffening of the drill shaft to help reduce flexure due to side loads. The penultimate stage was that of a full trial on a human cadaveric specimen. The procedure was carried out in the same way that it would be in the operating theatre. The manoeuvrability and positioning of the drill unit was found to be acceptable and the operative site was easily reached. It was noted however, though not in this case, that proximity to that lateral wall of the mastoidectomy was very close to the drill shaft when trying to position the drilling axis normal to the surface of the cochlea. The fine positioning of the drill bit was also successful and allowed the clinician to choose the precise location of the cochleostomy. The drilling process was completed successfully and breakthrough was detected and controlled to within 12 μm of the distal surface. The drilling transients were very similar in shape, magnitude and duration to that of the porcine cochlea, thus it is possible to conclude that porcine cochleae are a good model on which trials with the drilling system can be based.

Now that the device performance has been successfully validated and its limitations identified, the validation and verification process can be concluded by conducting a full research clinical trial on a live human subject.

Chapter 8

The Clinical Trial

8.1 Clinical Trial Objectives

There are many surgical procedures that require a surgeon to work at the limit of their perception and this number is increasing with new minimally invasive and micro-surgical techniques being pioneered all the time. What are required are smart tools that build on the clinicians skills to perform tasks that are beyond their ability to control. The surgical micro-drill is unique in that it uses sensory feedback not only to provide feedback to the clinician but it actively uses this feedback to interpret the state at the tool tip and actively makes decisions on how the procedure progresses. This trial will be the final stage in the validation and verification of this tool as a surgical system. The outcome of this trial will not only determine the suitability of this particular device for its intended purpose but will have much wider implications for general surgical practice. This device will be the first of its kind to be deployed in the operating theatre, as such the primary goal of this clinical trial is as a proof of concept for the use of smart tools in surgery. Although only a small number of trials will be conducted *(up to three)* it will provide a qualitative assessment of the suitability of smart tools for use in the surgical environment.

8.2 System Setup

The complete surgical setup prior to draping is shown in figure 8.1. The computer

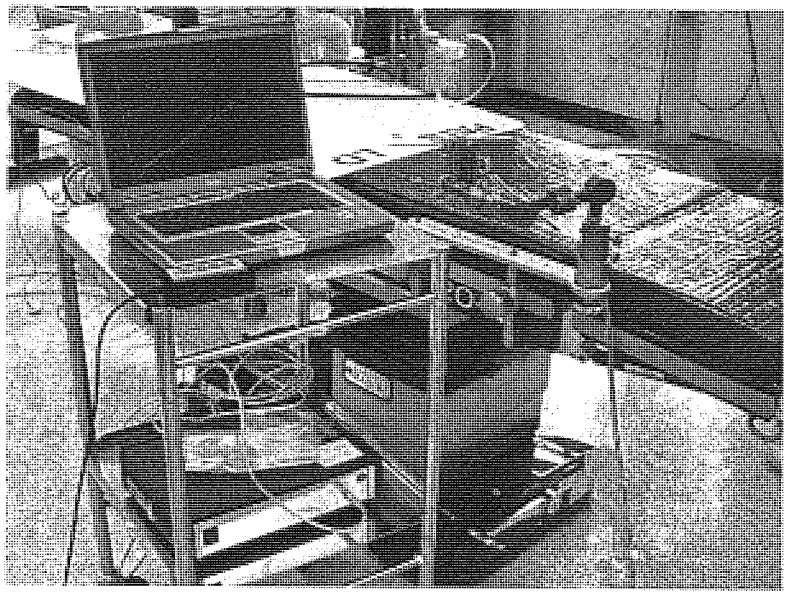

Figure 8.1: *Complete surgical setup.*

and system controller are placed on a stainless steel surgical trolley. The drilling system can be seen in the correct position for the drilling of a left cochlear. Before the system is prepped for surgery a diagnostic and sensor calibration is performed to ensure optimal system performance. This also saves time on the setup after the patient is brought into theatre.

8.2.1 Theatre Layout

The new theatre layout is shown in figure 8.2. The layout represents a typical setup for the drilling of a right cochlear. The key additions to the operating theatre equipment are $20a$ and $20b$, the surgical drilling systems and a trolley containing the control and display unit. The drill unit is mounted on the operating table directly in front of the clinician. The control and display unit is located opposite the clinician so that the display can be easily observed. This also means the secondary controls are easily accessible to the assisting surgeon

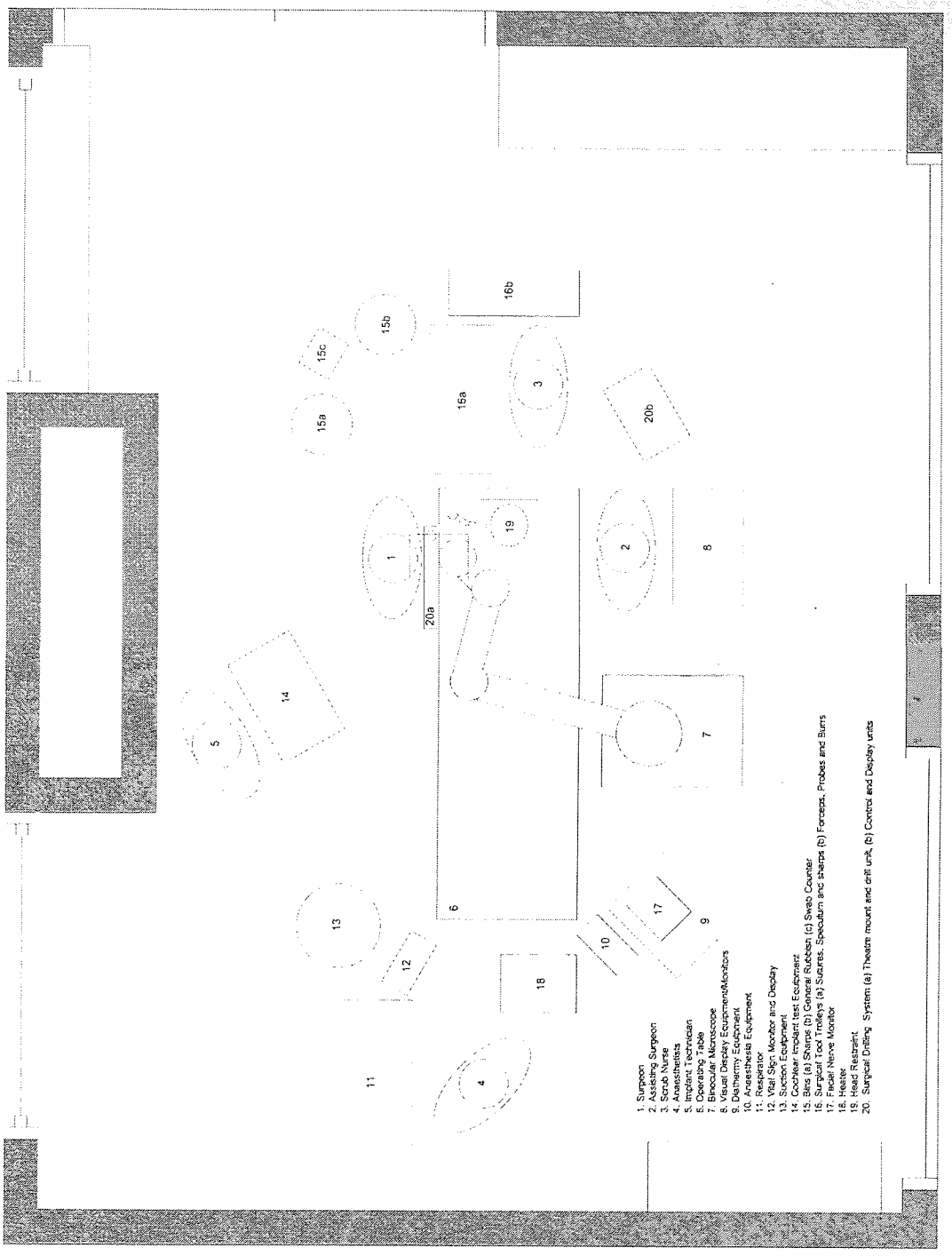

Figure 8.2: *Clinical trial operating theatre layout.*

should intervention be necessary.

8.2.2 Sterility

Given the importance of sterility in the operating theatre a sterilisation and draping procedure was designed. The instrument was designed is such a way that all parts that come into direct contact with the patient are removable and can be sterilised using standard techniques already established within the hospital. The chief example of this is the drill shaft and sheath. Both can be removed from the drill and cleaned, firstly in an ultrasonic bath containing a strong sterilising agent. This is to remove any debris or detritus that may have built up on the part. Secondly the part is sterilised at high pressure and temperature in an autoclave to ensure that any biological contaminants that remain are killed and broken down. Once the parts have been cooled and dried they are encapsulated in a sterile instrument packet, which is in turn placed in another sterile packet. The packaged burrs are shown in figure 8.3. The double packaging enables instruments

Figure 8.3: *The sterilised drill shafts and sheaths.*

to be stored and handled by non-sterile members of staff. When it comes to using the item contained within, a non-sterile member of staff can open the outer

packaging without contaminating the inner packet thus a sterile member of staff, such as the scrub nurse, can open the inner packet and the item can be removed by the clinician without fear of cross contamination. For the remaining parts of the drilling system they can be sterilised using standard cleaning agents used in the operating theatre for cleaning equipment such as the operating table and surgical instrumentation. This is as simple as wiping the equipment down with alcohol based sterile wipes. This is sufficient for any parts that are connected to the operating table or that are located within a draped area as these regions are considered non-sterile. For the exposed areas, these are covered either by sterile polythene camera sheaths or by surgical drapes.

8.2.3 Draping Procedure

The draping of a patient is a fairly complex process. When the patient is brought into the operating theatre they are the least sterile and handling the patient poses the greatest risk of cross contamination. As such draping is performed by two sets of staff, non-sterile and sterile. Non-sterile members simply wear surgical scrubs and gloves, sterile members wear surgical gowns and sterile latex gloves that cover them from the neck down. The patient is brought in and is moved onto the operating table. After all support and monitoring equipment has been attached the entire patient is covered in sterile drapes with the exception of the operation site. It is at this point that the drilling system is mounted and draped. The drilling system is draped in two separate stages, first the support section is draped and then the drill unit is draped separately. The procedure for the mounting system is described in figure 8.4 and that of the drill unit is described in figure 8.5.

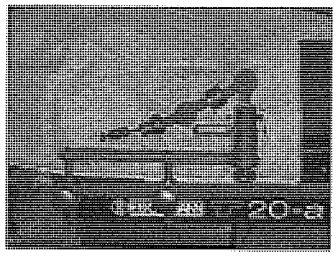

The arm and theatre mount are cleaned with sterile wipes and mounted on the side of the operating table and is moved to one side.

The area is not yet sterile and as such this is carried out by a non-sterile member of staff.

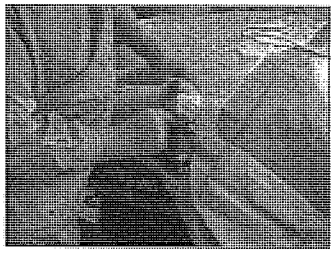

A sterile member of staff then covers the patient and the lower portion of the arm with a sterile drape. Care is taken to avoid touching the arm and mount. The drape is folded back to prevent the sterile side becoming contaminated.

The arm is placed inside a sterile camera drape and the drape is extended down to cover the whole arm and the valve assembly.

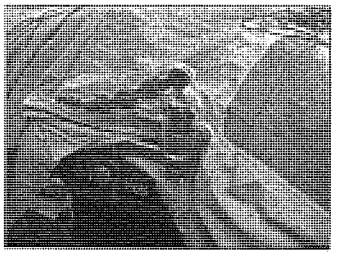

The camera drape is trimmed to length and the folded back drape is pulled forward to cover the theatre mount.

A second drape is clipped around the base of the locking arm covering the gas cylinder and the piercing screw. This covers all exposed parts of the locking arm leaving the valve accessible.

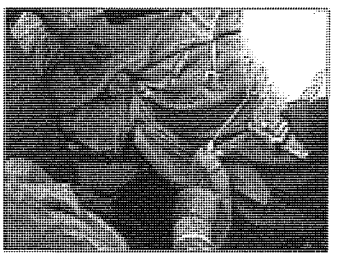

Lastly the locking arm is folded back out of the way and a third drape covers the entire assembly.

When the arm is required a non-sterile member of staff reaches beneath the sterile drape, looses the theatre clamps and slides the unit into position then re-tightens the clamps.

Figure 8.4: *Draping procedure for the theatre mount and locking arm.*

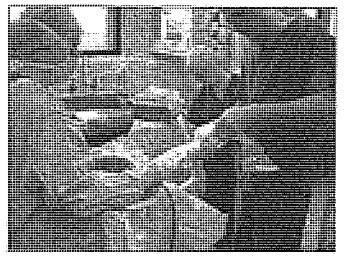

Like the mounting system the drill unit is first wiped down with sterile wipes. A sterile camera drape is then help my a sterile member of staff, whiles a non-sterile member drops the drill unit into the drape.

The non sterile of the drape can then be extended to cover the drill unit and the control cables.

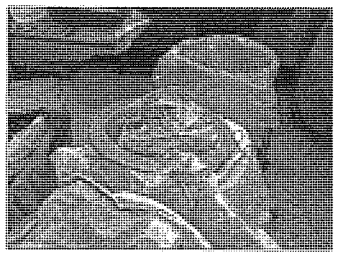

Once draped the drill unit its placed along side the operating table with the other surgical instruments ready for use.

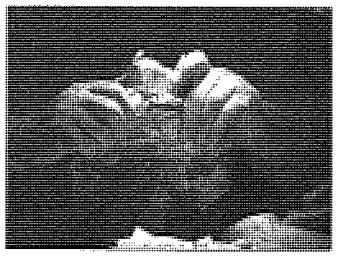

When the time comes to setup the drill unit, the draped unit is taken and mounted on the locking arm.

Care must be taken to push the drape into the 'V' groove so the drill unit does not pierce the drape when the clamp is tightened.

A small incision about 1 cm long is made in the drape over the hole in which the drill shaft locates.

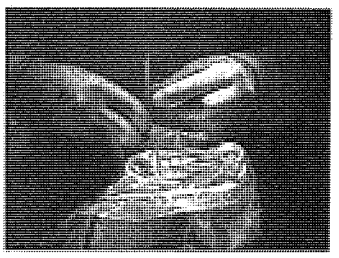

The drill shaft and sheath are removed from their sterile packaging.

The drill shaft is placed through the hole in the drape, the sheath is then placed over the shaft and the boss end is placed through the drape and is screwed into the drill chassis.

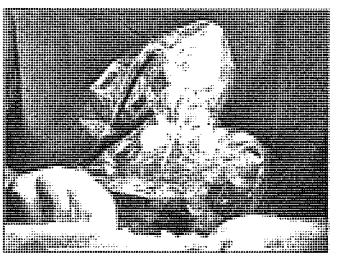

The boss is screwed tight clamping the polythene and sealing the drape.

The system is now sterile and ready to use.

Figure 8.5: *Draping procedure for the drill unit.*

8.2.4 Drilling Protocol

The drilling protocol dictates how the drilling system is used in the operating theatre, an example protocol is shown in figure 8.6. In the centre column shows the drilling actions, the left columns shows the control actions and the right shows the interactions required by the operator. The stages identified by 'WAIT' are the key points at which the clinician must confirm that they are happy for the system to continue onto the next phase. For the purposes of patient safety there should be complete quiet in the operating theatre and the clinician should clearly announce the progression between drilling phases. This ensures that the team is aware what the device is doing and the current drilling phase it is in. This will also ensure that the clinician can hear audible notifications from the computer.

8.3 Surgical procedure

The surgical technique employed is based on that described in section 5.3.3.1 with a few exceptions. The key stages of the conventional and new surgical procedures are shown in figure 8.7. The first deviation from the conventional procedure is the setup of the clinical micro-drilling system just after the patient is brought in. The theatre mounting system is mounted on the same side of the operating table as the ear to be operated on and is draped according to the procedure outlined in section 8.2.3. Although this is not technically part of the surgical technique, it is a key part in the setup and use of the drill. Ordinarily the clinician creates the cochleostomy using the Skeeter® (6) hand drill as soon as the access is prepared. The hole is formed, flushed with saline and then plugged with wadding to lower the risk of contamination while the remainder of the procedure is performed. This is done primarily because this is the most intricate part of what can be a fairly lengthy procedure. Thus it is best performed early before fatigue has a chance to set in. The risks of this include loss of perilymph and a greater risk of infection due to prolonged exposure. As the intention is to use the micro-drilling system to perform the cochleostomy the opening of the cochlear can be left to the last moment prior to electrode insertion. As such the implant well is milled

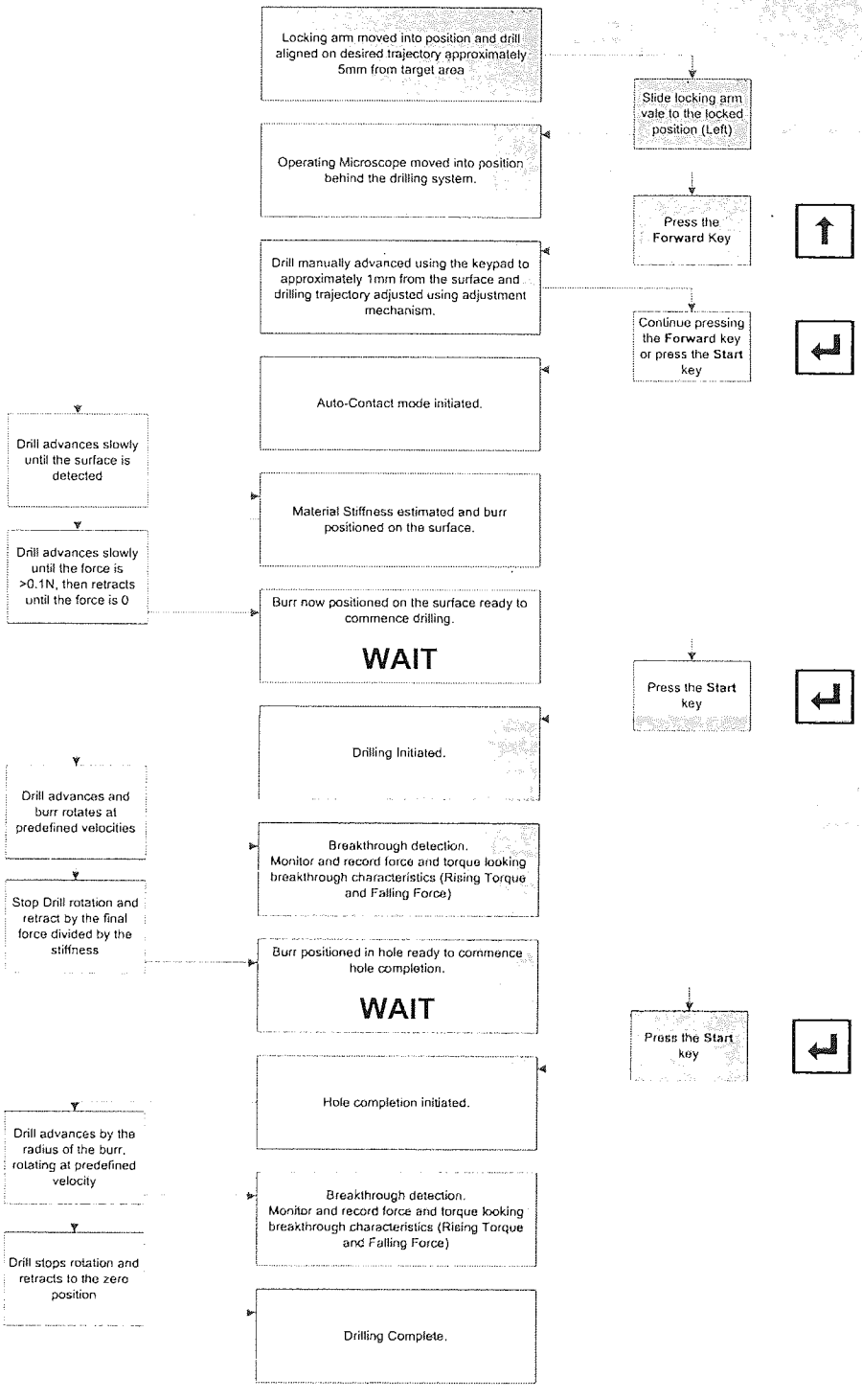

Figure 8.6: *Surgical drilling protocol.*

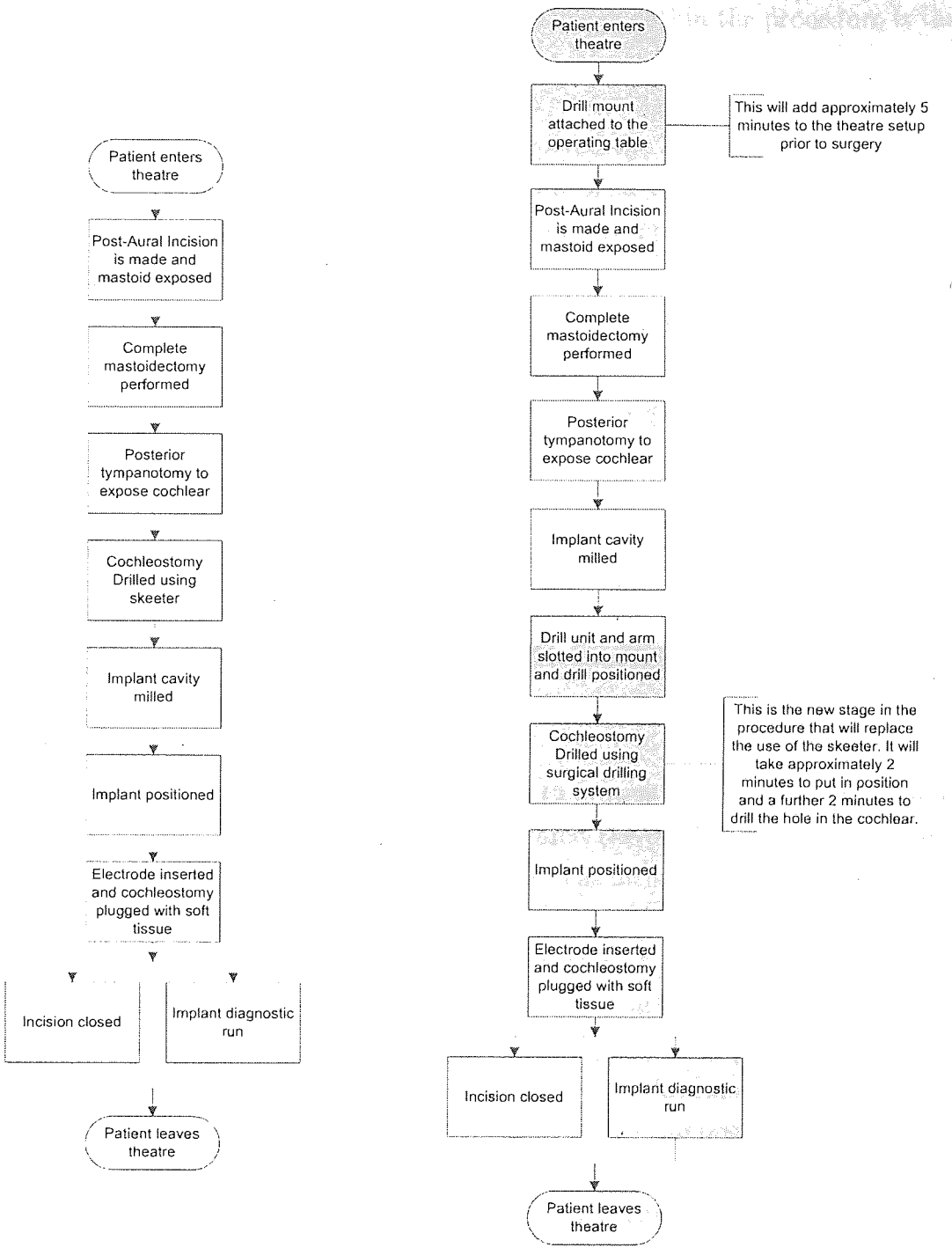

Figure 8.7: *The old (left) and the new (right) surgical techniques.*

and the implant site prepared before rather than after the preparation of the cochleostomy. Obviously the most significant change within the procedure is the use of the surgical micro-drill to perform the cochleostomy.

It was this procedure that was used in the clinical trials.

Once the patient and equipment were prepared the surgeon could begin creating the access way to the middle ear. This was done in the usual manner with a post aural incision followed by the creation of a complete mastoidectomy and posterior tympanotomy. The prepared access is shown in figure 8.8. The posterior

Figure 8.8: *Prepared access to the middle ear.*

tympanotomy was then plugged with wadding to prevent debris entering the middle ear. With the access to the cochlear prepared the implant well was created. When the milling was completed the entire area was flushed with saline to remove all debris. This completed all the tasks that could be performed prior to electrode insertion so it was then necessary to drill the cochleostomy. The drilling system was slid along the mounting rail so that the support arm was level with the patients head, and the arm was extended. The drill unit was attached and the drill shaft and sheath inserted as described in figure 8.5, the clinician can then position the system ready for drilling. Figure 8.9 shows the clinician position the drill unit within the posterior tympanotomy. Once roughly positioned, the surgical microscope can be moved into position and the hole location and drilling trajectory can be finely adjusted. Figure 8.10 shows the clinician using the surgical microscope to visualise the drill tip and using the adjustment controls to precisely position the burr. With the drilling trajectory and hole position correct the surgeon ini-

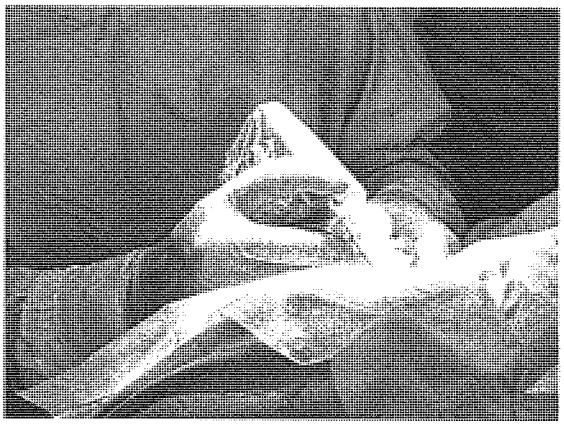

Figure 8.9: *Clinician positioning the drill unit.*

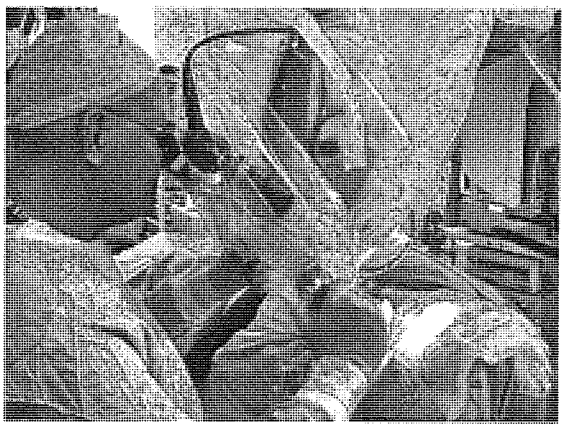

Figure 8.10: *Clinician using a surgical microscope to view the drill tip.*

tiates the drilling process, monitoring the drills progress on the computer and inspecting the drill tip between stages. Figure 8.11 shows the clinician operating the drilling system via the hand held remote control. Upon completion, the drill

Figure 8.11: *Clinician operating the drill system using the hand-held remote.*

was removed and the hole inspected. The partially completed cochleostomy is shown in figure 8.12. The hole was of the correct size and partially complete with

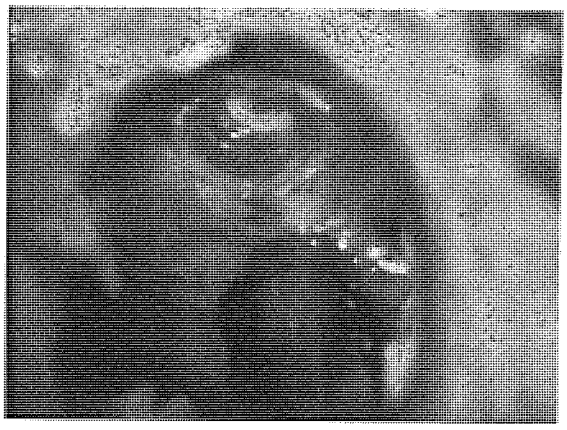

Figure 8.12: *Clinical trial: Partially completed cochleostomy.*

the membrane intact, preserving the integrity of the cochlea. The area was then flushed and all debris and blood removed. The membrane was then opened gently using a scalpel, this prevented the ingress of contaminants into the cochlea and the pressure wave that would normally be induced by the drill bursting through the membrane and displacing perilymph. This created a small aperture in the

Figure 8.13: *Completed cochlear implantation.*

membrane through which the implant electrode could be inserted. The outer edge of the membrane acted as a seal as the electrode was inserted thus the electrode had to be inserted very slowly to prevent pressure building up within the cochlear. Figure 8.13 shows the implanted electrode in position. After insertion the procedure continued as normal with the clinician closing the incision while an implant diagnostic is performed by an implant technician. The closed incision is shown in figure 8.14. This concluded the procedure and the patient was removed

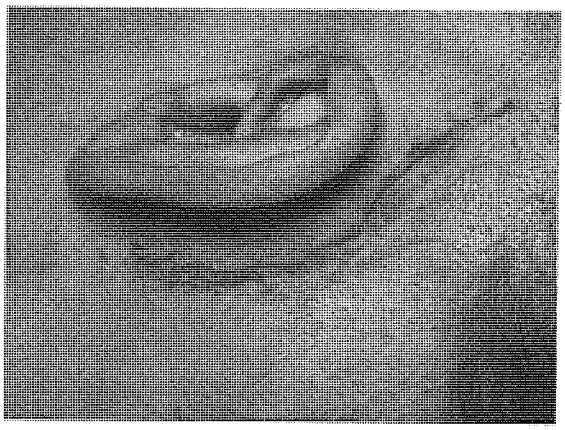

Figure 8.14: *The closed incision, completing the procedure.*

to recovery and the operating theatre was cleaned down ready for the following procedure.

8.4 Trial Results

A series of three clinical trials were conducted, each of which had a successful outcome.

The first trial could not be brought to its conclusion due to anatomical limitations that prevented the burr reaching the desired cochleostomy site. A Partial hole was drilled, however, the distal surface could not be reached due to the lateral wall of the mastoid coming into contact with the drill shaft sheath, deflecting the burr. Despite breakthrough not being reached, the drilling system performed well in all other aspects. The drilling protocol ensured that the operation of the device went smoothly. One potential issue that was highlighted by the operator of the device was that the adjustment mechanism and clamps were difficult to rotate due to the drape slipping. This had potential to make fine positioning of the device difficult. The drill unit with the modifications made as a result of learning from the first trial is shown in figure 8.15. To prevent these issue re-occurring

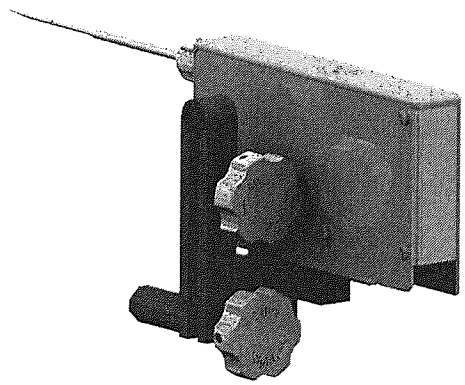

Figure 8.15: *Modifications made to the drill unit.*

the drill shaft was stiffened and the drill shaft sheath shortened to make the profile of the drill shaft assembly slimmer to prevent it fouling anatomical features. Knurled covers were added to the thumbscrews to make gaining purchase easier through the polythene drape. In both cases neither problems occurred again and

the learning and experience led to later trials running smoother. This led to faster setup and draping times and more efficient position of the drilling unit. The remaining trials were both completed successfully, figure 8.16 shows a set of force and torque transients from a successful clinical test. The total drilling time

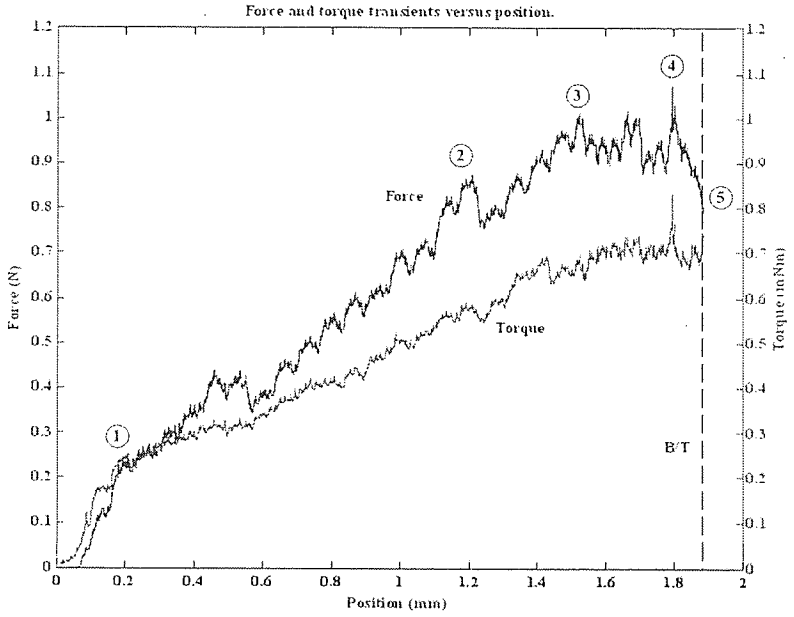

Figure 8.16: *Force and torque transients from a research clinical trial.*

was approximately three minutes, over a total displacement of 1.89 *mm*. Looking at the drilling transients, the most striking feature is the prominence of the fluctuations induced by the patients respiration, in addition to this the heart beat is also detected. These transients are superimposed on the base signal occurring at frequencies of approximately 0.25 Hz and 60 Hz respectively. Further to this the patient appears to take an extended breath approximately every 60 *seconds*. This can be seen as feature **2** on figure 8.16, this recurring feature at point **2** was logged each time it occurred. The steep gradient at the beginning of the transient indicates that the initial cutting rate was very low, this is likely to be due to there being insufficient force to cut. The burr beds in and the cutting rate increases at point **1** and normal drilling commences. Like the porcine cochlear the thickness of the cochlear wall is insufficient for equilibrium drilling to occur so the transients are approximately linear between points **1** and **3**. However, at

point **3** movement of the patient results in a the axial force increasing above the force limitation threshold resulting in a reduction in the linear feed rate, and the initiation of force limited feed rate. The net result of this is a leveling of the gradient. At point **4** the system experiences an external disturbance which is detected and logged by the system at the patient suddenly moving toward the drill. This is likely to have been caused by something knocking against the operating table. The onset of breakthrough was detected at point **5**. In this example breakthrough was successfully detected and controlled. The estimated drilling parameters are shown in table 8.1.

Table 8.1: *Estimated drilling parameters.*

Parameter	Value	Units
$Thickness$	0.44	mm
$Stiffness$	1.65	N/mm
$Burr\ Penetration$	14	μm

Breakthrough was detected and controlled within 15 μm of the distal surface without damaging the endosteal membrane. The hole was then successfully completed.

8.5 Conclusions

The clinical trial saw the surgical drilling system successfully deployed in the operating theatre. The device integrated seamlessly with existing equipment and procedures. In general the device was found to be easy to use and simple to operate, with the exception of the first trial in which fine positioning of the drill unit was found to be difficult through the polythene drape. This was rectified by the addition of grips on the thumbscrews and the reduction of the drill shaft profile. The remaining trials were successful and demonstrated that the system is capable of controlling the penetration of the burr to within 15 μm of the distal surface.

It was shown that the system successfully differentiated between environmental disturbances, such as the patient's breathing, external vibration, and the onset

of breakthrough. It proceeded to control the drill penetration to a high degree of accuracy. The partially complete holes were then completed and the procedures finished successfully, in doing the clinician observed that trauma to the cochlea appeared greatly reduced and the delayed opening of the cochlear also reduced the loss of perilymph.

The new surgical procedure successfully limited the duration that the internal cochlear was exposed. Although insufficient trials were conducted to draw firm conclusions based on statistical data the clinician felt that the drilling system demonstrated clear benefits over the conventional technique.

By visual inspection the clinician observed that the hole that was formed by the device was in the optimal position and the membranous cochlear remained intact. This represents the ideal outcome when using the manual technique with the additional benefits introduced by the smart tool. These include reducing the skill level required to perform the operation to this standard, reduced drilling time and above all, it offers control and repeatability.

Chapter 9

Conclusions

9.1 Summary

This thesis has described the design and development of the first autonomous surgical robot to be deployed in the operating theatre, from the conceptual design to the successful completion of a research clinical trial.

The system developed combined a mechatronic tool that integrated a smart tool point to relay real-time information about the state of the tool-tissue interaction. The smart tool point employed a multi-modal sensing strategy combined with an embedded control system to to actively control the progression of drilling process independently, self-referencing to the deforming tissue. The device successfully demonstrated the ability to accurately control the penetration of a cutting burr through compliant tissues of unknown mechanical properties and unknown boundary conditions at the medial surface.

The clinical trial saw the system detect and control the penetration of the cutting burr to within 20 μm of the distal surface. The system clearly demonstrated that it is possible to build on a clinicians skills by enhancing their sensing and control capabilities to achieve high quality clinical results in parallel with reducing the time and skill level required.

This body of work took the drilling concept from the compliant drilling model originally developed by Brett *et al* (42) and the learning from the development of the first prototype device and used it as a basis for the design of a new autonomous surgical drilling system. The work has:

1. explored the characteristics of the drilling of compliant materials and used this model to develop a control strategy for minimising burr penetration;

2. the requirements of two possible applications as well as general surgical requirements were investigated;

3. a specification for the final design was derived taking into account the surgical, technical and environmental requirements defined by the technique and its applications.

4. A complete drilling system was designed, manufactured and underwent a vigorous validation and verification process which,

5. culminated in a successful series of research clinical trials.

The characteristics of the drilling of compliant materials were explored and the process was broken down into a series of key stages that could be uniquely identified from the drilling transients. A number of control strategies were investigated to control each stage in such a way that the state of the drilling process could be derived and controlled to minimise drill penetration upon breakthrough and then complete the hole with minimum protrusion. The most appropriate strategies were chosen, expanded and integrated to form a technique for the drilling of compliant materials. A specification for the final system was derived based on the requirements of the drilling technique and those of the surgical technique.

Previous work in this area was reviewed and an original prototype was rebuilt and used to evaluate the control strategies investigated. Key areas of improvement were identified and, as a result, new sensing and hardware control strategies were explored. Additional learning was gained from the use of the instrument and was used to further develop the technical specification for the new device. The key deficiencies of previous systems identified were the sensor resolution and tool

support. A number of feasibility studies were conducted to identify alternative sensing strategies in which a novel torque measurement technique was developed.

Conventional surgical techniques were reviewed in detail and their key risks and limitations identified. By developing and understanding of how and why these procedures are carried out in they way they are, the ways in which a robotic system could offer the most benefit came to light. In addition, existing surgical robotic systems were reviewed and used to formulate an approach to the design of a system that would be suitable for clinical deployment. A clinical and environmental specification for the robotic surgical system was then defined.

A tool support was designed based on the requirements defined by the surgical applications and the stability requirements of the technique. To ensure that the design was suitable, rapid prototyping was used to build a scale model that could be evaluated.

A complete system was designed and built based on the derived specification. The system, comprising of an embedded controller, support system and a sensor guided mechatronic tool was manufactured and assembled. A control interface was designed and written and the compliant drilling technique was implemented in the firmware of the embedded controller.

The complete system then underwent an intense verification process in which each sub-module was tested and a series of laboratory trials were conducted to evaluate the system as a whole. As part of the verification process a series of porcine trials were successfully conducted and a method of estimating the drill penetration was established. It was found that the system could detect breakthrough within 20 μm of the distal surface with extremely low false-positive and failure detection rates of less than 1% as shown in figure 7.5. This led to a trial on a cadaveric specimen in which breakthrough was detected within 18 μm of the distal surface and controlled without penetration of the endosteal membrane.

On successful completion of the verification process the device was used in a series of dummy operating theatre trials in which the surgical team were trained and the surgical procedure finalised. This included the selection of the procedure to be performed, the setup and removal of the device, sterilisation, draping procedures and the operating protocols.

In parallel to this NHS ethics approval was sought to enable a research clinical

trial to be conducted. On receipt of the ethics approval and permission to perform the trial a series of clinical trials was conducted.

The micro-drilling system successfully demonstrated that penetration of compliantly or compliantly mounted tissue can be achieved extremely accurately without damage to the underlying tissues at the medial surface. In this application this meant the penetration of the bony cochlea whilst leaving the membranous cochlea intact. Penetration was controlled to within 15 μm of distal surface.

9.2 Concluding Remarks

This system which was designed with surgical deployment in mind, represents a major step forward in surgical robotics. It is the first device of its kind to be successfully deployed in the operating theatre, demonstrating that all the benefits that robotic systems represent can be brought to the operating table.

Three of the major hurdles facing surgical robotic systems are cost, patient safety and surgical opinion.

This system has demonstrated that a complex, smart control system can be implemented on a basic, 8-bit hardware platform without the need for expensive and bulky support equipment. The custom design of the drilling unit enabled the device to have a very small foot print that could be used alongside standard theatre equipment and be integrated into the surgical environment with minimal disruption to the work flow. Potentially making this kind of device very cost effective.

Two of the key principles behind the safe design of autonomous tools for use in the operating theatre are the design of custom tools specific to individual tasks and the inclusion of the surgeon in the control loop.

This not only improves safety, but also ensures that the clinician does not feel that the control of the procedure has been taken out of their hands. This is key if autonomous tools are to be successfully adopted in general surgical practice.

The concept is to build on a surgeon's skills by performing tasks that are beyond human perception to detect and control, not to replace a surgeon with a robot. The intention being to assist, reducing the skill level required to perform

complex and often risky surgical tasks to a high quality, thus standardising procedures and making them safer, more cost efficient and thus available to a much wider patient base.

To date, tele-manipulator systems were the only surgical robots to have been successfully deployed commercially in the operating theatre that can manipulate soft tissues, albeit under the control of the operator. One of the major limitations has been seen to be the lack of tactile feed back to the clinician. This system is unique due to the way in which it uses real-time data from the tool tip to derive the state of the tool-tissue interaction. The system uses this state information to actively control the way in which the tool interacts with the tissue, governing the way in which the drilling process progresses. This sensor guided strategy enables the tool to self-reference to the deforming tissue and navigate without the need for pre-opertive scan data. It is this capability that enables the system to operate in circumstances where the boundary conditions are unknown without the need to restrain the patient.

If smart surgical tools were integrated into existing surgical robotic systems and used in conjunction with their pre-operative planning and intra-operative tracking capabilities it may lead the way for more complicated soft-tissue procedures to be performed robotically. The same could be said for MIS and MAS procedures, for example Natural orifice translumenal endoscopic surgery or *NOTES* (60); if smart tool points were integrated into endoscopic and laparoscopic instruments it could further aid clinicians in understanding what is happening at the tool tip by relaying information describing the tool tissue interaction that could be used for both control, tactile feedback and navigation.

Above all, this research has demonstrated that smart tool points have a place in the operating theatre.

Figure 9.1 shows the surgical team in the operating theatre next to the operating table with the drilling system attached.

Figure 9.1: *The surgical team at the Queen Elizabeth Hospital, Birmingham, UK.*

9.3 Future Work

During the course of the work a number of possible avenues for future work came to light. These covered many different areas and are summarised in this section.

9.3.1 Patient Safety

One of the major hurdles facing the adoption of robotic surgical techniques in general surgical practice is patient safety. This device, by design, is intrinsically safe due to the slow, controlled manor in which drilling is executed. In the unlikely event that breakthrough is not detected the clinician has several seconds to observe and halt the drilling procedure manually before there is any risk of damage. As such, even if any damage does occur it is likely to be less traumatic than that of the conventional technique. Additional safety features were also incorperated such as the force limitiation and the operating protocol to make the device as safe as possible for use in the operating theatre. Despite this, a number of further potential enhancements became apparent throughout the course of the research. The key improvements are listed below:

1. Simplification of the user interface;
2. elimination single failure modes in safety critical systems;
3. integration of manual back-drive capability;
4. integration additional sensing capability.

Points **1**, **3** and **4** will be discussed in the subsequent sections. In the case of point **2**, a single failure mode is a single failure of a part or component that results in in-operation or malfunction of the device. If this were to happen in a safety critical system it would obviously pose an unnecessary risk to the patient. The most obvious example in the micro-drilling system is the force sensor. If this part were to fail, an excessive force could be applied to the patient resulting in harm. To prevent this from occurring additional redundancy should be built into the device. This could be, but not necessarily so, another force sensor or a means

of simply detecting the fault. For example a simple limit switch on the cantilever or an actuator that is force limited. This can be used to detect the fault and alert the operator or take appropriate action, making the device safer to use.

9.3.2 Design Considerations

A number of design improvements were identified some resulting from new technologies that have since become available and some from experience with the device itself.

9.3.2.1 Mechanical Design

Two areas identified for improvement were that of the force sensing and the linear actuation of the drill unit.

Force Sensing

One of the limitations of the device was differentiating between tissue movement along the tool axis and that of lateral motion. While the force and torque characteristics give a clear indication in theory, in practice it is difficult to separate. The inclusion of a multi-axis force sensor in the drill sheath mounting would provide a measurement of drilling forces exerted at the tool tip perpendicular to the drilling axis and would also provide information on whether the drill unit itself was in contact with the patient. This will impact patient safety as well as drill performance as the risk of applying excessive force, that would not necessarily be detected, would be reduced.

Linear Motion

The system designed employed a conventional fine pitch lead screw to generate the linear motion along the drilling axis. While this approach has many benefits including very precise velocity and position control it is somewhat limited in several ways:

1. The achievable velocity range is very low;
2. Lead-screws are prone to wear resulting in decreased accuracy;
3. No back-drive capability.

Items **1** and **3** are particularly important as they have a direct effect on patient safety. If in the event of an emergency the drill system has to be removed quickly, this is hampered by no back drive capability and thus the drill must be actuated to retract and enable safe removal. As the actuator is designed for very low velocities, high velocities are unachievable and as such increases the time needed to retract the device. If this back-drive capability were present, the surgeon could simple pull the device back and safely remove it. One such technology that would allow this are the new generation of piezo motors. These devices can provide velocities as low as 100 nm/s up to 150 mm/s at resolutions down to 50 nm. These motors operate using a friction drive principle and provide a maximum linear force of a few newtons thus can be manually back-driven safely. Due to the nature of the devices and the choice of materials these devices are also highly wear resistant making them ideal for this application.

9.3.2.2 Electronic Design

While the system control architecture performed well and was sufficient for this series of clinical trials, additional memory and processing power would have been of benefit. The firmware implemented in the device was written in a very efficient manner yet the algorithms employed were very simple. Despite this, the memory limitations of the micro-controller used as the HLC imposed restrictions on the program code length thus the algorithm complexity had to minimised. Another problem with this specific device was that the core program memory was volatile, that is the code has to be downloaded from the host computer each time the device is switched on. This made the presence of the computer necessary when the system is first setup. As such a more advanced processor with a larger amount of non-volatile memory and faster core processor would enable the system to make more use of the information available to it, improving performance. A suitable device for inclusion would be a digital signal processor (DSP) or FPGA.

In addition to the use of more advanced algorithms, if this device were to be developed into a commercial device further self-testing and diagnostic capability would have to be integrated. The inclusions of additional force sensors would also increase the likely processing overhead.

At present the system requires the presence of a computer, ultimately this is desirable in terms of both safety and cost. Although all the data processing is embedded in the devices present incarnation, the visual display and configuration is performed by the host computer. An ideal solution would be to integrate a display and a simple interface to allow setting of the parameters used by the micro-drill controller. Given that the interface requirements for this system are simple, a touch-screen display would be a good solution. An interface of this kind would reduce both cost and system complexity.

9.3.2.3 Interface Design

As this was a research device the software provided significantly more functionality than is required. The level of control and configurability was not required in the operating theatre and thus can be simplified significantly.

9.3.2.4 Control Improvements

To date little work has been done on the effect of the angle of drilling, some preliminary work was carried out that identified the range over which the current system will operate effectively, however, how this affects the tool-tissue interaction is little understood. The inclusion of a multi-axis force sensor will go some way to understanding this, however, further work is required and the findings will need to be integrated into the control algorithms.

Further work also needs to be carried out on the modeling of soft tissues which is an area in which little work has been done, this will lead to more effective strategies of compliance estimation. This research used a simple approach to account for the tissue deformation, however, this was identified as a limitation on the achievable accuracy.

9.3.3 Further Applications

There are a number of other applications that this technique may be successfully applied to should further work be undertaken, one example of this the implantation of bone anchored hearing aids. Another area of future work is the use of this instrument in a hand held capacity. Some preliminary work has been done in this area with encouraging results, however it was necessary to provide audible force feed back to the operator. As well as new applications, the use of the current system could be used to make improvements to existing techniques in cochlea implantation, for example it may be well suited for use in the suprameatal approach developed by Baumgartner *et al* (35). All of these future applications are discussed in greater detail in A.4.

References

[1] National institutes of health, medical arts and photography branch. http://www.nidcd.nih.gov/, Jan 2007. 1, 5.1, 5.2, 5.3, 5.4, 5.5, 5.6, 5.7, 5.8

[2] http://www.altera.com/, Mar 2007. 6.3.1.5

[3] Maxon dc motor key information. http://www.maxonmotor.co.uk, May 2008. 4.2.1.2, 4.2.1.2, 4.2.1.2, 6.2.2.1, 6.2.2.1

[4] http://www.acrobot.co.uk/, May 2008. 3.1.2

[5] http://www.avagotech.com/, May 2008. 6.3.1.4

[6] http://www.medtronic.com/neuro/midasrex/ehs.html, Jan 2008. 5.3.2.1, 5.3.3.1, 8.3

[7] http://www.microchip.com/, Feb 2008. 4.2.1.2, 6.3.1.3

[8] http://www.acrobot.co.uk/Sculptor.html, May 2009. 3.1.2

[9] http://www.analog.com/, May 2009. 6.3.1.4

[10] http://www.cypress.com/, May 2009. 6.3.1.2

[11] http://www.freehandsurgeon.com/, May 2009. 3.1.1

[12] http://www.idt.com/, May 2009. 6.3.1.4

[13] http://www.igus.co.uk/, May 2009. 6.2.2.2

[14] http://www.integra-ls.com/, May 2009. 3.1.1

[15] http://www.intuitivesurgical.com/, May 2009. 3.1.1, 3.1.3

[16] http://www.mazorst.com/SpineAssist-product.asp, May 2009. 3.1.1

[17] http://www.micro-epsilon.co.uk/, May 2009. 6.2.2.2, 6.3.2

[18] http://www.pfizer.com/, May 2009. 5.3.3.1

[19] http://www.prosurgics.com/, May 2009. 3.1.1

[20] http://www.renishaw.com/en/10712.aspx, May 2009. 3.1.1

[21] http://www.robodoc.com/, May 2009. 3.1.4

[22] http://www.staubli.com/en/robotics/, May 2009. 3.1.3

[23] http://www.ti.com/, May 2009. 6.3.1.4

[24] S. Aiono, J. M. Gilbert, B. Soin, P. A. Finlay, and A. Gordan. Controlled trial of the introduction of a robotic camera assistant (endoassist) for laparoscopic cholecystectomy. *Surg Endosc*, **16**(9):1267–1270, Sep 2002. 3.1.1

[25] B. Allota. Study on a mechatronic tool for drilling in the osteosynthesis of long bones: tool/bone interaction, modelling and experiments. *Int. Jnl. of Mechatronics*, **6**:447:459, 1996. 3.2

[26] M. Asai. Analysis of the best site on the stapes footplate for ossicular chain reconstruction. *Acta Otolaryngol*, **119**:356:361, 1999. Stockh. 5.3.2.2

[27] D.A. Baker. *A technology for controlled compliant drilling of bone applied to the stapedotomy procedure.* PhD thesis, Bristol University, 1998. 1.1, 2.2, 2.2.1, 4.1, 4.1.1.4

[28] D.A. Baker, P.N. Brett, M.V. Grffiths, and L. Reyes. A mechatronic drilling tool for ear surgery: A case study of some design characteristics. *Mechatronics*, **6**:461:477, 1996. 3.3

[29] D.A. Baker, P.N. Brett, M.V. Griffiths, and L. Reyes. Surgical requirements for the stapedotomy tool: data and safety considerations. In *Proc. 18th Annual International Conference of the IEEE Bridging Disciplines for Biomedicine Engineering in Medicine and Biology Society*, **1**, pages 214–215, 31 Oct.–3 Nov. 1996. 4.1

[30] D. Bansal, D.J. Evans, and B. Jones. Application of the real-time predictive maintenance system to a production machine system. *International Journal of Machine Tools & Manufacture*, 2005. 4.2.1.2, 4.2.1.2

[31] D. Bansal, D.J. Evans, and B. Jones. A real-time predictive maintenance system for machine systems - an alternative to expensive motion sensing technology. In *Proc. Sensors for Industry Conference*, pages 39–44, 2005. 1

[32] D. Bansal, D.J. Evans, and B. Jones. A real-time predictive maintenance system for machine systems. *International Journal of Machine Tools & Manufacture*, **44**:759:756, 2006. 4.2.1.2, 1

[33] D. Bansal, R.P. Taylor, and P.N. Brett. Controller design for the drive system of a clinical micro-drilling system. Unpublished, 2004. 1, 4.2.1.2

[34] J. Barksdale. *The Encyclopedia of the Chemical Elements.* Reinhold Book Corporation, Illinois, 1968. 6.2.1.2

[35] W.D. Baumgartner, A. Jappel, J. Kronenberg, J. Hamzavi, K. Frei, and M. Stach. Cochlear implantation without mastoidectomy - the vienna experience. In *Proceedings of the 8th International Cochlear Implant Conference*, **1273**, pages 122–124, November 2004. 9.3.3, A.4.2

[36] P.P. Benham, R.J. Crawford, and C.G. Armstrong. *Mechanics of Engineering Materials.* Longman Group Limited, 2nd edition, 1996. 2.2.1, 2.2.3, 4.2.1.1, 4.2.1.1

[37] P.N. Brett. Automatic tool for microdrilling a stapedotomy. *Mechanical Incorporated Engineer*, **6**:112, 1994. 2.1

[38] P.N. Brett. An automatic technique for micro-drilling a stapedotomy in the stapes flexible footplate. *Proc. Instn. Mech. Engrs. Part H*, **209**:255:262, 1995. 2.2.2, 3.1, 3.3, 4.1

[39] P.N. Brett. Simulation of resistance forces acting on surgical needles. *Proc. Instn. Mech. Engrs. Part H*, **211**:335:247, 1997. 3.2

[40] P.N. Brett. Evaluation of the response of operators to force feedback at the tip of a steerable endoscope. *World Congress on Medical Physics and Biomedical Engineering*, 2000. Chicago, USA, July 23-28. 2.3.2.3

[41] P.N. Brett, D.A. Baker, R.P. Taylor, and M.V. Grffiths. Controlling the penetration of flexible bone tissue using the stapedotomy microdrill. *Proc. Instn. Mech. Engrs. Part I*, **218**:343:351, 2004. 3.2, 4.1

[42] P.N. Brett and M.V. Griffiths. Automated tools for surgical applications involving non-rigid tissues. In *Proc. International Conference on Systems, Man and Cybernetics 'Systems Engineering in the Service of Humans'*, pages 351–354, 17–20 Oct. 1993. 1.4, 2.1, 9.1

[43] S. Burrell. The bone anchored hearing aid:the third option for otosclerosis. *J Laryngol Otol Suppl.*, **7**:21:31, 1996. 5.2.2, 5.5.3

[44] G. Chen, M.T. Pham, and T. Redarce. Sensor-based guidance control of a continuum robot for a semi-autonomous colonoscopy. *Robotics and Autonomous Systems*, **57**(6-7):712 – 722, 2009. 3.2

[45] C. Choi. Predicting the effect of post-implant cochlear fibrosis on residual hearing. *Hearing Research*, **205**:193:200, 2005. 5.3.3.2

[46] N.L. Cohen. Cochlear implant soft surgery: fact or fantasy? *Otolaryngol Head Neck Surg*, **117**(3 Pt 1):214–216, Sep 1997. 5.3.3.2

[47] C.J. Coulson, A.P. Reid, D.W. Proops, and P.N. Brett. Ent challenges at the small scale. *Int J Med Robot*, **3**(2):91:96, Jun 2007. 5.1, 5.5.3, 7.4

[48] B.L. DAVIES. Application software for a robot for prostate surgery. *Proceedings of the 1st International Workshop on Mechatronics in medicine and surgery*, page 31:39, 1992. MediMech, Spain, 26-28 October. 3.1.4

[49] B.L. DAVIES. Active compliance in robotic surgery - the use of force control as a dynamic constraint. *Proc. Instn. Mech. Engrs. Part H*, **211**:285:292, 1997. 3.1.2

[50] B.L. DAVIES. The safety of medical robots. *Proc. 29th Int Symp. on Industrial Robots*, page 7:11, 1998. Beyond 2000. 2.3.2.2, 3.1

[51] B.L. DAVIES, K.L. FAN, R.D. HIBBERD, M. JAKOPEC, AND S.J. HARRIS. A mechatronic based robotic system for knee surgery. In K.L. FAN, editor, *Proc. Intelligent Information Systems IIS '97*, page 48:52, 1997. 3.1.2

[52] B.L. DAVIES, R.D. HIBBERD, W.S. NG, A.G. TIMONEY, AND J.E.A. WICKHAM. A surgeon robot for prostatectomies. In R.D. HIBBERD, editor, *Proc. Fifth International Conference on Advanced Robotics 'Robots in Unstructured Environments', 91 ICAR*, page 871:875 vol.1, 1991. 3.1

[53] B.L. DAVIES, S. STARKIE, S.J. HARRIS, E. AGTERHUIS, V. PAUL, AND L.M. AUER. Neurobot: a special-purpose robot for neurosurgery. In S. STARKIE, editor, *Proc. IEEE International Conference on Robotics and Automation ICRA '00*, **4**, page 4103:4108 vol.4, 2000. 6.6.4

[54] J.M. DRAKE, J.M. DRAKE, M. JOY, A. GOLDENBERG, AND D. KREINDLER. Computer and robotic assisted resection of brain tumours. In M. JOY, editor, *Proc. Fifth International Conference on Advanced Robotics 'Robots in Unstructured Environments', 91 ICAR*, pages 888–892 vol.1, 1991. 3.1

[55] H. DUDLEY, D. CARTER, AND R.C.G. RUSSELL. *Rob & Smiths Operative Surgery: Ear. Fourth Edition.* Butterworths, London, 1986. 5.3.2.1

[56] M.S. ELJAMEL. Robotic application in epilepsy surgery. *Int J Med Robot*, **2**(3):233–237, Sep 2006. 3.1.1

[57] B. Fei, W.S. Ng, Chauhan S., and C.K. Kwoh. The safety issues of medical robotics. *Reliability Engineering & System Safety*, **73**(2):183:192, August 2001. 7.2

[58] N. Fox. Space, sterility and surgery: circuits of hygiene in the operating theatre. *Soc. Sci. Med.*, **45**:649:657, 1997. 5.4.1

[59] C.A. Grimbergen and J.E.N. Jaspers. Robotics in minimally invasive surgery. In *Proc. IEEE International Conference on Systems, Man and Cybernetics*, **3**, pages 2486–2491, 10–13 Oct. 2004. 5

[60] I. Halim and A. Tavakkolizadeh. Notes: The next surgical revolution? *Int J Surg*, **6**(4):273–276, Aug 2008. 9.2

[61] S.J. Harris, S.J. Harris, Q. Mei, R.D. Hibberd, and B.L. Davies. Experiences using a special purpose robot for prostate resection. In Q. Mei, editor, *Proc. th International Conference on Advanced Robotics ICAR '97*, page 161:166, 1997. 3.1.4

[62] S. Hartland. Bone anchored hearing aid wearers with significant sensorineural hearing losses (borderline candidates): patients results and opinions. *J Laryngol Otol Suppl.*, **21**:41:46, 1996. 5.2.3

[63] R. Isermann. Process fault detection based on modelling and estimation methods - a survey. *Automatica*, **20**:387:404, 1984. 4.2.1.2

[64] S. Jovanovic. Co2 laser stapedotomy with the one-shot techniqueclinical results. *Otolaryngol Head Neck Surg*, **131**:751:757, 2004. 5.3.2.2

[65] A. Kadhim. Bone anchored hearing aids: reality, failure and current status. *Ir Med J.*, **97**:312:314, 2004. 5.2.2

[66] P. Kazanzides, J. Zuhars, B. Mittelstadt, and R.H. Taylor. Force sensing and control for a surgical robot. In J. Zuhars, editor, *Proc. IEEE International Conference on Robotics and Automation*, pages 612–617 vol.1, 1992. 3.1.4

[67] A. KONARSKA. Surgical problems in some otosclerosis cases. *International Federation of Otorhinolaryngological Societies*, **14**:97:100, 2003. 5.3.2.2

[68] Y. KWOH. A robot with improved absolute position accuracy for ct guided stereotactic brain surgery. *IEEE Transaction on Biomedical Engineering*, **35**:153:160, 1988. February. 3.1.1

[69] S. LAVALLEE. A new system for computer assisted neurosurgery. In *Proc. 11th IEEE Engineering in Medicine and Biology Conf.*, page 926:927, 1989. Seatle. 3.1.1

[70] Q.H. LI, L. ZAMORANO, A. PANDYA, R. PEREZ, J. GONG, AND F. DIAZ. The application accuracy of the neuromate robot–a quantitative comparison with frameless and frame-based surgical localization systems. *Comput Aided Surg*, **7**(2):90–98, 2002. 3.1.1

[71] F. LINTHICUM. Histopathology of otosclerosis. *Otolaryngologic Clinics of North*, **26**:335:352, 1993. 5.2.2

[72] X. MA, P.N. BRETT, M.T. WRIGHT, AND M.V. GRIFFITHS. A flexible digit with tactile feedback for invasive clinical applications. *Proc Inst Mech Eng [H]*, **218**(3):151–157, 2004. 3.2

[73] E. MONAHAN AND A. SHIMADA. Computer-aided navigation for arthroscopic hip surgery using encoder linkages for position tracking. *Int J Med Robot*, **2**(3):271–278, Sep 2006. 3.1.1

[74] R. MULHALL. Impact blasting with glass beads. *Metal Finishing*, **105**:65:71, 2007. 6.2.1.2

[75] F.R. ONG AND K. BOUAZZA-MAROUF. The detection of drill bit breakthrough for the enhancement of safety in mechatronic assisted orthopaedic drilling. *Mechatronics*, **9**(6):565 – 88, 1999. 3.2

[76] T. PARKER. Towards a mechatronic tool for the epidural procedure. *Proceedings of 2nd Int. Conf. On Mechatronics and Machine Vision in Practice (M2VIP)*, page 189:192, 1995. Hong Kong, 12-14 September. 3.2

[77] I. Petra, D.J. Holding, K.J. Blow, B. Tam, Xianghong Ma, and P.N. Brett. The design of a flexible digit towards wireless tactile sense feedback. In *Proc. ICARCV 2004 8th Control, Automation, Robotics and Vision Conference*, **1**, pages 468–473, 6–9 Dec. 2004. 3.2

[78] I. Petra, D.J. Holding, X. Ma, P.N. Brett, and K.J. Blow. Fast and accurate tactile sense feedback estimation for innovative flexible digit for clinical applications. *Electronics Letters*, **42**(14):790–792, 6 July 2006. 3.2

[79] C. Priwin and G. Granstrm. The bone-anchored hearing aid in children: a surgical and questionnaire follow-up study. *Otolaryngol Head Neck Surg*, **132**(4):559–565, Apr 2005. A.4.3

[80] L. Reyes. Mechtron design limited. Derby, UK. 4.1, 6.2

[81] P. Roland. Method for hearing preservation in cochlear implant surgery. *Operative Techniques in Otolaryngology*, **16**:93:100, 2005. 1, 5.3.3.2, 5.2

[82] D. Rothbaum. Task performance in stapedotomy: Comparison between surgeons of different experience levels. *Otolaryngol Head Neck Surgery*, **128**:71:77, 2003. 5.3.2.2

[83] R. Sachidananda. Bone anchored hearing aid versus stapedectomy: Analysis of patient benefits. *Otolaryngology Head and Neck Surgery*, page 76, 2005. Birmingham, United Kingdom. 5.2.2, 5.5.3

[84] A. Sepehr. In-situ oct imaging of porcine cochlear microanatomy. *Otolaryngology - Head and Neck Surgery*, **137**:128:129, 2007. 7.4

[85] G. Shand. Shand systems limited, May 2008. `http://www.shand-systems.com/`. 6.3

[86] M. Shoham, S. Brink-Danan, A. Friedlander, and N. Knoller. Bone-mounted miniature robotic system for spine surgery. In *Proc. First IEEE/RAS-EMBS International Conference on Biomedical Robotics and Biomechatronics BioRob 2006*, pages 917–920, February 20–22, 2006. 3.1.1

[87] P.S. Slack and X. Ma. Time dependency assessment of muscular fatigue index and hand tremor under operating conditions. In *Proc. 29th Annual International Conference of the IEEE Engineering in Medicine and Biology Society EMBS 2007*, pages 4822–4825, 22–26 Aug. 2007. 1.2

[88] E.H. Spencer. The robodoc clinical trial: a robotic assistant for total hip arthroplasty. *Orthop Nurs*, **15**(1):9–14, 1996. 3.1, 3.1.4

[89] K. Stidham. Cochlear hook anatomy: Evaluation of the spatial relationship of the basal cochlear duct to middle ear landmarks. *Acta Otolaryngol*, **119**:773:777, 1999. 5.3.3.1

[90] G.T. Sung and I.S. Gill. Robotic laparoscopic surgery: a comparison of the da vinci and zeus systems. *Urology*, **58**(6):893–898, Dec 2001. 3.1.3

[91] R. Taylor, P. Jensen, L. Whitcombe, A. Barnes, R. Kumar, D. Stoianovici, P. Gupta, Z. Wang, E. deJuan, and L. Kavoussi. An integrated robot system architecture augmentation. *An Integrated Robot System Architecture*, **18**:1201:1210, 1999. 3.1.2

[92] R.H. Taylor. A perspective on medical robotics. *IEEE J PROC*, **94**(9):1652–1664, Sept. 2006. 3.1

[93] J. Troccaz, J. Troccaz, S. Lavallee, and E. Hellion. A passive arm with dynamic constraints: a solution to safety problems in medical robotics. In S. Lavallee, editor, *Proc. International Conference on Systems, Man and Cybernetics 'Systems Engineering in the Service of Humans'*, pages 166–171 vol.3, 1993. 3.1.2

[94] C. Turner. Preservation of residual acoustic hearing in cochlear implantation. *International Congress Series*, **1273**:243:246, 2004. 5.3.3.2

[95] A.A. Wagner, I.M. Varkarakis, R.E. Link, W. Sullivan, and L. Su. Comparison of surgical performance during laparoscopic radical prostatectomy of two robotic camera holders, endoassist and aesop: a pilot study. *Urology*, **68**(1):70–74, Jul 2006. 3.1.1

[96] J. WAHRBURG. Concept of a novel laser probe for minimal invasive applications in neurosurgery. *Int. Jnl. of Mechatronics*, **6**:179:190, 1996. 3.2

[97] J. WAHRBURG, I. GROSS, P. KNAPPE, S. PIECK, S. KUNZLER, AND KERSCHBAUMER F. An interactive mechatronic assistance system to support surgical interventions. In *Computer Assisted Radiology and Surgery, Proceedings of the 18th International Congress and Exhibition*, **1268**, pages 431–436, 2004. 3.1.4

[98] R. WESTPHAL, S. WINKELBACH, T. GSLING, T. HFNER, J. FAULSTICH, P. MARTIN, C. KRETTEK, AND F.M. WAHL. A surgical telemanipulator for femur shaft fracture reduction. *Int J Med Robot*, **2**(3):238–250, Sep 2006. 3.1.3

[99] A. WOLF AND B. JARAMAZ. Mbars: Mini bone attached robotic system for joint arthroplasty. In *Proc. First IEEE/RAS-EMBS International Conference on Biomedical Robotics and Biomechatronics BioRob 2006*, pages 1053–1058, February 20–22, 2006. 3.1.4

[100] P. YEN. A telemanipulator system as an assistant and training tool for penetrating soft tissue. *Int. Jnl. of Mechatronics*, **6**:423:436, 1996. 3.2

[101] N. YOUNG. Cochlear implantation, operative techniques in otolaryngology. *Head and Neck Surgery*, **14**:263:267, 2003. 5.3.3

Appendix A

Technical Documentation

A.1 Circuit Diagrams

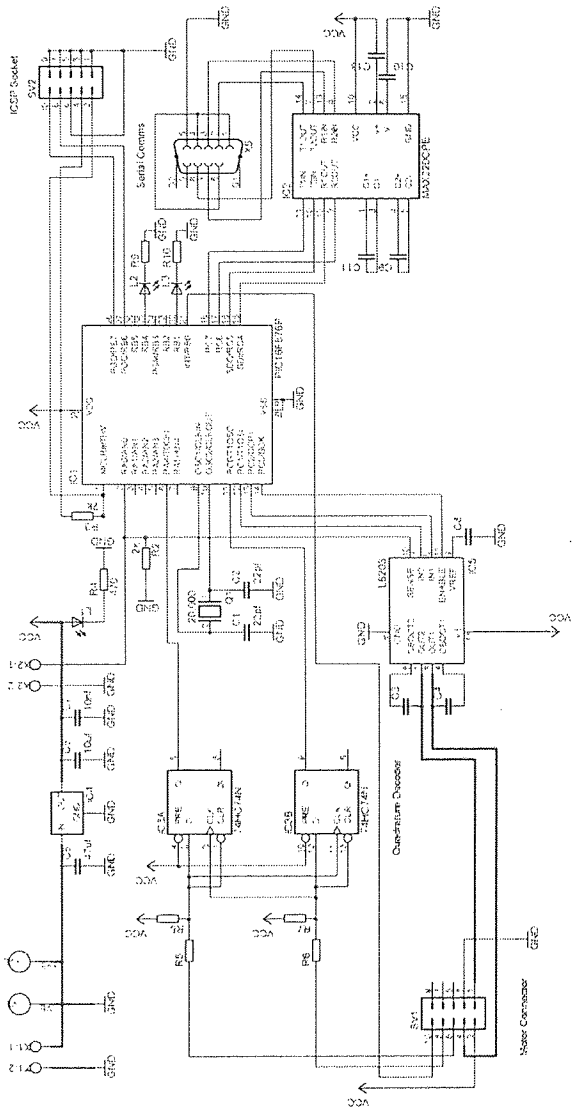

Figure A.1: *Circuit diagram for the test rig controller.*

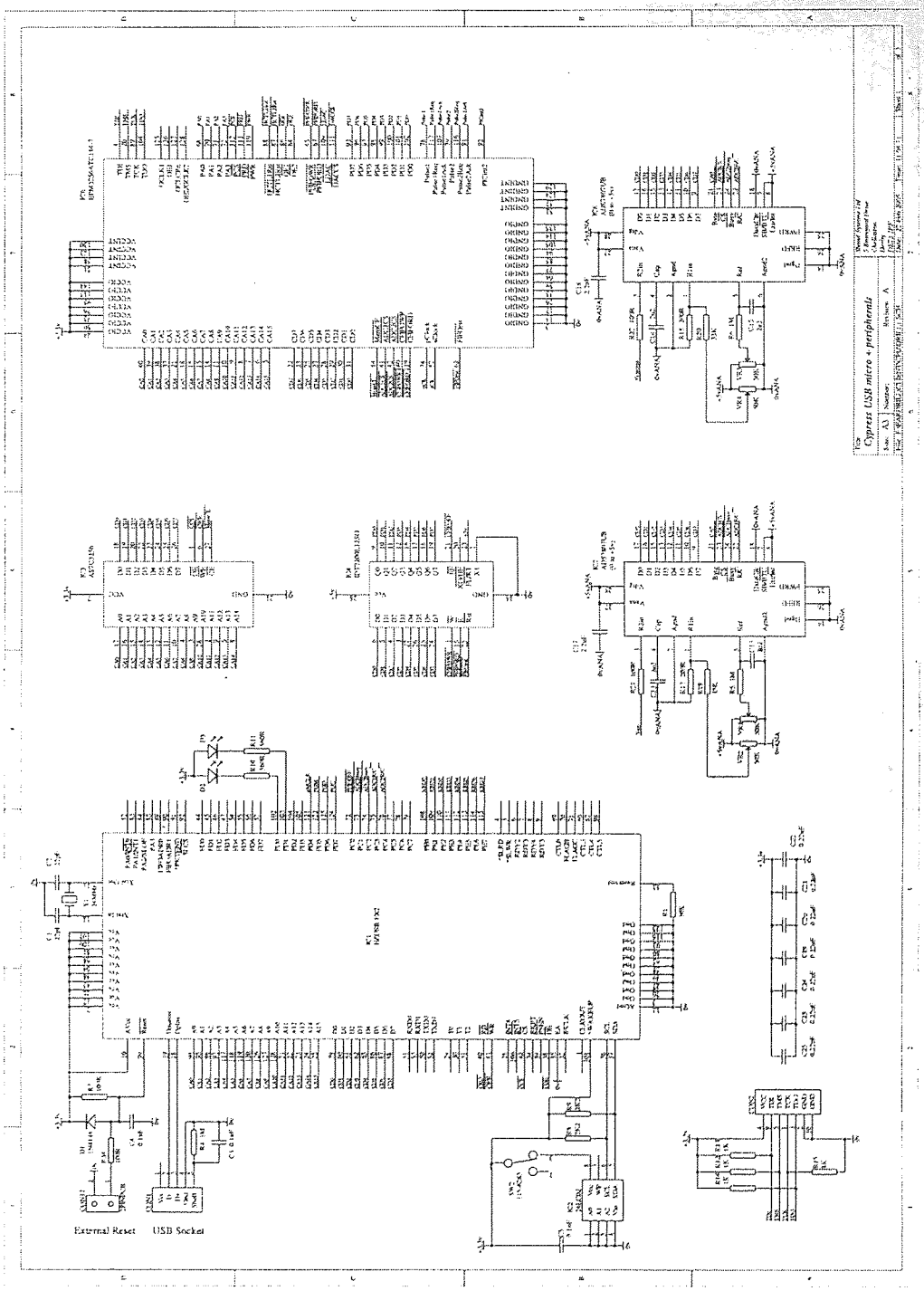

Figure A.2: *Circuit diagram for the High Level Controller (HLC).*

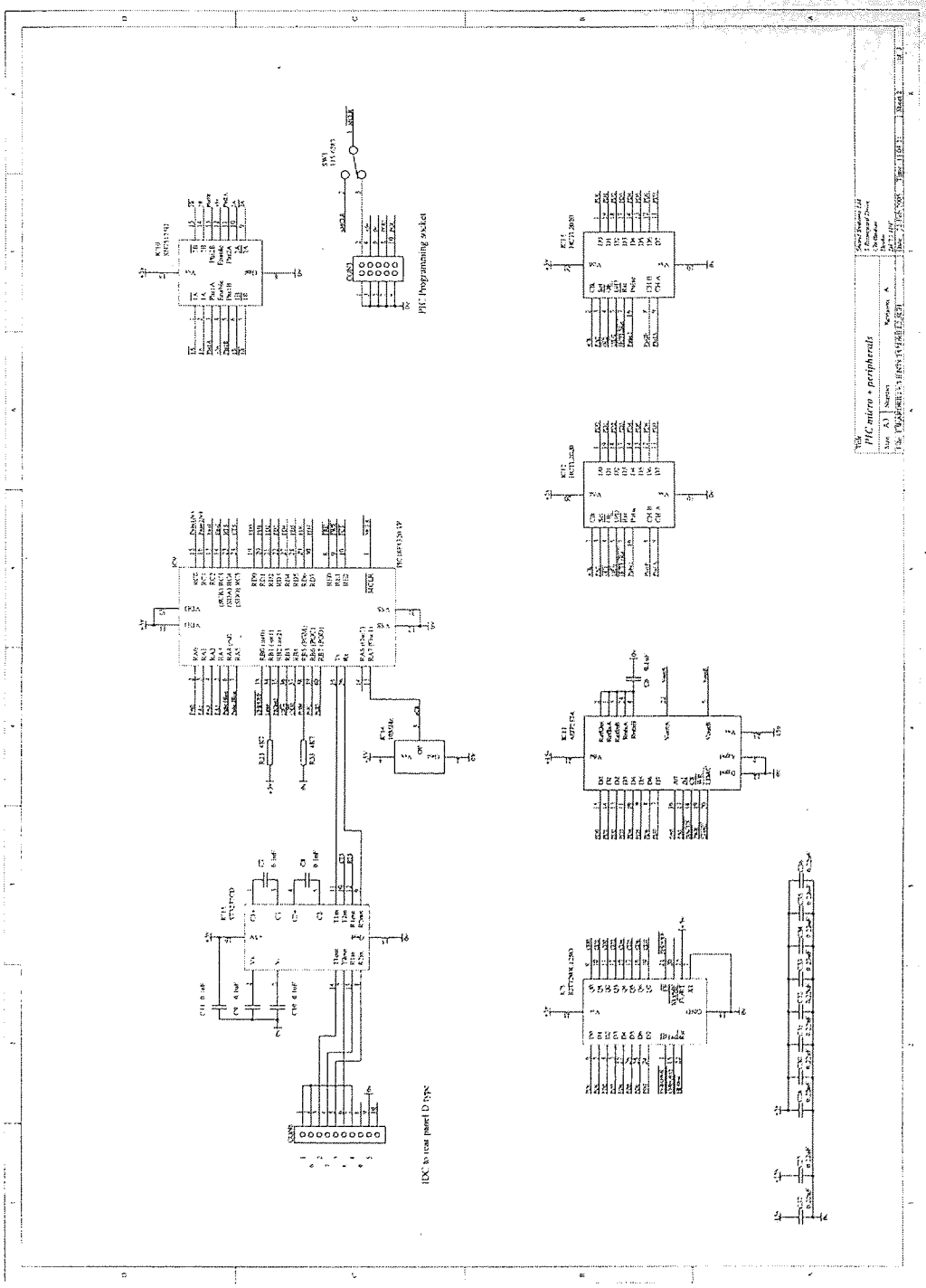

Figure A.3: *Circuit diagram for the Low Level Controller (LLC).*

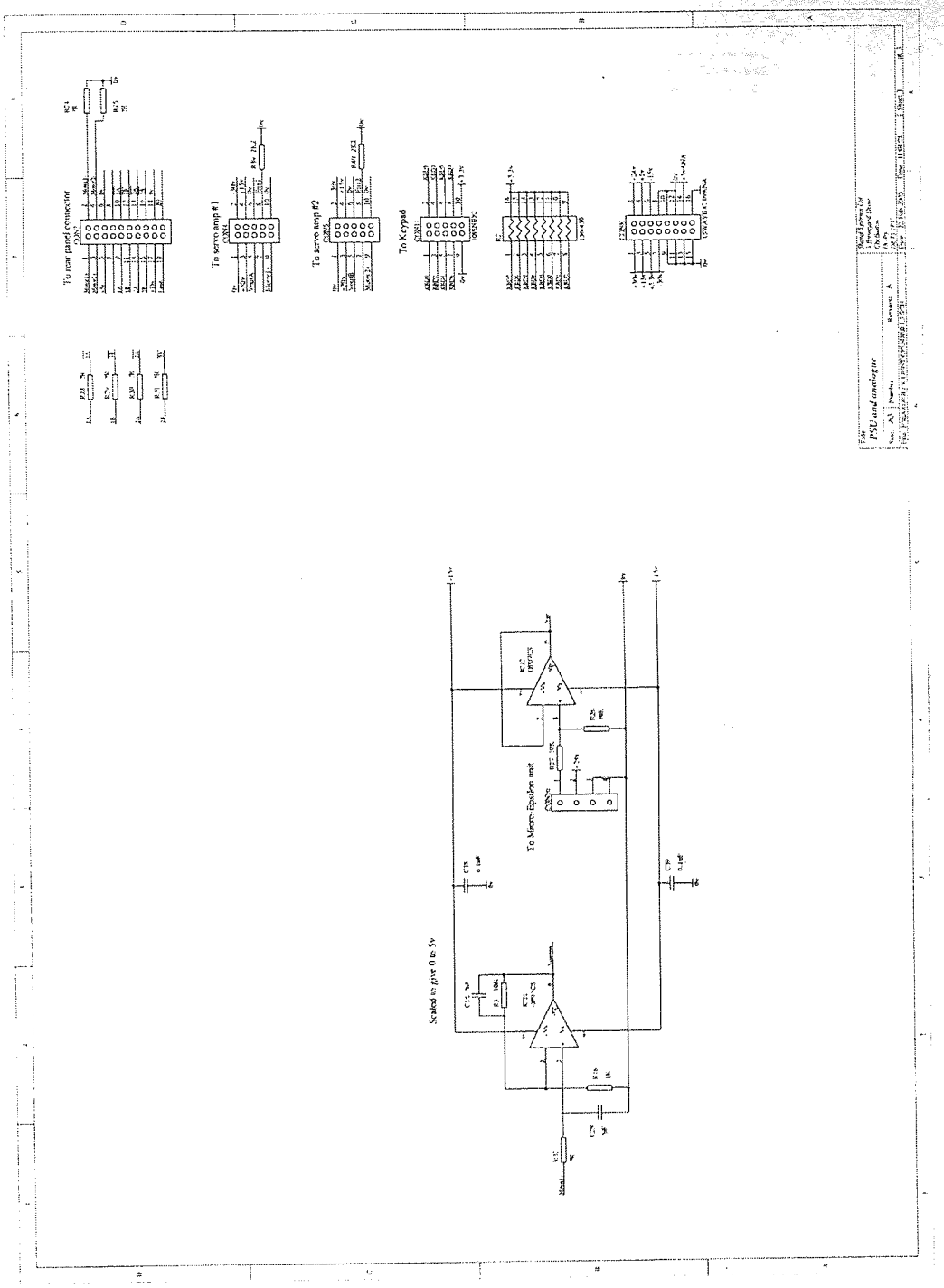

Figure A.4: *Circuit diagram for the power supply unit (PSU).*

A.2 Firmware Flow Diagrams

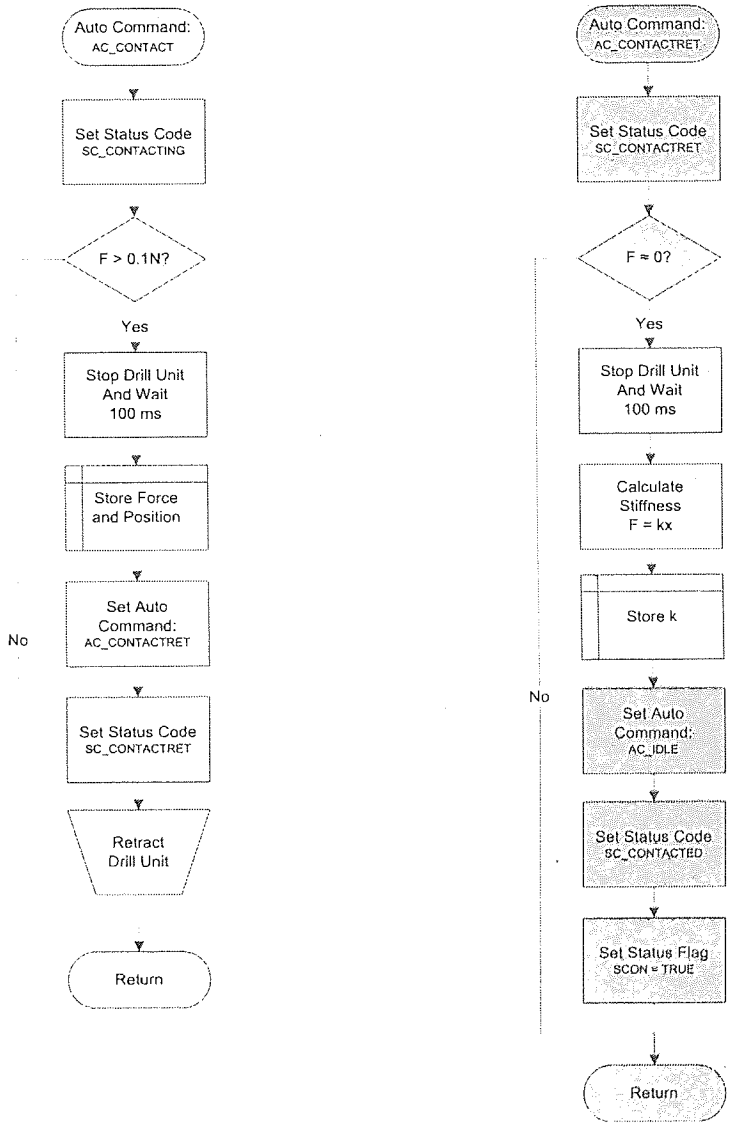

Figure A.5: *AutoCommand contact sequences.*

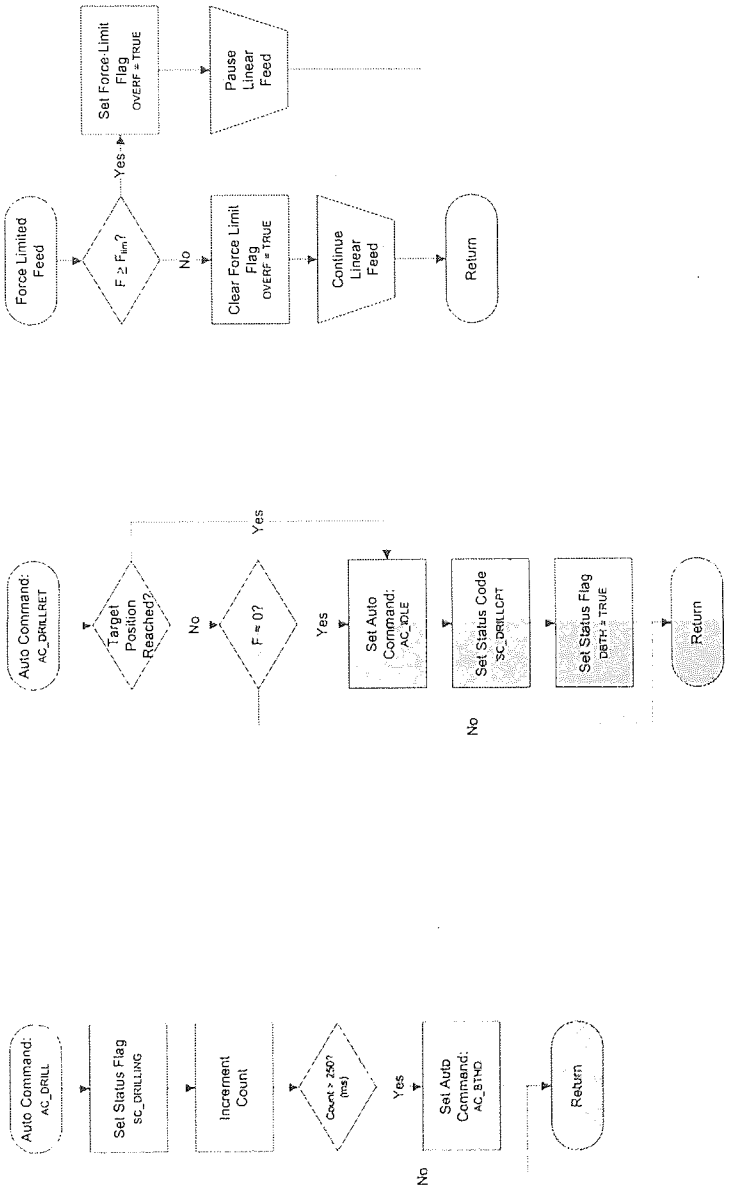

Figure A.6: *AutoCommand investigative drilling sequences.*

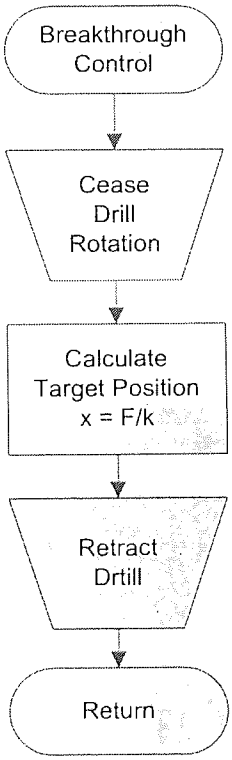

Figure A.7: *AutoCommand breakthrough control sequence.*

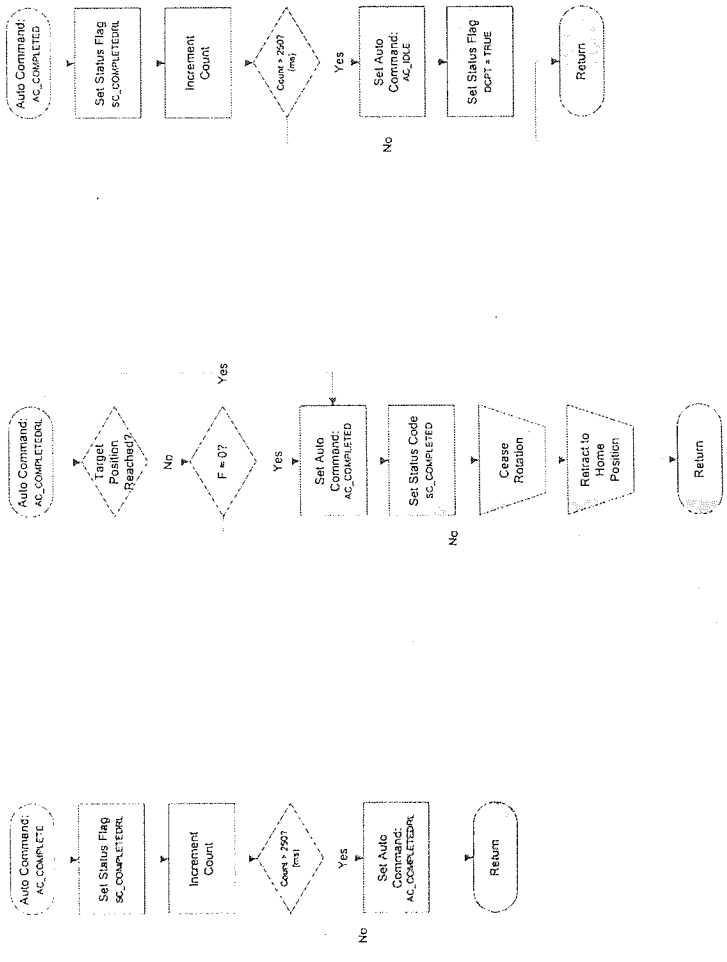

Figure A.8: *AutoCommand hole completion sequence.*

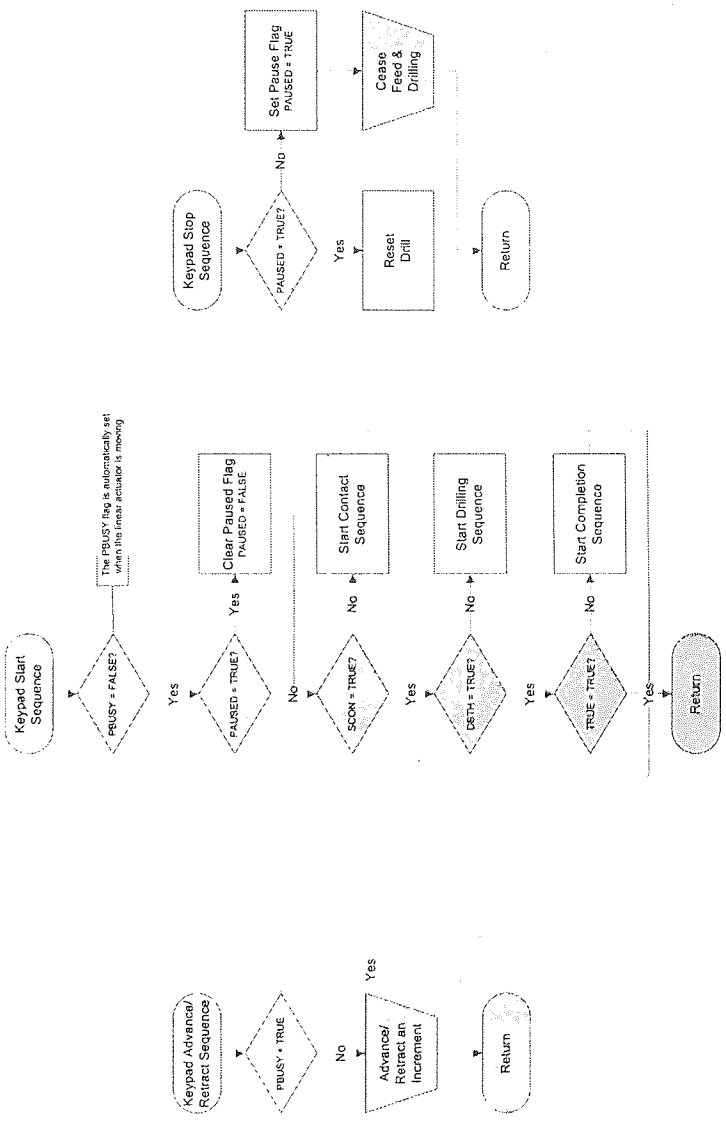

Figure A.9: *Keypad sequences, Advance/Retract(left), Start(center), Stop(right).*

A.3 Software Functions

The specific functions of the GUI described in the previous section are described in detail in figure A.10.

The key functions of the interface are indicated by the numbered balloons and are as follows:

1. **Force**
   This displays the current force applied to the drill tip.

2. **Force Offset**
   This displays the force offset calculated when the drilling system was initialised to compensate for hysteresis in the force sensor.

3. **Torque**
   This displays the current torque applied to the drill tip.

4. **Drill Velocity**
   This displays the actual drill rotational velocity set point.

5. **Drill Set Velocity**
   This displays the drill rotational velocity set point stored within the instrument.

6. **Current Position**
   This displays the current position of the linear actuator.

7. **Set Position**
   This is the target position of the linear actuator stored in the instrument.

8. **Set Velocity**
   This is the target position of the linear actuator stored within the instrument.

9. **Time**
   This shows the duration of the current drilling process.

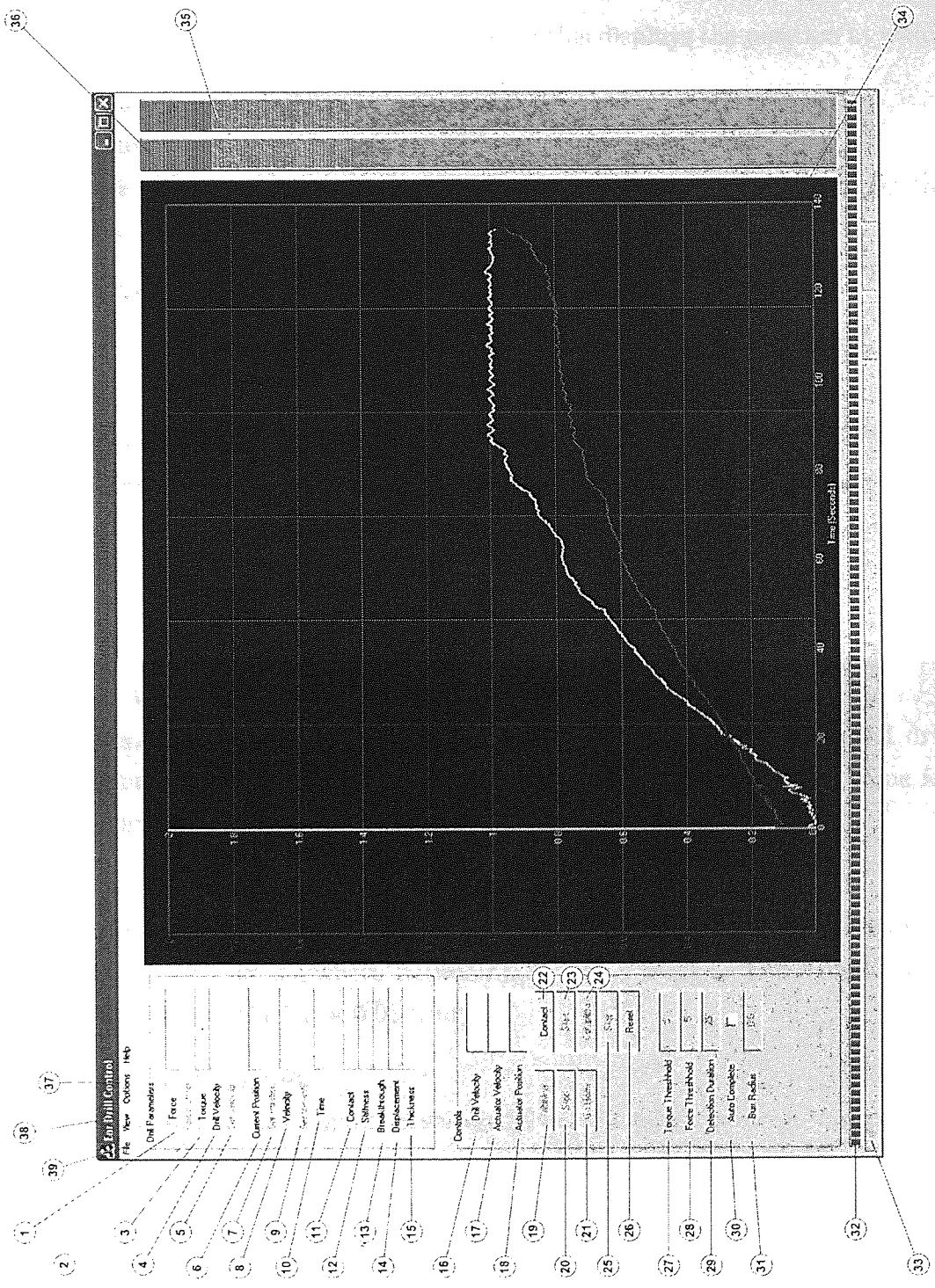

Figure A.10: *Host software graphical user interface and key functions.*

10. **Contact**
    If the contact routine has been completed this displays the position at which contact with the target was achieved.

11. **Stiffness**
    This is the calculated stiffness of the target material as calculated by the contact routine.

12. **Breakthrough**
    If the drilling routine has been completed the position at which breakthrough occurred is displayed here.

13. **Displacement**
    On detection of breakthrough the displacement and thickness of the target can be calculated and is displayed here.

14. **Thickness**
    This estimated target thickness is displayed here.

15. **Drill Velocity**
    This is an editable box in which the operator can enter the desired drill rotational velocity anywhere between 0 and 50 rps. The default value for this threshold is 25 rps.

16. **Actuator Velocity**
    This is an editable box in which the operator can enter the desired linear actuator velocity anywhere between 0.01 and 4 mm/s. The default value for the linear velocity is 0.01 mm/s.

17. **Actuator Position**
    When manual control mode is selected from the Options menu the operator can manually enter a desired target position for the linear actuator anywhere between 0 and 25 mm. When the device is used in theatre none of the manual operations are available.

18. **Initialise**
    This button is only enabled when the drill system is first turned on, before

the system is placed in Automatic mode. This button starts the linear actuator initialisation sequence.

19. **Stop**
    This stop button is available only when the drilling system is performing a manual operation for example moving to a manually entered position, moving to the home position or running the initialisation sequence.

20. **Go Home**
    When manual mode is enabled this returns the linear actuator to the home position.

21. **Contact**
    When placed in Automatic Mode via the Options Menu this is the only of the autonamous functions that is available initially. This button initiates the first phase of the control strategy, the contact sequence. *This sequence can also be initiated via the hand held remote, in which case the GUI is updated automatically.*

22. **Start**
    When the contact sequence is completed this button becomes available. When pressed it starts the drilling sequence, the second phase of the control strategy. *This sequence can also be initiated via the hand held remote, in which case the GUI is updated automatically.*

23. **Complete**
    After breakthrough has been detected and controlled this button becomes available. When pressed this initiates the hole completion sequence, the final phase in the control strategy. *This sequence can also be initiated via the hand held remote, in which case the GUI is updated automatically.*

24. **Stop**
    When the drilling system is performing any of the autonomous control sequences this button becomes enabled. When pressed the current sequence is paused and the corresponding sequence button is re enabled. The sequence can be restarted by clicking the button again. *This sequence can*

also be initiated via the hand held remote, in which case the GUI is updated automatically.

25. **Reset**
    This performs an emergency reset which retracts the drill at maximum velocity to the home position and ceases drill rotation.

26. **Torque Threshold**
    The is an editable box in which the operator can enter the torque threshold used for breakthrough detection. The default value for this threshold is 5.

27. **Force Threshold**
    The is an editable box in which the operator can enter the force threshold used for breakthrough detection. The default value for this threshold is -5.

28. **Detection Duration**
    The is an editable box in which the operator can enter the desired detection duration used for breakthrough detection in ms. This determines the number of milliseconds that the breakthrough condition must remain true and can be used to control the diameter of the aperture of the drilled hole. The default value for the detection duration is 25 ms.

29. **Auto Complete**
    When this option is enabled the hole completion sequence is initiated without the operators intervention upon the detection of breakthrough.

30. **Burr Radius**
    This is an editable box in which the radius of the cutting burr is entered. This is used on the calculation of the position parameters for the breakthrough control and hole completion sequences.

31. **Progress Bar**
    This progress bar represents the duration of the drilling process, reaching 100% at 600 seconds. The software can acquire a maximum of 10 minutes of data.

32. **Status Bar**

    This bar shows any additional relevant data such as the current date and time, status updates from the device, data file name and any error codes from problems that may have occurred.

33. **Transient Graphs**

    This is the graphing screen. This displays real time data coming from the drilling system and is updated every tenth of a second. The graph can display both force and torque simultaneously or individually, as well as force and torque gradient data and velocity information. The graph can also be maximised to fill the entire screen and individual segments can be zoomed in on to aid visualisation. The scale of the axis can be change from the View menu using the plot settings dialog.

34. **Force Status Bar**

    This is a bar chart that shows a visual representation of the current threshold parameters. As the predefined threshold is approached the bar turns red indication that the threshold has been reached.

35. **Torque Status Bar**

    This is the similar as the Force status bar in that is displays the Torque Threshold status. When both bars become red simultaneously, this indicates that the breakthrough condition is current satisfied.

36. **Options Menu**

    This is a simple drop down menu that provide access to some of the more advance configuration options such as:

    - Manual setting of the force offset,
    - Enable/Disabling of the PID controller,
    - Enable/Disable of Automatic Mode,
    - Capture of data directly to the hard drive,
    - Management of the command log.

37. **View Menu**
    The view menu provides access to the display option and additional dialogs including:

    - Status Dialog,
    - System Console,
    - System Settings,
    - Patient information dialog,
    - Plot settings, data selection and location.

38. **File Menu**
    The file menu provide access to overall system actions such as connect, reset and refresh as well as standard file functions. These include:

    - Connection to the device,
    - File dialogs (Save, Save As and Open),
    - Reset Device (Hard Reset),
    - Refresh Interface.

A.4 Further Applications

A.4.1 Electrode Insertion

Another potential development of the drilling system is its use for controlled electrode insertion. Although specific to the cochlea implant procedure it may present significant benefits through improved electrode placement and reduced trauma.

Electrode insertion is part of the cochlea implant procedure and one which poses similar risks to the drilling of the cochleostomy. The electrode, which is approximately 25 *mm* in length, is inserted through the cochleostomy into the spiral lamina of the cochlea. To keep the electrode straight a wire splint passes

through its length which is withdrawn as it is inserted. A natural curl makes it form a spiral as it is inserted. This process is again performed by hand by the surgeon. If inserted too rapidly, the electrode can cause severe damage to the membranous cochlea and heavy fluid displacement.

When the drilling of the cochleostomy is complete, the drilling axis remains inline with the hole and thus is along the same trajectory along which the electrode will be inserted. Given that the drill unit already integrates a precision linear feed, force sensing and rotary motion, it is thought a simple lead screw assembly in an alternative drill shaft sheath could be used to withdraw the splint whilst the electrode is advanced by the drilling unit. The rate at which the splint is withdrawn could be precisely controlled such that the curl of the electrode matches that of the spiral of the cochlea. Combined with a slow linear feed and force feedback, contact with internal structures may be controlled or even avoided all together and perilymph displacement reduced.

A.4.2 Suprameatal Approach

The use of smart tools in surgery presents many potential benefits, some of which may not yet be immediately apparent. For example, the standardisation of surgical practice and the exploration of less invasive surgical techniques. A further example of the way in which this technology may add additional benefit to the cochlea implant procedure is through the use of alternative access routes to the inner ear. One such approach is that developed by Baumgartner *et al* (35). Using this approach, the bulk of the procedure is performed via the ear canal, similar to the way in which the stapedotomy is performed. A separate route for the electrode is made by drilling a 2 *mm* suprameateal tunnel. This route avoids both the sensitive structures within the ear and the facial nerve, significantly reducing the risk of complications. A drawback of this approach is that the surgeon is required to work through significantly smaller access way making the task more technically demanding. The use of the micro-drilling system in this approach would reduce the complexity of the procedure and ensure an optimally located, minimally traumatic cochleostomy. The procedure could then be further enhanced

using the insertion technique described in the previous section.

A.4.3 BAHA

The implantation bone anchored hearing aids (BAHA) is another application that could benefit from the use of a system such as this. The implantation of a BAHA involves the drilling of a hole through the skull behind the ear in the mastoid region where the temporal bone is thickest, into which an abutment is fitted. To reduce the risk of post-operative complications the hole into which the abutment is fitted is required to be as deep as possible, up to 5 *mm*. In the conventional procedure the hole is drilled until this depth is reached or until the drill reached the dura protecting the brain. The latter is often the case with children and thus carries a high degree of risk (79). The drilling system could be adapted to perform such a task potentially reducing the likelihood of damaging the dura. As preparation of the abutment aperture is the most critical stage of the procedure the drilling system could carry out the task with a higher level of precision, and a higher level of consistency than currently possible. By reducing the skill requirements to achieve success, the method offers potential to widen access to this treatment and the resulting precision-fit of the BAHA would result in more efficient conductive sound transmission.

A.4.4 Smart Tool Points

In reviewing potential applications it became apparent that general drilling procedures may be able to take advantage of the use of smart tool points without the associated cost of the robotic systems to support them. Given the success of this device in discriminating between true features in the drilling transients and noise, an experiment was conducted to evaluate the potential for inclusion of smart tool points in standard surgical instruments. Figure A.11 shows the force and torque transients when using the drill unit alone with the linear feed disabled in an unsupported, hand-held capacity.

This was a laboratory trial on compliantly mounted egg shell. It was found

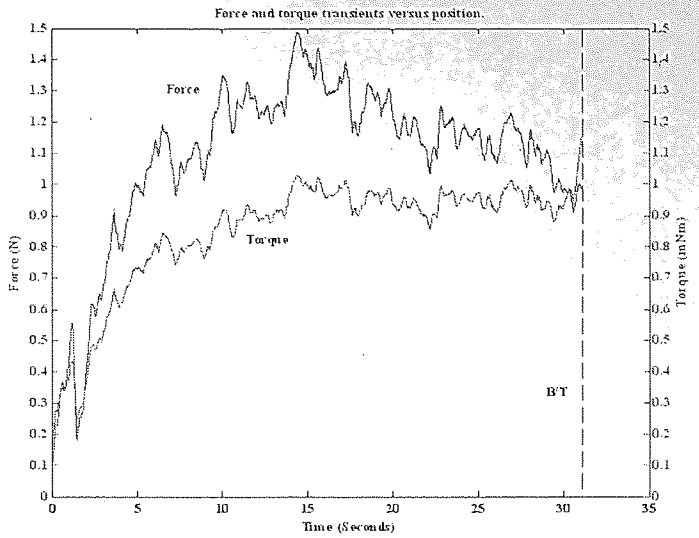

Figure A.11: *Drilling transient when using the micro-drill in a hand-held capacity.*

that in order for this to work, force feedback had to be provided to the operator via an audible tone that increased in pitch as the force increased. Without this it was found that the force levels were extremely unstable, often resulting in excessive force being applied to the target. Despite the noisy transients, breakthrough was detected within 25 μm of the distal surface. This demonstrates that the use of this technique in conventional surgical instruments is an avenue that should be explored. Smart tool points have the capacity to revolutionise conventional surgical procedures whether it be by actively controlling mechatronic tools, simply relaying additional tactile information to the clinician or as part of a larger robotic system.